UNIVERSITY OF SALAMANCA
INSTITUTE FOR NEUROSCIENCE OF CASTILLA Y LEÓN
AUDITORY NEUROSCIENCE LABORATORY
Doctoral Program in Neurosciences

STIMULUS-SPECIFIC ADAPTATION AND DEVIANCE DETECTION IN THE AUDITORY CORTEX

Thesis submitted for the degree of

Doctor in Neuroscience

By

Javier Nieto Diego

Under the supervision of

Prof. Dr. Manuel Sánchez Malmierca

Salamanca, June 2017

MANUEL SÁNCHEZ MALMIERCA, CATEDRÁTICO DE UNIVERSIDAD DEL DEPARTAMENTO DE BIOLOGÍA CELULAR Y PATOLOGÍA DE LA UNIVERSIDAD DE SALAMANCA Y DIRECTOR DEL INSTITUTO DE NEUROCIENCIAS DE CASTILLA Y LEÓN

CERTIFICA

que la tesis doctoral titulada:

STIMULUS-SPECIFIC ADAPTATION AND DEVIANCE DETECTION IN THE AUDITORY CORTEX

ha sido redactada en inglés, contiene un resumen en español y describe el trabajo de investigación realizado por Javier Nieto Diego bajo mi dirección durante los últimos 4 años.

Esta memoria de tesis recoge una caracterización y análisis detallados de las propiedades fisiológicas y anatómicas de la adaptación a estímulos específicos (*stimulus-specific adaptation*, SSA) en la corteza auditiva de la rata, y su estrecha relación con los mecanismos neuronales de detección de la discrepancia (*deviance detection*) y de la codificación predictiva (*predictive coding*). Los datos presentados en esta memoria constituyen una aportación original y puedo afirmar que ponen de manifiesto un gran avance en el área de las Neurociencias en general, y de la Neurociencia Auditiva en particular.

Por todo ello, considero que esta tesis reúne la calidad y rigor científico necesarios para que sea defendida en la Universidad de Salamanca como requisito para que Javier Nieto Diego opte al título de 'Doctor con mención de Doctor Internacional' por la Universidad de Salamanca.

Y para que así conste, firmo el presente certificado en Salamanca, a 4 de Junio de 2017.

Prof. Manuel Sánchez Malmierca

Por muy cerrada la noche, e incierto el camino,
lucía siempre en lo alto del firmamento una estrella;
su luz me trajo hasta aquí, acompañando mis huellas,
para realizar un sueño y perseguir mi destino.
…Y si algún día lo encuentro, sé que será junto a ella.

ACKNOWLEDGEMENTS

Many people have participated, directly or indirectly, in this research project. I want to thank them all and acknowledge their contribution to scientific knowledge.

Gracias… a todo el personal del INCYL, por hacer que tantas cosas funcionen. En representación de todos ellos, gracias a Ana por recibirme cada mañana con una sonrisa.

Gracias… a David, Flora, Dani, Yann y Blanca, por enseñarme cada detalle del trabajo en el laboratorio, y por tantas horas de discusión científica e inspiración.

Gracias… a Guillermo, Gloria y Catalina, cuya contribución a este trabajo va mucho más allá del compañerismo y la buena disposición, ellos forman parte de esto tanto como yo.

Thanks… to Adrian, Alan, Bernhard, Christoph, Daniel, Dexter, Heather, Iria, José Luis, Juanita, Ned, Patrick, and Ryszard, for serious help to improve my manuscripts.

Thanks… to Heather, for showing me how to record properly from auditory cortex.

Thanks… to Bernhard, for being the best possible host in Donders, and for many hours of exciting and inspiring scientific and philosophical conversation.

Gràcies… a Carles, per la seva especial contribució a aquest treball, i pels anys de col·laboració i amistat entre els nostres laboratoris.

Gracias… a Manolo, por ser el mejor jefe que uno pueda imaginar, y también un gran amigo. He taught me almost everything I know about how to thrive in science, and many important things about how to thrive in life.

Gracias… a mis padres, a mis hermanos y a toda mi familia, por darme tantos hogares.

Gracias… a mis amigos, por limpiar mi cabeza con un buen vino de tanto en tanto.

Gracias… a todos mis maestros y profesores, por abrir cientos de ventanas en mi mente.

Gracias a María, por creer en mi cuando yo mismo no lo hacía.

This work ha been funded by a fellowship from Spanish Junta de Castilla y León (Consejería de Educación, Programa ERIDI 2007-2013), using funds from European Social Fund (Operational Programme ESF Castilla y León 2007-2013), by an exchange grant from the Network of European Neuroscience Schools (NENS), by the Spanish MINECO projects BFU2013-43608-P and SAF2016-75803-P, by the Spanish JCYL project JCYL-SA343-U14 to MSM, and by a Explora-Ciencia grant PSI2013-49348-EXPLORA.

ORIGINAL PUBLICATIONS

This thesis is based on the following publications:

Peer reviewed published article:

Nieto-Diego J and Malmierca MS (2016). Topographic Distribution of Stimulus-Specific Adaptation across Auditory Cortical Fields in the Anesthetized Rat. PLoS Biology 14:e1002397.

Article under review:

Nieto-Diego J, Parras GG, Carbajal GV, Valdés C, Escera C and Malmierca MS (2017). Hierarchical Prediction Error in Neuronal Responses along the Auditory Neuraxis. *Under review in Nat Commun*.

ABBREVIATIONS

A1, primary auditory cortex

AAF, anterior auditory field

ABR, auditory brainstem response

BCSC, baseline-corrected spike count

CAS, cascaded sequence

CF, characteristic frequency

CSI, common stimulus-specific adaptation index

DCIC, dorsal cortex of the inferior colliculus

DEV, deviant / measure of the response to deviant tones

DW, difference wave

EEG, electroencephalography

ERP, event-related potentials

FRA, frequency response area

fMRI, functional magnetic resonance imaging

IC, inferior colliculus

iMM, index of neuronal mismatch

iPE, index of prediction error

iRS, index of repetition suppression

LCIC, lateral cortex of the inferior colliculus

LFP, local field potentials

LLR, long latency responses

MAS, many-standards sequence

MEG, magnetoencephalography

MGB, medial geniculate body

MGD, medial geniculate body, dorsal division

MGM, medial geniculate body, medial division

MGV, medial geniculate body, ventral division

MLR, middle latency responses

MMN, mismatch negativity

MUA, multi-unit activity

Nd, negative deflection of the LFP

PAF, posterior auditory field

Pd, positive deflection of the LFP

PEP, prediction error potential

PSTH, peri-stimulus time histogram

RCIC, rostral cortex of the inferior colliculus

RP, repetition positivity

RS, repetition suppression

SDF, spike-density function

SFR, spontaneous firing rate

SI, stimulus-specific adaptation index

SRAF, suprarhinal auditory field

SSA, stimulus-specific adaptation

STD, standard / measure of the response to standard tones

VAF, ventral auditory field

TABLE OF CONTENTS

ABSTRACT

Neurons in primary auditory cortex, thalamus and midbrain show stimulus-specific adaptation (SSA), a reduction in response to repetitive stimuli that does not affect neuronal responses to deviant tones. This has been proposed as a neuronal correlate of the mismatch negativity (MMN), a special evoked potential in response to deviant tones. However, three important requirements remain to be demonstrated in order to support the SSA-MMN link: (1) MMN is generated mainly within higher-order auditory cortical areas, whereas cortical SSA has only been recorded in A1 of different species. (2) MMN is a mid-long latency response, peaking between 100-200 ms in humans, whereas SSA has only been observed in early responses of A1 neurons. And finally, (3) neuronal responses to oddball stimulation have not been tested for deviance detection–enhancement of responses to deviant events—in addition to SSA, which is an essential property of any *bona-fide* mismatch response. In this study, I set specific objectives to investigate the relation between SSA and MMN, and moreover, I will test the Hierarchical Predictive Coding account for the MMN at the neuronal level, showing that single neuron responses to oddball stimulation represent prediction error, which is hierarchically organized along the auditory system.

INTRODUCTION

This thesis is about how the sounds around us are represented in the brain. In particular, I study how the representation of a sound changes according to the context in which it is presented. And, yet more specifically, I will focus on how specific modulations (reduction or enhancement) of neuronal responsiveness to a sound may help to detect relevant sounds, while ignoring irrelevant ones. Thus, I start this account introducing the general properties and functional significance of rapid sensory adaptation for efficient coding. I continue with an overall description of the mammalian auditory system, highlighting its hierarchical organization. Then, I will introduce the main subject of the present thesis: *the representation of novelty in the auditory system*. Adaptation and deviance detection will be shown to be tightly related and complement each other to detect relevant sounds in the environment. I will expose the main discoveries and controversies that have dominated the relationship between the two in the past decades. Last, I will introduce and discuss the principles that govern the "hierarchical predictive coding" framework of brain function, which will appear as a unifying principle capable of reconcile and shed new light into this conundrum.

NEURONAL ADAPTATION AND SENSORY CODING

Ever since I learned that our perceptions about the world are direct consequences of the electrical activity of neurons within our brain, I wanted to know more about that. How was that sensory information represented in living, biological tissue? When I first learned that my Ph.D. research will be on neuronal adaptation, I thought "well, this is as good a starting point as any other in neurophysiology". I would learn how neurons respond to different stimuli, and then I would study how these responses vary when the stimulus is repeated. Thus, it was exciting as much as it concerned, indirectly, the study of how neurons encode and transmit information about external events. I could not imagine, however, that adaptation would be, precisely, the central principle of how neurons encode, transmit and process information along sensory systems.

To adapt or to die: Phenomenology of neuronal adaptation

Adaptation can be defined as a transient change in function that takes time to develop, and time to dissipate (Whitmire and Stanley, 2016). This is an essential feature of all life, spanning over timescales from evolution down to rapid interactions, and involving a plethora of diverse biological mechanisms, from molecules to cell and animal behavior. But with a common result: the ability of organisms to change their behavior in response to changes in the environment. In particular, nervous systems have evolved essentially to detect and react to changes in their environment. Thus, for the nervous system, adaptation is not only ubiquitous, but one of its fundamental principles of organization and function. In principle, adaptation can refer to any form of change that leads to an improvement in function, but in sensory physiology the term "adaptation" usually refers to a decrease in neuronal response over short time periods (milliseconds to a few minutes), whereas the term "facilitation" is reserved for the opposite effect. However, rather than a single behavior, "adaptation" has ended up describing a range of

phenomena with distinct underlying mechanisms and diverse effects on neuronal responses and information encoding (Maravall, 2013). Figure 1 illustrates different forms of neuronal adaptation, as revealed by different stimulus configurations.

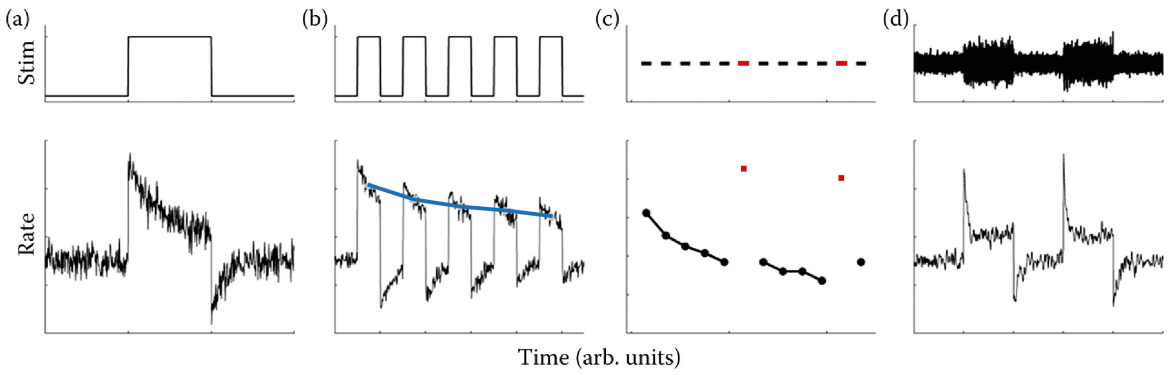

Figure 1. Different forms of adaptive behavior in neuronal firing. (a) Perstimulatory adaptation, or gradual decrease in firing rate along a continuous stimulus presentation, can be observed in the auditory system from auditory nerve fibers up to cortex (Pérez-González and Malmierca, 2014; Eggermont, 2015). (b) Neuronal habituation, or decline in average response to each one of a series of repetitive stimuli, is a form of neuronal habituation to the stimulus (Condon and Weinberger, 1991). (c) Stimulus-specific adaptation, a special form of repetition suppression that leaves responses to other, different stimuli unaffected, can be interpreted as a form of change detection (Movshon and Lennie, 1979; Ulanovsky et al., 2003). (d) Adaptation to stimulus variance, a more complex form of adaptation observed to changes in the statistical distribution of some parameter of a random stimulus, such as the variance of a Gaussian white noise (Fairhall et al., 2001). Adapted from Maravall (2013).

Despite its many different expressions, most forms of neuronal adaptation gravitate around the idea of adaptation to stimulus statistics. The response properties of a neuron are changed according to the local distribution of inputs present in the current environment. To understand why adaptation is so inextricably linked to sensory coding, and how the neuron can achieve this adaptive behavior, we must draw attention to some more basic aspects of sensory physiology. The main function of sensory neurons is to represent the state of the external world into a common code of electrical signals that can be further processed and used in the brain to generate adaptive behavior. The basic principles of sensory coding, which now we take for granted, were established almost 100 years ago back in early 20th century (Adrian and Zotterman, 1926; Rieke, 1999; Maravall, 2013):

1. Neurons transmit information through discrete, all-or-none (*i.e.*, digital) action potential signals. In sensory systems, this information relates to the current state of relevant aspects of the environment, and its specific nature is determined by the position of each particular neuron in the topology of connections within the brain.
2. There is a quantitative relationship between the magnitude of the neuronal response and specific stimulus parameters, such as frequency or intensity. These relationships emerge more clearly when the combined, simultaneous activity of many neurons is taken into account.

3. The rules that link stimulus variables and neuronal response magnitude vary over time, depending not only on the current stimulus parameters, but also on the *context* and on the *history of stimulation*. Neurons adjust their codes according to changes in the environment. In other words, neurons *adapt*.

This latter property (adjust the coding strategy according to local context) is critical for an efficient neuronal function, since the optimal coding strategy for a neuron at any point in time depends on the locally prevailing stimulus statistics. Furthermore, this adjustment of neuronal coding properties reveals that sensory systems are capable of tracking changes in recent stimulus history over many temporal scales, from tens of milliseconds to minutes (Fairhall et al., 2001; Ulanovsky et al., 2004; Ayala and Malmierca, 2013; Robinson et al., 2016) [1].

The function of a prototypical neuron is well summarized in the simple linear-nonlinear-Poisson (LNP) model (Figure 2), which is a simplified mathematical description of the input-output transformation performed by the neuron (Simoncelli et al., 2004; Schwartz et al., 2006). The LNP model of neuronal firing splits neuronal function into two complementary aspects of neuronal responses to different stimuli: (1) selectivity (L filter), or preference of the neuron for certain range of stimulus parameters—or forms of energy—, and (2) sensitivity (N function), or absolute firing rate of the neuron in response to increasing amounts of synaptic input—intensity of energy. As stated above, this input-output mapping of the neuron can be changed through adaptation. Depending on which step (L or N) is affected, two major types of adaptation can result:

(a) **Dynamic range adaptation** is the rapid adjustment in sensitivity of the input-output (N) function according to the distribution of synaptic input values, p(s), being received by the neuron (Figure 3). Typically, the N function of the neuron shifts and scales so that its operation point (point of maximum slope) coincides with the mean of the p(s) distribution, and its dynamic range matches the variance of the p(s) distribution (Figure 3). This is generally considered a gain control mechanism (Maravall et al., 2007; Wark et al., 2007; Robinson and McAlpine, 2009), often referred to as adaptive gain rescaling. This form of adaptation has been demonstrated at multiple stages of processing across different sensory modalities (Fairhall et al., 2001; Dean et al., 2005; Maravall et al., 2013), and its functional relevance will be explained in the next section.

(b) **Receptive field adaptation** is the rapid adjustment in selectivity of the L filter according to the probability distribution of stimulus feature values in the current stream of stimulation. This is a form of rapid receptive field plasticity (Froemke et al., 2007), that can take different forms (Figure 4)—often with opposite effects—such as general decrease in selectivity around the adaptor stimulus (Dhruv and Carandini, 2014), small shifts in neuronal selectivity, both repulsive—away from the adaptor—(Dragoi et al., 2000; Dhruv and Carandini, 2014), and attractive (Kohn and Movshon, 2004), or sharpening of tuning around the adaptor (Kohn and Movshon, 2004). How tuning is altered depends on the

[1] This is a fundamental property of adaptation processes, indicative of an exquisite sensitivity to higher-order stimulus statistics—beyond mere global probability—orchestrated by a multiplicity of underlying mechanisms, from ion channel dynamics to complex network dynamics (Wark et al., 2007; Maravall, 2013). However, I will not deal with this aspect of adaptation in this thesis, and just mention it here for the sake of completeness.

brain region and stimulation paradigm used (Kohn, 2007). Usually, the neuron becomes less selective to the most common stimulus feature values, and retains, or even enhances[2], selectivity to the less common ones (Dragoi et al., 2000; Kohn, 2007; Maravall, 2013). This behavior amounts to a form of change or novelty detection, in which a stimulus evokes a larger response when it is unpredictable (Ulanovsky et al., 2003). Thus, it is not surprising that this form of adaptation has been linked to higher-level inference processes in the brain, as reflecting the ability of sensory neurons to encode not only the physical features of the stimulus, but also its relevance and degree of match/mismatch within the ongoing context. Like the previous one, this form of adaptation has been described at different stages of processing within all sensory systems that have been investigated (Kohn and Movshon, 2003, 2004; Ulanovsky et al., 2003; Reches and Gutfreund, 2008; Malmierca et al., 2009; Antunes et al., 2010; Duque et al., 2012; Ayala et al., 2013; Dhruv and Carandini, 2014; Musall et al., 2015; Nieto-Diego and Malmierca, 2016).

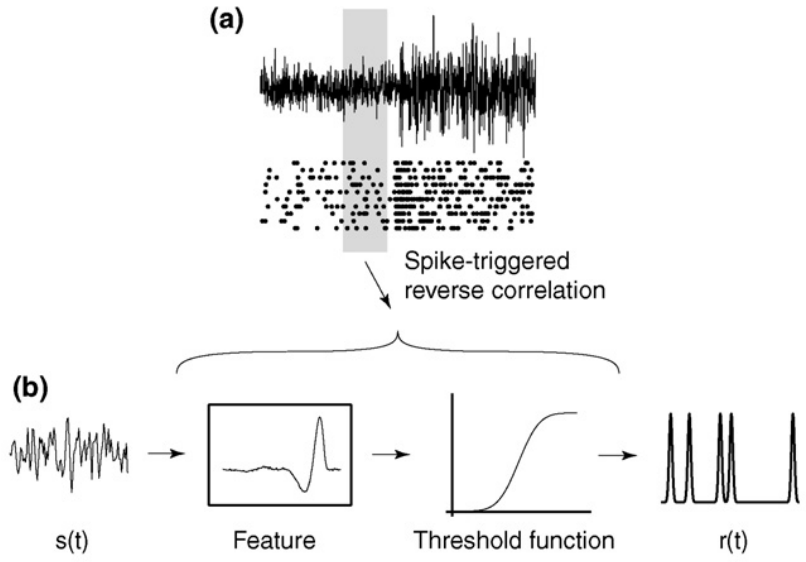

Figure 2. LNP model of neuronal firing. The LNP model summarizes the input-output transformation of a neuron in three steps: (1) Linear filter (L), that determines the total synaptic input to the cell according to its feature selectivity, (2) Nonlinear response function (N), that transforms synaptic input (in, membrane potential) into probability of firing a spike (fr = nl(in)), and (3) Poisson process (P), that generates random spikes according to a random Poisson distribution of mean firing rate. The parameters of the first two steps (L and N) can be estimated by presenting many different stimuli and determining the firing rate of the neuron in response to them. This can be done in a direct way (averaging many presentations of the same stimulus), but it is becoming more and more common to perform a "spike-triggered averaging" process, to determine the "canonical" stimulus that best drives the neuron. From Wark et al. (2007).

In this thesis, I will focus on the second type of adaptation—receptive field adaptation—, since it is the one potentially mechanism underlying change detection (Ulanovsky et al., 2003;

[2] This difference (retain or enhance selectivity) is more than a mere subtlety. It will be a central question of this thesis, and will be fully addressed in Study 2.

Maravall, 2013; Malmierca et al., 2014), and this work is centered on the neurophysiological mechanisms of mismatch detection in the auditory system. In particular, I will center on stimulus-specific adaptation (SSA), a form of receptive field adaptation as measured with the oddball paradigm, a simple form of stimulus probability distribution in which the stimulus takes one of two possible values, one with more probability than the other (Ulanovsky et al., 2003). Despite its apparent simplicity, this paradigm will reveal fundamental properties of sensory processing, and how information about the environment is represented in the brain.

Why to adapt? Functional roles of adaptation

From the previous section it should be clear that rapid sensory adaptation, in its many forms, is a pervasive property of all sensory systems that evolution has promoted many times independently in a wide range of organisms and processing stages of sensory systems. Therefore, it must certainly provide important advantages over "non-adapting" approaches. Many functional benefits of neuronal adaptation have been proposed, including, among others:

- ✓ Efficient use of the limited dynamic range of the neuron to represent a much wider range of stimulus intensities (Fairhall et al., 2001; Dean et al., 2005).
- ✓ Efficient use of channel information transmission capacity (Maravall et al., 2007; Wark et al., 2007).
- ✓ Gain control of neuronal firing rate (Robinson and McAlpine, 2009).
- ✓ Enhanced discriminability of small changes in stimulus intensity (Dean et al., 2005; Wark et al., 2007) or along a specific stimulus feature (Dragoi et al., 2002; Ulanovsky et al., 2004; Kohn, 2007; Musall et al., 2014).
- ✓ Redundancy reduction, through decorrelation of spikes in neuronal population activity (Müller et al., 1999; Benucci et al., 2013).
- ✓ Equalization of population firing rates, or "neuronal homeostasis" (Benucci et al., 2013).
- ✓ Basis for regularity encoding (Yaron et al., 2012; Malmierca et al., 2014).
- ✓ Sensory memory trace formation (Haenschel et al., 2005).
- ✓ Change detection and novelty detection (Ulanovsky et al., 2003; Musall et al., 2014).

However, the common principle behind the many functional benefits of adaptation was already identified by Horace Barlow more than 50 years ago: efficient coding (Barlow, 1961). Instead of following a rigid coding scheme to represent sensory events, neurons change their coding strategy as a function of time to exploit any non-random structure in the ongoing distribution of sensory inputs (i.e., regularities), to diminish redundancy in neuronal messages and maximize the information transmitted about the stimulus, with the minimum energy expenditure. But, how is this very demanding and ambitious goal achieved by the two main types of adaptation described in the previous section? This can be understood in the following way:

(a) Figure 3 illustrates the functional benefits of dynamic range adaptation. If the distribution of strength of synaptic inputs (reflecting stimulus intensity such as luminance of an image of loudness of a sound) changes as shown in the top panels (from the blue to the green distribution), the most efficient strategy of the neuron is to shift its input-output function

(N) to match the corresponding cumulative distribution (bottom panels). In this manner, the most common stimulus values in the local context are represented by the full dynamic range of the neuron. Extrapolating this strategy to the population code, dynamic range adaptation allows the nervous system to represent a range of stimulus intensities that usually spans over many orders of magnitude (e.g. sounds from 0 to 90 dB means from 20 μP to 20×10^9 μP, and a similar thing happens for luminance) with a much modest range of firing (typically 0-100 Hz). Moreover, the mapping between them (stimulus intensity and firing rate) will be optimal in that all firing rate levels will be used with similar probability (Figure 3).

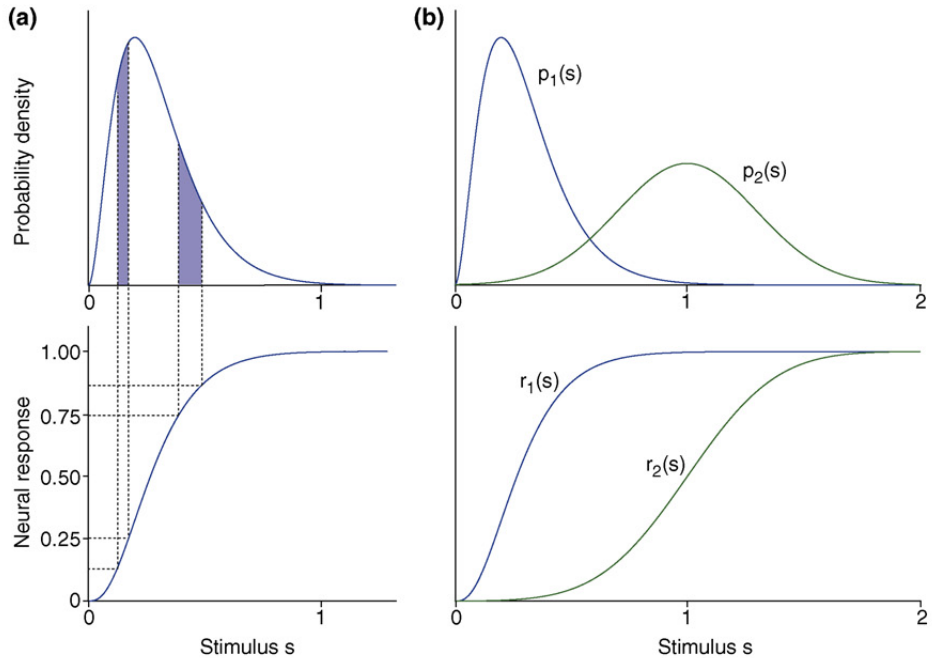

Figure 3. Dynamic range adaptation. (a) Given a stimulus energy distribution (top), the maximally efficient mapping from stimulus to response is the integral of the stimulus distribution (bottom) known as the cumulative distribution. This mapping transforms equal probability in the stimulus distribution (shaded areas) to equal response ranges, making all responses equally likely. **(b)** When the stimulus distribution changes, for example, from $p_1(s)$ to $p_2(s)$ (top), the maximally efficient mapping also changes. The new mapping, $r_2(s)$, is the cumulative distribution of $p_2(s)$. In this case, both the mean and the variance of the stimulus distribution change, leading to a shift in the half-maximum and a decrease in gain (slope) of $r_2(s)$, respectively. From Wark et al. (2007).

(b) On the other hand, the functional benefits of receptive field adaptation can be fully explained by basic principles of information theory (Shannon and Weaver, 1998). Sensory relays recode sensory messages so that their redundancy is reduced but comparatively little information is lost. If a stimulus becomes repetitive, or otherwise highly predictable, its informational content (or entropy) decays rapidly, and there is no point in wasting neuronal resources signaling its occurrence. To paraphrase Barlow's own words, "News is only news if it conveys really *new* information". The general effect of neuronal selectivity adaptation is

that the activity of the neuron represents not only a particular feature of the stimulus, but also the amount of information associated with the occurrence of that stimulus within the current context. Put simply, the most common and expected a stimulus is, the less information we obtain by knowing that it occurred. On the other hand, infrequent or otherwise unexpected sensory events contain a lot of information, and therefore they must be signaled by strong neuronal activity. Thus, in contrast to the situation for dynamic range adaptation (Figure 3), now stimuli in the center of the distribution (the most common stimulus values) elicit the weakest responses, whereas outliers (in any direction) will elicit the strongest responses (Garrido et al., 2013).

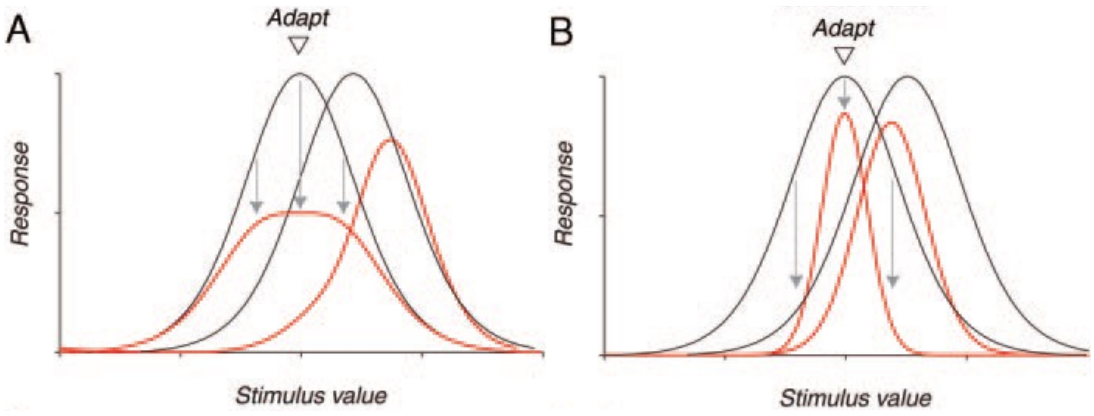

Figure 4. Different forms of receptive field adaptation. (A) Adaptation has been found to alter V1 neuronal tuning by reducing responses to stimuli similar to the adapter most strongly, as indicated by the longer downward arrows for the adapted value than for offset values. Flank adaptation causes a repulsive shift in tuning. Tuning before adaptation is shown in black; after adaptation, in red. (B) In MT, adaptation affects responses at the adapted value least, resulting in narrower tuning (center pair of tuning curves) and attractive shifts in preference (offset pair of tuning curves). C: tuning curve slope depends on the distribution of stimuli used to drive the cell. A high variance distribution (light gray histogram in the background) results in shallower tuning (dotted line); a low variance distribution (dark gray histogram) results in steeper tuning (solid line). Adapted from Kohn (2007).

In summary, adaptation operates on the neuronal code to optimize neuronal resources and maximize information transmission capacity. However, there are also some side effects of sensory adaptation, such as impaired detectability of a repetitive stimulus (Musall et al., 2014), perceptual distortions and after-effects (Clifford et al., 2000; Jin et al., 2005), or complication of population activity decoding schemes (Clifford et al., 2007; Seriès et al., 2009). But clearly, the benefits of adaptation overweight its potential disadvantages.

How to adapt? Underlying mechanisms and models

The gradual attenuation of neuronal responses after stimulus repetitions can be explained by many different theoretical models, including neuronal fatigue, sharpening of tuning and facilitative effects (Grill-Spector et al., 2006). However, only empirical studies can reveal the actual biological mechanisms behind each kind of neuronal adaptation. The many different

types of adaptation, its ubiquity in sensory processing and the ability of neuronal responses to adapt to stimulus statistics over many spatial and temporal scales, suggest the existence of a combination of different molecular, cellular and network mechanisms. These different systems must be operating in parallel at many levels and with different time scales (Maravall, 2013; Malmierca et al., 2014).

As already pointed out, both components of the LNP model can be affected by adaptation, and each one would lead to different outcomes (Clifford et al., 2007; Maravall et al., 2007). Thus, it is reasonable to think of cellular mechanisms whose net effect is to decrease the firing rate of the cell, by acting on either neuronal sensitivity (N function) or selectivity (L filter), or both. This view provides us with the following categorization of mechanisms:

(a) **Intrinsic neuronal mechanisms.** Rapid changes in cellular dynamics, particularly passive (ion conductance) and active (firing threshold) membrane properties can easily explain changes in neuronal sensibility, that would translate into non-specific decrement of neuronal activity (fatigue-like effects) and also most forms of dynamic range adaptation. Indeed, intrinsic membrane properties have been shown to contribute to adaptive changes of coding in the sensorymotor cortex (Schwindt et al., 1988), barrel cortex (Díaz-Quesada and Maravall, 2008), visual cortex (Carandini and Ferster, 1997; Sanchez-Vives et al., 2000) and auditory cortex (Abolafia et al., 2011), but calcium-dependent changes in gain participate in contrast adaptation as early as in the retina (Kim and Rieke, 2001). In general, sodium- and calcium-dependent potassium currents are the most likely mechanism behind firing rate adaptation—reviewed in Malmierca et al. (2014). Importantly, supporting its central role in neuronal adaptation, the intrinsic response dynamics of single neurons display multiple timescales (La Camera et al., 2006), a central feature of sensory adaptation as discussed in the first section.

(b) **Synaptic mechanisms.** Intrinsic membrane mechanisms are well understood, but they cannot solely explain stimulus- or input-specific effects underlying receptive field adaptation (Nelken, 2014; Malmierca et al., 2015). A suitable mechanism would be activity-dependent depression of thalamocortical synapses, as shown for the auditory (Wehr and Zador, 2005) and somatosensory (Chung et al., 2002) cortex, that could easily underlie stimulus-specific adaptation in narrow frequency channels (Taaseh et al., 2011; Khouri and Nelken, 2015). Other synaptic mechanisms include lateral inhibition (Qin and Sato, 2004), increased inhibition (Zhang et al., 2003) or excitatory/inhibitory imbalance (Oswald et al., 2006). Interestingly, intrinsic and synaptic mechanisms may interact synergistically to provide computational capabilities of change and novelty detection (Puccini et al., 2007).

(c) **Network mechanisms.** It is highly unlikely that one single neuron, by itself, is able to recognize and habituate to complex background regularities in the environment. Simple network mechanisms, such as disynaptic feedforward inhibition (Wehr and Zador, 2003; Isaacson and Scanziani, 2011), can largely underlie adaptation effects. Because the excitatory and inhibitory inputs interact in a complex manner, adaptation of these two components will have profound effects on the feature selectivity and timing of responses (Whitmire and Stanley, 2016), and a tight balance between excitation and inhibition may lie at the foundation of efficient coding (Denève and Machens, 2016). Moreover, complex interactions between excitatory and inhibitory circuit components can not only shape the

effects of adaptation on neuronal tuning, but even explain selective response enhancements through input-specific disinhibition (Solomon and Kohn, 2014). Finally, it has been shown through computational modeling that differential adaptation of populations of presynaptic neurons (even through intrinsic mechanisms) can lead to stimulus-specific effects in brain activity (Jääskeläinen et al., 2004; Grill-Spector et al., 2006; Whitmire and Stanley, 2016) or even to changes in neuronal tuning (Jin et al., 2005; Solomon and Kohn, 2014).

It is important to mention here the important role that neuromodulation (Edeline, 2012) and top-down signals (Malmierca et al., 2015) may have in shaping neuronal activity at different stages of processing. However, the only chemical modulator that has been shown to mediate input-specific adaptation effects is the cholinergic system (Ayala and Malmierca, 2015), consistent with its known role in short-term receptive field plasticity (Froemke, 2015). Some neurotransmitter systems, such as ionotropic GABA(A) receptors, modulate the strength of adaptation in an unspecific gain control manner (Pérez-González et al., 2012; Duque et al., 2014). But, other hitherto untested neuromodulators, such as dopamine or serotonin, may also play a role in adaptation.

Of course, it is likely the combination of intrinsic, synaptic and network mechanisms what allows the complex adaptive behavior found in neuronal responses. For example, the ultimate network model for repetition effects is the proposed cortical microcircuit for predictive coding (Bastos et al., 2012). Furthermore, as will be highlighted later, adaptation might represent not only an effort to save energy and resources; even more important, it could be the signature of the inferential activity of the brain, underlying a more general principle of sensory physiology.

THE HIERARCHICAL ORGANIZATION OF THE AUDITORY SYSTEM

To hear may seem a simple task, at first glance. However, the auditory system faces one of the most challenging missions of all nervous system: auditory scene analysis (Bregman, 1990); and performs it with outstanding success, as Bregman exposed very convincingly[3]. Maybe for this reason, the mammalian auditory system shows a level of anatomical complexity that far exceeds that of other sensory systems such as the visual or somatosensory. Whereas there is only one relay between the retina and the primary visual cortex (the lateral geniculate nucleus of the thalamus), or two relays between the skin mechanoreceptors and the primary sensory cortex (cuneate nucleus and ventral posterior thalamus), in the auditory system we find five relay stations between the cochlea and primary auditory cortex (cochlear nuclear complex, lateral superior olive, nuclei of the lateral lemniscus, inferior colliculus, and medial geniculate body of the thalamus), with a high degree of parallel processing as well as different degrees of convergence and divergence. By the moment that a signal reaches the auditory cortex, it resembles very little the initial pressure signal that hit the eardrums in the first place. This may be one of the reasons why the cortical representation of sounds is so mysterious and poorly

[3] Imagine you are on the edge of a lake and a friend challenges you to play a game. Your friend digs two narrow channels up from the side of the lake. Halfway up each one, your friend stretches a handkerchief and fastens it to the sides of the channel. You are allowed to look only at the handkerchiefs, and from their motions to answer a series of questions: How many boats are there on the lake, and where are they? Which is the biggest one? Which one is closest? Is the wind blowing? Has any large object been dropped suddenly into the lake?

understood, in comparison with vision and touch. One main aim of this study is to shed some light into the nature of these representations.

Next, I will provide a brief description of the mammalian auditory system, with a specific focus on the rat distinctive features. For the greatest detail, see Malmierca (2003, 2015). The emphasis of this description will be on highlighting the hierarchical organization of the auditory system, especially from midbrain to cortex. A central theme in this respect will be the distinction between lemniscal, or first-order, and non-lemniscal, or higher-order, divisions within each anatomical level, including midbrain, thalamus and cortex.

Serial processing of sound along the pathway

The sound in the form of air pressure waves is transformed into mechanical waves in the middle ear, and in turn to liquid (endolymph) waves inside the cochlea. Up to that point, the oscillatory, wave-like nature of sound is still preserved with great fidelity. However, inside the cochlea, the basilar membrane (10-12 mm long in the rat, tightly coiled) acts as a hydromechanical frequency analyzer, and the inner hair cells (1000-1300 in the rat, arranged in a single row) act as mechanoelectrical transducers, producing a pattern of activity in the auditory nerve that bears little resemblance with the original sound wave. The auditory nerve is a bunch of up to 20.000 axons in the rat that convey information more similar to a multichannel digital sound system. The intensity (or energy) contained in the original wave has been separated into multiple frequency channels, and represented by the average firing rate of the corresponding bunch of fibers in the auditory nerve (Figure 5a). Thus, the activity of the auditory nerve contains a spectrogram of the original sound (Figure 5b), and that is the form of a sound that the brain is able to understand. In addition to operate as a frequency spectral analyzer, the cochlea is also a selective (dynamic) amplifier, thanks to the motility of its three rows of outer hair cells. These cells receive inputs from the brain that can control the sensitivity and selectivity of the cochlear filters. Therefore, the adaptive changes of selectivity and sensitivity mentioned in the previous section are present already at the transducer organ of the auditory system. Thus, the tonotopic code (different sound frequencies represented by the location of neurons along one spatial dimension) is generated in the cochlea—low frequencies in the apex, high frequencies at the base—and will remain the central principle of organization along the pathway, up to primary auditory cortex. This is essentially similar between all species of mammals, and the major difference is the range of frequencies to which the ear responds. In rats, the frequency range is from 0.25 to 70 kHz, but the optimal range is between 8 and 32 kHz.

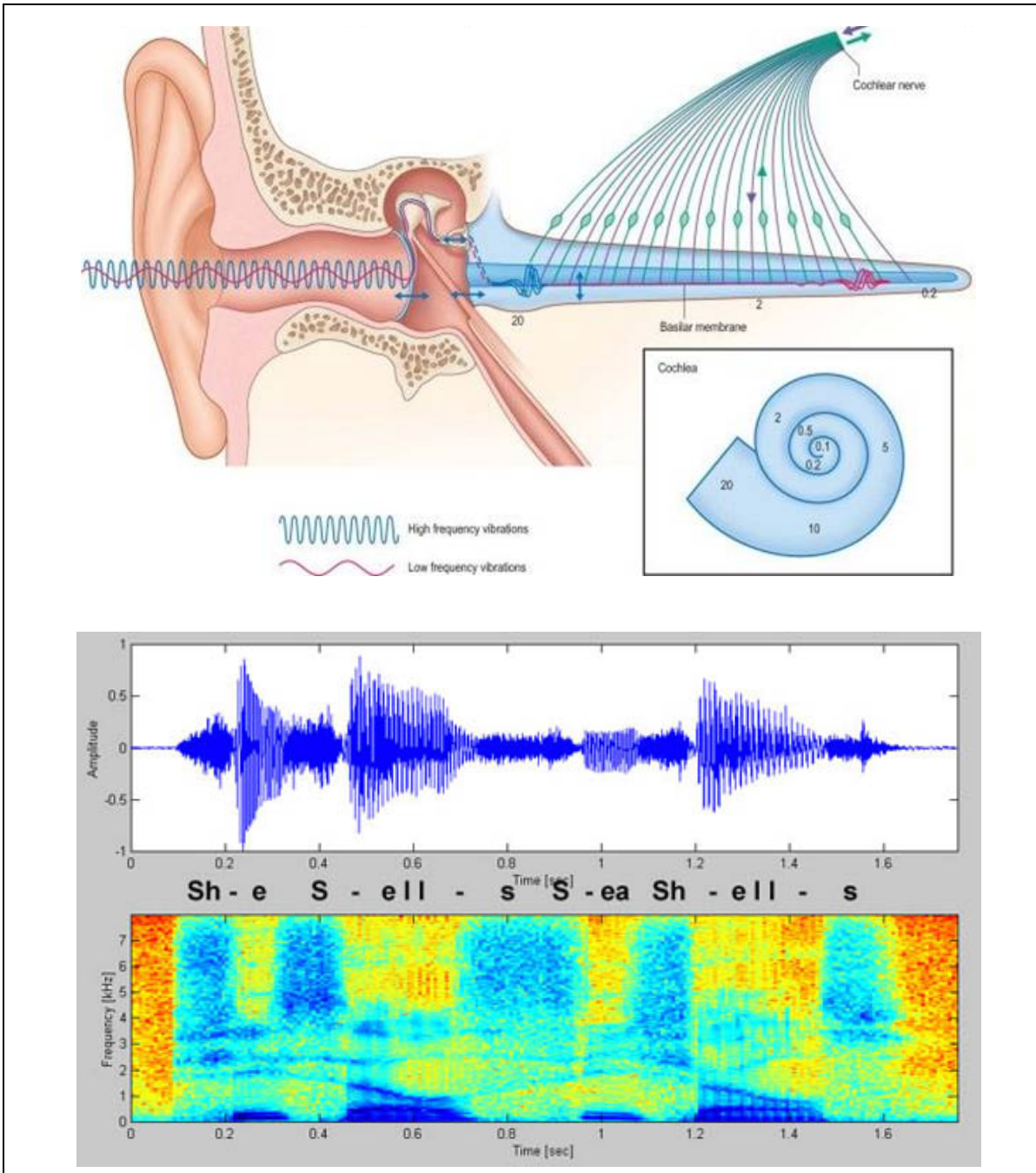

Figure 5. Transduction of sound. (a). The basilar membrane performs a spectral analysis of sound pressure waves entering the ear, inducing a tonotopic pattern of electic activity in the fibers of the auditory nerve. Source: https://i.stack.imgur.com/TNUxK.jpg. (b) The pattern of activity that enters the brain is roughly equivalent to a spectrogram of the original sound wave. Source: https://qph.ec.quoracdn.net/main-qimg-5ea3c55f647865a852b5f5cde6688cff-p

The auditory nerve bifurcates in a tonotopical pattern as soon as it enters the cochlear nuclear complex (CNC), the first relay of the central auditory system. The CNC is by itself a masterpiece of engineering that dwarfs the most sophisticated digital signal processor built by humans. Here, the transduced signal reaches many different and well-characterized neuronal types. Each one of them will process a separate aspect of the signal, and relay it to the next processing stage in the chain (Figure 6). Thus, the CNC is the origin of many processing parallel streams dedicated to different aspects of sound: position in space, spectral (frequency)

composition, loudness, spectral patterns, temporal patterns, etc. (Popper and Fay, 1992). These functions are carried out by the superior olivary complex and the nuclei of the lateral lemniscus (Figure 6), most of them using combined information from both ears, before all signals converge in the inferior colliculi (IC) of the midbrain.

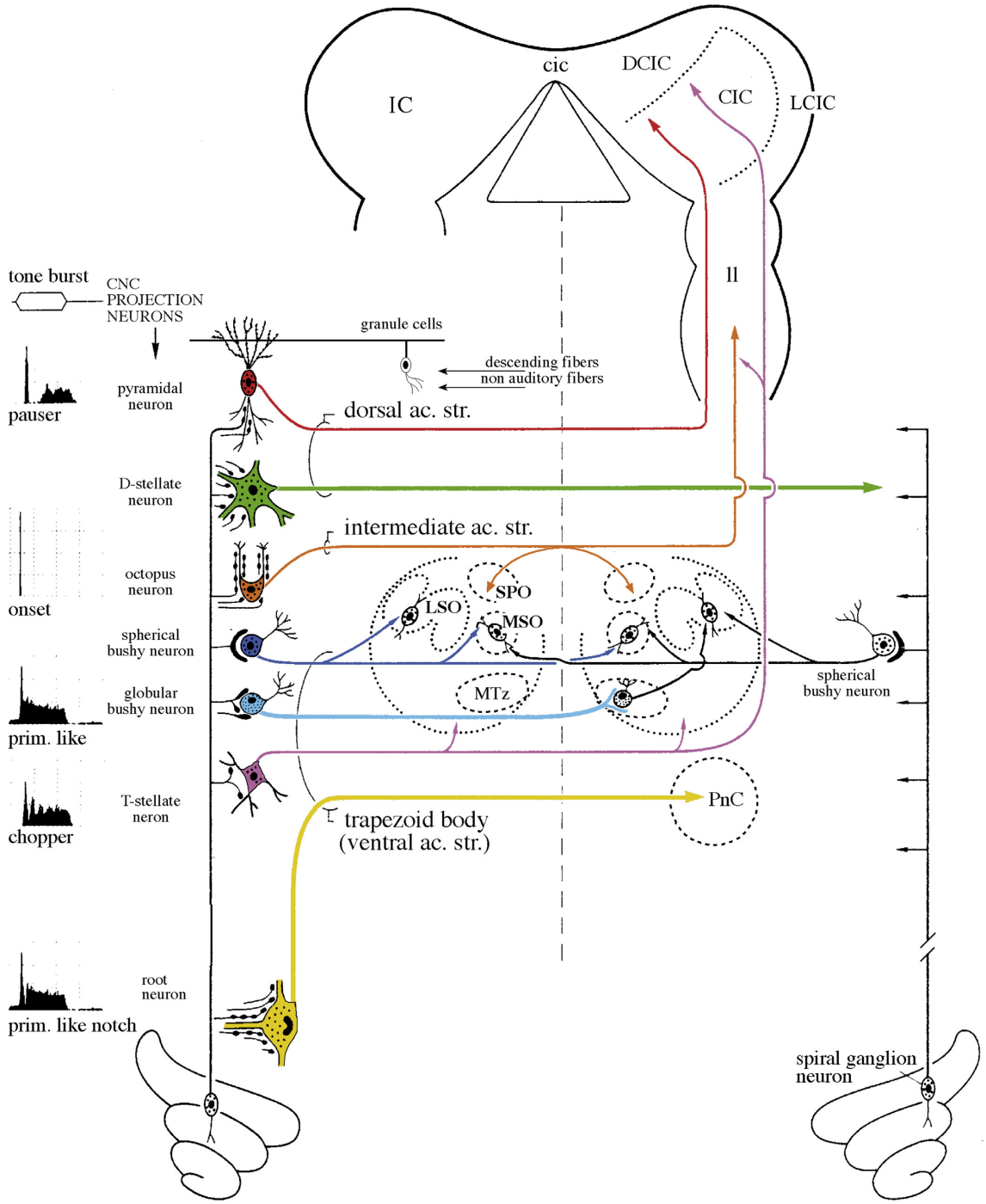

Figure 6. Schematic diagram of the ascending auditory pathway up to midbrain. Main projecting cell types of the CNC in rat are shown, with their corresponding physiological response profiles. From Malmierca (2015).

The IC is an obligatory relay center for most ascending auditory tracts. Each IC receives ascending input from both ears, but mostly from the contralateral side. The rat IC has an ellipsoid shape, with diameters of 3.5 and 2 mm, slightly tilted towards the caudomedial direction. In terms of size, the rat IC is the largest auditory structure, with around half a million neurons, including glutamatergic, glycinergic and GABAergic neurons. This points to a central role in complex sound processing, comparable to the role of V1 in the visual system (King and Nelken, 2009). Furthermore, the IC is the anatomical level where the distinction between lemniscal and non-lemniscal pathways first emerges[4]. The IC is organized in a central nucleus (CNIC), or lemniscal relay, surrounded by cortical or "shell" areas, considered non-lemniscal. Ascending information from the brainstem arrives massively, and tonotopically, to the CNIC, defined by the presence of thin fibrodendritic laminae that constitute the structural basis for its tonotopic organization[5]. Thus, a whole lamina of complex neuronal tissue is dedicated to process a single, frequency-band, or narrow frequency channel. Correspondingly, neurons within these lamninae show narrow frequency selectivity (Table 1). About 25% of CNIC neurons are GABAergic, and the CNIC is under strong inhibitory influence by both GABA and glycine. The cortical areas surround the CNIC on the sides (rostral cortex, RCIC and lateral cortex, LCIC) and at the top (dorsal cortex, DCIC). Their layered circuitry resembles that of the neocortex, pointing to advanced pattern recognition capabilities. These regions receive input from the CNIC (Saldaña and Merchán, 1992; Malmierca et al., 1995), but they are multisensory integration centers that concentrate projections from heterogeneous sources and also massive influence from the auditory cortex (*v.i.*). This integrative, higher-order nature is reflected in the receptive field properties of its neuronal units (see Table 1) and in the absence of a clear tonotopic organization.

Information leaving the IC is funneled into the medial geniculate body (MGB), a smaller structure prominent in the posterodorsal surface of the rat thalamus. The MGB, like all other thalamic nuclei, is an obligatory relay station and the last opportunity for subcortical processing for every signal that enters the cortex. However, it is more than a simple relay station, or at least not a passive one. The thalamus is known to actively regulate the flow of information from periphery to cortex (Sherman, 2007), and between cortical areas (Llano and Sherman, 2008). Furthermore, thalamic neurons can dynamically change their firing mode, and thus modify the functional connectivity between distant cortical regions in real time (Guillery and Sherman, 2002). The MGB is unique in that it receives massive inhibitory influences from the IC (Winer et al., 1996), in addition to the excitatory projections, reflecting the important role of inhibition in shaping auditory spectrotemporal receptive fields. The CNIC projects to the ventral division (MGV), which relays the lemniscal information to primary auditory cortex in a strict tonotopic manner. The frequency representation in the MGV is also laminar—following a dorso-ventral gradient from low to high frequencies—and the physiological responses of single units correspond to the lemniscal pathway (Table 1). The MGV contains large, bi-tufted relay neurons that respond transiently to contralateral pure tone stimulation. Paralleling the

[4] This important organizational principle will be discussed in the next section.

[5] The representation of frequency in the CNIC is reflected in measurements of best frequencies along its major axis, revealing that best frequency increases with depth in a stepwise manner (Malmierca et al., 2008).

organization of the CNIC, these neurons have highly oriented dendritic arbors arranged in the direction of the afferent fibers, and constitute the basis for the laminar organization of the MGV. The non-lemniscal divisions of the MGB, the dorsal (MGD) and medial (MGM) divisions, are anatomically and functionally distinct from the MGV, and receive a projection from the cortical regions of the IC. They are reciprocally connected to non-primary auditory cortical areas, but receive also a driving input from primary auditory cortex. Accordingly, their physiology is more heterogeneous than in MGV (Table 1) and they do not present a clear tonotopic organization. The MGD contains tufted and stellate neurons, whose cell bodies and dendrites are not oriented in any particular fashion. The MGM is a narrow disc of tissue, with large, sparsely distributed cell bodies. The MGM contains a tonotopic map in its anterior sector, but much less ordered than in MGV. Non-lemniscal thalamic subdivisions subserve advanced, higher-order functions, corresponding to their position in the auditory hierarchy, reciprocally connected with the non-primary areas of the auditory cortex (*v.i.*).

Finally, the auditory cortex (AC) is the site of ascending projection from the MGB of the thalamus, localized bilaterally in the temporal lobes. The auditory cortex represents the highest level of processing within the auditory system. Basic spectral and temporal analysis has already been performed by subcortical circuits, and in fact animals do not need the auditory cortex for simple perceptual or audiomotor tasks such as frequency discrimination or sound localization (Kelly and Kavanagh, 1986; Gimenez et al., 2015). The auditory cortex deals with complex structure of sound: the formation and recognition of auditory objects (Nelken, 2004). In general, activity in auditory cortex is related to complex, or higher-order aspects of perception and behavior (Sutter and Shamma, 2011; Li et al., 2017), starting with the recognition of fine temporal modulations (Cooke et al., 2007). In addition, it is the site of highest neuronal plasticity for learning and memory about the objects that populate the complex structure of the auditory world (Weinberger, 2004).

The auditory cortex forms part of the mammalian neocortex, a highly modular structure resulting from the extensive repetition of a common pattern, suggesting a shared underlying computational principle (Mountcastle, 1997). In the horizontal dimension, the neocortex is organized in six layers (this number can vary between areas, but six is the most common for sensory cortices). The middle layers (layer IV, and also lower layer III in auditory cortex) are dense in cell bodies and present a granular aspect from which they take the name "granular layer/s"; these cells project only to the local tissue. Thus, layers I-III are called "supragranular", whereas layers V-VI are "infragranular"; both have pyramidal cells that project out of the cortex. In the vertical dimension, neurons are grouped in columns (about 500 microns in diameter), and neurons within the same column tend to show similar receptive field properties (Mountcastle, 1997). Finally, a third common principle of cortical organization is the functional division in areas, specialized in processing of different types of information (such as auditory, visual, association, objects, locations, etc).

In contrast to the subcortical regions, which are largely conserved in mammals, there are important species differences in the number of identified auditory cortical areas (from 5 in mice and rats to 10-12 in primates and around 30 in humans), their tonotopic organization, response properties or reciprocal connectivity. However, a common feature of all species investigated is

the presence of one or more primary auditory fields, surrounded by, and connected to, non-primary auditory fields, in turn connecting to higher-order multisensory association areas (Winer and Schreiner, 2011). In primates, these areas are called core, belt and parabelt. respectively. Primary or core cortex contains a dense granular layer that receives strong, direct input from the MGV, and contains one or more complete tonotopic representations of the audible frequency range of the animal. By contrast, belt areas lack a thick granular layer and receive their major ascending input from non-lemniscal divisions of the MGB (and from projection cells in supragranular layers of primary areas). Belt areas do not show a clear tonotopic organization, and in fact are usually more difficult to drive with pure tones (Table 1). The parabelt would comprise all auditory areas not directly connected to primary cortex, and its cellular physiology remains largely unexplored (Rauschecker and Romanski, 2011).

The rat auditory cortex also contains a "core" region made of the primary auditory cortex (A1) and two other primary fields: anterior auditory field (AAF) and ventral auditory fields (VAF). Additionally, the rat AC comprises at least two distinct non-primary fields in the "belt" regions, the posterior and the suprarhinal auditory fields (PAF and SRAF, respectively) (Doron et al., 2002; Kimura et al., 2003; Rutkowski et al., 2003; Donishi et al., 2006; Polley et al., 2007). These non-primary fields correspond to the dorsal and ventral secondary auditory cortex in the rat stereotactic atlas of Paxinos and Watson (2014). Unfortunately, there are no magic stains or molecular markers that cause one cortical region in the rat to stand out unambiguously from another. Also, the lack of gross anatomical landmarks (the rat is lissencephalic) complicates individual comparisons across animals. However, electrophysiological mapping studies have shown a robust organization of multiple response properties that follow a particular spatial organization (Polley et al., 2007; Higgins et al., 2010). That makes it feasible to locate the relative position of each field in a single animal through elecrophysiological mapping in vivo. The major reference to define the extension of these fields is the progression of their characteristic tonotopic gradients. The boundaries between them are defined by inversions or bifurcations of these gradients (Figure 7). They differ also in the distribution of other physiological characteristics, such as absolute response thresholds, spectral tuning bandwidth and response latency (Polley et al., 2007), but these are not as reliable cues as the frequency gradients. The rat A1 contains the typical six layers of granular cortex, which extend over about 1.1 to 1.2 mm (Figure 8). Ascending thalamic inputs from MGV to A1 terminate in layers III/IV, between 350 and 650 μm depth, and also at the junction of layers V and VI. Supragranular layers (I/II and upper III) extend only 350 μm below the pia surface, wheras infragranular layers (V and VI) occupy the deep half of the cortex, around 600 μm (Games and Winer, 1988; Polley et al., 2007; Smith et al., 2012). Granular layers are abundant in small stellate cells with smooth dendrites. Supragranular layers are dense in small pyramidal cells, with regular spiking firing profiles, that project locally and to higher-order cortical areas.

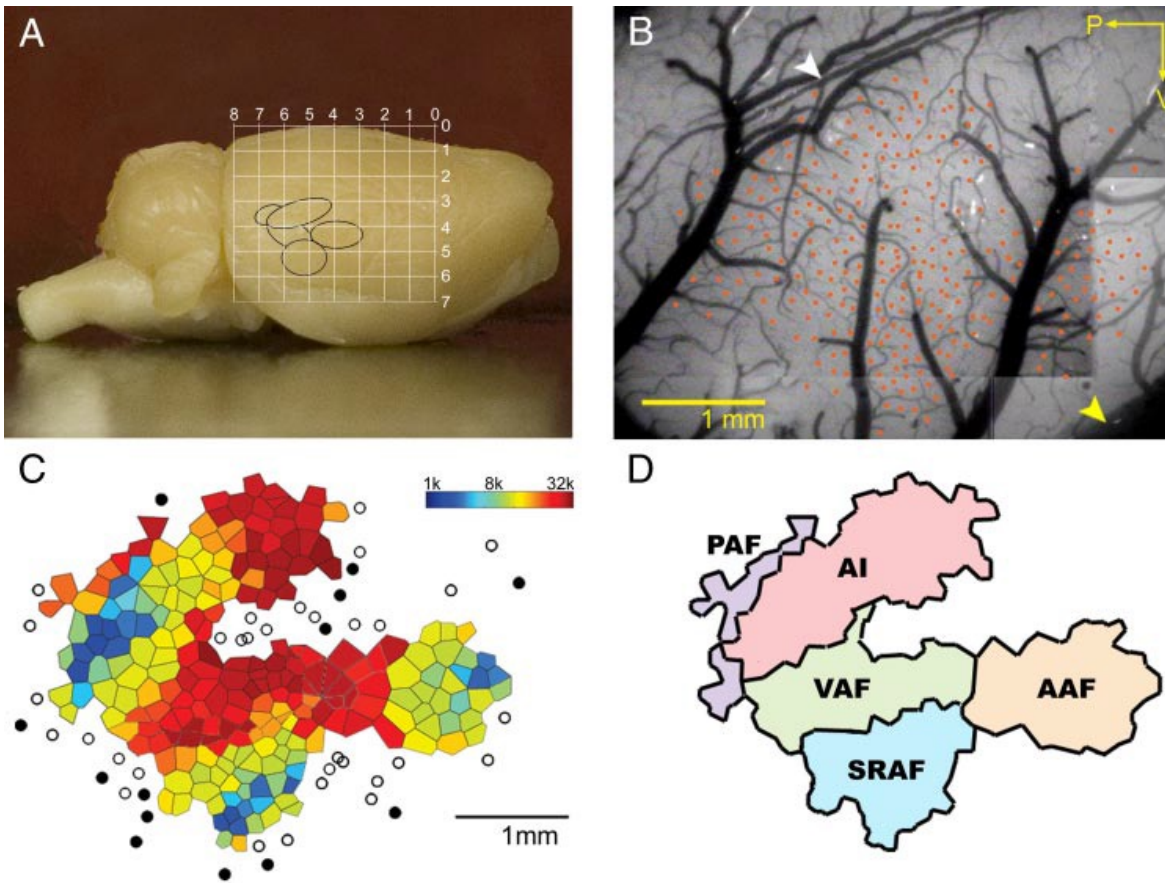

Figure 7. Physiological division of rat auditory cortex. A. The rat auditory cortex is easy to reach, completely exposed in the lateral aspect of the temporal lobe, between 3 and 7 mm posterior to bregma. **B.** The pattern of vasculature can be used to reference relative electrode positions, but otherwise varies significantly between subjects. **C.** A physiological mapping of the whole auditory cortex in one rat, showing the tonotopic gradients of characteristic frequency that define the boundaries between fields. **D.** The five different auditory cortical fields identified in the rat: A1, VAF and AAF are primary fields, whereas SRAF and PAF are considered higher-order, given their reciprocal connections with higher-order thalamic relays. From Polley et al. (2007).

Infragranular layers contain larger pyramidal cells with intrinsically bursting firing patterns (especially layer V, but layer VI also contains bitufted and multipolar neurons) that project to a variety of subcortical targets (*v.i.*). The columnar organization of auditory cortex is reflected anatomically by a system of intrinsic fibers perpendicular to the surface, spanning 200-800 um in width and made up of terminal axons that extend through all cortical layers. Functionally, it is reflected in the fact that neurons along the direction perpendicular to the pia surface tend to have the same frequency preference. But the modular organization of the auditory cortex goes beyond small columns. Different properties such as spectral bandwidth, intensity tuning or binaural interactions seem to be organized in patches or complex metagradients that, unlike the tonotopic gradients, extend beyond the limits between cortical fields (Polley et al., 2007). Like other cortical regions, all areas of auditory cortex are rich in a large variety of inhibitory (GABAergic) interneurons with many potential roles in controlling and synchronizing neuronal

activity (DeFelipe et al., 2013), but in the case of the auditory cortex, inhibitory influences may have an even more important role for shaping spectrotemporal receptive fields and encoding of temporal information (Schinkel-Bielefeld et al., 2012; Bendor, 2015). Unfortunately, there are no detailed studies on the morphology and distribution of inhibitory interneurons in the rat auditory cortex, but most probably all cell types except pyramidal neurons are GABAergic in the rat auditory cortex, as in other mammals (Malmierca, 2015).

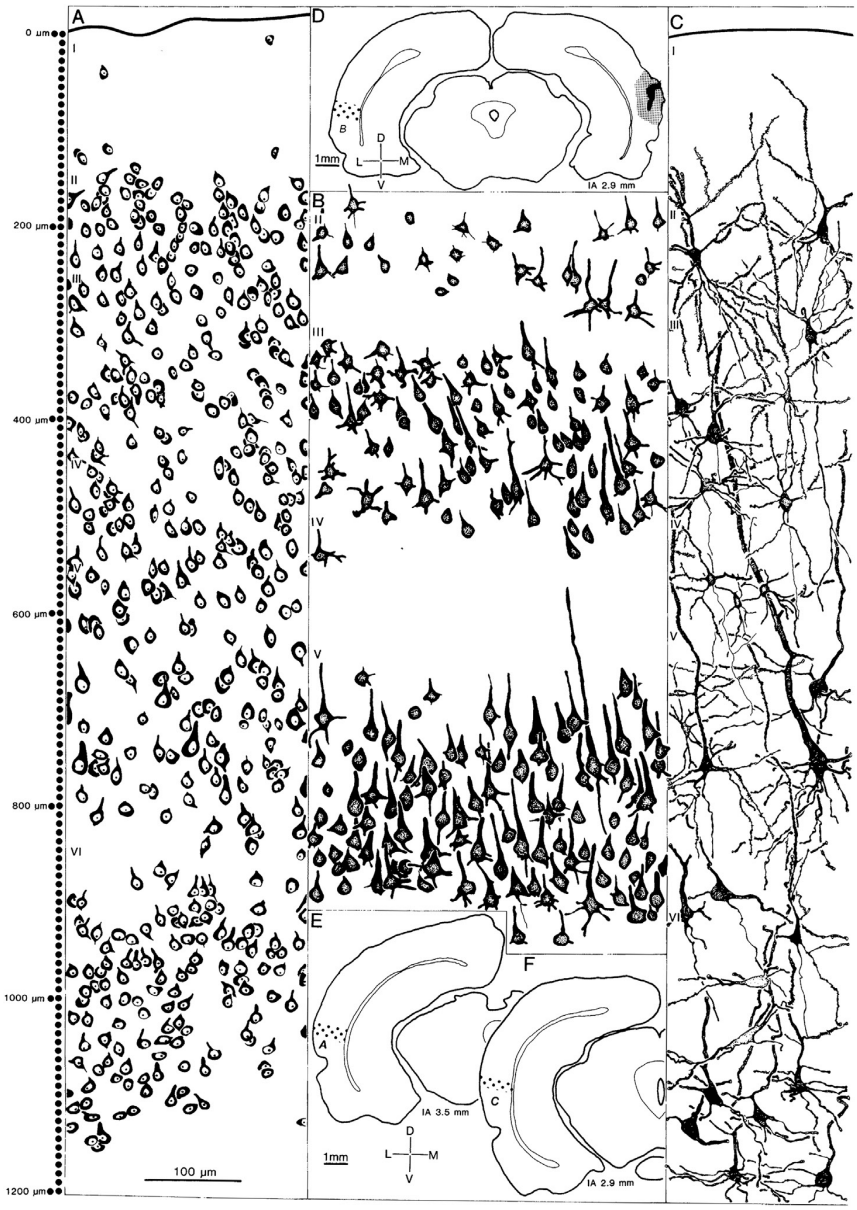

Figure 8. Cytoarchitecture of the rat primary auditory cortex. (A) Neuronal types and laminar boundaries in the primary auditory cortex (Te1, Au1) seen in Nissl stained sections. (B) HRP labeled cells after injections into the contralateral AC and ipsilateral IC. (C) Golgi impregnated material. Note different cell types, neuronal density and dendritic branching patterns in each of the six layers. (D-F) Insets showing from which panels B, A and C were drawn, respectively. From Games and Winer (1988).

Primary cortical fields A1, VAF and AAF are reciprocally topographic connected to lemniscal MGV, through strictly tonotopic ascending and descending projections. However, cortical fields are organized in isofrequency contours, whereas MGV follows a laminar tonotopy. Therefore, the topographic correspondence between primary thalamus and cortex is not trivial, and a whole isofrequency line of MGV neurons must converge into each cortical column (Imaizumi and Lee, 2014). More specifically, each isofrequency line of A1 receives input from the rostral half of a isofrequency lamina of MGV, whereas VAF receives from the caudal MGV (Storace et al., 2010). A1 projects to the secondary PAF and SRAF, and these in turn project to a variety of non-auditory areas and to the amygdala (see Table 1). Non-primary PAF is reciprocally connected with MGD and MGM, whereas SRAF is connected with the MGM (Kimura et al., 2003, 2005; Smith et al., 2012; Storace et al., 2012). The extensive corticofugal projections from auditory cortex will be discussed in a separate section.

Primary and non-primary representation of sound

The mammalian neocortex is hierarchically organized. This principle makes it such a versatile and computationally powerful structure, and is reflected also at the anatomical level, in the asymmetric pattern of reciprocal connections between functional areas (Felleman and Van Essen, 1991). Generally speaking, lower-level areas send "feedforward" projections from supragranular layers, terminating mainly in layer IV of the next area in the hierarchy. On the other hand, each area sends a "feedback" reciprocal projection from infragranular layers, terminating outside of layer IV (mainly in layers I and VI) of the hierarchically lower cortical area (Figure 9a). This organizational principle defines a hierarchical processing chain that can be followed with anatomical methods (Figure 9b). The only deviation of this homogeneity, both at anatomical and physiological levels, is the distinction between primary and non-primary (or higher-order) areas. Primary sensory areas have a thick granular layer, and are reciprocally connected with the corresponding specific thalamic relay (LGN, MGV, VPM… according to sensory modality). The descending projection from layer VI of a primary area does not go to a lower cortical area (since there is none), but back to the first-order thalamus (Shipp, 2007). Correspondingly, non-primary areas are reciprocally connected with higher-order (or unspecific) thalamic relays (Figure 11 and Figure 12). However, thalamocortical relations are asymmetric, and the main driving input to higher-order cortical areas comes from lower areas through and indirect, transthalamic route through higher-order thalamic relays (Llano and Sherman, 2008; Sherman and Guillery, 2011). Thus, the cerebral cortex does not function in isolation, but in intimate relation with the thalamus, and the thalamocortical system constitutes a functional unit. Whatever happens in a cortical area is reflected in its corresponding thalamic relay, and reciprocally, so that the hierarchical organization of cortical areas is also reflected in the thalamus. Of course, information represented in thalamus and cortex show important differences, and the thalamocortical transformation of information is well documented in all sensory systems (Maravall et al., 2013; Dhruv and Carandini, 2014), including auditory (Wang et al., 2008; Imaizumi and Lee, 2014; Eggermont, 2015). At any rate, the distinction between primary and non-primary regions is also a central aspect of thalamic anatomy and function, and every sensory sector of the thalamus is divided into specific, or first-order, and nonspecific, or higher-order, relays (Sherman and Guillery, 1996).

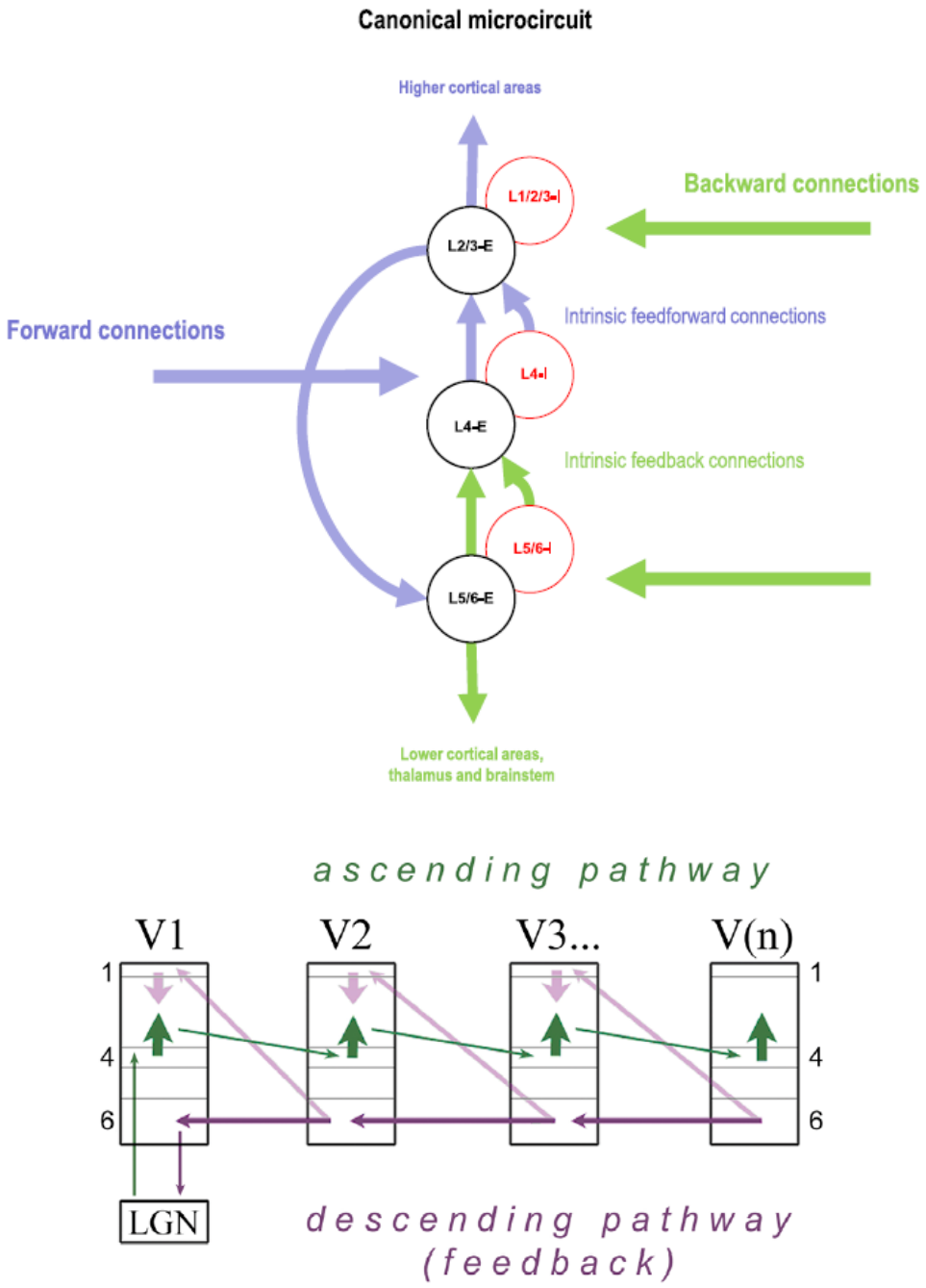

Figure 9. Canonical cortical circuits. (a) Every column of neocortex follows the same patterns of connectivity and information flow within the column. Afferent signals enter middle (granular) layers of cortex, which project locally; supragranular layers are reciprocally connected to hierarchically higher cortical areas; infragranular layers project to hierarchically lower cortical areas, as well as to subcortical targets. From (Bastos et al., 2012). **(b)** The cortical hierarchy is defined by the pattern of reciprocal, asymmetric connections between areas. Figure shows a schematic representation of the visual hierarchy, but the same principles hold for auditory, somatosensory and even motor systems. From Shipp (2007).

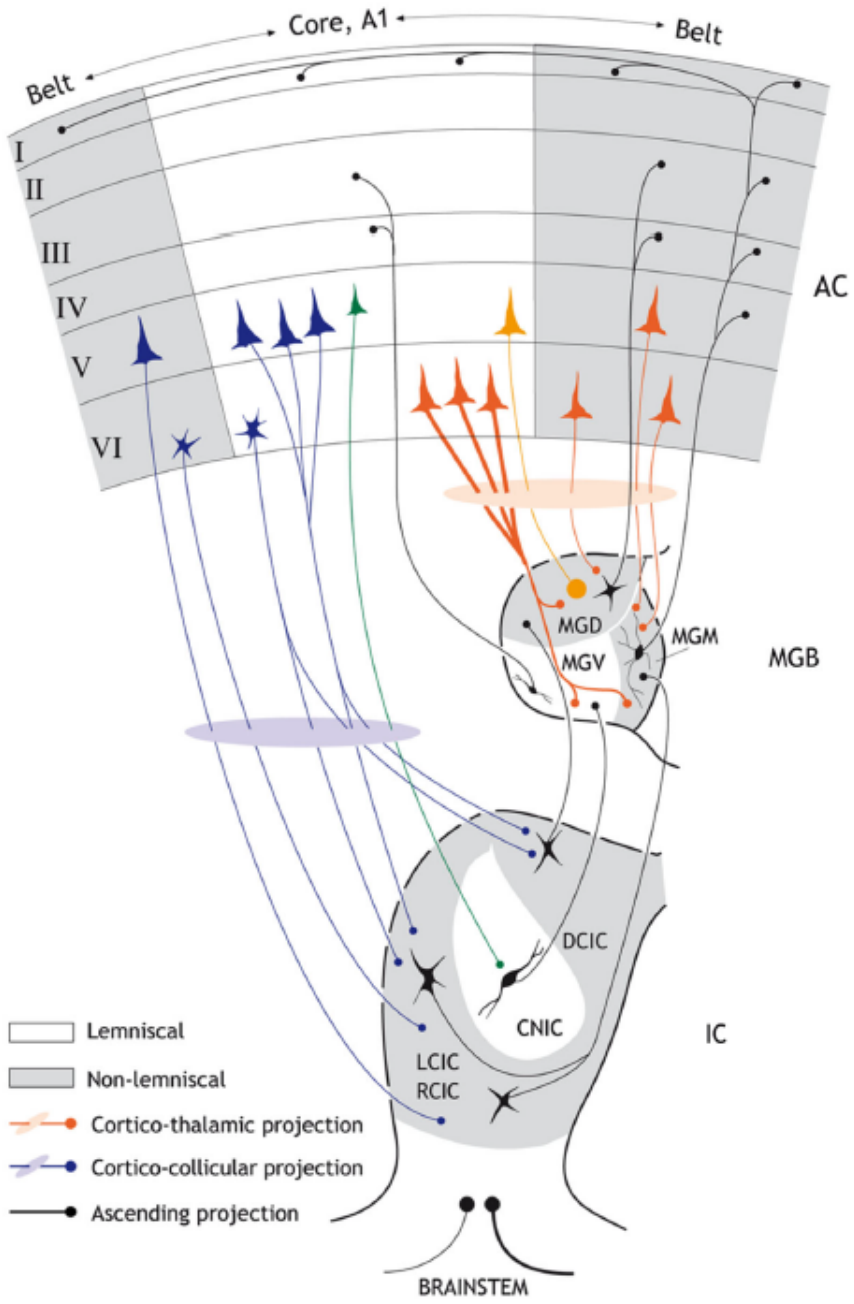

Figure 10. Auditory corticothalamic and corticocollicular projections. Non-lemniscal (or non-primary) divisions are highlighted as gray areas. Black lines indicate ascending projections. Red lines indicate major cortico-thalamic connections and purple lines major cortico-collicular projections. The major cortico-collicular projections emerge from pyramidal neurons in layer V. Larger pyramids project to cortical areas of the IC. By contrast, the major cortico-thalamic projection emerge from pyramidal neurons in layer VI, terminating in small boutons. A less dense projection from layer V pyramidal cells also terminate in large, driving-like terminals. From Malmierca et al. (2015).

These general principles of primary vs non-primary modes of sensory processing are particularly clear in the auditory system. Experimental evidence from molecular, cellular and

behavioural studies supports the notion that lemniscal and non-lemniscal pathways are involved in distinctive auditory functions. Lemniscal projections carry tonotopically organized and auditory specific information, whereas the non-lemniscal pathway forms part of an integrative system that plays an important role in polysensory integration, temporal pattern recognition, and certain forms of learning (Hu, 2003). Moreover, in the case of the auditory system, the distinction between primary (or first-order) and non-primary (or higher-order) divisions can be extended also to the IC, since it is divided into lemniscal CNIC and non-lemniscal cortical regions, with corresponding connections to primary MGV and higher-order MGD and MGM.

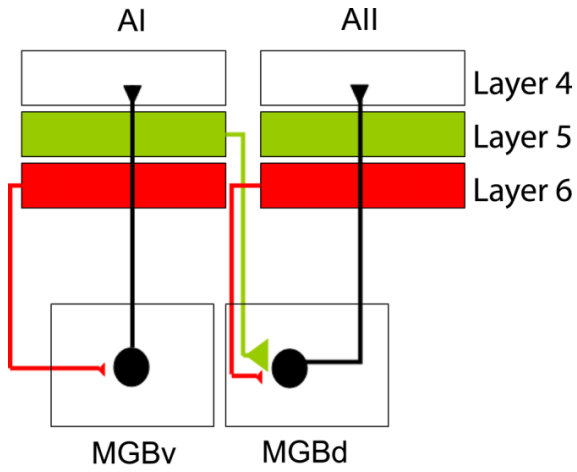

Figure 11. Corticothalamic relations. Primary and higher-order auditory cortical areas are reciprocally connected to first- and higher-order auditory thalamic relays, respectively. In addition, there is an indirect, transthalamic route from primary to higher-order areas, emerging from layer V in primary areas, through higher-order MGB, to layer IV in higher-order areas. From Llano and Sherman (2008).

At the level of the auditory cortex, primary and non-primary auditory cortical areas have been shown to subserve qualitatively different functions and represent different aspects of auditory stimuli (Carrasco and Lomber, 2010, 2011). Non-primary areas of cat auditory cortex are specialized for the spatial localization of acoustic stimuli or the recognition of auditory patterns (Lomber and Malhotra, 2008). Lesions of these areas are associated with impairment of the discrimination of temporal patters of sounds or of complex acoustical signals such as speech sounds that differ mostly in the pattern of their harmonics (Lomber and McMillan, 2011). In the MGB, lemniscal and non-lemniscal thalamic divisions show clear anatomic and physiological differences at the cellular level (Bartlett and Smith, 1999). Non-lemniscal thalamic divisions (MGD and MGM) are implicated in multisensory integration, processing of communication signals, auditory learning and emotional significance of sounds (Lee, 2015). The non-lemniscal nuclei of MGB send and receive feedforward and feedback projections among a wide constellation of midbrain, cortical, and limbic sites, which support potential conduits for auditory information flow to higher auditory cortical areas, mediators for transitioning among arousal states, and synchronizers of activity across expansive cortical territories (Figure 12). The differentiation between lemniscal/non-lemniscal pathways begins in the IC, and is reflected in the macro- and micro structural as well as physiological properties.

For example, the CNIC is tonotopically organized and receives mainly ascending input from the auditory periphery, whereas cortical regions are heterogeneous in cytoarchitecture, sources of inputs and physiological response characteristics (Table 1). Moreover, this correlates with the anatomical relations between IC and the rest of the pathway. Neurons in the CNIC are mainly under the influence of the lower centers, while neurons in cortical regions are mainly under the influence of the descending pathways. Overall, the dicotomy between lemniscal/primary/first-order regions and non-lemniscal/non-primary/higher-order[6] ones is a critical distinction along the auditory pathway from midbrain to cortex, and in fact, they could be considered two parallel, and to some degree, independent pathways within the auditory system (Lee and Sherman, 2011).

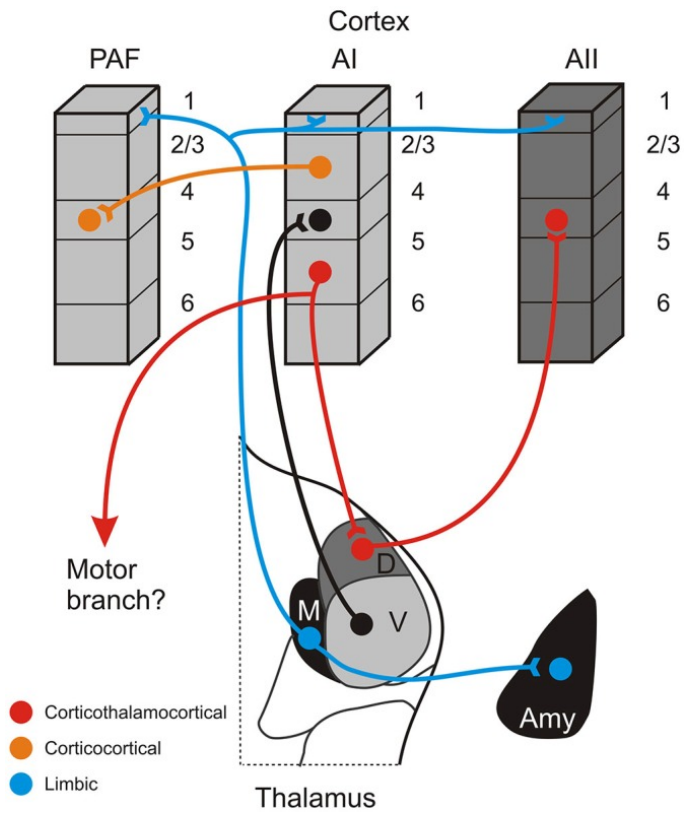

Figure 12. Schematic summary of some connections of the non-lemniscal auditory thalamus. The corticothalamocortical pathway links primary and higher-order cortical areas (in red). The same layer V projection neurons may also branch to innervate lower motor centers. This pathway is distinct from the direct corticocortical connections that link many auditory areas, such as A1 and PAF (in orange). A complementary system, putatively involved in affective processing of auditory information and synchronizing activity across cortical territories (in blue), has widespread terminations in layer I of multiple areas and the amygdala (Amy). From Lee (2015).

In summary, primary regions are the first to receive the ascending input from the periphery, and contain a representation of the physical features of sounds, at different dimensions and

[6] These terms will be used interchangeably throughout this manuscript.

levels of complexity. The lemniscal pathway is tonotopically organized, and spectral processing is carried out more or less independently in separate, narrow frequency channels. On the other hand, higher-order divisions (at all levels, IC, MGB, AC) are more dedicated to processing the sounds in relation to their context. In particular, their responses are more related to the meaning or behavioral relevance of sounds, rather than to their particular physical features, something that has been shown in animals (Atiani et al., 2014) and humans (Kropotov et al., 2000). These important physiological differences are also reflected anatomically, such as in the large, extensive dendritic arbors of neurons in cortical regions of the IC, that span across many different frequency channels. Table 1 summarizes the main differences between primary and non-primary structures in the rat auditory system, separate for IC, MGB and AC, both at the anatomical and physiological level. As will be discussed in the next section, and most relevant for our studies, a very important physiological difference between them is their relative degree of neuronal adaptation and their sensitivity to acoustic change (Kraus et al., 1994; Kropotov et al., 2000; Antunes et al., 2010; Duque et al., 2012; Nieto-Diego and Malmierca, 2016).

Table 1: The importance of being non-lemniscal. Comparative of anatomical and physiological differences between primary and non-primary divisions within each level of the auditory system from midbrain to cortex.

IC	
PRIMARY	NON-PRIMARY
ANATOMY	
• CNIC • Main ascending input from brainstem • Laminar organization • Confined dendritic arborizations	• RCIC, LCIC, DCIC • Receive inputs from heterogeneous sources • Higher influenced by corticofugal projections • Extense dendritic arborizations (especially LCIC)
PHYSIOLOGY	
• Strict tonotopic organization • Frequency processing in narrow, independent channels • Narrow, V-shaped receptive fields • Predominance of sustained responses, selective to different physical features of sounds • Very low levels of SSA	• No clear tonotopic organization • Multisensory integration • Broad receptive fields • High context-sensitivity (eg. SSA) • Predominance of onset responses signaling relevant events • Longer response latencies than in CNIC • Strong levels of SSA

MGB	
PRIMARY	NON-PRIMARY
ANATOMY	
• MGV • Main ascending input from ipsilateral CNIC • Fibrodendritic laminar structure • Large bi-tufted relay cells • Project to primary AC (layer IV)	• MGD, MGM • Ascending input from DCIC (MGD) and LCIC (MGD and MGM) • MGM receives from auditory, somatosensory and visual structures • Heterogeneous mixture of cells • Project to non-primary AC (layer IV) • MGM projects diffusely to all areas (layer I) • MGM projects directly to amygdala
PHYSIOLOGY	
• Strict tonotopic organization • Purely acoustic function • Neurons respond transiently and sensitively to pure tone stimulation • Short latencies and well-tuned to a best frequency • Narrower frequency selectivity than MGD and MGM • Low levels of SSA	• No clear tonotopic organization • Weaker responses to pure tone stimulation • Broad or complex receptive fields to pure tones (e.g. multipeaked) • Preference for complex, modulated stimuli • Longer response latencies (although MGM has units with very short latencies) • MGD involved in acoustic attention and discrimination of sound patterns (Bordi and LeDoux, 1994) • MGM involved in multisensory integration and emotional learning (fear conditioning) • Strong adaptation to repetition and SSA
AC	
PRIMARY	NON-PRIMARY
ANATOMY	
• A1, VAF, AAF in Te1 • Located in “core” in Te1 region • Thick granular layer • Main ascending input from MBV • Project back to MGV from layer VI • Project up to non-primary areas from layer II/III	• PAF in Te2, SRAF in Te3 • Thinner cortical width (1000 μm) with less prominent granular layer • Main ascending input from MGD • Project back to MGD, MGM and primary areas, from layers V/VI • PAF projects to posterior parietal cortex • SRAF projects to insular cortex

PHYSIOLOGY	
• Well-tuned to pure tones • Clear tonotopic gradients • Confined, V-shaped or narrow receptive fields • A1 and AAF mostly monotonic, but VAF contains most non-monotonic, low-threshold units • Respond to physical features of sounds • Short response latencies to pure tones and noise bursts • Low degree of context-dependence • Low degree of adaptation to repetition • Response facilitation to rapidly repeated sounds. Synchronize responses to up to 20 Hz trains	• SRAF, PAF • Weaker responses to pure tones • Broad or disorganized receptive fields for pure tones. • Preference for spectrotemporally complex, broad-band sounds such as modulated white noise • Longer response latencies • Responses more influenced by meaning or contextual significance of sounds • High degree of adaptation to repetition even at slow presentation rates • PAF initiates a dorsal stream for auditory spatial processing and directed attention to sounds (Kimura et al., 2004, 2005) • SRAF initiates a ventral stream for emotional processing of sounds (Kimura et al., 2005, 2007; Donishi et al., 2006)

There and back again: feedback loops in the auditory pathway

As we have seen, auditory nuclei at different levels are usually reciprocally connected. Within auditory cortex, primary areas send ascending projections to higher-order areas, which in turn, send feedback projections to primary areas (Figure 9b). Analogously, the MGV sends an ascending, tonotopic projection to primary auditory cortex, but in turn, the auditory cortex sends back a "feedback" projection to MGV. Furthermore, this feedback projection is around 10 times as dense as the forward projection, and in fact the corticothalamic projection is the heaviest projection of the whole brain, comparable only to the corticospinal tract (Winer and Schreiner, 2011). But the auditory cortex does not send projections only to MGV. The corticofugal projections are targeted to the whole MGB, IC, SOC, CNC, striatum, amygdala, central gray, pontine nuclei, and others. Judging only from their size, descending projections must play a fundamental role in sensory processing. However, this role has remained largely unknown for decades, or assumed to provide "modulation" or "gating" to ascending sensory-evoked responses. Today, we have a rather complete picture of these projections, and the view is changing from that "modulatory" nature, to a more protagonist role in shaping neuronal receptive fields (Sillito et al., 2006) or assisting in higher sensory functions such as figure-ground separation (Hupé et al., 1998). But descending projections are especially important for a recent and comprehensive theory of brain function, the so-called predictive coding framework, as will be explained in the next section.

A schematic depiction of the corticothalamic and corticocollicular projections is shown in Figure 10. The corticothalamic projection from primary auditory areas can be split in two separate projections. One arises mainly from pyramidal neurons of layer VI, and reaches the

MGV in a highly topographic manner, terminating in small terminal boutons, putatively of modulatory nature. The other arises mainly from layer V, and reaches higher-order thalamic relays, such as the MGD, terminating in large, type-II terminals of putative driver nature (Bartlett et al., 2000; Llano and Sherman, 2008). This driver projection would be part of the transthalamic pathway connecting primary and higher-order areas indirectly, with a thalamic gating in between (Sherman and Guillery, 2011). Higher-order areas of auditory cortex also send feedback projections to thalamus. In this case, the modulatory projection from layer VI is sent back to the MGD or MGM, from which these non-primary areas receive their ascending inputs. The driver corticothalamic projection from layer V is sent mainly to MGM (Figure 10), from which they could reach higher-order association areas (Kimura et al., 2003, 2007). The auditory cortices also send an important direct projection to the IC, bypassing the MGB (Figure 10). The heaviest of them is the projection from large pyramids in layer V of primary A1. This projection is mostly ipsilateral and topographic, such that low-frequency regions of A1 project to dorsolateral region of the IC, and the high-frequency regions of A1 project to the ventromedial region of the IC. Most cortico-collicular projections, from both primary and non-primary areas, target the cortical (non-lemniscal) regions of IC, although the CNIC also receives a smaller, weaker projection from A1 (Saldaña et al., 1996). Corticofugal projections arise from pyramidal cells, and are therefore glutamatergic. However, all corticothalamic projections send collaterals to the auditory sector of the thalamic reticular nucleus, and therefore they can also exert an important inhibitory action. Similarly, the auditory cortex may have inhibitory effects on the IC through the activation of local inhibitory connections within the IC. This is confirmed by physiological studies that demonstrate the excitatory and inhibitory effects of the auditory cortex on MGB neurons, as well as IPSPs in IC neurons after auditory cortex stimulation (Malmierca et al., 2015). Not only the auditory cortex sends descending projections to lower auditory centers. Important descending projections arise also from the IC to the brainstem, and from the SOC to the cochlea (Malmierca, 2015).

The auditory pathways are usually described sequentially, the ascending connections first, the descending connections last, just to present them in some systematic way. However, the connections of the auditory system would be best described as a series of nested loops of reverberating ascending and descending information, each next loop surrounding the previous one to add the next layer of auditory processing (Winer, 2006; Malmierca, 2015). In fact, the opportunities for a continuous interaction between descending projections and ascending inputs are numerous, and it is likely that these interaction, more than the activity of each pathway separately, be the physiological foundations of auditory perception. Interestingly, some authors consider that these descending projections carry the "feedforward" signal, representing the main internal activity of the brain, while the (much narrower) ascending information would be used only as a "feedback" to confirm that incoming signals are consistent with the current internal representation of the external world (Friston, 2005). This would be analogous to peeking outside the window just to confirm that "it is cloudy and raining outside". Only if the ascending input contradicts our hypothesis about the world, a strong ascending signal will be relayed up the hierarchy to trigger the adjustment of the internal model. Thus, the interplay between the ascending and descending information may be the basis of deviance detection, as we explain next.

AUDITORY DEVIANCE DETECTION AND SSA

As highlighted by Barlow in its seminal work (*v.s.*), new or unexpected sensory events are high in information content, and require more elaborate processing than sensory inputs that are repetitive or can be anticipated (Barlow, 1961). Thus, a basic network mechanism to automatically separate the "standard" input—that is, the background and other irrelevant, repetitive aspects of the auditory scene—from singular "deviant" events is warranted. Adaptation may provide a filter for repetitive patterns in the environment, preventing redundant information to reach higher processing levels. However, adaptation depends only on the number of times that a certain stimulus feature has been recently encountered, irrespective of the complex structure of the input in predictable patterns. Thus, adaptation does not allow separating uninformative events from more informative (unexpected) ones that occur with roughly the same frequency in the auditory scene. The ability to detect specific sensory events that do not match expectations created from the regularities encountered in recent sensory streams—*deviance detection*—is an important aspect of auditory scene analysis, which might be the basis of a fast and efficient formation and segregation of auditory objects (Grimm and Escera, 2012). Brain responses specifically elicited by deviant events are generally called mismatch responses (Harms et al., 2016), and represent the empirical demonstration of the invisible, underlying process of deviance detection.

Hierarchical organization of the auditory deviance detection system

An increasing body of evidence from single-unit recordings in animals to scalp auditory evoked potentials in humans indicates the ubiquitous presence of suppression of brain responses to invariant aspects of the sensory input, often accompanied by an enhanced responsiveness to new or rare information on multiple levels of auditory processing (Bendixen et al., 2012; Escera et al., 2014; Shiga et al., 2015; Aghamolaei et al., 2016). In the human auditory system, the detection of new or deviant events has been directly associated with the mismatch negativity, or MMN (Näätänen et al., 2007), a particular response of the auditory event-related potentials as measured with electoencephalogram (EEG) or magnetoencephalogram (MEG). Traditionally, the MMN is measured during an auditory oddball paradigm, in which a sequentially repeated standard stimulus is occasionally replaced by a rare stimulus that deviates in any of its physical features from the standard (Figure 13). The MMN is defined as the difference wave between brain responses to deviant and standard tones, assuming that responses to standard tones represent the "obligatory" component of the response, and after removing this component to the response to deviant tones, what is left is the component of the response specifically due to the occurrence of a deviant event. The MMN is typically a slow, negative deflection of the mid-late ERP (circa 150 ms from deviance onset). Brain generators of MMN have been localized bilaterally in the auditory cortex (both primary and non-primary), responsible for the sensory memory mechanisms (Giard et al., 1990), with a potentially important contribution form prefrontal regions (with a right lobe predominance) (Giard et al., 1990; Alho, 1995; Maess et al., 2007; Näätänen et al., 2007) related to involuntary attention switch caused by auditory change (Escera et al., 1998, 2003).

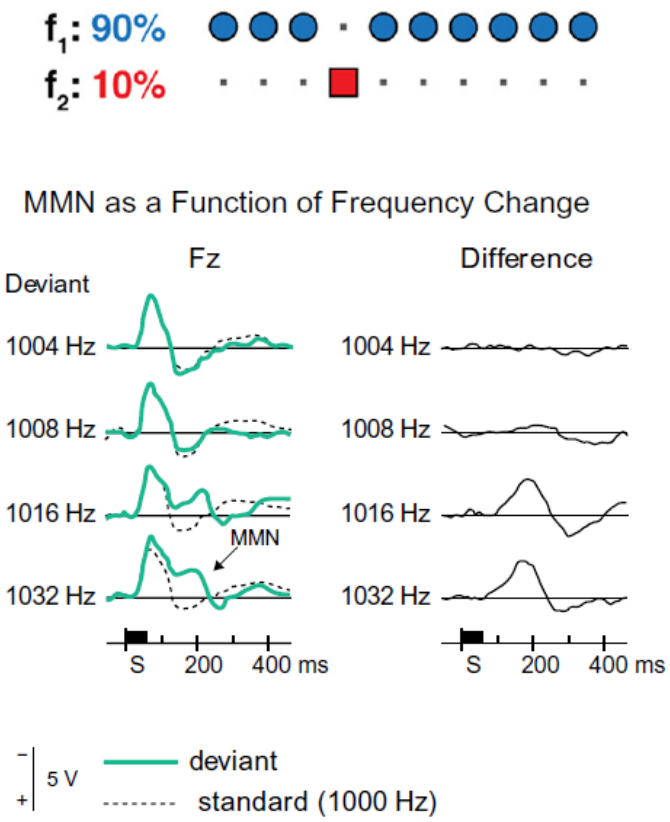

Figure 13. The mismatch negativity (MMN). (a) Schematic representation of the oddball paradigm. A series of standard (blue) tones is randomly interrupted by a deviant (red) tone of different frequency f_2. **(b)** Evoked potentials in response to deviant and standard tones are different within a particular time window, and this difference (MMN) increases with increasing separation of the deviant frequency. Adapted from Näätänen (2007).

The detection of a stimulus that violates a previously established regularity requires the use of short-term sensory memory. Thus, the MMN is thought to reflect a memory formation and comparison process, revealing higher pre-cognitive abilities of the auditory cortex (Näätänen et al., 2001; Winkler, 2007). Indeed, different studies have shown that MMN elicitation requires the previous presentation of a minimum number of repetitions of the rule, that increase with the complexity of the regularity that has to be encoded (Näätänen et al., 2005; Escera et al., 2014). Importantly, MMN is an automatic brain response, which does not require the subject's attention to the stream of sounds, and can be readily recorded from distracted, asleep, anesthetized, and even coma patients. This feature makes it a convenient tool for clinical and basic research in auditory perception, but also highlights the ability of sensory systems to automatically perform complex comparisons between stimuli, which persists across different states of awareness (Näätänen et al., 2001).

The MMN reflects a basic perceptual process that can be detected in different sensory modalities, including somatosensory (Kekoni et al., 1997; Shinozaki et al., 1998; Akatsuka et al., 2007), olfactory (Pause and Krauel, 2000) and visual (Czigler et al., 2002; Astikainen et al., 2013), for different types of change or regularities, at different levels of abstraction, further

pinpointing to its close relation to cognitive processes. The oddball design can be used to test sensitivity to simple changes in a physical feature of the stimulus, such as frequency, location, pitch, intensity, duration, modulation frequency, roughness, etc. However, more elaborated designs also reveal MMN for changes in complex regularities, defined by the relationships or precedence rules between discrete sounds, but not on a specific feature per se (Alain et al., 1994; Tervaniemi et al., 1994; Gomes et al., 1997). The most important reflection of this is the MMN generated by violations of grammar rules in mother-tongue sentences (Näätänen et al., 1997; Pulvermüller and Shtyrov, 2003; Pulvermüller et al., 2008; Hanna et al., 2014).

Cognitive brain research using the MMN has continued for the last four decades, there now being more than 2000 research articles[7] using, or referring to, the MMN. The significance of MMN lays in its wide range of practical applications in both basic and clinical research (Näätänen et al., 2007, 2012):

- ✓ Indicator of early cognitive development in newborns, toddlers and even from the fetus.
- ✓ Indicator of the functional condition of the NMDA-receptor system.
- ✓ Index of the different brain pathologies underlying schizophrenia and a wide range of different clinical conditions and diseases.
- ✓ Tool in genetic research of pshychopathology.
- ✓ Predictor of coma outcome.
- ✓ Index of primitive sensory intelligence in audition.
- ✓ Index of brain mechanisms of speech perception and understanding.

However, the MMN is not the earliest electrophysiological response for regularity violations in humans (Escera et al., 2014). The whole human auditory ERP includes the auditory brainstem response (ABR), reflecting mainly early (1-10 ms), subcortical activity, the middle-latency responses (MLR), reflects early activity (12-50 ms) in primary auditory cortex, and the long-latency reponses (LLR) which include the MMN (Picton, 2010). The MLR is characterized by a sequence of waveforms labeled as N0, P0, Na, Pa, Nb and Pb (Figure 14).

The MMN is a long-latency auditory ERP, thus reflecting a higher-order stage of processing over already elaborated and filtered information. In fact, higher-order areas of auditory cortex are more sensitive to the deviance per se that primary areas, which are more sensitive to the physical or purely sensory aspects of sound (Kropotov et al., 2000; Opitz et al., 2005; Maess et al., 2007). Primary auditory areas seem to be able to encode only simple rules, such as local deviants (AAA**B**), whereas higher-order cortical areas can detect violations of complex rules, such as global deviants (AAABAAABAAA**A**) (Wacongne et al., 2011; Recasens et al., 2014). Different neuronal populations appear to be involved in the MMN generation for a simple acoustic feature and for a sequential pattern (Alain et al., 1998, 1999).

[7] PubMed search "mismatch negativity" yielded 2406 results as to April, 2017.

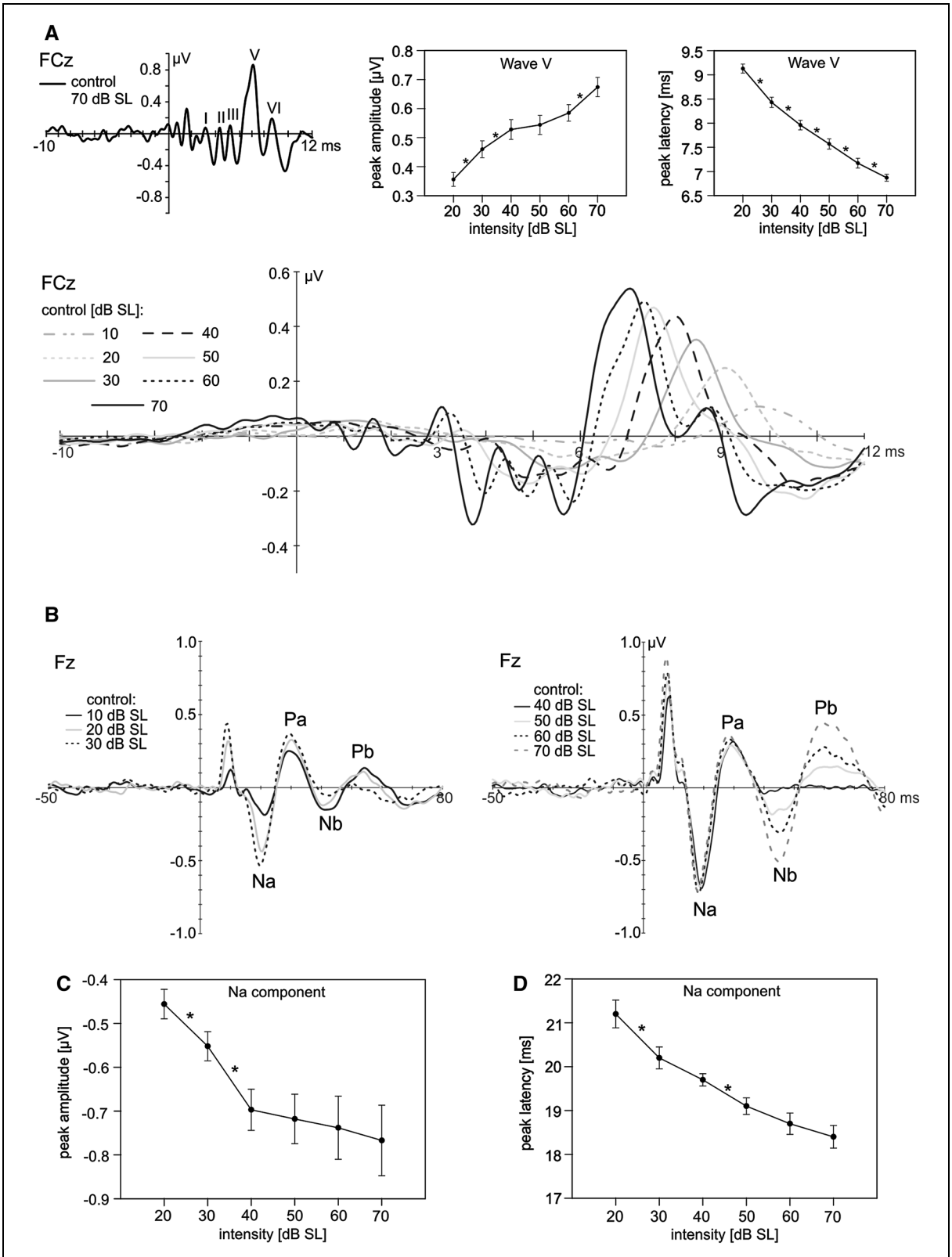

Figure 14. Different components of the human auditory ERP. (A). Auditory brainstem response (ABR). **(B)** Middle latency responses (MLR). From Althen et al. (2011).

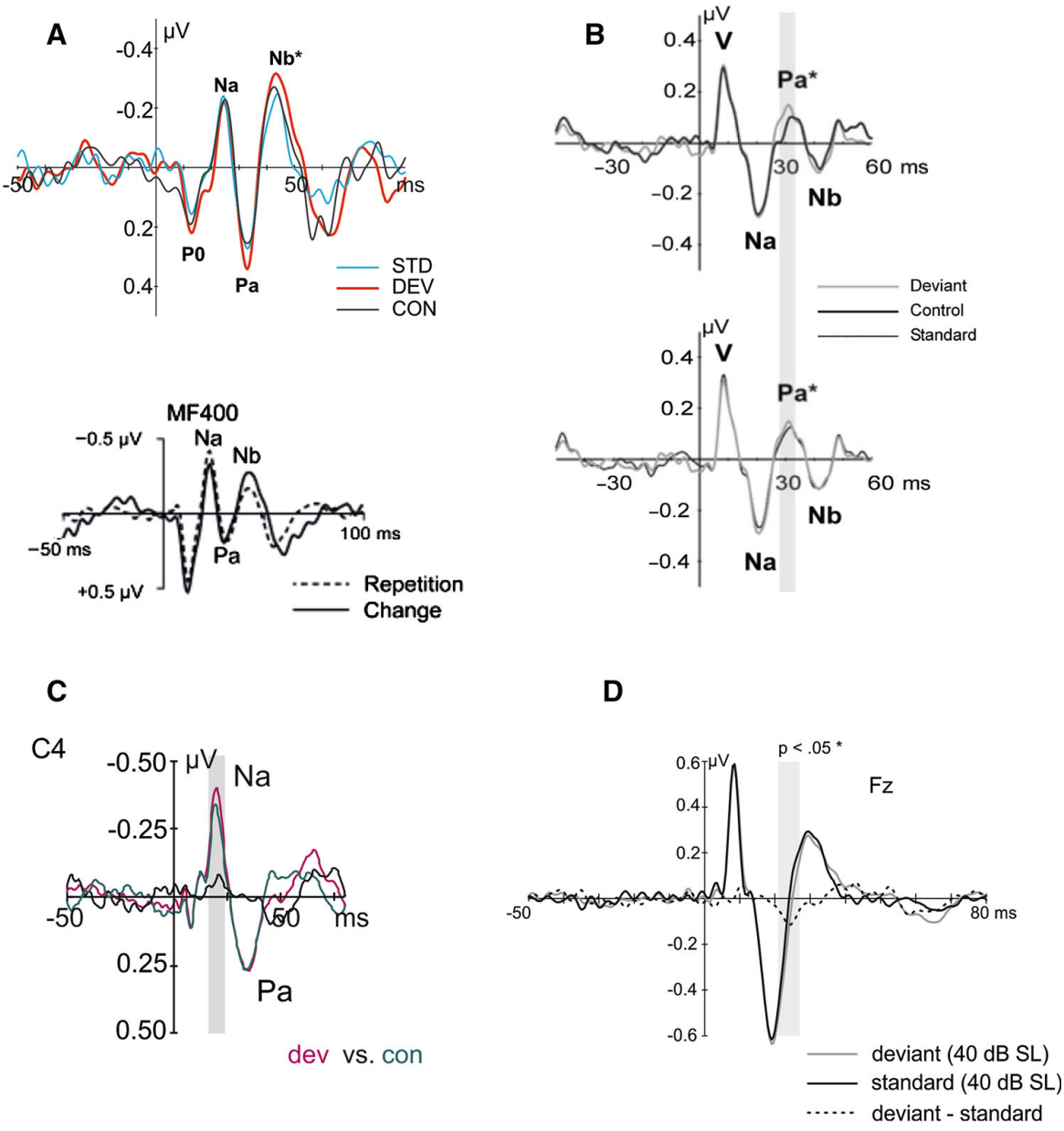

Figure 15. Early electrophysiological correlates of deviance detection in the MLR range. Frequency changes produce specific modulations of the Nb **(A)** and Pa **(B)** components of the MLR. Location deviants enhance the Na component **(C)** and intensity deviants induce a negativity by the Na to Pa transition **(D)**. From Escera et al. (2014).

Simple feature deviants can be detected already at the MLR (Figure 15). Pure tone frequency deviants produce a specific enhancement of the Nb component of the MLR, at around 40 ms from change onset (Grimm et al., 2011), even within natural auditory scenes (Puschmann et al., 2013), which is not observed for other features such as intensity, duration or location (Leung et al., 2012). This Nb modulation is confined to the Heschl's gyrus, where the primary auditory cortex is located (Recasens et al., 2014). Other study found signs of deviance detection for noise tokens even earlier than Nb, in the Pa component of the MLR (around 30 ms) (Slabu et al., 2010). The Na component (25 ms) is enhanced by the occasional feature

change in the interaural time differences (Cornella et al., 2013). Intensity deviants produced a more negative potential at the transition from Na to Pa component (Althen et al., 2011), and temporal regularity violations led to enhanced Pa and Nb responses (Leung et al., 2013). Moreover, deviance-related responses can be observed at even earlier stages, at the level of the brainstem, as revealed by FFR recordings (Slabu et al., 2012) and fMRI (Cacciaglia et al., 2015). By contrast, violations of complex regularities do not modulate early responses such as MLR or ABR. A series of studies used a combined approach to dissociate simple and complex rule effects at different hierarchical levels of the auditory processing, directly revealing the hierarchical organization of the human auditory deviance detection system, starting from early levels of processing. One study combined simple (ITD) and complex (alternating pattern) rule violations within a single conjunction paradigm (Cornella et al., 2012). Both violations elicited an MMN, but only the simple rule produced an enhanced Na response. Other study used a feature conjunction paradigm in combination with an oddball paradigm, to reveal MMN for both rules, but deviance-related Nb enhancement only for the oddball condition (Althen et al., 2013). Finally, in a MEG study, MMN responses were generated for both local and global rule violations, but deviance-related Nbm and Pbm responses were only observed in the local rule violation condition (Recasens et al., 2014). Taken together, these studies suggest that simple regularities are encoded in the early processing stages, whereas encoding complex regularity requires the higher levels of the auditory hierarchy. Thus, depending on the structure and parameters of the stimulus sequence, an MMN elicited by a certain acoustic change can reflect any, or even the combination, of memory traces at different levels (Ritter et al., 1995; Näätänen et al., 2007).

SSA and the link to MMN

Given the great success of MMN as a clinical and experimental tool, animal models of MMN were developed including monkey (Javitt et al., 1992), cat (Csépe et al., 1987), rat (Ruusuvirta et al., 1998), mouse (Umbricht et al., 2005) and guinea pig (Kraus et al., 1994), as helpful tools to gain insight into the cellular mechanisms of MMN generation and the disruption thereof (Nelken and Ulanovsky, 2007; Todd et al., 2013).

Totally independent of the MMN research, a different and apparently unrelated phenomenon was being described in single neurons of the visual and auditory systems: stimulus-specific adaptation (SSA; Movshon and Lennie, 1979; Condon and Weinberger, 1991; Müller et al., 1999; Ulanovsky et al., 2003). SSA was a special form of neuronal adaptation, by which neuronal responses vanished upon repetition of a stimulus, but retaining their ability to respond to different, infrequent stimuli. Thus, SSA exhibited the hallmarks of behavioral habituation, defined as the "gradual diminution of the response to a stimulus following the repeated presentation of the same, or similar, stimulus": (a) stimulus specificity, (b) rate sensitivity and (c) dishabituation, a recovery following the presentation of another stimulus. These properties precluded a simple explanation of SSA based on changes in the general responsiveness of the cell through, for example, intrinsic membrane mechanisms (Nelken and Ulanovsky, 2007).

A simple yet powerful idea established the link between SSA and MMN: to use an oddball paradigm to study adaptation in single cortical neurons (Ulanovsky et al., 2003). As with scalp-

recorded MMN, single neuron responses to deviant tones were stronger than to the same tones when presented as standards. The key point of this seminal study was to demonstrate that single cortical neurons showed a differential response to standard and deviant tones under oddball stimulation, just as MMN but at the cellular level (Figure 16) [8]. Moreover, SSA mimicked most of the defining properties of MMN, beyond the differential responses to standard and deviant tones (Nelken and Ulanovsky, 2007). Critically, the magnitude of SSA/MMN increased with the magnitude of deviance (Figure 54), decreased with the probability of deviant occurrence, and decreased with the inter-stimulus interval (Table 2). All these striking parallelisms led the authors of that study to postulate SSA as a neuronal correlate of the MMN potential recorded epidurally. At the same time, they recognized important limitations or discrepancies between SSA and MMN (Table 2): (1) SSA was measured from spike responses of single units in primary auditory cortex, whereas the MMN is a large-scale voltage measure with a major contribution from (excitatory and inhibitory) post-synaptic potentials generated throughout the whole auditory cortex, with a predominant role of non-primary areas; (2) SSA was observed with a latency of 20-30 ms, which is way earlier than the 100-150 ms of the MMN, making it impossible to establish a simple, direct link between the two.

Since the process of deviance detection must involve more or less complex memory operations, it was commonly thought a task that only the cerebral cortex could perform. Analogously, given the sophistication of SSA and its similarities to MMN, it was assumed that SSA was a unique and emerging property of cortical neurons. However, a series of studies using single unit recordings in animal models challenged this idea, showing strong and consistent SSA in the midbrain (IC) (Pérez-González et al., 2005; Reches and Gutfreund, 2008; Malmierca et al., 2009; Duque et al., 2012; Ayala and Malmierca, 2013; Dutta et al., 2016) and thalamus (MGB) (Yu et al., 2009; Antunes et al., 2010; Bäuerle et al., 2011; Duque et al., 2015), with very similar properties to the SSA described in auditory cortex (Malmierca et al., 2014; Pérez-González and Malmierca, 2014; Duque et al., 2015).

One of the most important and consistent discoveries concerning subcortical SSA was that SSA seemed to be a characteristic property of the non-lemniscal auditory pathway. This held true in IC (Malmierca et al., 2009; Duque et al., 2012) and MGB (Antunes et al., 2010), where SSA was virtually absent in their primary, or lemniscal, division, whereas it was strong and widespread in the non-lemniscal divisions, to the point that the level of SSA could be used as a hallmark of non-lemniscal neurons (Duque et al., 2015). Thus, primary auditory cortex was the

[8] An important improvement in methodology boosted by the studies by Ulanovsky et al. was the systematic use of the "reverse" condition. Instead of using one single oddball sequence, and compare the responses to standard and deviant tones (which were physically different stimuli), the same physical tone was presented first as a deviant and then as a standard, and responses to both conditions, for the same physical tone, were compared. This control for the effect of the physical features of the stimulus was not essential in human scalp studies, because large-scale potentials to pure tones were similar in shape and amplitude irrespective of frequency of the tone, but it was mandatory in single unit studies, since responses of single units in primary auditory cortex are highly dependent on the physical parameters of the sound.

first primary auditory station showing consistent SSA, pinpointing A1 as a site of generation of SSA, that could be transmitted down through the corticofugal pathway (*v.s.*). However, this subcortical SSA did not require the intervention of auditory cortex, demonstating that SSA is a rather ubiquitous phenomenon that can emerge independently at different hierarchical levels (Antunes and Malmierca, 2011; Anderson and Malmierca, 2013; Malmierca et al., 2015).

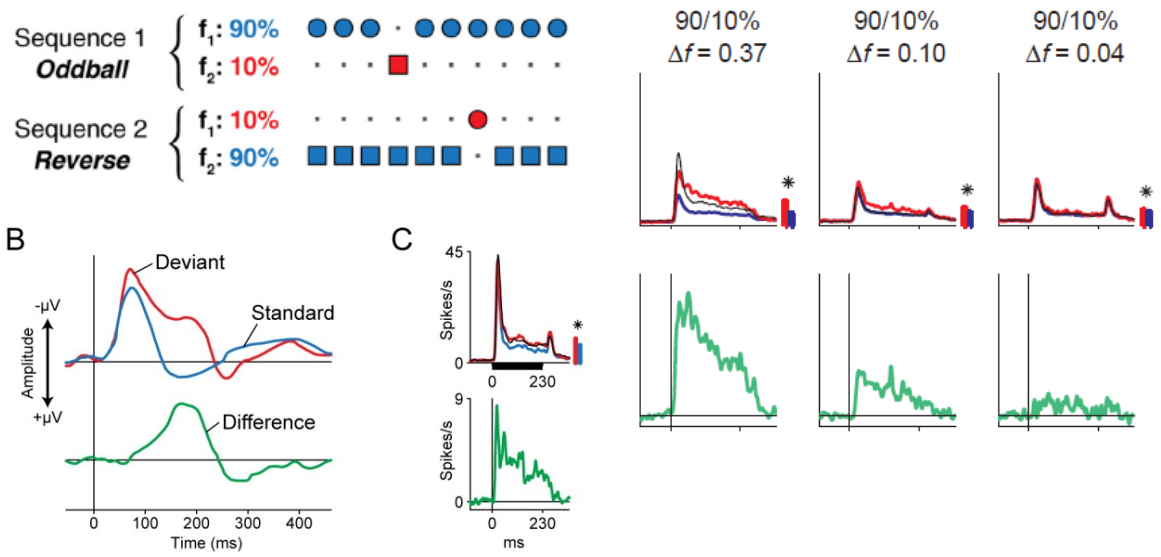

Figure 16. SSA as a neuronal correlate of MMN. (A) The oddball paradigm, including a reverse condition, to present the same physical stimulus in the role of deviant and standard. **(B)** The MMN is the difference between evoked responses to deviants and standards. **(C)** In response to the same stimulation paradigm, single neurons in A1 also respond differentially to deviants and standards, irrespective of their physical frequency (D) The magnitude of the difference signal (DS, in green) measured from spike responses in A1 shows exactly the same dependence as the MMN on the frequency separation between deviant and standard tones. Adapted from Ulanovsky et al. (2003) and Pérez-González and Malmierca (2014).

The combination of discoveries from cortical and subcortical SSA studies produced a picture in which SSA seemed to be a prevalent property of the non-lemniscal auditory pathway, that could be a direct correlate of the earlier indicators of deviance detection seen in human EEG studies, but just upstream of the true MMN generation (Nelken and Ulanovsky, 2007; Grimm et al., 2015). The complete MMN signal, as recorded in human and animal preparations, seemed to be generated later with the key participation of non-primary auditory areas. However, the picture of SSA in the auditory system was incomplete, since no one had ever recorded SSA from non-primary auditory cortex, and thus the map of SSA in the auditory pathway was yet to be completed (Figure 17), even though the very discoverers of the SSA-MMN link predicted that SSA in non-primary auditory cortex could be a more direct correlate of the real MMN (Nelken and Ulanovsky, 2007).

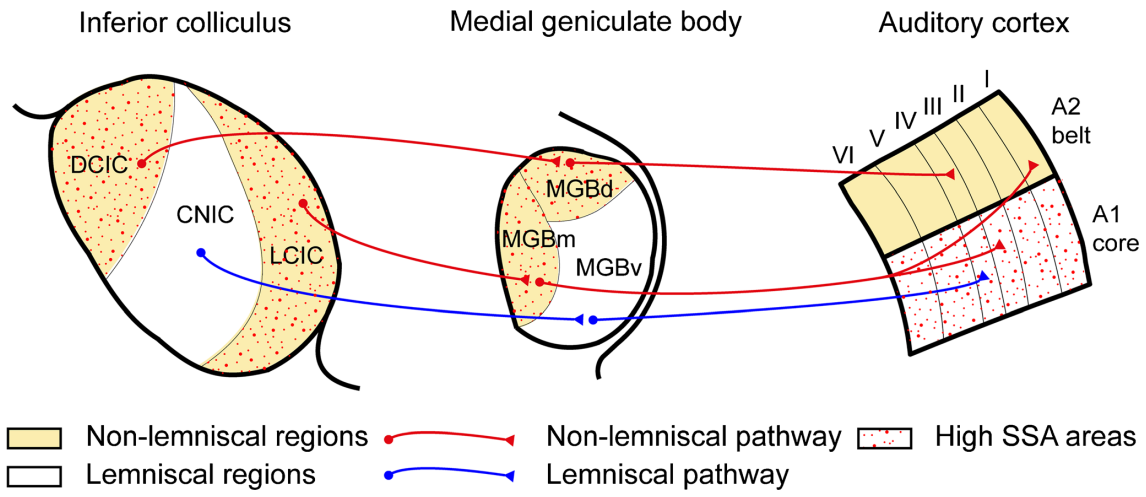

Figure 17. Distribution of SSA along the auditory pathway. At subcortical levels, SSA is sharply segregated to the non-lemniscal auditory pathway. However, as of 2015, the level of SSA in non-primary auditory cortex remains to be determined. From Duque et al. (2015).

In summary, SSA met all the requirements to be a neuronal correlate of the MMN, but there were two major limitations in the SSA-MMN link:

(a) Anatomical location: MMN is generated mainly in non-primary auditory cortex, whereas SSA had only been demonstrated in primary auditory cortex (A1).
(b) The latency of SSA in A1 (and subcortical structures) was much earlier than the latency range of MMN, separated by a physiological abysm of 50-100 ms.

Additionally, there was a key requirement yet to be demonstrated for SSA to be considered a genuine mismatch response, underlying deviance detection in auditory neurons, as exposed in the following section.

Table 2. Similarities and differences between MMN and SSA. Most relevant for Study 1 and Study 2 are the important discrepancies that still prevent the acceptance of SSA as a direct neuronal correlate of the MMN. Adapted and extended from (Nelken and Ulanovsky, 2007).

SIMILARITIES	
MMN	**SSA**
MMN appears in epidural recordings in monkeys, cats and rats (Javitt et al., 1992; Pincze et al., 2002; Harms et al., 2014).	SSA appears in extracellular single-unit recordings in A1 of monkeys, cats and rats (Ulanovsky et al., 2003; von der Behrens et al., 2009; Taaseh et al., 2011; Fishman and Steinschneider, 2012).
MMN is generated in auditory cortex (Alho, 1995).	SSA can be recorded in A1 (Ulanovsky et al., 2003; von der Behrens et al., 2009; Taaseh et al., 2011; Fishman and Steinschneider, 2012).

Magnitude of MMN increases with frequency separation between standard and deviant (Näätänen, 1992).	Magnitude of SSA increases with frequency separation between standard and deviant (Ulanovsky et al., 2003; Malmierca et al., 2009).
Magnitude of MMN decreases with the probability of deviant sound (Näätänen, 1992).	Magnitude of SSA decreases with the probability of deviant sound (Ulanovsky et al., 2003; Malmierca et al., 2009).
Magnitude of MMN decreases with the interstimulus interval (Näätänen, 1992).	Magnitude of SSA decreases with the interstimulus interval (Ulanovsky et al., 2003; Malmierca et al., 2009).
MMN latency is longer than the latency of responses to standard sounds (Näätänen, 1992).	SSA latency (in AC) is longer than the latency of responses to standard sounds (Ulanovsky et al., 2003).
MMN gets more pronounced over the time course of the stimulation (trial nr.), following many timescales simultaneously.	SSA gets more pronounced over the time course of the stimulation (trial nr.), following many timescales simultaneously.
MMN analogs can be recorded from subcortical MGB (Kraus et al., 1994).	SSA is strong and widespread in non-lemniscal divisions of subcortical IC and MGB (Malmierca et al., 2009; Yu et al., 2009; Antunes et al., 2010; Duque et al., 2012).
MMN shows a dependency on the sequential structure of the stimulation (Winkler and Schröger, 2015; Koelsch et al., 2016).	SSA shows a dependency on the sequential structure of the stimulation (Ulanovsky et al., 2004; Yaron et al., 2012).
DIFFERENCES	
MMN	**SSA**
Neuronal generators of MMN show a major contribution from non-primary AC to the "cognitive" component and A1 to the "sensory" component (Kropotov et al., 2000; Opitz et al., 2005; Maess et al., 2007; Shiramatsu et al., 2013).	SSA is widespread in A1, but it is unknown whether it appears in non-primary AC, and whether it is different from SSA recorded in A1 (Nelken and Ulanovsky, 2007; Nelken, 2014).
MMN peaks around 150-200 ms in humans, and around 80-100 ms in rodents (Näätänen, 1992; Todd et al., 2013).	SSA peaks around 20-30 ms in A1 of cats and rats (Ulanovsky et al., 2003; Taaseh et al., 2011).
A "genuine" MMN still exists when controlling for repetition effects with the many-standards or cascadic controls (Jacobsen and Schröger, 2001; Opitz et al., 2005;	A larger response to deviants than to many-standards or cascadic controls has not been shown unambiguously for SSA in A1 (Farley et al., 2010; Taaseh et al., 2011; Fishman and

Ruhnau et al., 2012).	Steinschneider, 2012) –but see (Chen et al., 2015).
MMN exists for intensity deviants and for unexpected omissions of the standard stimulus (Näätänen, 1992; Yabe et al., 1997; Wacongne et al., 2011).	SSA has not been shown unambiguously for intensity deviants, and responses to omitted stimuli have not been recorded in AC (Ulanovsky et al., 2003; von der Behrens et al., 2009; Fishman, 2014; Duque et al., 2016).

The MMN conundrum: adaptation vs memory trace models

The discovery of SSA moved the focus of attention from responses to deviants to responses to standards, and was followed by studies in humans claiming that the whole MMN phenomenology could be due to SSA of overlapping populations of cortical neurons (Jääskeläinen et al., 2004), without the need to call for higher, memory-driven mechanisms to produce a differential response to deviants and standards. Thus, the field of MMN research was divided between supporters of two theories, which were pushed far enough so as to seem mutually exclusive (May and Tiitinen, 2010; Fishman, 2014) (Figure 18):

(a) Memory-trace model: the MMN is a distinct component of the ERP generated by comparator neurons that make use of a memory trace of recent history stimulation. Without the presence of a previous regularity to create this memory trace, no MMN is generated.
(b) Adaptation (SSA) model: The MMN, as a difference signal, results from suppression of the response to the standard stimulus, due to repetition effects. The response to the deviant in the oddball paradigm is just the normal, unadapted response to that stimulus.

The "just SSA" hypothesis of MMN was rapidly and exhaustively refuted in a convincing way by Näätänen and colleagues (Näätänen et al., 2005). The main argument for the memory-trace model was the demonstration of MMN for deviants in rather complex and abstract types of regularities, and also for feature deviants that directly defied the adaptation model, such as intensity deviants and omitted stimuli (Fishman, 2014). On the other hand, the efforts of the adaptation community were centered on developing computational models simulating all the MMN-related brain responses, by modeling only adaptation processes (May and Tiitinen, 2010).

Even though the memory-trace supporters were convinced that higher cognitive processes had to be involved in MMN generation, they also acknowledged that adaptation of responses to the repetitive standard could be contributing to some degree to the difference wave called MMN. In other words, the "cognitive" component of the MMN could be "contaminated" by adaptation effects (Näätänen et al., 2005; Opitz et al., 2005). This was a long held debate that was not particularly productive, but led to the realization that there was a second uncontrolled factor (beyond differences in physical features of deviant and standard stimuli) that needed to be accounted for in MMN studies: presentation rate. Since the standard stimulus appears with much higher presentation rate (probability) than the deviant, it is subject to more adaptation, and in this way the stronger responses to deviants could result just from release from SSA. Based on responses to the oddball paradigm alone, there is no way to determine how much of

this difference is due to adaptation to the standard, and how much to the deviant nature of the rare tones.

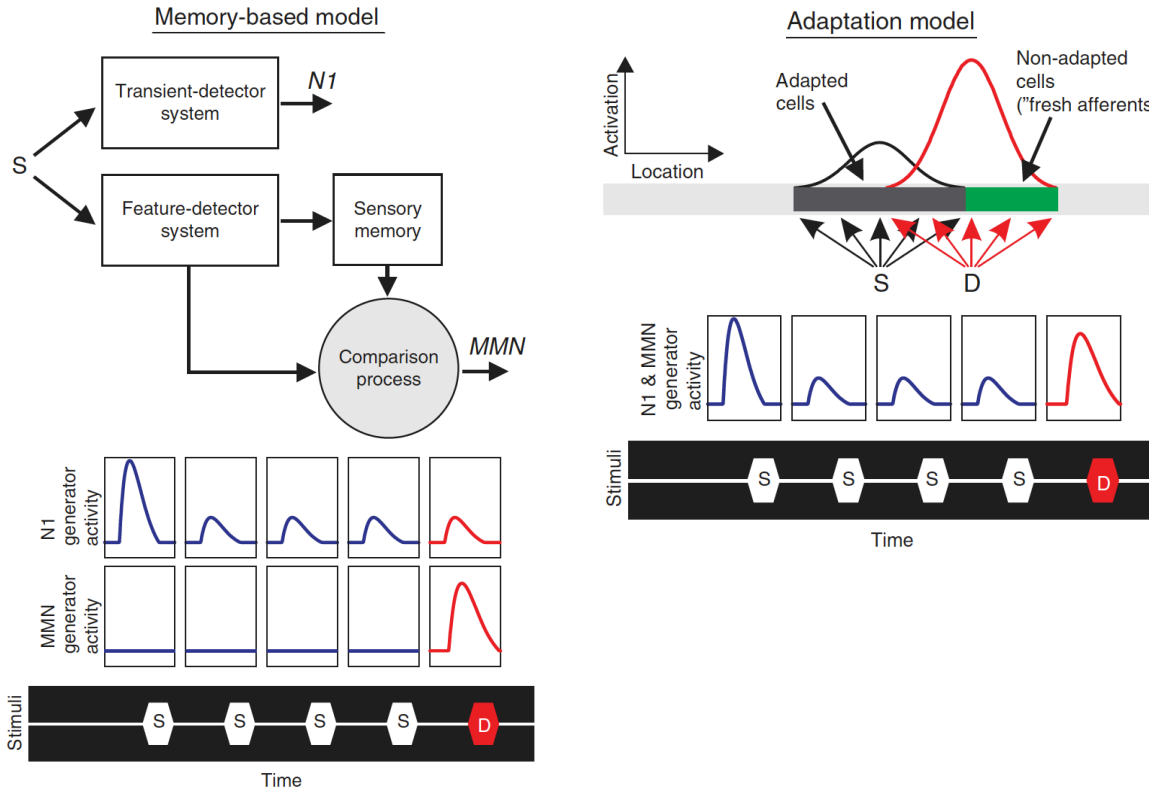

Figure 18. Two competing hypothesis of MMN generation. Left: In the memory-based model, a stimulus is analyzed by an N1-generating "transient detector" system, and a separate, MMN-generating "comparator system" that first analyzes the stimulus features and generates a sensory memory trace. Then, it compares the features of incoming stimuli with representations of past stimuli in the sensory memory store, and, when the two differ, an MMN response is generated. The N1 is largest for the first standard. In contrast, the MMN generator reacts only when the deviant follows (and breaks) an already established memory trace for the standards. Right: In the adaptation model, the standards and deviants activate overlapping neuronal populations. The repetitive standard leads to cells tuned to the standard to become adapted. When the deviant is presented, non-adapted cells/synapses—"fresh afferents"—contribute to an enhanced response. Note that now the MMN generator responds vigorously to the first standard of the sequence. It also produces attenuated responses to the subsequent standards. In this model, the N1 and MMN are generated by the same neural populations, and the MMN is, essentially, an enhanced N1 response. From May and Tiitinen (2010).

One of the most widely used tools to control for adaptation effects in MMN was the so-called "many-standards control" (MAS) (Jacobsen and Schröger, 2001). The many-standards control sequence is just a random presentation of a number of different stimuli (4-10), such that each of them appeared the same number of times in an unpredictable order and with the same probability as the deviant in an oddball sequence. Then, instead of comparing responses to a

tone in the deviant and standard conditions, which could differ due to adaptation effects at different presentation rates, a direct comparison between deviant and control conditions (for the same physical stimulus) is performed, to reveal the specific effect of deviance in neuronal responses (Figure 19).

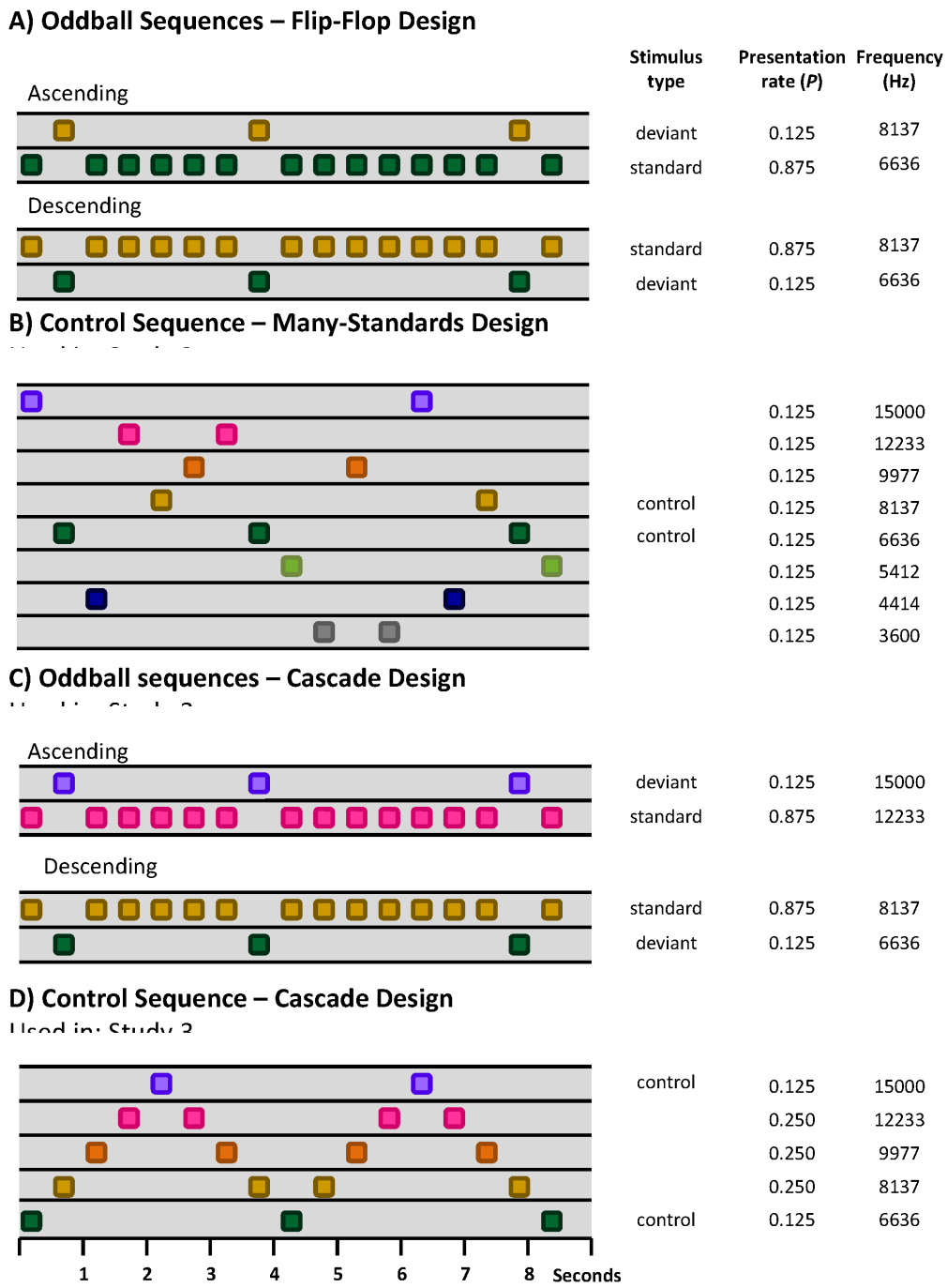

Figure 19. Control sequences used to demonstrate deviance detection. Using this design, or a variation of it, each physical stimulus can be presented as a deviant (the rare tone in an oddball sequence) or in a neutral condition, such as in the many-standards or cascade context, where it appears in the same positions but is not a perceptual deviant. From Harms et al. (2014).

The main rationale behind this design is that, in the MAS control conditions, each tone has the same (low) probability of occurrence as a deviant tone in the oddball sequence, so it is not repetitive (as the standard), and therefore is free of repetition effects (e.g. repetition suppression), but it does not stand out from the statistical context (as the deviant), and therefore it is not perceived as a deviant. The cascaded (CAS) sequence was recently designed as an improvement to the many-standards, that controls for additional key factors beyond presentation rate of the deviant tone (Ruhnau et al., 2012; Harms et al., 2014). First, the tone immediately preceding a deviant is the same in the oddball (a standard) and cascaded sequences. This improves the estimation of the overall adaptation state of the system by the time the deviant tone is played, and controls for the potential sensitivity of the neuron to a rise or fall in frequency between two successive tones. Second, the cascaded sequence mimics the regular structure of the oddball sequence, with the important difference that now the target tone *conforms* to the rule, instead of being a deviant. Essentially, these sequences would capture the baseline brain response to a neutral stimulus, in a context where it is neither repetitive, nor deviant. They have been successfully applied in both the auditory (Maess et al., 2007; Lohvansuu et al., 2013) and visual (Astikainen et al., 2008; Kimura et al., 2009) domains, to separate repetition effects from mismatch responses proper.

These control conditions soon became the *de-facto* method to separate deviance detection from adaptation effects (Jacobsen and Schröger, 2001; Opitz et al., 2005; Grimm et al., 2011; Stefanics et al., 2014), to the point that the critical comparison "DEV>CTR" was considered a fundamental requirement to interpret any brain response as a "mismatch response" (Harms et al., 2016). This requirement would extend to responses of single neurons. Thus, if SSA recorded in single neurons with the oddball paradigm was to be considered a neuronal correlate of deviance detection, one of these control had to be used to prove that responses to deviant were enhanced in relation to the control condition. Some studies used these controls to validate animal models of MMN (Shiramatsu et al., 2013; Harms et al., 2014). However, initial attempts to find signs of deviance detection in single neurons of primary auditory cortex of different animal preparations, including awake rat (Farley et al., 2010), awake monkey (Fishman and Steinschneider, 2012) and anesthetized rat (Taaseh et al., 2011) yielded inconclusive results. Only a recent study in mouse A1 (Chen et al., 2015) and another in rat barrel cortex (Musall et al., 2015) showed deviance detection in late responses of single units, using the MAS control sequence.

As a result of this controversial debate, the memory trace community was almost obsessed about eliminating the "contamination" of adaptation effects from their results, to obtain the "purified" electrophysiolical signals of brain activity directly involved in memory comparison processes (Horváth et al., 2008). Thus, the suppression of responses to standard stimuli due to repetition were regarded not only as irrelevant, but even discarded as detrimental to the research (Stefanics et al., 2014). However, soon the phenomenon of repetition suppression (RS) was regarded as interesting per se, and proposed as an electrophysiological indicator of the very formation of the memory trace required for the detection of a sensory mismatch (Haenschel et al., 2005; Garrido et al., 2009a; Costa-Faidella et al., 2011a). Thus, the MMN community started to understand that adaptation and deviance detection were just two complementary aspects of the same phenomenon, or two sides of the same coin (Schröger et al., 2014; Stefanics

et al., 2016), that contributed to the segregation of uninformative and highly informative sensory event in separate processing streams, as postulated by Barlow many decades ago. In fact, to make a relevant event pop out from the context, it is equivalent to (a) enhance neuronal responses to the relevant sensory events or (b) attenuate neuronal responses to irrelevant sensory events; but a combination of the two seems the most effective strategy. And, an important feature of the MAS and CAS control sequences is that they allow for the decomposition of neuronal responses to oddball stimulation into adaptation and deviance detection components, thus facilitating their separate study and experimental manipulation.

One of the main critiques to the memory trace model was that the underlying neuronal mechanisms were not detailed in any way, specific enough such as, for example, developing a computational model (May and Tiitinen, 2010). But, an elegant theory about cortical responses to diverse sensory inputs, as measured with non-invasive methods (fMRI, MEG/EEG...), was being completed, and will be extremely helpful to reconcile the MMN controversy.

The predictive coding account of MMN

The aforementioned hierarchy of electrophysiological markers of mismatch detection based on regularity encoding—in addition to MMN—operating from early stages of auditory processing, provides empirical support to the hierarchical predictive coding framework (Friston, 2005), seamlessly fitting it as the sum of thousands of neuronal prediction error signals (Bendixen et al., 2012; Phillips et al., 2016). Predictive coding is a unifying account of general brain function (Rao and Ballard, 1999; Friston, 2009), which gives a detailed specification of old general ideas dating back to Helmholtz in the 19th century (Swanson, 2016), formulated in rigorous mathematical models. According to this theory, the thalamocortical system—and by extension the whole brain—works like a hierarchical Bayesian inference system (Mumford, 1992; Friston, 2005). Sensory-evoked neuronal responses represent prediction error, which is relayed up the hierarchy. At the same time, higher stations are constantly trying to anticipate the future, and send descending signals to actively suppress the evoked, ascending neuronal activity, and thus minimize prediction error (Figure 20). Predictive coding principles seem to govern sensory systems from very early stages of signal transduction and representation, conditioning the more basic principles of sensory physiology, such as center-surround receptive fields in the retina (Srinivasan 1982).

As discussed earlier, a puzzling, common feature of all sensory systems is the existence of massive descending, efferent, or "backwards", projections (both cortico-cortical, from higher to lower areas, and corticofugal). For decades neuroscientists have wondered… What are they for? Undoubtedly, massive descending projections must have a central role in brain function, or evolution would not have favored them. Both afferent and efferent signals, and the interaction between them, are important in this theory. Higher sensory areas store a model of the current state of the surrounding world, and use sensory inputs to complete and update this model according to empirical evidence coming from the senses. Signals coming out of the brain towards the senses (for example, from a higher to a lower cortical sensory area) contain an abstract description, or code, of the expected state of things at that lower level. In practical terms, at the primary sensory areas this efferent code is a prediction of what the next sensory

input is going to be. And physiologically, the effect of these "prediction" signals is to cancel out the afferent, sensory signal, whenever it is correctly predicted. This is because afferent signals represent prediction error: when the sensory signal has not been anticipated at one particular level of the hierarchy, and thus canceled by efferent predictions, the afferent error signal will progress up the hierarchy.

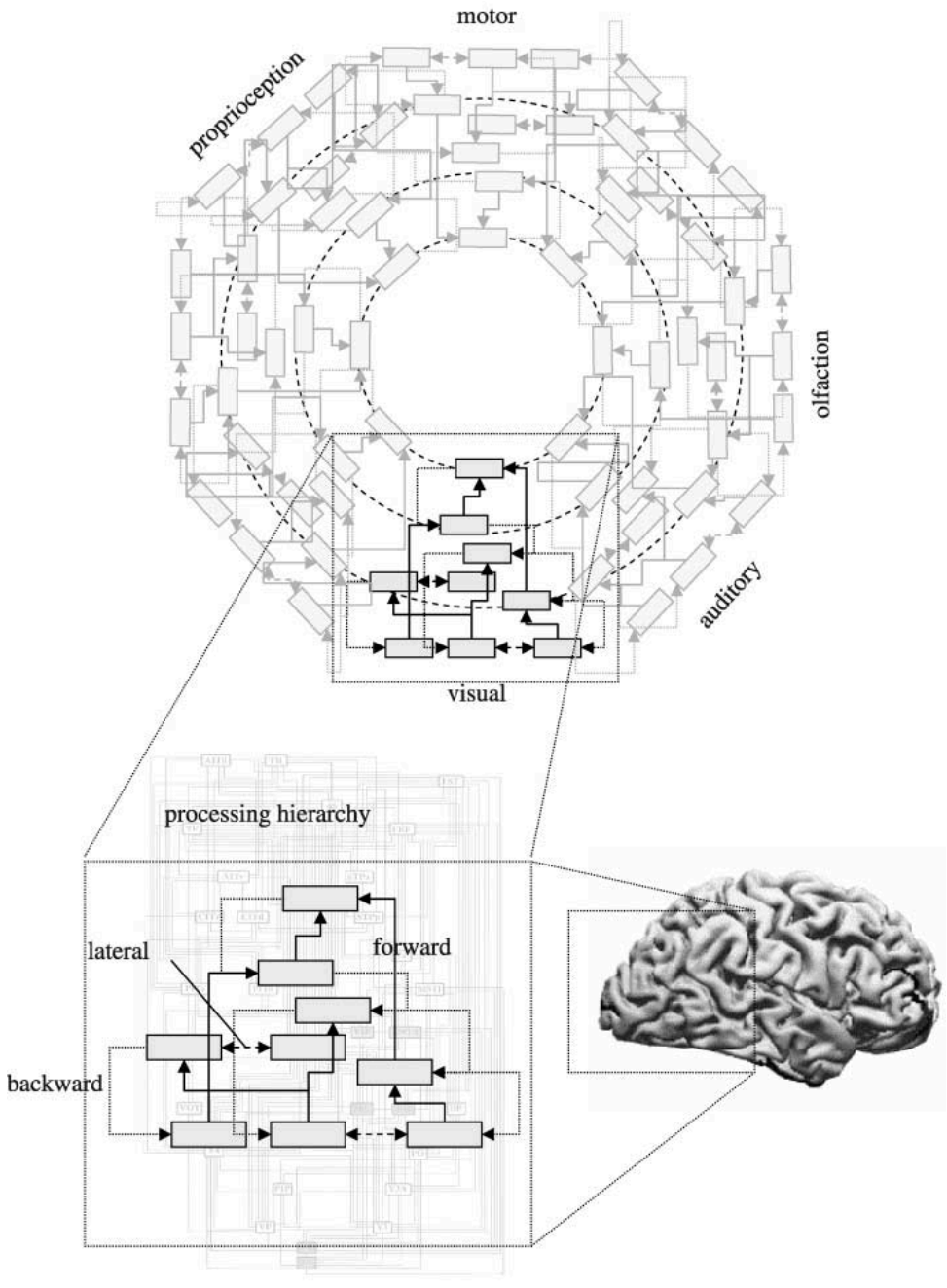

Figure 20. Hierarchical message passing in the brain. The schematic depicts hierarchical structures in the brain and the distinction between forward, backward and lateral connections. Each hierarchical level sends predictions downwards and prediction errors upwards. From Friston (2005).

Moreover, predictive coding not only describes its hypothesis in theoretical, abstract terms, but also gives a detailed description of how these operations of generation of predictions and prediction errors are implemented in the circuits of the mammalian neocortex (Mumford, 1992; Friston, 2005; Bastos et al., 2012). Supragranular layers of any sensory cortical area would contain mainly "error units", which project to higher hierarchical areas, sending upwards the prediction error signals computed at that level. These prediction errors arrive to granular layers of higher areas, just as the normal, ascending input from thalamus to primary areas (Figure 21). On the other hand, infragranular projection neurons would act as "predictive units", sending their predictions down to lower hierarchical areas. These predictions are spread in a diffuse way through layer I of the lower area, so that they can be used to cancel out the ascending input (Figure 21). Importantly, the generation of predictions and prediction errors operate in a hierarchical manner (Friston, 2005; Garrido et al., 2008; Bastos et al., 2012), so that all areas generate predictions and prediction errors, but higher-level areas generate predictions about more abstract aspects of the external world, encompassing wider spatial and temporal extensions, that are used by lower areas to generate more specific predictions about sensory inputs based on the local context.

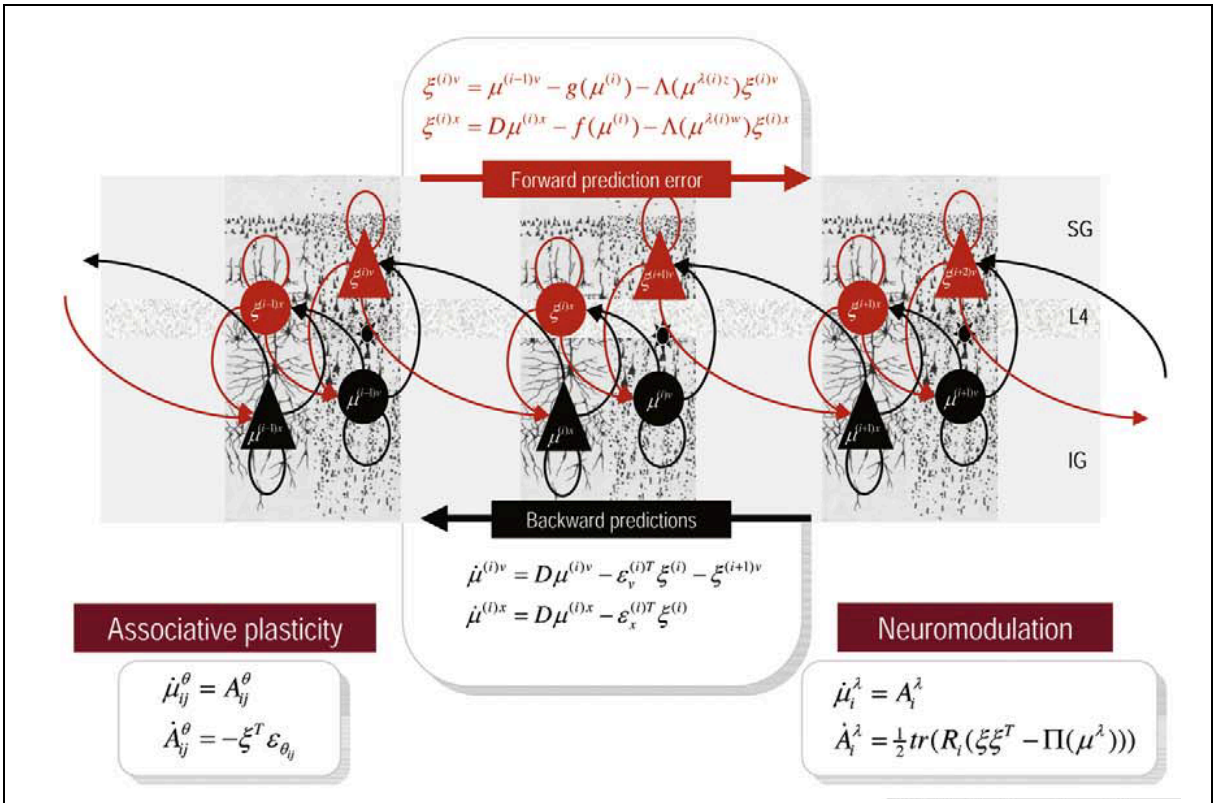

Figure 21. Neuronal architecture for predictive coding. Within each area in the processing hierarchy, the sources of forward and backward connections are superficial and deep pyramidal cells, respectively. Forward driving connections convey prediction error from a lower area to a higher area, and backward connections construct predictions. The equations represent a gradient descent on free-energy under specific hierarchical dynamic models. State units are represented in black, and error units in red. SG: supragranular layers; IG: infragranular layers. From Friston (2009).

Importantly for MMN research, predictive coding worked as a kind of unification theory, providing a model capable of reconcile the processes of adaptation and mismatch detection, making them complementary instead of mutually exclusive (Garrido et al., 2009b; Stefanics et al., 2016). Predictive coding research provided the memory trace community with a neurobiologically informed account of the MMN, which postulated memory effects in the form of predictions, and also mismatch detection signals in the form of prediction errors. Adaptation, or more generally repetition suppression, would reflect the process of model validation as more sensory evidence is observed in favor of the next prediction. Mismatch responses, on the other hand, would reflect prediction error signals relayed up the hierarchy to trigger a model adjustment process to better explain the observed inputs (Winkler et al., 1996; Summerfield et al., 2008; Garrido et al., 2009a). This dialogue between higher and lower areas continues until a consensus between predictions and the actual inputs is established (Friston, 2005).

Thus, according to the predictive coding hypothesis, two complementary processes are involved in MMN generation (Figure 22a). The first occurs when the standard tones are played, a memory trace of the recent history of stimulation is formed and used to generate predictions about upcoming inputs, which are propagated in a top-down fashion and compared against actual sensory signals. As long as they coincide, a "memory match" leads to *adaptation*, or attenuation of brain responses to repeated stimuli (Näätänen and Picton, 1987; Haenschel et al., 2005; Baldeweg, 2006; Grill-Spector et al., 2006; Summerfield et al., 2008; Summerfield and de Lange, 2014). The second occurs when a deviant stimulus is played, a prediction error signal is relayed bottom-up, and this "memory mismatch" leads to *deviance detection* or amplification of responses to unpredicted stimuli (Winkler, 2007; Garrido et al., 2009b; Winkler and Czigler, 2012; Lieder et al., 2013; Stefanics et al., 2014). Therefore, MMN generation is a dual phenomenon, and both processes (adaptation and deviance detection) are of equally importance and necessary (Schröger et al., 2014).

Moreover, this theory also explains why responses to deviants are stronger than responses to equally rare tones that are not deviants, e.g. in the context of the MAS control (Figure 22). Descending projections from one higher to a lower area come in two different types: driving and modulatory (Bastos et al., 2012). Driving projections convey the predictions as such, if there are any. Their effect on the lower area will be mainly inhibitory (through its action on GABAergic interneurons), in order to cancel out prediction error in the lower area. Modulatory projections, on the other hand, would represent the *precision* of these predictions, that is, the degree of confidence on them (Moran et al., 2013; Auksztulewicz and Friston, 2016a). If the accumulated sensory evidence strongly supports the predictions made, these modulatory projections will sensitize error units in the lower area, so that any small discrepancy with the predictions is amplified. On the other hand, if the predictions are weak, not solid, or based on scarce sensory evidence, these modulatory projections will not be very active, so that prediction errors are not amplified. And this can explain the quintessence of MMN: its dependence on the previous formation of a rule through the repetition of a pattern. When the standard is repeated over and over, the confidence that it will be repeated again increases, that is, a prediction is generated with increasing precision. Thus, when a deviant tone is received, error units are highly sensitized and the prediction error generated is amplified, producing a strong MMN (Figure 22a). However, in the context of the control condition, many different predictions are generated, but

none of them with great precision, since they are based on weak sensory evidence (Figure 22b). That is the reason why the target tone in the MAS sequence generates a prediction error (because it was unpredicted), but not very strong (because it does not break a strong prediction).

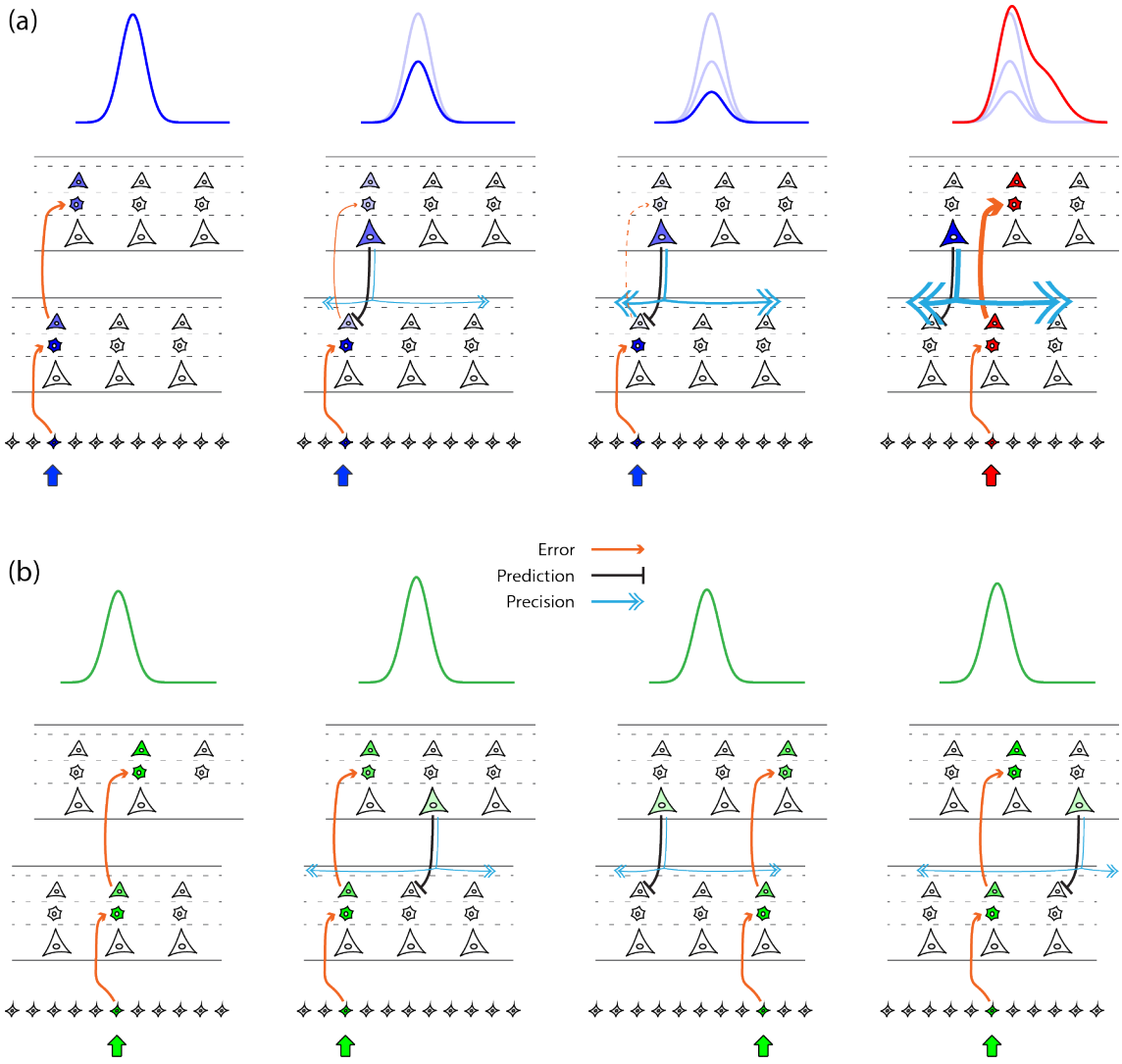

Figure 22. Predictive coding account of MMN generation. Each schematic represents two reciprocally connected areas of auditory cortex, a lower and a higher one. Granular layers receive ascending inputs, supragranular layers forward prediction errors, and infragranular layers send backward predictions (black connections) and the precision thereof (light blue connections). **(a)** As the standard tones are played, a prediction is generated with increasing precision. The prediction itself has an inhibiting effect, producing repetition suppression. The precision is a modulatory signal that will take effect only when a deviant tone is played, amplifying the prediction error generated, and thus leading to a strong MMN. **(b)** When the random tones of the many-standards control are played, predictions are weak (with low precision), and the prediction error generated by each tone is not as big as the MMN generated by the deviant.

In summary, the predictive coding framework unifies SSA and memory-trace models of MMN generation, making both complementary and equally important aspects. However, it implies the existence of active mechanisms of repetition suppression, with strong top-down influences, as opposed to mere, passive synaptic adaptation due to repeated use of the same afferents:

(a) Repetition suppression is a neuronal correlate of the memory trace formation, but at least part of it requires the formation of predictions in higher levels that are used to attenuate responses to expected inputs in lower levels.
(b) A specific enhancement of responses (error signals) occurs when the current stimulus does not match the expected input, and this requires memory and comparison processes.
(c) The subpopulation of neurons responsible for the "true" MMN or deviance detection component is the family of "error units", putatively pyramidal cells in supragranular layers. Therefore, the MMN can be considered a distinct component of the auditory ERPs.

HYPOTHESES AND OBJECTIVES

The link between the MMN and SSA was proposed fourteen years ago (Ulanovsky et al., 2003). Moreover, SSA could be a neuronal correlate of the more general theory of predictive coding (Friston, 2005; Garrido et al., 2009b). However, several issues remain, preventing the acceptance of SSA as a genuine neuronal correlate of the MMN and/or earlier mismatch brain responses (Fishman, 2014).

The first issue is a discrepancy in their anatomical location. While MMN is generated mainly within non-primary auditory cortex, SSA has only been recorded in primary auditory cortex. At the same time, in subcortical structures, it is already well established that SSA is much stronger in non-lemniscal, or non-primary subdivisions (Malmierca et al., 2009; Antunes et al., 2010; Duque et al., 2012). However, detailed studies on SSA within the different cortical fields beyond A1 were lacking. Since SSA is stronger in the non-lemnical regions of the IC and MGB, it is reasonable to hypothesize that SSA in the non-primary regions of auditory cortex would also be stronger than in A1. Indeed, previous studies on the general response properties of the auditory cortex reported that non-primary neurons in the cat (Irvine and Huebner, 1979; Schreiner and Cynader, 1984) and rat (Doron et al., 2002; Polley et al., 2007; Pandya et al., 2008) auditory cortex adapt more strongly than in A1. Even studies in human subjects have shown differential adaptation between primary and non-primary cortical areas (Kropotov et al., 2000; Jääskeläinen et al., 2004; Opitz et al., 2005). Moreover, two recent studies that mapped auditory event-related potentials in the rat showed robust MMN-like responses in non-primary auditory cortical fields (Jung et al., 2013; Shiramatsu et al., 2013).

The second issue, and even a more limiting one, is a problem of temporal development. While MMN is a mid-late response, peaking at 80-120 ms in rats, SSA in animal models has been observed only within the first 20-30 ms of neuronal responses. These discrepancies in location and latency led the discoverers of SSA to postulate that it would be a direct correlate of earlier indices of deviance detection (MLR generated in A1), only indirectly leading to the MMN within higher-order auditory areas (Nelken and Ulanovsky, 2007).

The third issue, and probably the most critical one, is of higher conceptual nature. To be considered a *bona fide* mismatch response, any brain signal must meet an important criterion: the critical comparison with an appropriate control in which the tone is presented with the same probability, but in a context in which it is not a deviant from any rule (Harms et al., 2016). Responses of single neurons to deviant tones in the oddball paradigm need to pass that critical test to be considered as genuine mismatch responses, reflecting deviance detection at the neuronal level. However, at the cellular level, mismatch responses could also arise from a simpler neurophysiological mechanism (May and Tiitinen, 2010; Fishman, 2014), namely, stimulus-specific adaptation (SSA) (Ulanovsky et al., 2003), or response decrement with stimulus repetition (Whitmire and Stanley, 2016) that leaves neuronal responses to different stimuli—e.g. the deviant—almost unaffected.

Finally, neuronal responses to oddball stimulation could perform deviance detection under the principles of predictive coding. If that is true, prediction errors should increase from lower

to higher hierarchical levels. Yet, whereas it is now clear that large-scale mismatch responses to oddball stimulation indeed reflect the predictive activity of the auditory and other sensory systems (Stefanics et al., 2014; Phillips et al., 2016), even at early processing stages (Bendixen et al., 2012) including subcortical midbrain and thalamus (Escera and Malmierca, 2014), and also in animal models (Shiramatsu et al., 2013; Todd et al., 2013; Harms et al., 2015), this predictive activity remains to be demonstrated at the neuronal level.

Therefore, as the main driver of this research, I hypothesize that:

1. ***SSA, defined as a differential response to deviants and standards under oddball stimulation, will be found in non-primary auditory cortical areas, and indeed, it will be stronger there than in primary auditory cortex.***
2. ***Neuronal responses within non-primary areas will have longer latencies and durations, so that SSA will be present in these non-primary areas at longer response latencies, matching better the time range of the actual MMN.***
3. ***Responses of single neurons to deviant tones in the oddball paradigm reflect deviance detection, in addition to just SSA, and thus can be considered genuine mismatch responses.***
4. ***Enhanced responses to deviant tones represent neuronal prediction error, which will increase from lower to higher hierarchical levels of the auditory pathway as postulated by the hierarchical predictive coding framework.***

Thus, the main objective of this thesis is to validate SSA (or more rigorously speaking, neuronal responses to the oddball paradigm) as a neuronal correlate of the MMN, underlying deviance detection at the cellular level. More specifically, to test the previous hypotheses, I will set the following objectives:

1. Create a physiological map of SSA throughout the auditory cortex of the rat, to detect any principle of organization of SSA in gradients or metagradients (Polley et al., 2007). Critically, the mapping must include all primary as well as non-primary fields of the rat auditory cortex, which are already well described and easy to delineate physiologically (Rutkowski et al., 2003; Polley et al., 2007; Profant et al., 2013). This will complete the picture of SSA in the auditory pathway (Figure 17).
2. Investigate the level of SSA throughout the different time ranges of neuronal responses, especially within non-primary fields, where evoked responses to sound are expected to be of longer latency and duration (Schreiner and Cynader, 1984; Polley et al., 2007). Analyze any significant variation of SSA level throughout the neuronal responses from onset to offset.
3. Probe neuronal responses to the oddball paradigm for genuine deviance detection, using the many-standards and cascadic controls for repetition effects (Ruhnau et al., 2012). Use responses to the control condition to decompose neuronal responses into "Repetition Suppression" and "Prediction Error".
4. Perform these recordings within all the main stations of the auditory pathway where SSA has been investigated previously, both at cortical and subcortical levels, and study any systematic progression of prediction error along the auditory hierarchy.

Objectives 1 and 2 will be addressed in study I, through the creation of physiological maps of SSA throughout the auditory cortex. This will require the use of a simple oddball paradigm and multi-unit recordings. Objectives 3 and 4 are more ambitious, and will be the focus of study II, requiring the use of the many-standards and cascadic controls, in addition to the oddball paradigm, and careful recordings of well-isolated single units from different nuclei of the auditory pathway. This is a colossal work that will likely require the collaboration of other members of the lab for the collection of large amounts of data.

MATERIALS AND METHODS

Experimental Design

In Study 1, Multiunit activity (MUA) was recorded with self-manufactured glass-coated tungsten electrodes (1–5 MΩ impedance at 1 kHz) (Merrill and Ainsworth, 1972; Bullock et al., 1988; Ayala et al., 2016). A single electrode was positioned orthogonal to the pial surface (forming a 30º angle with the horizontal plane) and advanced 350–550 μm into the thalamorecipient layers IIIb–IV using a piezoelectric micromanipulator (Sensapex) until we observed a strong spiking activity synchronized with the train of searching stimuli. Once a suitable recording site was reached, the frequency response area (FRA) was determined using 75 ms pure tones at varying frequencies and intensities (Figure 24A; 0.5–44 kHz logarithmically spaced at 0.25 octave steps, 0–70 dB SPL at 10 dB steps, 375 ms onset-to-onset interval, 1 to 3 randomized repetitions of each stimulus). The FRA was displayed on a computer screen using custom software, and the frequency-tuning curve was automatically outlined as the minimum sound intensity that elicited a firing rate over 20–40% of the maximum firing for each frequency. Thus, the minimum response threshold and characteristic frequency (CF) were computed for each site (excluding isolated "islands" of spontaneous activity), and a two frequencies (f_1, f_2) were selected to use in the oddball paradigm (Ulanovsky et al., 2003) at 20–30 dB above threshold. The two stimuli were selected so as to evoke strong responses of similar magnitude at that recording site. In some cases, one or more extra pairs of stimuli were selected to ensure at least one recording met this requirement. Two oddball sequences with fixed parameters (250 trials each, 75 ms stimulus duration, 0.5 octaves frequency separation, 10% deviant probability, 300 ms onset-to-onset interval, minimum of 3 standard tones before a deviant) were presented for every pair of stimuli thus selected. In one of the sequences the low frequency (f_1) was the "standard" and the high frequency (f_2) was the "deviant", and in the other sequence their roles were swapped. The order of presentation of these two sequences was randomized across sites.

The goal of Study 2 was to test responses of single neurons of the central auditory system of the rat for signs of predictive activity under oddball stimulation. We recorded extracellular single neuron activity in response to sinusoidal tones in different auditory centers of the rat brain (Figure 32A,B). Rats were deeply anesthetized prior to surgery preparation and during the whole recording session. One single neuron (or small cluster of neurons in Study 1) was recorded at a time, using one tungsten electrode inserted into the brain, and local field potential (LFP) activity was simultaneously recorded from the same electrode. Surgical, electrophysiological and histological procedures are detailed below.

All stimuli presented were sinusoidal pure tones of 75 ms duration, including 5 ms raise/fall ramps. For each recorded neuron, the frequency-response area (FRA) was first computed, as the map of response magnitude for each frequency/intensity combination (Figure 33). To obtain this FRA, a randomized sequence of tones was presented at a 4 Hz rate, randomly varying frequency and intensity of the presented tones (3-5 repetitions of all tones). Then, we selected 10 evenly-spaced tones (0.5 octave separation) at a fixed sound intensity (usually 20-30 dB

above minimal response threshold), so that at least two of them fell within the FRA or close to its limits (see Figure 32C and Figure 33). These 10 frequencies were used to create the control sequences shown in Figure 32C. Additionally, adjacent pairs of them were used to present different oddball sequences. All sequences were 400 tones in length, at the same, constant presentation rate of 3 Hz (for AC) or 4 Hz (for IC and MGB). A faster presentation rate was used for subcortical recordings, to compensate for the relative slowing down of preferred repetition rates from brainstem to cortex (Eggermont, 2014).

To test the specific contribution of deviance to the neuronal responses, we used oddball sequences (Ulanovsky et al., 2003; Dehaene et al., 2015) (Figure 32C). An oddball sequence consisted of a repetitive tone (the standard), occasionally replaced by a different tone (the deviant), with a p=0.1 probability, in a pseudorandom fashion. The first 10 tones of the sequence were always the standard tone, and a minimum of 3 standard tones always preceded each deviant. Oddball sequences were either ascending or descending, depending on whether the deviant was of a higher or lower frequency than the standard, respectively (Figure 32C). To control for the overall presentation rate of the target tone, as it reduces neuronal responses at high rates, we used two different control sequences, namely, the many-standards and cascaded sequences (Taaseh et al., 2011; Ruhnau et al., 2012) (Figure 32C). The many-standards control sequence was a random presentation of the 10 selected tones, such that each of them appeared the same number of times in an unpredictable order, with the only constraint that a single tone was never repeated in a row. Two cascaded control sequences, ascending and descending, were built as a repetitive series of groups of the 10 tones, arranged by ascending/descending frequency, respectively (Figure 32C). Since all sequences were 400 stimuli long, at the same presentation rate, a tone appeared with the same overall presentation rate in the DEV, MAS and CAS conditions, a total of 40 times along the 400-stimuli sequence. The cascaded sequence was recently designed as an improvement to the many-standards, that controls for additional key factors beyond presentation rate of the deviant tone (Ruhnau et al., 2012; Harms et al., 2014). First, the tone immediately preceding a deviant is the same in the oddball (a standard) and cascaded sequences. This improves the estimation of the overall adaptation state of the system by the time the deviant tone is played, and controls for the potential sensitivity of the neuron to a rise or fall in frequency between two successive tones. Second, the cascaded sequence mimics the regular structure of the oddball sequence, with the important difference that now the target tone *conforms* to the rule, instead of being a deviant.

Thus, using this design, every tone presented as a deviant was also presented as a standard (in a different oddball sequence) and in the context of the many-standards and cascaded control sequences. These four conditions, and by extension also response measures to them, will be denoted DEV, STD, MAS and CAS, respectively. Note that there were two variants of the DEV condition (ascending/descending), which were compared with the corresponding ascending/descending CAS condition. The STD condition was averaged, for each frequency, across ascending/descending versions of the oddball sequence (as indicated in Figure 32C). The order of presentation of these sequences was randomized across neurons, with a silent pause of ~30 seconds between sequences. If the neuron could be held for long enough, the same protocol was repeated at different sound intensities.

Surgical procedures

Experiments were performed on 48 adult, female Long-Evans rats (12 in Study 1 and 36 in Study 2) with body weights between 200–250 g. The experimental protocols were approved by, and used methods conforming to the standards of, the University of Salamanca Animal Care Committee and the European Union (Directive 2010/63/EU) for the use of animals in neuroscience research. Each individual animal was used to record from only one auditory station, either IC, MGB or AC. The initial surgical procedures were identical in each case, and the electrophysiological procedures differed only in the location of the craniotomy, and placement/orientation of the recording electrode, for each different station.

Surgical anesthesia was induced and maintained with urethane (1.5 g/kg, i.p.), with supplementary doses (0.5 g/kg, i.p.) given as needed. Dexamethasone (0.25 mg/kg) and atropine sulfate (0.1 mg/kg) were administered at the beginning of the surgery and every 10 h thereafter to reduce brain edema and the viscosity of bronchial secretions, respectively. After the animal reached a surgical plane of anesthesia, the trachea was cannulated for artificial ventilation and a cisternal drain was introduced to prevent brain hernia. The animal was then placed in a stereotaxic frame in which the ear bars were replaced by hollow specula that accommodated a sound delivery system. Corneal and hind-paw withdrawal reflexes were monitored to ensure that a moderately deep anesthetic plane was maintained as uniformly as possible throughout the recording procedure. Isotonic glucosaline solution was administered periodically (5–10 ml every 6–8 hours, s.c.) throughout the experiment to prevent dehydration. Body temperature was monitored with a rectal probe and maintained between 37–38°C with a homoeothermic blanket system (Cibertec).

For IC and MGB recordings, a craniotomy was performed in the left parietal bone to expose the cerebral cortex overlying the left IC/MGB. The dura was removed, and the electrode was advanced with an angle of 20º for the IC, and in a vertical direction for the MGB. For AC recordings, the skin and temporal muscles over the left side of the skull were reflected and a 6×5 mm craniotomy was made in the left temporal bone to expose the entire auditory cortex (see Figure 1 in ref. (Nieto-Diego and Malmierca, 2016)). The dura was removed and the exposed cortex and surrounding area were covered with a transparent layer of agar to prevent desiccation and to stabilize the recordings. The electrode was positioned orthogonal to the pial surface, forming a 30º angle with the horizontal plane, to penetrate through all the cortical layers of one same cortical column.

Electrophysiological recording procedures

Experiments were performed inside a sound-insulated and electrically-shielded chamber. All sounds were generated using an RX6 Multifunction Processor (TDT) and delivered monaurally (to the right ear) in a closed system through a Beyer DT-770 earphone (0.1–45 kHz) fitted with a custom-made cone and coupled to a small tube (12 gauge hypodermic) sealed in the ear. The sound system response was flattened with a finite impulse response (FIR) filter, and the output of the system was calibrated in situ using a ¼-inch condenser microphone (model 4136, Brüel & Kjær), a conditioning amplifier (Nexus, Brüel & Kjær) and a dynamic signal analyzer (Photon+, Brüel & Kjær). The output of the system had a flat spectrum at 76 dB

SPL (±3 dB) between 500 Hz and 45 kHz, and the second and third harmonic components in the signal were ≤ 40 dB below the level of the fundamental at the highest output level (90 dB SPL). Prior to surgery and recording sessions, we recorded auditory brainstem responses (ABR) with subcutaneous electrodes to ensure the animal had normal hearing. ABRs were collected using TDT software (BioSig) and hardware (RX6 Multifunction Processor) following standard procedures (0.1 ms clicks presented at a 21/s rate, delivered in 10 dB ascending steps from 10 to 90 dB SPL).

Action potentials and local field potentials (LFP) were recorded with hand-manufactured, glass-coated tungsten electrodes (Bullock et al., 1988) (1–4 MΩ impedance at 1 kHz). One individual electrode was used to record one single neuron at a time. The electrode was advanced using a piezoelectric micromanipulator (Sensapex) until we observed a strong spiking activity synchronized with the train of searching stimuli. The signal was amplified (1000×) and band-pass filtered (1 Hz to 3 kHz) with an alternate current differential amplifier (DAM-80, WPI). This analog signal was digitized at a 12K sampling rate and further band-pass filtered (with a second TDT-RX6 module) separately for action potentials (between 500 Hz and 3 kHz) and LFP (between 3 and 50 Hz). Stimulus generation and neuronal response processing and visualization were controlled online with custom software created with the OpenEx suite (TDT) and Matlab (Mathworks). A unilateral threshold for automatic action potential detection was manually set at about 2–3 standard deviations of the background noise. Spike waveforms were displayed on the screen, and overlapped on each other in a pile-plot to facilitate isolation of single units. Only when all snippet waveforms were identical and clearly separable form other smaller units and the background noise, the recorded action potentials were considered to belong to a single unit.

Sounds used for stimulation were white noise bursts or pure tones with 5 ms rise-fall ramps. Sounds used for searching for neuronal activity were trains of noise bursts or pure tones (1–8 stimulus per second). We used short stimulus duration for searching (30 ms) to prevent strong adaptation. In addition, type (white noise, narrowband noise, pure tone) and parameters (frequency, intensity, presentation rate) of the search stimuli were varied manually when necessary to facilitate release from adaptation, and thus prevent overlooking responses with high SSA. Once a single neuron was isolated and confirmed to be stable, the whole stimulation protocol was applied, as described in the first section "Experimental Design".

Histological procedures and anatomical localization of recording sites

AC experiments. At the end of the surgery, a magnified picture (25×) of the exposed cortex was taken (Nieto-Diego and Malmierca, 2016) with a digital SLR camera (D5100, Nikon) coupled to the surgical microscope (Zeiss) through a lens adapter (TTI Medical). The picture included a pair of reference points previously marked on the dorsal ridge of the temporal bone, indicating the absolute scale and position of the image with respect to bregma. This picture was displayed on a computer screen and a micrometric grid was overlapped to guide and mark the placement of the electrode for every recording made. Recording sites (250–500 μm spacing) were evenly distributed across the cortical region of interest while avoiding blood vessels. The vascular pattern was used as a local reference to mark the position of every recording site in the

picture, but otherwise differed largely between animals. To confirm the actual depth and cortical layer of the recorded neurons, at the end of the experiment we made electrolytic lesions at one to four of the recording sites, at the same depth that recordings were made. Five auditory cortical fields were identified according to tone frequency response topographies (Nieto-Diego and Malmierca, 2016). The limits and relative position of the auditory fields were determined for each animal at the end of the experiment, using the characteristic frequency (CF; the tone frequency that elicits a significant neuronal response at the lowest intensity) gradient as the main reference landmark (Polley et al., 2007; Nieto-Diego and Malmierca, 2016). We consistently observed distinct tonotopic gradients within the different fields, with a high-frequency reversal between VAF and AAF (rostrally), a low-frequency reversal between A1 and PAF (dorsocaudally) and a high-frequency reversal between VAF and SRAF (ventrally). We identified the boundary between A1 and VAF as a 90° shift in the CF gradient in the ventral low-frequency border of A1, and the boundary between A1 and AAF as an absence of tone-evoked responses in the ventral, high-frequency border of A1 (Nieto-Diego and Malmierca, 2016). We used these boundaries to assign each recording to a given field. The CF of each recording track was computed as the average CF of all neurons recorded in that track, including a fast multi-unit activity FRA recording made between 400-550 μm depth, corresponding to layers IIIb-IV of the auditory cortex.

IC and MGB experiments. Each recording track was marked with electrolytic lesions for subsequent histological localization of the neurons recorded. At the end of the experiment, the animal was given a lethal dose of sodium pentobarbital and perfused transcardially with phosphate buffered saline (0.5% $NaNO_3$ in PBS) followed by fixative (a mixture of 1% paraformaldehyde and 1% glutaraldehyde in rat Ringer's solution). After fixation and dissection, the brain tissue was cryoprotected in 30% sucrose and sectioned on a freezing microtome in the transverse or sagittal planes into 40 mm-thick sections. Sections were Nissl stained with 0.1% cresyl violet to facilitate identification of cytoarchitectural boundaries. Recording sites were marked on standard sections from a rat brain atlas (Paxinos and Watson, 6th Edition) and neurons were assigned to one of the main divisions of the IC (central nucleus, dorsal, lateral or rostral cortex) or the MGB (ventral, dorsal and medial division), respectively. The stained sections with the lesions were used to localize each track mediolaterally, dorsoventrally and rostrocaudally in the Paxinos atlas. To determine the main IC or MGB subdivisions, cytoarchitectonic criteria, i.e., cell shape and size, Nissl staining patterns and cell packing density, were used. This information was complemented and confirmed by the stereotaxic coordinates used during the experiment to localize the IC/MGB. After assigning a section to each track/lesion, the electrophysiological coordinates from each experiment and recording unit, i.e., beginning and end of the IC/MGB, as well as the depth of the neuron, were used as complementary references to localize each neuron within a track.

Statistical Analysis

All data analyses were performed with the Matlab^{TM} software, using the built-in functions, the Statistics and Machine Learning toolbox, or custom scripts and functions developed in our laboratory. Peri-stimulus time histograms (PSTH) were generated for every stimulus/condition tested. Only the last standard tones preceding each deviant were used for the analyses, except for

the time course analysis, where all standard trials were analyzed. Every PSTH was analyzed to test for significant auditory responses and to extract several different metrics of response strength and latency. For these analyses, the original PSTH was smoothed with a 6 ms gaussian kernel ("ksdensity" function in Matlab) in 1 ms steps to estimate the spike-density function (SDF) over time, and the baseline spontaneous firing rate (SFR) was determined as the average firing rate during the 75 ms preceding stimulus onset. For any given time window, the excitatory response was measured as the area below the SDF and above the baseline SFR. This measure will be referred to as "baseline-corrected spike count" (BCSC). To test for statistical significance of the BCSC we used a Monte Carlo approach. First, 1000 simulated PSTHs were generated using a Poisson model with a constant firing rate equal to the SFR. Then, a "null distribution" of BCSC was generated from this collection of PSTHs, following these same steps. Finally, the p-value of the original BCSC was empirically computed as $p = (g + 1) / (N + 1)$, where g is the count of "null" measures greater than or equal to BCSC and $N = 1000$ is the size of the "null" sample. Note that using this approach, the minimum p-value that can be obtained is $1/1001 \approx 0.001$.

When a significant evoked activity was detected, onset and offset latencies of the whole excitatory response were computed as follows. First, a "noise" threshold was computed, as the firing rate below which the pure-spontaneous simulated SDFs remained 97.5% of the time. Every SDF, including the simulated ones, was scanned for stretches of "signal" above this threshold, and the amount of "signal" for each stretch was measured as the area below the SDF and above the SFR during that particular interval. Using the distribution of all the signal stretches thus found within the 1000 pure-spontaneous SDFs, a Monte Carlo test was used to compute empirical p-values for every stretch of signal found in the target SDF under study. For each significant signal stretch ($p < 0.05$), the start/end times (T_{on}, T_{off}) were determined as the time points when the SDF trace cuts the noise threshold, and onset/offset latencies of the whole excitatory response (*ONSET*, *OFFSET*) were defined as the T_{on}/T_{off} of the first/last significant excitatory component of the response, respectively. Peak firing rate amplitude was defined as the maximum firing rate reached by the SDF within the analysis window, minus the SFR baseline, and peak latency as the time point respect stimulus onset that this peak takes place. Finally, the duration of the whole significant response interval was defined as *OFFSET* – *ONSET*, and the duration of the strong peak of the response, or "half-peak response duration", was measured as the total length of time that the SDF remains above 50% of the peak amplitude.

Study 1. In order to quantify and compare SSA levels between the five fields, we computed the frequency-specific SSA index for each stimulus, SI(f_1) and SI(f_2), and the common SSA index (CSI) for every recording site, in the usual way (Ulanovsky et al., 2003):

$$SI(f_i) = \frac{DEV(f_i) - STD(f_i)}{DEV(f_i) + STD(f_i)}\,; \qquad i = 1,2$$

$$CSI = \frac{\sum DEV(f_i) - \sum STD(f_i)}{\sum DEV(f_i) + \sum STD(f_i)}\,; \quad i = 1,2$$

where $DEV(f_i)$, $STD(f_i)$ are baseline-corrected spike counts in response to frequency f_i when it was a deviant and standard, respectively. The CSI was calculated only for recordings with significant auditory responses to at least one frequency in the oddball paradigm (either as deviant or as standard). In cases where more than one stimulus pair was tested at the same recording site, we selected only one to compute SSA for that site, according to the following criteria: (1) Recordings with significant responses to both frequencies (either as deviant or as standard) were always preferred to recordings with significant response to only one of them. (2) We selected the recording with most similar responses to f_1 and f_2 (as deviants); the similarity between responses was measured as their ratio, f_1/f_2 or f_2/f_1, whichever was less than 1. (3) If there were two or more recordings with similar deviant-to-deviant ratios (difference of ratios < 0.1), we selected the one with the lowest sound level (SPL) used for stimulation.

For the analysis of the LFP signal, we aligned the recorded wave to the onset of the stimulus for every trial, and computed the mean LFP for every recording site and stimulus condition (deviant, standard), as well as the difference wave (DW = deviant – standard). Then, grand-averages were computed for deviant, standard and DW across the whole auditory cortex and for every field separately. The p-value of the grand-averaged DW was determined for every time point with a two-tailed t-test, Bonferroni-corrected for 204 comparisons (overall significance level of 0.05), and the time intervals where a significant DW was observed were computed. For each individual (mean) LFP wave, the peak amplitude and latency were computed within two time windows: [10–40 ms] and [50–90 ms], corresponding to the first negative deflection (Nd) and second positive deflection (Pd) seen in the grand-averages within all fields. When comparing response features between fields, such as onset latency or CSI, we used non-parametric Kruskall-Wallis or Friedman tests, given the non-normal nature of these measures. Each of these tests was followed by a post-hoc multiple comparison test, using the Dunn-Sidak method at a 5% significance level, to detect specific differences between fields. For the sake of readability, p-values for all tests are reported using an upper bound equal to the minimum power of ten or half a power of ten that is greater than the actual p-value (*e.g.*, $p < 5 \cdot 10^{-6}$).

For the time course analysis, we first computed the average standard and deviant response at each absolute position within the sequence, for all neurons tested, within each cortical field separately. A single-trial spike count for any given PSTH was computed as the number of spikes between the previously determined *ONSET* and *OFFSET* times, minus the baseline SFR. Then, we fitted these time series to different models (linear, exponential, double exponential, polynomial inverse and power law with two or three coefficients) using the "fit" function in Matlab, that also computes the coefficient of determination (adjusted-r^2) of the whole fit and confidence intervals for the fitted parameters.

To quantify the topographical organization of a feature map and test for statistical significance thereof, we used the "MapTools" library in Matlab, applying the topographic product statistic (Yarrow et al., 2014). This metric was used instead of other alternatives (Pearson and Spearman linear correlation, Zrehen measure, etc) due to the highly non-normal nature of the data under study (*i.e.*, CSI) and assuming a local, linear nature of the topography of the CSI. To generate averaged maps for CF, CSI and other response features, we followed a spotlight-average approach: starting with the set of sample points where actual recordings were

made, and the associated values of the feature, we computed the averaged feature value for any other point in the map from its nearest neighbors. Specifically, we placed a bivariate Gaussian kernel of 100 μm radius:

$$\ker(x, y) = \frac{1}{2\pi r} \cdot \exp\left\{\frac{\sqrt{x^2 + y^2}}{2r^2}\right\}$$

centered on every sample point and multiplied it by its associated feature value. Then we summed all these functions over the entire map and divided the result by the sum of all kernels at every point, to compute a weighted average throughout the whole surface. Thus, the feature value *V* at every point of the map was calculated as:

$$\mathrm{V}(\mathrm{x}, \mathrm{y}) = \frac{\sum_{\mathrm{i}=0}^{\mathrm{n}} \mathrm{v_i} \cdot \ker(\mathrm{x} - \mathrm{x_i}, \mathrm{y} - \mathrm{y_i})}{\sum_{\mathrm{i}=0}^{\mathrm{n}} \ker(\mathrm{x} - \mathrm{x_i}, \mathrm{y} - \mathrm{y_i})}$$

where x, y are the coordinates of a generic point in the map, and x_i, y_i (i = 1, …, n) are the sample points used to generate the map. To impose a limit on the influence span for every point, this weighted average was computed only for points where the sum of all kernels (denominator in the last formula) was greater than 0.05. Further, to avoid single-point averages, we computed *V(x,y)* only when at least 2 neighboring sample points had been used for averaging.

To combine data from different animals, we followed an iterative process to improve the quality of the alignment in successive stages. We first generated the CF map for the case with the greatest number of recordings (shown in Figure 23). Then, we applied a manual shift to each of the remaining maps in turn so as to put them into register with the former. We used the CF gradient, the "unresponsive spot" at the wedge between A1, AAF and VAF and the low-frequency centers in A1, AAF and SRAF, as main references to determine, for each animal, the absolute position of the map with respect to bregma (Polley et al., 2007). Finally, we computed the topographic product statistic for the whole set of aligned recordings. This alignment was refined and the test statistic was recalculated until no improvement was detected in the correlation. We repeated this process for every animal until the alignment was completed.

Study 2. Peri-stimulus time histograms (PSTH) were generated for each stimulus/condition tested, and analyzed as explained above. Only the last STD tones preceding each DEV tone were used for the analyses. We used two types of sequences to control for repetition effects (*v.s. Experimental Design*), namely the many-standards and cascaded sequences (Figure 32D). However, only one of them is required to decompose neuronal mismatch into repetition suppression and prediction error (Figure 32D). In the following, we describe the analysis performed using the CAS condition as control, since the analysis using the MAS sequence is completely analogous. Baseline-corrected spike count responses of a neuron to the same tone in the three conditions (DEV, STD, CAS) were normalized using the formulas:

DEV_N = DEV/N;

STD_N = STD/N;

$CAS_N = CAS/N;$

Where

$N = \sqrt{DEV^2 + STD^2 + CAS^2}$

is the Euclidean norm of the vector (DEV, STD, CAS) defined by the three responses. This normalization procedure always results in a value ranging 0 to 1, and has a straightforward geometrical interpretation (Figure 34B,H): Normalized values are the coordinates of a 3D unit vector (DEV_N, STD_N, CAS_N) with the same direction of the original vector (DEV, STD, CAS), and thus the same proportions between the three response measures. From these normalized responses, indices of neuronal mismatch (iMM), repetition suppression (iRS), and prediction error (iPE) were computed as:

iMM = $DEV_N - STD_N$,

iRS = $CAS_N - STD_N$,

iPE = $DEV_N - CAS_N$,

These indices, consequently, always range between -1 and 1, and provide the following quantitative decomposition of neuronal mismatch (Figure 32D) into repetition suppression and prediction error:

iMM = iRS + iPE

As shown in Figure 37, the iMM is largely equivalent to the typical SI, or "SSA index" (*v.s.*), commonly used in most previous studies of SSA in single units (Ulanovsky et al., 2003; Taaseh et al., 2011).

For the analysis of the LFP signal, we aligned the recorded wave to the onset of the stimulus for every trial, and computed the mean LFP for every recording site and stimulus condition (DEV, STD, CAS), as well as the "prediction error potential" (PEP = $LFP_{DEV} - LFP_{CAS}$). Then, grand-averages were computed for all conditions, for each auditory station separately. The p-value of the grand-averaged PEP was determined for every time point with a two-tailed t-test (Bonferroni-corrected for 200 comparisons, with family-wise error rate FWER<0.05), and we computed the time intervals where PEP was significantly different from zero (Figure 36).

All statistical tests used were distribution-free tests (or "nonparametric", namely the Wilcoxon signed-rank test and Friedman test), given the non-normal nature of our dataset (baseline-corrected spike counts, normalized responses, indices of neuronal mismatch, repetition suppression and prediction error). Only the difference wave for the LFPs (PEP in Figure 36) was tested using a t-test, since each LFP trace is itself an average of 40 waves, and thus approximately normal (according to the Central Limit Theorem). Linear models used to test significant average iPE within each auditory station (Figure 35B,D) and significant effects of *nucleus*, *hierarchy*, *SPL*, *direction*, and interactions between them, were fitted using the 'fitlm' function in Matlab, with robust options.

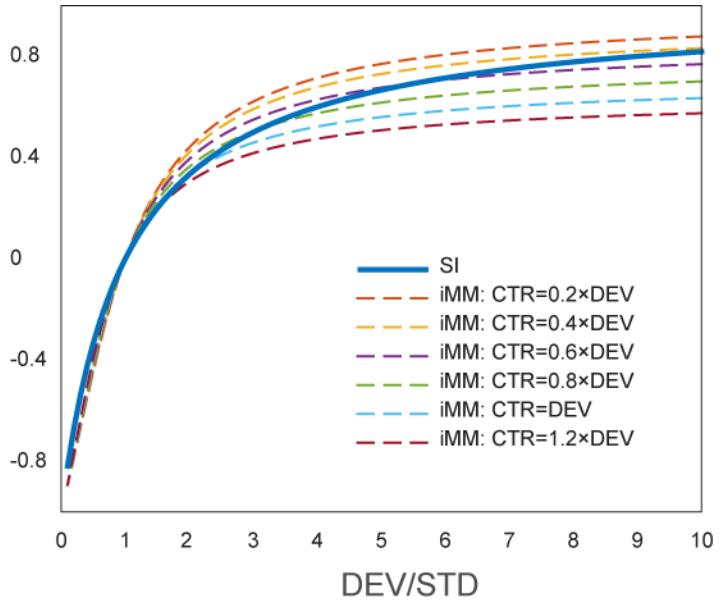

Figure 37: Quantitative comparison between iMM and the "classical" SI. The SI trace is plotted as a function of the DEV/STD ratio, since it does not take into account the control condition. Different iMM traces are plotted (dashed lines), as a function of the relative magnitude of the response to control condition with respect to DEV response (CTR/DEV), from low (CTR=0.2*DEV) to high (CTR=1.2*DEV) hypothetical responses to the control. The two indices (the SI and the iMM for different CTR response magnitudes) take values very close to each other under most conditions, except for very extreme and rare cases in which the response to the control condition is much larger than DEV of much smaller than STD.

RESULTS

STUDY 1: TOPOGRAPHIC DISTRIBUTION OF SSA IN THE AUDITORY CORTEX

The main goal of Study 1 was to generate a complete and fine-grained map of SSA across all known cortical fields in the rat. Despite interspecies differences, the rat auditory cortex shares many common anatomical and physiological features with other species (Takahashi et al., 2005; Polley et al., 2007; Smith et al., 2012), including primary and non-primary regions. Detailed electrophysiological mapping studies (Polley et al., 2007; Pandya et al., 2008; Profant et al., 2013) have identified at least five tonotopically organized fields in the rat auditory cortex. The primary auditory cortex (A1), the anterior auditory field (AAF) and the ventral auditory field (VAF) are all considered primary fields (Polley et al., 2007; Storace et al., 2012). Additionally, two distinct non-primary regions have been identified, the posterior auditory field (PAF), located in the dorso-caudal border of A1, and the suprarhinal auditory field (SRAF), in the ventral margin of the auditory cortex (Kimura et al., 2004, 2007; Polley et al., 2007; Smith et al., 2012). My results demonstrate that, although SSA is indeed present in A1 and the other two primary fields, it is markedly stronger in the non-primary fields PAF and SRAF, consistent with the SSA observed in non-lemniscal parts of the IC and MGB. Another important finding in these data is that SSA observed in auditory cortex is robust up to 200 ms after stimulus onset, well within the latency range of the MMN-like potentials in the rat (Harms et al., 2015). These data suggest the existence of a hierarchically organized system for SSA processing (Grimm and Escera, 2012), and reinforce the notion that non-primary SSA is a more direct neural correlate of the MMN than the SSA observed in A1.

To study the topographic distribution of SSA across the auditory cortex I recorded a total of 816 multiunit activity (MUA) clusters from layers IIIb/IV within all cortical fields from the left auditory cortex in 12 animals (total number of recordings by field: A1, 167; AAF, 121; VAF, 164; SRAF, 169; PAF, 119). Local field potentials (LFP) were simultaneously recorded from the same electrode in 4 of the animals. In each animal I made a microelectrode mapping (15–25 tracks/mm^2) covering at least three fields (Figure 23A shows an example with 132 recording sites from all fields). Most recordings (89%) were made between 300 and 600 μm depth, corresponding to cortical layers IIIb/IV (Smith et al., 2012). Five auditory cortical fields were identified according to tone frequency response topographies. The limits and relative position of the auditory fields were determined for each animal at the end of the experiment, using the characteristic frequency (CF) gradient as the main reference landmark (Figure 23B). I consistently observed distinct tonotopic gradients within the different fields (Polley et al., 2007; Higgins et al., 2010; Profant et al., 2013), with a high-frequency reversal between VAF and AAF (rostrally), a low-frequency reversal between A1 and PAF (dorsocaudally) and a high-frequency reversal between VAF and SRAF (ventrally). Thus, I identified the boundary between A1 and VAF as a 90° shift in the CF gradient in the ventral low-frequency border of A1, and the boundary between A1 and AAF as an absence of tone-evoked responses in the ventral, high-frequency border of A1 (Figure 23B). I used these boundaries to assign each recording to a given field.

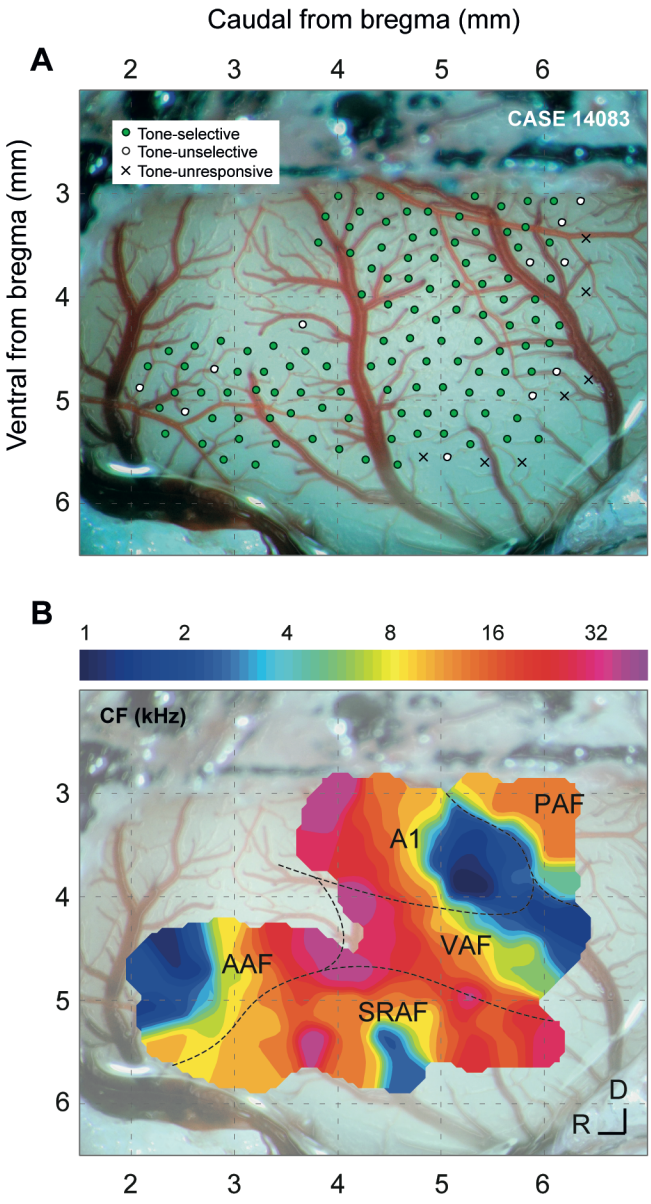

Figure 23. Experimental setup. A. Sample case with 132 MUA recording sites from layers IIIb/IV throughout the cortical fields in one representative animal. At every site, the CF was determined (if possible) and I presented an oddball paradigm. Sites are classified according to pure-tone selectivity (Selective: tone-responsive with a clear CF; Unselective: tone-responsive, but with an unstructured FRA or otherwise lack of a clear CF; Unresponsive: no significant responses to pure tones). **B.** Outline of the different cortical fields in this particular case, as derived from the tonotopic gradients. Each field shows a characteristic CF gradient (Polley et al., 2007), A1 being the most easily identifiable.

At every recording site, I presented an oddball paradigm (two sequences of 250 trials, 10% deviants, 300 ms onset-to-onset interval, 0.5 octaves frequency separation) using a pair of pure tones at 20–30 dB above CF threshold, which elicited clear responses of similar magnitude. Figure 24 shows representative MUA recordings from each auditory cortex field. Figure 24A

shows their FRAs and the pair of stimuli f_1 and f_2 selected for the oddball paradigm, and Figure 24B shows comparative responses to each frequency when presented as either standard (blue) or deviant (red) in the oddball paradigm.

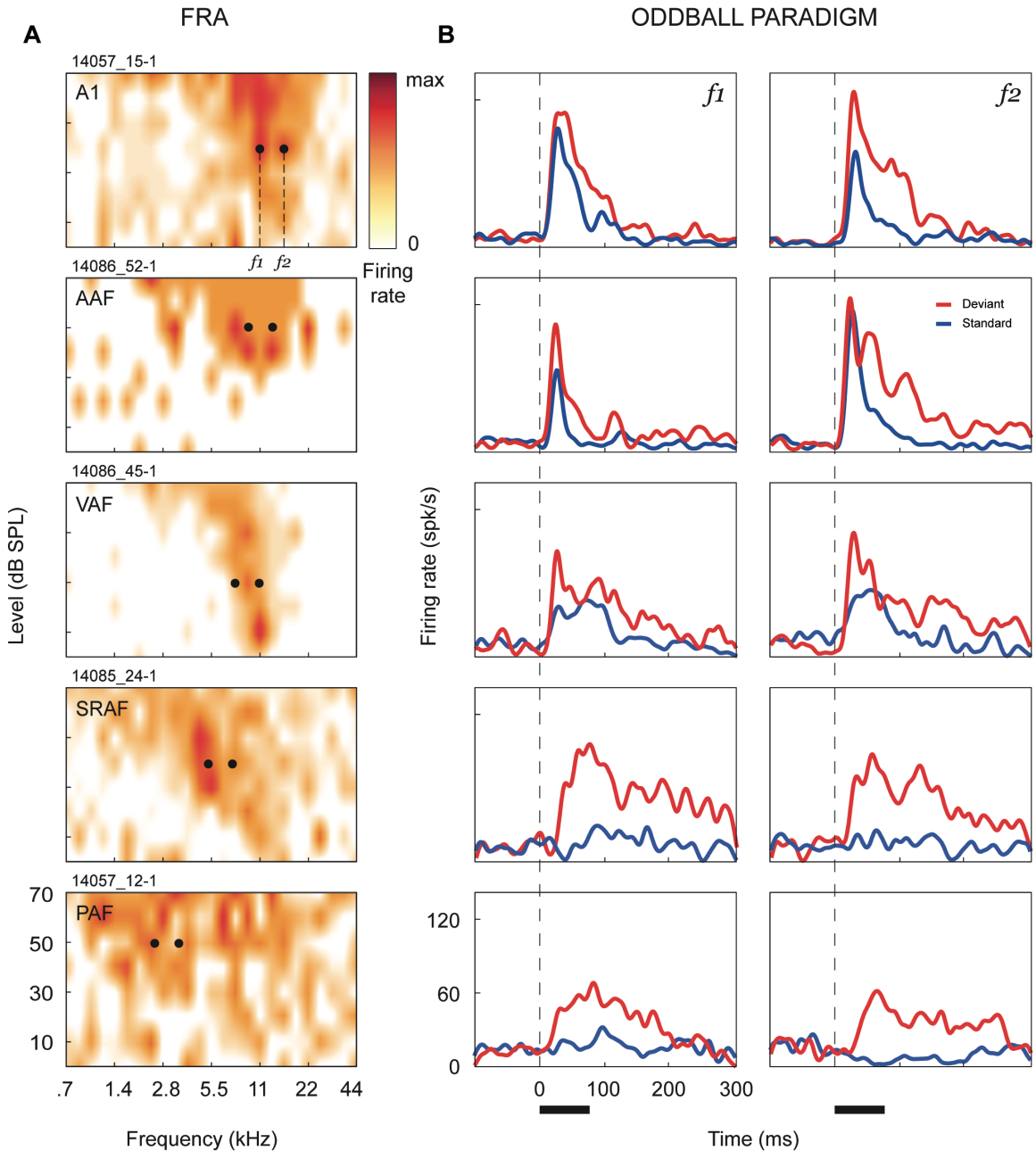

Figure 24. Stimulation paradigm. A. Representative FRAs from each auditory cortex field. Firing rate (red shading, normalized to max response) is represented as a function of frequency and intensity of the tones presented, and the frequency-tuning curve has been outlined (minimum sound intensity that elicits a firing rate over 20–40% of the maximum firing for each frequency, excluding isolated "islands" of spontaneous activity). I selected a pair of frequencies, separated by 0.5 octaves, which elicited responses of similar magnitude at 20–30 dB above threshold. These frequencies were then presented within an oddball paradigm (250 tones, 10% deviants, 300 ms onset-to-onset interval, 75 ms tone duration). **B.** Corresponding responses to the oddball

paradigm. Each plot compares spike-density functions (see Materials and Methods) in response to the same frequency, computed from the 25 deviant trials (red) and the 25 standard trials just preceding a deviant (blue). Responses to standard tones were significantly reduced in all fields, as compared to deviants, but this adaptation is much stronger in the non-primary fields (SRAF and VAF). Black horizontal bar: stimulus duration.

SSA is stronger in non-primary fields

The main aim of this study was to quantify and compare SSA levels between the five cortical fields. Thus, I computed the frequency-specific SSA index for each stimulus, SI(f_1) and SI(f_2), and the common SSA index (CSI) for every recording site, using baseline-corrected spike counts during stimulus presentation (5 to 80 ms from stimulus onset; see Materials and Methods). Figure 25A shows a series of scatterplots illustrating the joint distribution of SI(f_1) and SI(f_2), for the whole population and for each field separately, and Figure 25B illustrates corresponding histograms of CSI distributions (total number of recording sites included in this analysis, as detailed in Materials and Methods, are also indicated). In all cases, points are symmetrically clustered around the main diagonal, with no significant differences between the median SI(f_1) and SI(f_2) for any field (paired Wilcoxon signed rank test, $p > 0.1$ in all fields), indicating that adaptation was equal on average for f_1 and f_2. The drift of the population medians towards the upper-right corner (Figure 25A) reveals a gradual shift of the cloud of points, from A1 to PAF fields, towards higher levels of SSA. The global population shows a CSI distribution that is slightly skewed to the right (Figure 25B, top panel). The origin of this skewness emerges once we split these distributions into the five cortical fields: the CSI distributions for the primary fields, especially A1 and AAF, are more symmetrical, centered on medium CSI values and spanning the full range of possible values (Figure 25B). The same distributions for the non-primary fields, SRAF and PAF, on the other hand, are clearly asymmetric, sharply skewed to the right towards the extreme positive CSI values, with a virtual absence of low CSI values. Moreover, the center of the distribution progressively moves to the right (*i.e.*, towards higher CSI values) from A1 to PAF, (CSI, [Q_1, median, Q_3]: **A1**, [0.22, **0.38**, 0.61]; **AAF**, [0.32, **0.50**, 0.68]; **VAF**, [0.39, **0.56**, 0.72]; **SRAF**, [0.57, **0.76**, 0.90]; **PAF**, [0.56, **0.76**, 0.89]), with the median CSI in every primary field being significantly smaller than in every non-primary field (Kruskall-Wallis test, $^2(4) = 121.43$, $p < 5\times10^{-24}$).

Correcting for baseline activity was required to measure the actual evoked response, given the high spontaneous rates seen in many recordings, particularly from the non-primary fields (spontaneous firing rate, mean ± SEM: A1, **8.2** ± 0.7 spk/s; AAF, **7.3** ± 0.6 spk/s; VAF, **10.7** ± 0.7 spk/s; SRAF, **9.2** ± 0.6 spk/s; PAF, **13.0** ± 1.0 spk/s). This correction may have a major impact when using a contrast index such as the CSI (Klein et al., 2014), so that higher CSI values in non-primary fields could result in part from this procedure. Therefore, we repeated the CSI calculation using the absolute spike counts for the same time window. As expected, all CSI values were overall reduced, but the same trend was observed between fields, since median CSI in all fields were lower than in SRAF; only CSI levels in PAF were differentially affected, so that they were no longer higher than in primary fields (CSI without baseline correction, [Q_1, median, Q_3]: **A1**, [0.14, **0.24**, 0.40]; **AAF**, [0.18, **0.30**, 0.45]; **VAF**, [0.21, **0.32**, 0.42]; **SRAF**, [0.26, **0.39**, 0.52]; **PAF**, [0.17, **0.25**, 0.42]). However, given the higher spontaneous rate

relative to evoked activity seen in PAF, uncorrected CSI does not faithfully represent the strong SSA (i.e., contrast) clearly observed in responses from this field (Figure 24B, Figure 27A). Therefore, I kept using these corrected measures for the rest of the analyses.

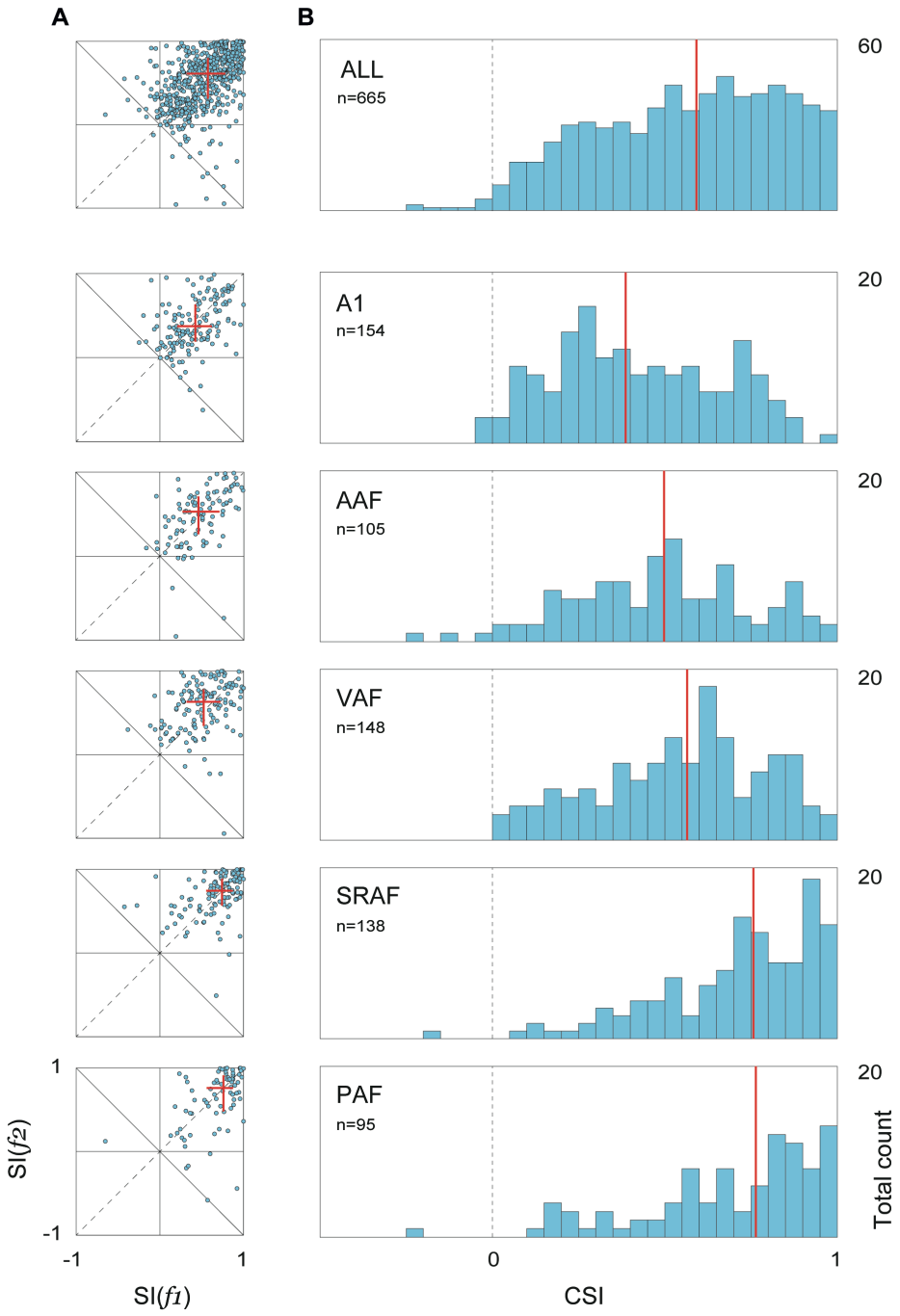

Figure 25. Distribution of SSA indexes within each field. A. Distribution of frequency-specific SSA indexes for the whole population and for each field separately. Red lines represent median and inter-quartile range for SI(f_1) and SI(f_2), showing a progressive increase in SSA from primary to non-primary fields. **B.** Corresponding distributions of the CSI. In the primary fields, distributions are symmetrical and centered in medium-CSI values,

but in the non-primary fields CSI distributions are sharply skewed to extreme levels of SSA. Red lines show distribution medians, which were statistically different between every primary and non-primary field (see text).

Consistent with previous studies (Polley et al., 2007), non-primary fields showed longer response onset latencies than primary fields for both deviant (mean ± SEM: A1, **11.6** ± 1.2 ms; AAF **11.1** ± 1.1 ms; VAF, **17.3** ± 1.5 ms; SRAF, **27.0** ± 2.0 ms; PAF, **23.9** ± 2.2 ms; Kruskal-Wallis test, $^{2}(4) = 152.78$, $p < 10^{-31}$) and standard tones (A1, **16.7** ± 1.7 ms; AAF, **22.5** ± 3.3 ms; VAF, **29.8** ± 3.5 ms; SRAF, **45.8** ± 4.7 ms; PAF, **50.0** ± 8.0 ms; $^{2}(4) = 77.59$, $p < 10^{-15}$). From these figures, it is apparent that onset latency was significantly delayed for standards as compared to deviants in all five fields (onset latency difference, standard – deviant, mean ± SEM: A1, **7.6** ± 1.5 ms; AAF, **13.6** ± 3.1 ms; VAF, **18.0** ± 3.1 ms; SRAF, **23.2** ± 3.8 ms; PAF, **31.8** ± 7.2 ms; all significantly greater than zero, Wilcoxon signed rank test, $p < 0.01$ in all cases). Thus, in addition to an overall reduction in spike counts, SSA also produced a delay in onset latency to the standard tones. Furthermore, this delay was significantly longer in non-primary fields than in primary fields A1 and AAF (Kruskal-Wallis test, $\chi^2(4) = 34.13$, $p < 10^{-6}$).

SSA is topographically organized in the auditory cortex

The sharp differences in SSA levels observed between primary and non-primary fields derive from a distinct topographic organization of adaptation throughout the whole auditory cortex (Figure 26). The absolute position of the map with respect to bregma differed between animals by up to 0.6 mm, but the relative position and orientation of the five cortical fields were highly conserved from one animal to the next. Thus, I constructed a synthetic map of CSI from all available data. Using the CF gradient as the main reference landmark, an appropriate shift was applied to each map to maximize the degree of CF coincidence between them (Figure 26A; *cf.* Figure 1 in (Polley et al., 2007) and Figure 1 in (Higgins et al., 2010)). I quantified the quality of the alignment as the local coincidence of CF values. The resulting correlation of CF between neighboring sites was next to maximal (Topological product, $P_T = 0.9686$, permutation test, $p < 0.001$) (Yarrow et al., 2014). Figure 26B shows the CSI map, while Figure 26C and Figure 26D show the corresponding maps of the response to deviant and standard stimuli (within the stimulus-fitted window), from which the CSI was computed. The CSI follows a statistically significant topographic distribution (Topological product, $P_T = 0.2342$, permutation test, $p < 0.001$), meaning that neighboring sites are likely to have more similar CSI values than more distant ones. To better determine the nature of this topography, I traced a boundary following the median iso-CSI contour (Figure 26B; median population CSI = 0.60), whenever this line enclosed a region of area greater than 0.5 mm^2. This procedure revealed an emergent organization of SSA, showing a large region of low-to-medium CSI values that covers the central and rostral portions of the auditory cortex, and two separate and distinct high-CSI regions confined to the posterodorsal and ventral margins of the map, respectively (Figure 26B). Remarkably, the CSI-based boundary that defines the posterodorsal high-CSI region matches almost perfectly the boundary between A1 and PAF previously traced from the CF gradient reversal (Figure 26A). Similarly, the iso-CSI contour that separates the ventral high-CSI region matches very well the caudal SRAF/VAF and rostral SRAF/AAF boundaries.

Finally, these high SSA regions revealed in Figure 26B can be seen also as regions of extremely low spike count to the standard stimuli in Figure 26D. Indeed, the "CSI" and "Standard" maps are almost complementary, such that regions of extreme CSI values correspond to those with virtually no response to standard stimuli, while regions of low-medium CSI match those with significant response to standards. This observation reveals a strong CSI dependence on the standard response being low, rather than on the deviant response being high. In fact, CSI was negatively correlated with both deviant (DEV) and standard (STD) response strength, yet much more strongly to the standard (Spearman correlation coefficient, $\rho(\text{CSI,DEV}) = -0.19$, $p < 10^{-6}$; $\rho(\text{CSI,STD}) = -0.81$, $p < 10^{-152}$). This also indicates that CSI values tend to be higher for neurons with an overall lower firing rate, as confirmed by a subsequent analysis (*v.i.*).

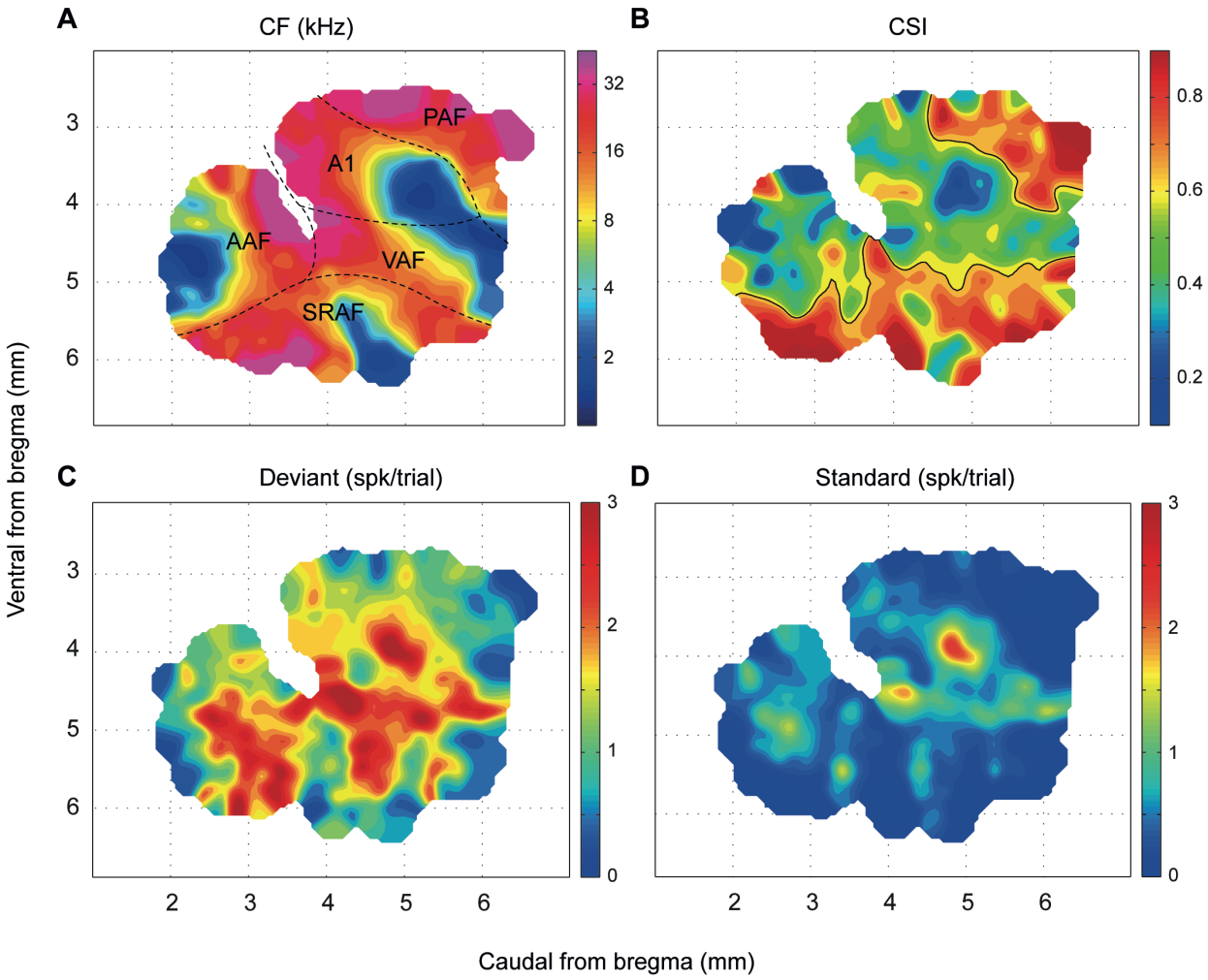

Figure 26. Topographic distribution of SSA throughout the auditory cortex. A. Synthetic map of the auditory cortex showing the location of the five cortical fields. The CF was used as the main reference to put into register the individual maps from the 12 animals. The high topographical correlation of the CF (see text) confirmed the robustness of the alignment. **B.** Topographic distribution of SSA in the auditory cortex. The CSI follows a statistically significant topography within the auditory cortex (see text), with the highest values being confined to

the non-primary fields. **C,D.** Topographic distribution of the responses to deviant and standard tones, respectively, from which the CSI was computed. Responses to standard tones were almost zero in the non-primary fields.

SSA occurs at the late component of the response

SSA was suggested as a potential neural correlate for the MMN, but previous studies neglected an analysis of the responses to deviant and standard tones at different temporal courses during stimulus presentation and beyond. Since I observed responses of long durations to deviant tones in many recordings (deviant response offset, mean ± SEM: A1, **162.6** ± 5.7 ms; AAF, **149.8** ± 6.9 ms; VAF, **194.2** ± 4.6 ms; SRAF, **196.4** ± 4.4 ms; PAF, **167.9** ± 7.4 ms), I wanted to further investigate the variation of the CSI across different components of the neural response. Hence, I computed baseline-corrected spike counts for different time intervals after stimulus onset (Figure 27A): *onset* (5–30 ms), *sustained* (30–80 ms), *offset* (80–105 ms) and *late* (105–200 ms). Corresponding CSI distributions and their topography for these different time windows are shown in Figure 27B and Figure 27C, respectively.

First, I compared median CSI between fields for every time window separately. For the *onset*, *sustained* and *offset* components, I found the same trend already observed for the stimulus-fitted response window: the median CSI in every primary field was significantly lower than in every non-primary field, and lowest of all in A1 (Figure 27B; Kruskall-Wallis test, *onset*: $\chi^2(4) = 73.95$, $p < 10^{-14}$, *sustained*: $\chi^2(4) = 109.81$, $p < 10^{-22}$; *offset*: $\chi^2(4) = 60.95$, $p < 10^{-11}$). The CSI for the *late* component of the response, however, behaved differently. At this time window, there were no significant differences in SSA between fields (Figure 27B; Kruskall-Wallis test, $\chi^2(4) = 7.78$, $p > 0.1$).

Then, I compared CSI levels within each field for the four time windows, to analyze the trend of SSA throughout the different response components. Within non-primary fields, I found no significant differences between median CSI measured at the four different time windows (Figure 27B; Friedman test, SRAF: $\chi^2(3) = 5.03$, $p > 0.1$; PAF: $\chi^2(3) = 4.72$, $p > 0.1$). By contrast, a highly significant window effect was found for the three primary fields (Friedman test, A1: $\chi^2(3) = 109.58$, $p < 10^{-22}$; AAF: $\chi^2(3) = 18.18$, $p < 0.001$; VAF: $\chi^2(3) = 55.3$, $p < 10^{-11}$). Post-hoc comparisons revealed that this effect was due to a specific increase of CSI at the *late* component (Figure 27B), with no significant differences between median CSI measured at the *onset*, *sustained* or *offset* components of the response, except for a slightly significant increase from the *sustained* to the *offset* component in A1, consistent with the overall trend. Therefore, SSA in the non-primary fields is maintained high throughout the entire response (Figure 27B,C). By contrast, SSA in the primary fields is moderate during stimulus presentation, followed by a specific enhancement in late components (Figure 27B,C), where SSA reaches the same levels found in non-primary fields.

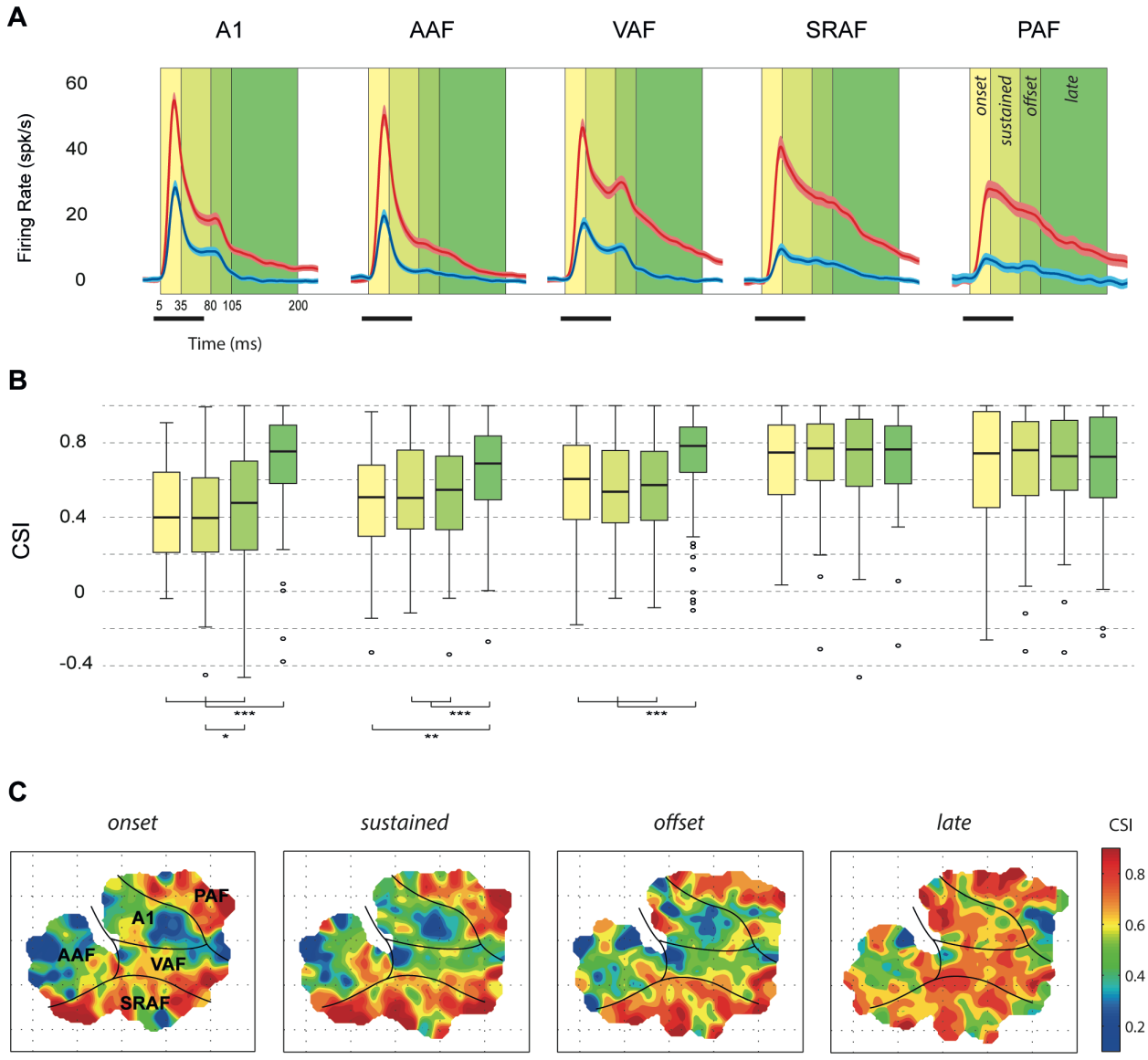

Figure 27. Variation of the CSI throughout the neural response. A. Grand-average responses (baseline-corrected firing rate, mean ± SEM) to standard (blue) and deviant (red) tones within each field. Many recordings showed significant responses beyond 100 ms from stimulus onset. **B.** Distribution of CSI values (thick bar: median, box: inter-quartile range, whiskers: full range excluding outliers) computed at different time windows with respect to stimulus presentation. In the non-primary fields, SSA was high through the entire response. In primary fields, median CSI was lower than in non-primary fields from *onset* to *offset* components but not for the *late* component, which showed CSI levels as high as in the non-primary fields. **C.** Topographic distribution of SSA for the four different time windows. Note that only the late-component CSI is high throughout the entire auditory cortex.

SSA depends on neuronal firing rate and frequency of stimulation

Upon visual inspection, regions with lowest SSA in the CSI landscape seemed to coincide with low-CF regions of the auditory cortex, particularly within A1 (Figure 26A,B). Since a strong dependence of SSA on frequency and intensity of pure-tone stimulation has been shown in the IC (Duque et al., 2012), I wanted to test whether a similar dependence was present in the

auditory cortex. Figure 28A shows a spotlight-average map of the SI across all frequency/intensity combinations tested in the whole set of recordings. High SSA is sharply skewed towards the high frequencies and low intensities of stimulation. When I analyzed primary and non-primary fields separately (Figure 28B,C) I observed that this dependence of the SI on frequency and intensity was more evident within primary (Figure 28B) than non-primary fields (Figure 28C). Additionally, average firing rate had a topographical distribution in the dataset, and was different between cortical areas (Figure 26C,D). Since firing rate may also have a strong impact on the amount of adaptation (Antunes et al., 2010), the topography of SSA could result in part from a topography of firing rates. Finally, the observed effect of stimulus intensity on the SI (Figure 28) might be an indirect consequence of the effect of firing rate, with higher intensities of stimulation producing higher firing rates and therefore lower SSA.

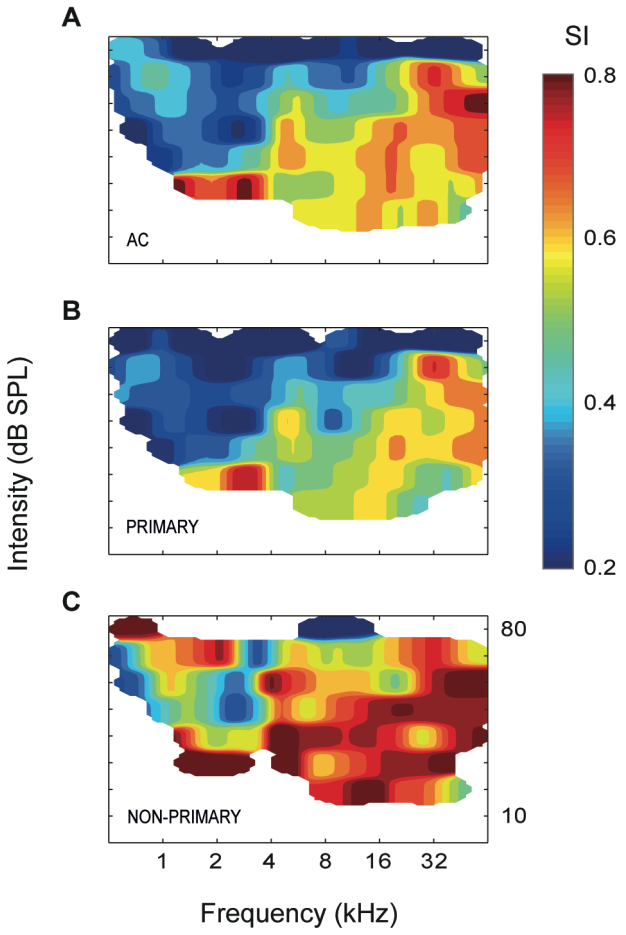

Figure 28. Dependence of SSA on the frequency and intensity of stimulation. A. Averaged SI for different values of frequency and intensity used in the oddball paradigm, for the whole set of recordings throughout the auditory cortex. SSA is significantly higher for high frequencies and low intensities of stimulation. **B.** The same effect of frequency and intensity on SSA is apparent when using all data from primary fields alone, with a virtual absence of SSA for low frequencies and high intensities of stimulation. **C.** In the non-primary fields, this frequency and intensity dependence is weaker than in the primary fields.

To address these observations quantitatively, I fit a multivariate linear regression model for the SI, following a stepwise strategy ('fitlm' function in Matlab, with robust fitting options). First, I used average spike count (*SPK*, as the sum of average response to deviant and standard stimuli) and frequency of stimulation (*OCT*, in octaves with respect to 1 kHz) as predictors. The resulting model was:

$SI = 0.51 - 0.046 \cdot SPK + 0.057 \cdot OCT$ ($F_{2,1215} = 166$, $p < 5 \times 10^{-64}$).

This model accounted for 21.3% of the variability of the SI, but more importantly it provided a specific quantification of each effect: on average, SI decreases 0.046 points per spike of the response, while it increases 0.057 points per octave of the stimulus. Then, I added intensity of stimulation (*SPL,* in dB SPL) as a factor to the model, obtaining:

$SI = 0.72 - 0.051 \cdot SPK + 0.050 \cdot OCT - 0.003 \cdot SPL$ ($F_{3,1214} = 122$, $p < 5 \times 10^{-69}$).

Thus, SI is also negatively correlated to intensity of stimulation. This model, however, explained 23% of the variability of the SI, only 1.7% more than the previous one. Therefore, most of the dependence of the SI on *SPL* is already explained by its dependence on *SPK*, confirming the fact that higher intensities produce lower SSA because of a higher firing rate. Therefore, we removed *SPL* from the model, and replaced it with *FIELD* as a categorical factor. Now, the explanatory power of the model increased to 30.6%, mainly due to overall higher SI in the non-primary fields:

$SI = 0.41 + 0.12 \cdot VAF + 0.24 \cdot SRAF + 0.20 \cdot PAF - 0.04 \cdot SPK + 0.05 \cdot OCT$ ($F_{6,1211} = 90.6$, $p < 10^{-94}$).

According to this model, mean SI is 0.41 in A1 and AAF (not significantly different from each other), 0.53 (0.41+0.12) in VAF ($p < 5 \times 10^{-9}$), 0.65 in SRAF ($p < 5 \times 10^{-28}$) and 0.61 in PAF ($p < 5 \times 10^{-16}$), and this difference cannot be explained by differences in firing rate within fields, since the *FIELD* factor explains an extra 9.3% of the SI variability. Note also that these are mean values, and therefore lower than the median values shown in Figure 25, given the rightwards skewness of the distributions.

As a final step, I tested this model for interactions between *FIELD* and the other three predictors separately, and I found significant interactions only between *FIELD* and *OCT*:

$SI = 0.19 - 0.24 \cdot VAF + 0.36 \cdot SRAF + 0.36 \cdot PAF + 0.078 \cdot OCT - 0.042 \cdot VAF \cdot OCT - 0.031 \cdot SRAF \cdot OCT - 0.034 \cdot PAF \cdot OCT$ ($F_{9,1208} = 43.8$, $p < 5 \times 10^{-68}$),

indicating that the effect of frequency was weaker in VAF ($p < 0.005$), SRAF ($p < 0.05$) and PAF ($p < 0.05$) than in A1 and AAF. Therefore, the dependence of SSA on firing rate (and, indirectly, on intensity of stimulation) is comparable among the five fields, but the observed dependence of SSA on frequency of stimulation is mainly due to the fact that A1 and AAF show lower SSA for low frequencies of stimulation, as illustrated in Figure 26A,B and Figure 28B. Incidentally, A1 and AAF are the cortical fields that show the most clear tonotopic gradient, one the mirror reversal of each other (Figure 26A) (Polley et al., 2007).

Since frequency and intensity of oddball stimulation were selected according to the frequency tuning and threshold of each recording site, and there is a tendency for tuning bandwidth in auditory cortex to decrease as a function of CF (Phillips and Irvine, 1981; Recanzone et al.,

1999), differences in SSA between fields could simply reflect differences in tuning bandwidth or CF threshold in the auditory cortex. To check this possibility, I analyzed the correlation between CSI and frequency tuning characteristics in our sample. Distributions of tuning bandwidth and threshold in our sample were consistent with previous mapping work in the rat (Polley et al., 2007). Particularly, PAF and AAF featured the broadest tuning bandwidth and highest response thresholds (Bandwidth 30 dB above threshold, in octaves, mean ± SEM: A1, **1.89** ± 0.06; AAF, **2.30** ± 0.1; VAF, **1.75** ± 0.06; SRAF, **1.98** ± 0.08; PAF, **2.95** ± 0.16; CF threshold in dB SPL, mean ± SEM: A1, **23.7** ± 0.9; AAF, **29.3** ± 1.3; VAF, **14.8** ± 0.9; SRAF, **22.5** ± 1.1; PAF, **28.3** ± 1.3). Both bandwidth and threshold in AAF and PAF were different from the other fields, but not to each other (Kruskal-Wallis test, bandwidth: $\chi^2(4) = 55.60$, $p < 5\times10^{-11}$; threshold: $\chi^2(4) = 96.03$, $p < 10^{-20}$). By contrast, CSI was 50% higher in PAF than in AAF, as already shown (Figure 25B). Similarly, CF threshold in VAF was significantly lower than in A1 or AAF, but the median CSI was not different between these primary fields (Figure 25B). Indeed, correlation between CSI and either tuning bandwidth or threshold was extremely weak in our sample (Spearman correlation coefficient: rho(CSI,BW30) = 0.083, p = 0.04; ρ(CSI,THR) = −0.09, p = 0.02). These considerations demonstrate that the distinct topography of SSA found in this study is genuine and not an artifactual effect of differences in other response properties between cortical fields.

Different time course of adaptation in primary and non-primary fields

In order to study the dynamics of adaptation to the repetitive stimuli over time, I averaged responses to standard and deviant stimuli across recordings for every trial number within the sequence, and plotted them in relation to the time elapsed since the beginning of the sequence, separately for each field (Figure 29A). Then, I fitted these responses to different simple models. None of the models tested could explain any amount of the variance of the deviant responses, indicating that deviant responses did not show dependence on trial number within any field. In sharp contrast, a power law model of three parameters, $y(t) = a \cdot t^b + c$, yielded very good quality fits for the responses to standards in all fields, explaining about 80% of their variability (adjusted-r^2: A1, **0.80**; AAF, **0.74**; VAF, **0.84**; SRAF, **0.83**; PAF, **0.69**) indicating that SSA in all fields matches stimulus statistics at many timescales (Drew and Abbott, 2006).

The most obvious difference between fields was that non-primary fields reached a much lower plateau at their final steady-state responses (gray dashed line in Figure 29B; c parameter (spk/trial): A1, **0.84**; AAF, **0.50**; VAF, **0.60**; SRAF, **0.22**; PAF, **0.17**; all significantly different from each other as derived from the 95% confidence intervals reported by the "fit" function in Matlab). Also, according to this model, adaptation was fastest in PAF, slowest in VAF and not significantly different between the other three fields (b parameter: A1, **−0.78**; AAF, **−0.93**; VAF, **−0.68**; SRAF, **−0.73**; PAF, **−1.32**). This result indicates a distinct high sensitivity of PAF to repetitive stimuli, needing only a few presentations to reach its fully adapted state. This phenomenon can be readily appreciated when analyzing the responses to the first 10 standard trials of the sequence (Figure 29B). Responses to standards in the non-primary fields adapt below half their initial strength with three (PAF) or four (SRAF) presentations of a stimulus (black arrows in Figure 29B), whereas in the primary fields it takes up to six (A1) presentations

to produce this same relative reduction. Therefore, adaptation occurs faster and is stronger in non-primary than in primary fields.

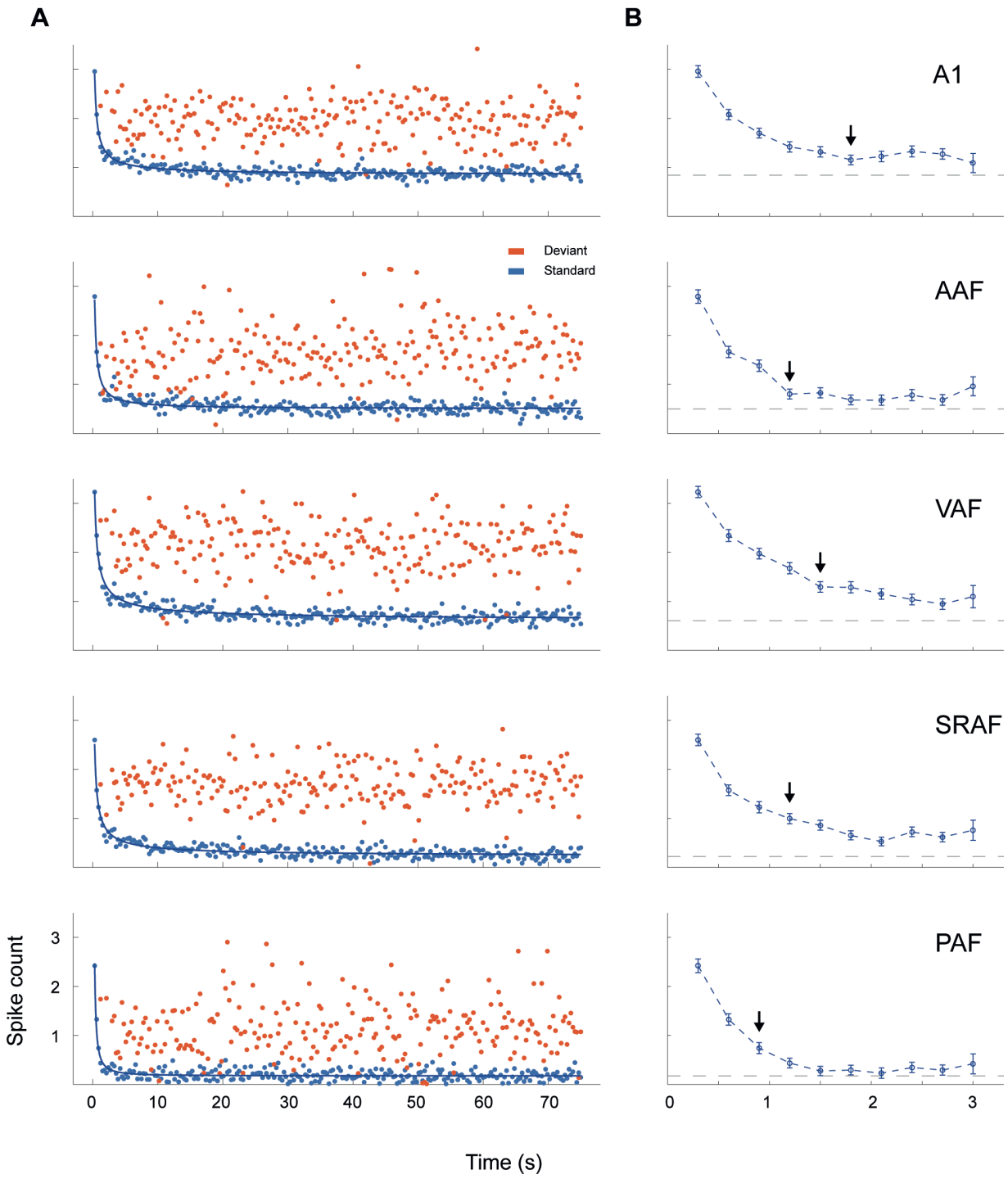

Figure 29. Time course of adaptation within each field. A. Average responses within each auditory cortex field in relation to the order of tone presentation, plotted for standard (blue) and deviant (red) tones separately. The course of standard responses over time followed a power law (thick blue lines), indicating that SSA matches stimulus statistics at many timescales. **B.** Detail of the average (mean ± SEM) standard responses for the first 10

presentations within the sequence. The arrows indicate the trial number where the response has fallen significantly below half of the response to the first tone presentation. Gray dashed lines indicate the steady-state plateau reached by standard responses at the end of the sequence (constant parameter of the power-law fit). Adaptation occurred faster in PAF than in any other field (see text), and reached a much lower plateau in non-primary than in primary fields.

SSA in the auditory cortex correlates with the difference wave of the local field potentials

Whereas SSA in spike responses is a local measure at the neuron level, the MMN is a large-scale brain potential. One reasonable way to bridge this gap is to probe the correlation between adaptation of neural responses and local field potentials (LFP), which represent average synaptic activity in local cortical circuits (Buzsáki et al., 2012). Thus, I recorded LFP simultaneously with MUA in 4 out of the 12 animals, with a total yield of 268 recording sites (A1, 49; AAF, 48; VAF, 55; SRAF, 54; PAF, 42; Unlocalized, 20). I averaged the recorded LFP waveforms evoked by standard and deviant tones for each field separately, and computed the difference wave (DW) at every time point after stimulus onset (Figure 30A). In all the five cortical fields, these potentials showed the typical morphology in response to pure tones (von der Behrens et al., 2009; Fishman and Steinschneider, 2012), with a fast negative deflection (Nd) followed by a slower positive deflection (Pd). These two components were present in responses to both standard and deviant tones, but their amplitudes were in all cases smaller for the standards, giving rise to a DW of similar shape but varying amplitudes (Figure 30A). For each recording, the peak amplitude and peak latency of the DW was measured for the Nd and Pd components, within a time window where the DW reached statistical significance at the whole population level (16 to 37.6 ms for Nd and 41.5 to 86.7 ms for Pd, respectively, paired t-test, Bonferroni correction for 268 comparisons, $p < 0.05$).

Peak amplitude of the DW at the Nd component showed a clear trend to be larger in primary than in non-primary fields, being significantly smaller in PAF than in the three primary fields, and smaller in SRAF than in AAF (Figure 30B; one-way ANOVA, $F_{4,243} = 8.24$, $p < 5\times10^{-6}$). This trend was still present, albeit much less clear, for the Pd component of the DW, being significantly smaller in PAF than in A1 and AAF, but not different between the other fields (Figure 30B; one-way ANOVA, $F_{4,243} = 3.74$, $p < 0.01$). Thus, the fast Nd component of the DW showed a topographical distribution within the auditory cortex, whereas the slower Pd component of the DW showed a more homogenous distribution across cortical fields. A similar pattern was apparent for the peak latencies of each of these components (Figure 30B). The Nd component of the DW peaked earlier in the primary than in the non-primary fields, significantly so between A1 or AAF and SRAF or PAF (mean ± SEM: A1: **24.6** ± 0.9 ms , AAF: **24.8** ± 0.8 ms , VAF: **28.3** ± 0.6 ms , SRAF: **31.1** ± 0.8 ms, PAF: **32.0** ± 1.7 ms; one-way ANOVA, $F_{4,243} = 11.78$, $p < 5\times10^{-8}$). Peak latencies for the Pd component, on the other hand, were not statistically different between fields (mean ± SEM: A1: **61.7** ± 2.0 ms , AAF: **57.4** ± 2.2 ms , VAF: **59.5** ± 2.0 ms , SRAF: **59.8** ± 1.7 ms, PAF: **61.4** ± 2.1 ms; one-way ANOVA, $F_{4,243} = 0.70$, $p = 0.59$). The steady progression of the Nd peak latency is consistent with a bottom-up propagation of the signal from primary to non-primary fields, whereas the

homogeneity of the Pd peak latency suggests a stronger contribution of intracortical processing and reciprocal interaction between fields.

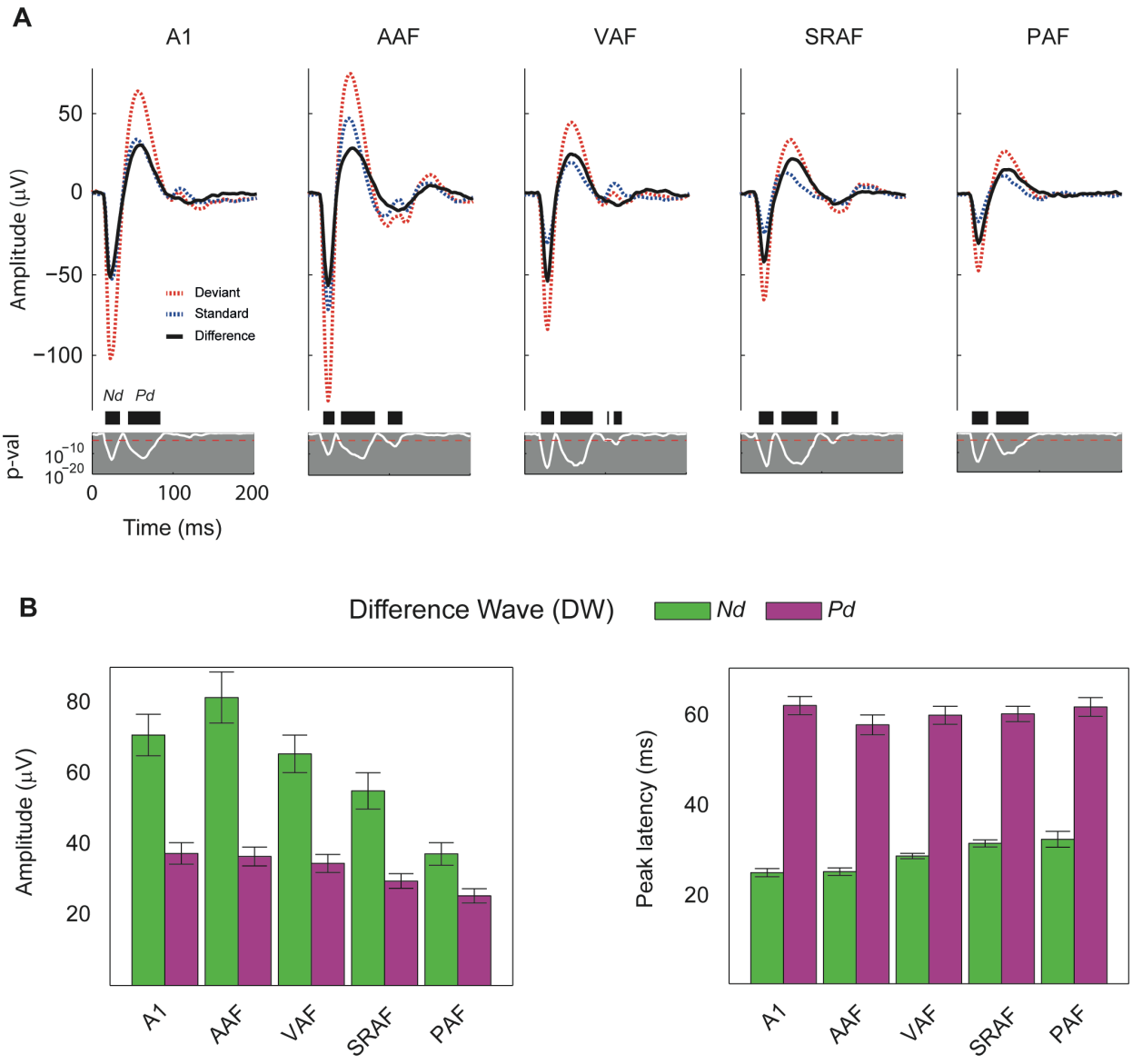

Figure 30. Adaptation in the LFP. A. Grand-average LFP traces in response to deviant (red) and standard (blue) tones, and the resulting difference wave (black), averaged for each cortical field separately. Two components of the difference wave (DW) were analyzed: the fast negative deflection (Nd) and the slower positive deflection (Pd). Note also a small but significant deflection of the LFP at longer latencies (>100 ms) in anteroventral fields (AAF, VAF and SRAF). White line: p-value of the DW. Black thick bars: time intervals showing a significant DW. Red dotted horizontal line: Bonferroni-corrected critical p-value (bilateral t-test). **B.** Peak amplitude and latency (mean ± SEM) of the Nd and Pd components of the DW within each cortical field. Note that the mean of the amplitudes/latencies of the individual DW components are not equal to the peak amplitude/latency of the same component in the grand-averaged DW.

To facilitate a more direct comparison between SSA for the MUA and for the LFP components, I also computed CSI values for the Nd and Pd peaks of the LFP (data not shown). Overall, SSA at both components of the LFP was appreciably lower than for the MUA (paired signed rank test for the whole set of recordings with LFP; CSI-Nd vs. CSI-onset, z-score = 6.98, $p < 5\times10^{-12}$; CSI-Pd vs. CSI-sustained, z-score = 10.12, $p < 5\times10^{-24}$), but it followed the same trend to be lower in the primary than in non-primary fields (Median CSI-Nd: A1, **0.32**; AAF, **0.31**; VAF, **0.45**; SRAF, **0.50**; PAF, **0.47**; Kruskall-Wallis test, $\chi^2(4) = 21.12$, $p < 5\times10^{-4}$. Median CSI-Pd: A1, **0.25**; AAF, **0.24**; VAF, **0.33**; SRAF, **0.37**; PAF, **0.40**; Kruskall-Wallis test, $\chi^2(4) = 13.09$, $p < 0.05$). Furthermore, CSI-Nd and CSI-Pd were strongly correlated with their corresponding CSI values at comparable time windows (Spearman correlation coefficient: ρ(CSI-Nd, CSI-onset) = 0.66, $p < 10^{-40}$; ρ(CSI-Pd, CSI-sustained) = 0.43, $p < 5\times10^{-12}$; ρ(CSI-Pd, CSI-offset) = 0.21, $p < 0.005$).

STUDY 2: HIERARCHICAL PREDICTION ERROR IN THE AUDITORY SYSTEM

In this study, with the collaboration of two determined laboratory mates, I recorded individual responses of subcortical and cortical neurons along the rat auditory pathway, using recently developed control sequences to separate repetition suppression from prediction error under oddball stimulation (Jacobsen and Schröger, 2001; Taaseh et al., 2011; Ruhnau et al., 2012; Harms et al., 2014). Our data show that differential responses to deviant and standard tones in oddball sequences indeed reflect active predictive activity, instead of a mere SSA in single neurons, and that this predictive activity emerges hierarchically from subcortical structures. These results unify three coexisting views of perceptual deviance detection at different levels of description: neuronal physiology, cognitive neuroscience and the theoretical predictive coding framework.

Evidence of prediction error in single auditory neurons

The predictive coding framework assumes that the same operations (generation of predictions and prediction errors) would take place at every hierarchical level of sensory systems (Friston, 2005), and this could in principle include subcortical processing stations (Auksztulewicz and Friston, 2016b). Unfortunately, there is a severe dearth of evidence for this, since research on predictive brain activity has until recently focused on cortical responses of varying source and latency (Bendixen et al., 2012; Phillips et al., 2016), and the role of subcortical structures in cognition, albeit increasingly acknowledged (Parvizi, 2009; Güntürkün and Bugnyar, 2016), remains largely unexplored. In order to collect a representative sample from different processing stations along the auditory pathway, we recorded a total of 207 neurons from the auditory midbrain (IC), thalamus (MGB) and cortex (AC) of anesthetized rats (Table 3), while stimulating the animal with sequences of pure tones (Figure 32A).

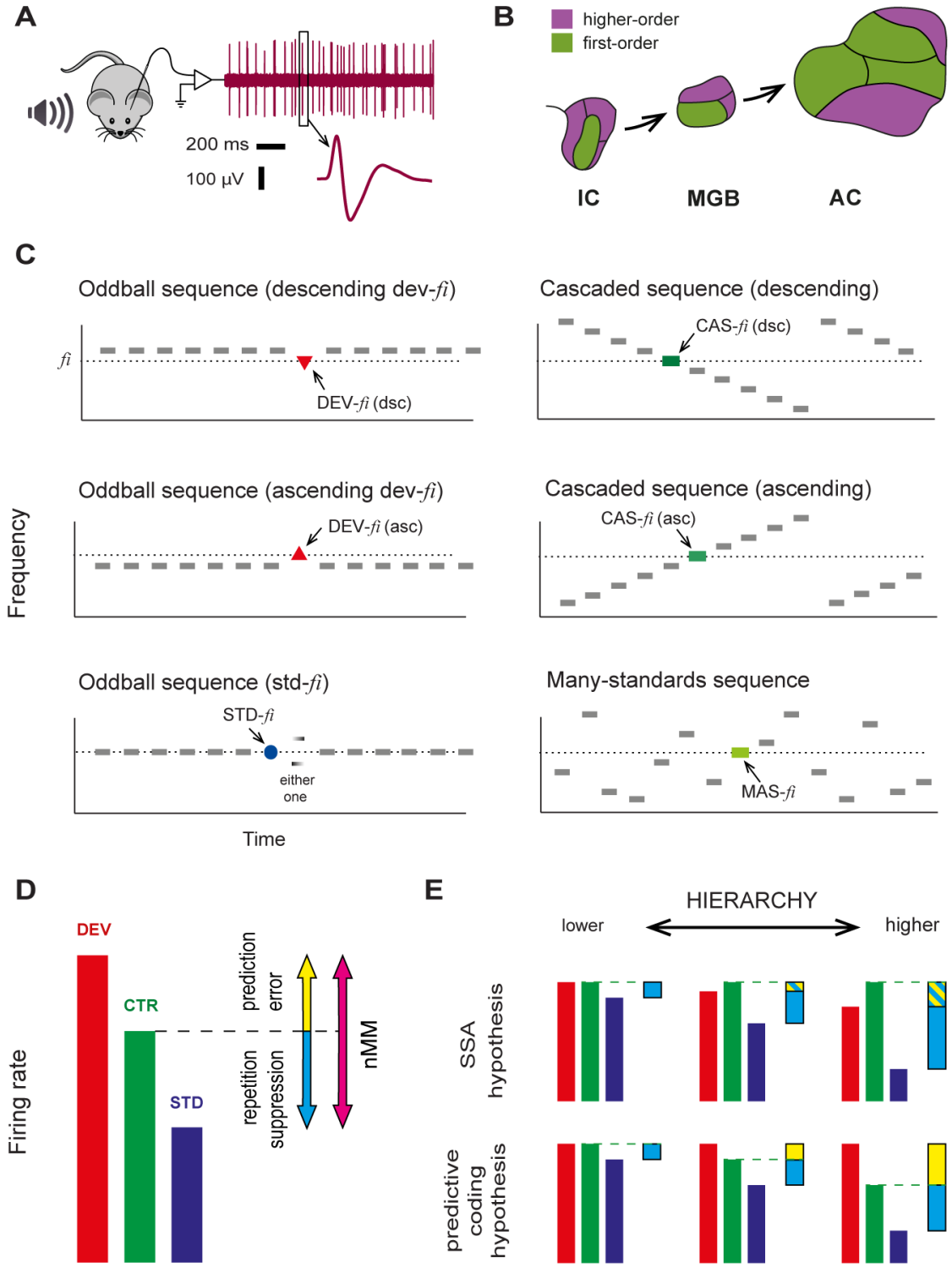

Figure 32. Experimental design for study 2. (A) Sketch of experimental setup. Isolated neurons were recorded from different auditory nuclei of anesthetized rats, while stimulating with pure tones. **(B)** Schematic representation of the rat auditory pathway form midbrain to cortex 3,30, divided into first- and higher-order regions. **(C)** Stimulation sequences. Using this design, each tone fi was presented in two experimental conditions (DEV and STD, in oddball sequences), and two control conditions (CAS/MAS) for adaptation effects. Note that ascending/descending DEV tones will be compared to the corresponding version of the CAS condition (see

Methods). **(D)** Decomposition of neuronal mismatch responses (nMM) to the oddball sequence using either one of the control conditions. **(E)** Predicted scenarios under two competing mechanisms explaining nMM. If SSA is the main mechanism underlying nMM, responses to STD tones will be more suppressed the more synapses information traverses along the auditory hierarchy, and responses to control (CAS/MAS) tones would be equal to, or stronger than, to DEV tones, since the average intertonal distance is larger in the controls than in oddball sequences 29. By contrast, if nMM reflects Bayesian inference, responses to DEV tones would be progressively larger than to the controls as the information propagates up the auditory hierarchy.

Recorded neurons were further grouped into "first-order" (*fo*) or "higher-order" (*ho*), depending on their particular location within each nuclei (Escera and Malmierca, 2014; Nieto-Diego and Malmierca, 2016), thus leading to 6 different processing stations (*fo*-IC, *ho*-IC, *fo*-MGB, *ho*-MGB, *fo*-AC, *ho*-AC; Figure 32B; see Methods). This distinction was made because higher-order (or non-primary) auditory regions represent a higher hierarchical level of processing (Atiani et al., 2014) and are known to be more sensitive to acoustic change and contextual influences than first-order (or primary) ones (Kraus et al., 1994; Escera and Malmierca, 2014; Nieto-Diego and Malmierca, 2016).

For each recorded neuron, we presented a set of oddball sequences, using tones selected from the neuron's frequency-response area (FRA), and a "neuronal mismatch response" (nMM) was computed as the difference between responses to deviant (DEV) and standard (STD) conditions for each tone (Figure 32D). To determine whether this difference (usually DEV > STD) reflected predictive activity, instead of (or in addition to) just SSA, we also presented two cascaded (CAS) sequences (ascending and descending) and one many-standards (MAS) sequence as controls (Ruhnau et al., 2012; Harms et al., 2014) (Figure 32C), containing all tones used in oddball sequences (see Methods). The main rationale behind this design is that, in the CAS/MAS control conditions, each tone has the same (low, 10%) probability of occurrence as a DEV tone in the oddball sequence, so it is not repetitive (as the STD), and therefore is free of repetition effects (e.g. repetition suppression), but it does not stand out from the statistical context (as the DEV), and therefore it is not perceived as a deviant (Ruhnau et al., 2012; Harms et al., 2014). Thus, responses to CAS/MAS control conditions are used as the reference yardstick with respect to which repetition suppression and prediction error effects can be discriminated (Figure 32D). If the neuronal mismatch response (nMM = DEV – STD) is caused entirely by SSA to the STD tone, responses to DEV and CAS/MAS control conditions should remain comparable through all hierarchical levels, or if anything, the response to DEV tones should undergo a slightly stronger suppression than to the controls, due to cross-frequency adaptation (Taaseh et al., 2011) (Figure 32E). By contrast, under the predictive coding framework, deviance detection is based on Bayesian inference (Friston, 2009), such that stronger prediction errors will be produced as more sensory evidence accumulates to increase the confidence and precision of current predictions (Garrido et al., 2009b; Stefanics et al., 2014; Auksztulewicz and Friston, 2016b). Therefore, stronger prediction errors should be elicited by DEV than by CAS/MAS tones, due to the lack of sequential stimulus repetitions in the controls (Ruhnau et al., 2012; Stefanics et al., 2014), and this effect should increase up the hierarchy (Figure 32E), since higher-order processing stations are able to code for more

complex regularities (Opitz et al., 2005; Bendixen et al., 2012; Wacongne et al., 2012; Escera and Malmierca, 2014).

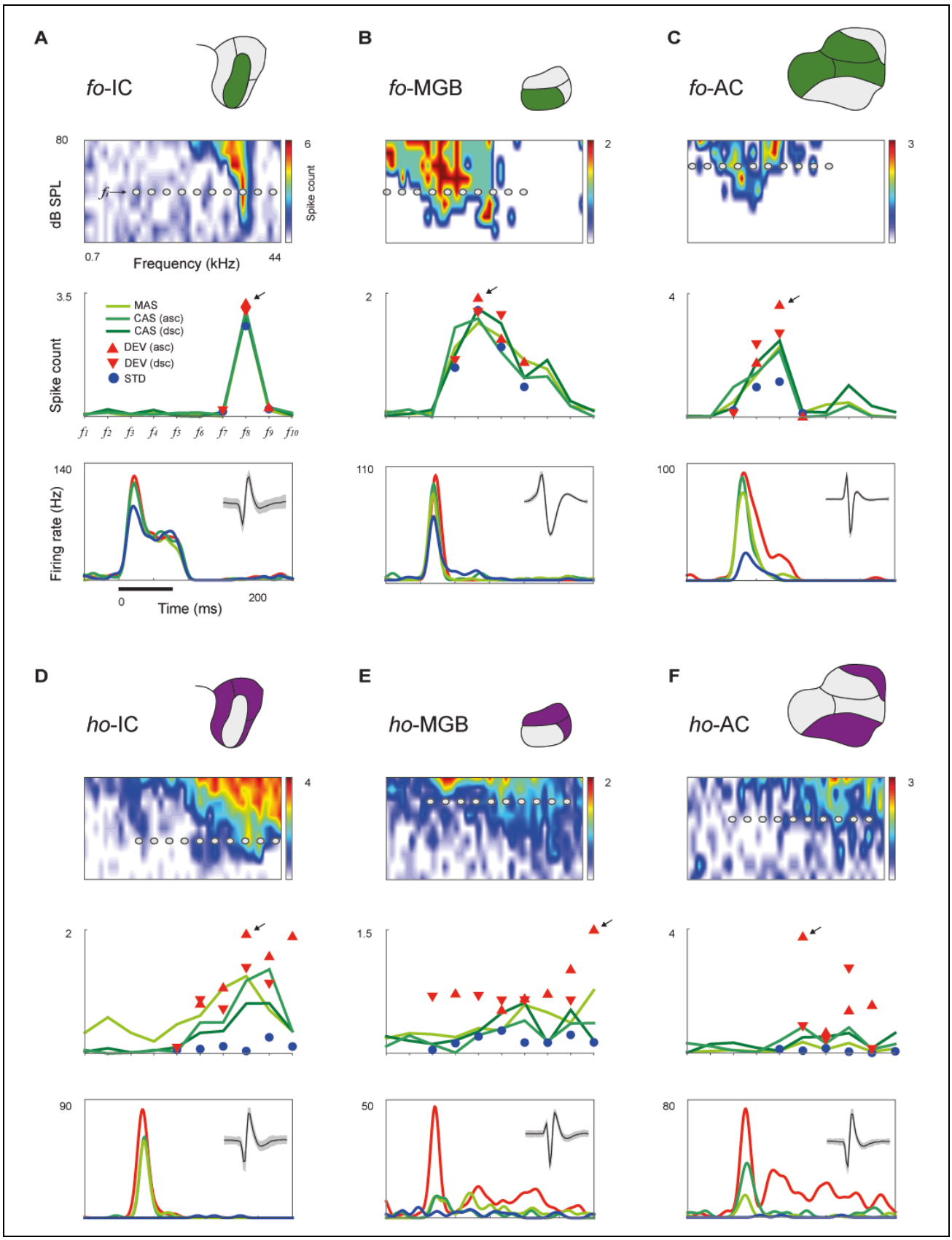

Figure 33. Prediction error in sample neuronal responses. Each panel shows responses of representative neurons within each station of the auditory pathway: (1) The FRA (representation of neuronal sensitivity to different frequency/intensity combinations) and the 10 tones selected to create the control sequences for that particular neuron (see Methods). (2) Measured responses of the neuron to each tone (baseline-corrected spike counts, averaged within 0–180 ms after tone onset), for all conditions tested. (3) Sample PSTH for each condition, for the tone with the highest response (either ascending or descending; indicated with an arrow). Stimulus duration is represented by the thick, horizontal line, and the isolated spike (mean ± SEM) is shown in the small inset. Both repetition suppression (STD < CTR) and prediction error (DEV > CTR) can be observed in responses to some tones, and this is particularly consistent for higher-order neurons (panels D-F).

Individual responses of representative neurons are shown in Figure 33. Responses of first-order neurons are mostly dependent on tone frequency, with little sensitivity to the different conditions, particularly at subcortical levels (Figure 33A,B). However, in *fo*-AC (Figure 33C), and most clearly in higher-order neurons (Figure 33E-F), strong response suppression to STD condition is apparent, but also, a higher firing rate in response to DEV tones, as compared to both MAS and CAS control conditions, was consistent across tested frequencies. This is, as just explained, the signature of prediction error at the single neuron level (Taaseh et al., 2011; Harms et al., 2015).

In the following, I will present only the results using the cascaded sequence as control, since it was designed as an improvement to the many-standards sequence that controls for additional factors beyond presentation rate of the deviant tone (Ruhnau et al., 2012; Harms et al., 2014) (see Materials and Methods, *Experimental Design*). However, the results using either CAS/MAS condition as a control were commensurable (Table 3), with no remarkable differences between them (Wilcoxon signed-rank test, $z = -0.125$, $p = 0.9$).

The contribution of prediction error to nMM increases along the auditory hierarchy

Single neuron responses to the three conditions (DEV, STD, CAS) for all tones tested in all neurons are represented in Figure 34A-F, separately for each processing station. Each pair of conditions, within each station, was tested for a difference in medians (Table 3). As expected, responses to DEV condition were stronger than to STD condition within all stations (Figure 34A-F; Table 3). This is a well described neuronal behavior across the auditory pathway (Escera and Malmierca, 2014), which has been referred to as SSA in previous studies (Ulanovsky et al., 2003), even though it was postulated to be the neuronal mechanism underlying deviance detection (Taaseh et al., 2011). Indeed, this nMM results mostly from suppression of the response to the repetitive STD condition (repetition suppression), since responses to STD were significantly weaker than to CAS condition within all stations (Table 3). Critically, responses to DEV tones were significantly higher than to CAS already within the *ho*-IC (Figure 34D; Table 3), and this difference increased progressively in the *ho*-MGB, and *ho*-AC (Figure 34E,F), where it was most apparent. Therefore, neuronal responses showed clear signs of prediction error at the population level, within all higher-order stations, but also within *fo*-AC (Figure 34C; Table 3), consistent with the observed effects in individual cases (Figure 33C-F).

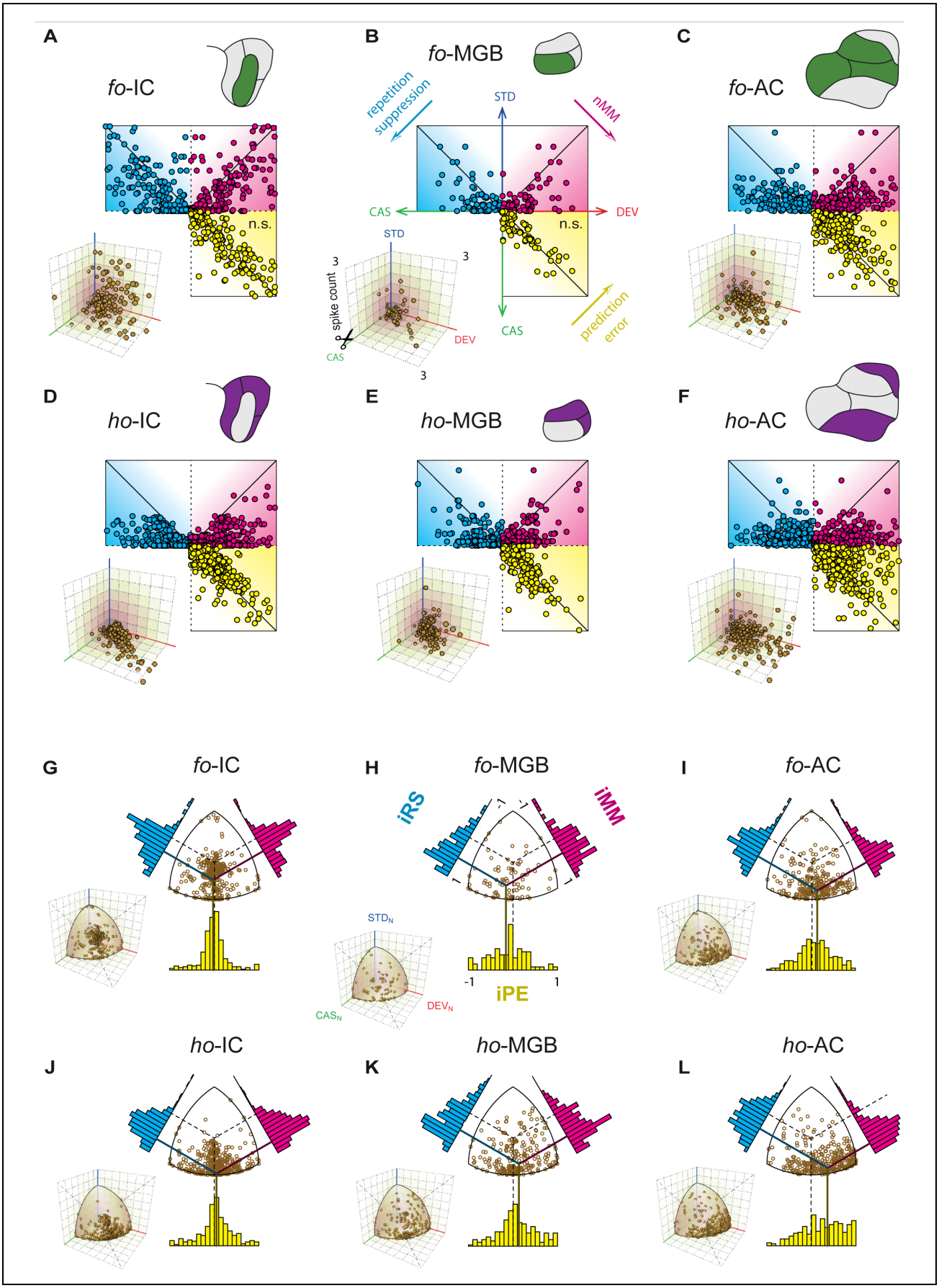
A
fo-IC
n.s.
B
fo-MGB
repetition suppression
STD
nMM
CAS
DEV
n.s.
CAS
prediction error
STD
spike count
3
3
DEV
CAS
3
C
fo-AC
D
ho-IC
E
ho-MGB
F
ho-AC
G
fo-IC
H
fo-MGB
iRS
iMM
STD_N
CAS_N
DEV_N
-1
1
iPE
I
fo-AC
J
ho-IC
K
ho-MGB
L
ho-AC

Figure 34. Prediction error at the population level. A-F. Responses to the three conditions (DEV, STD, CAS) for all points tested in all neurons, were represented on a 3D scatter, separately for each station. These points were then orthogonally projected onto the three "walls", to compare two responses at a time, and then the "box" was unfolded (after "cutting" along the CAS axes) to create the main, flat diagrams. Thus, each 2D point represents the response (baseline-corrected spike count) of a single neuron to one given tone for a pair of conditions. **G-L.** Distribution of normalized responses and indices of neuronal mismatch (iMM), repetition suppression (iRS) and prediction error (iPE). Each point in the 3D scatters from panels A-F represents a vector in response space (DEV, STD, CAS). The normalization is just the radial projection of this point onto the unit sphere centered on the origin (small insets), so the resulting vector (DEVN, STDN, CASN,) is a scaled version of the former. The flat diagram is a zenith view of the 3D sphere. Each diagonal (dotted black lines) represents the line where the corresponding index is zero, and the index will increase or decrease as a projected point moves away from this line. Histograms represent index distributions, with their means indicated by colored lines. Note the overall shift of the mean iPE towards positive values, from IC through MGB to AC, and from first- to higher-order divisions.

To quantify the relative contribution of repetition suppression and prediction error to nMM in neuronal responses, and to facilitate comparisons between different neurons/stations, I normalized the neural responses to the three conditions (DEV, STD, CAS) for each neuron/tone combination. I applied Euclidean vector normalization (Figure 34G), such that all normalized responses (DEV_N, STD_N, CAS_N) ranged between 0 and 1. Then, I computed three indices as the difference between normalized responses to pairs of conditions, ranging between –1 and +1 (Figure 34G). The "index of neuronal mismatch", **iMM** = DEV_N – STD_N, is the relative difference in responses to STD and DEV tones in the oddball paradigm. The iMM is quantitatively equivalent to the typical "SSA index" (Ulanovsky et al., 2003), used in previous studies (Figure 37). The "index of neuronal repetition suppression", **iRS** = CAS_N – STD_N, is the relative reduction of the response to a standard tone, as compared to the control. Thus, the iRS quantifies repetition effects (Baldeweg, 2006). Finally, and most importantly for this study, the "index of neuronal prediction error", **iPE** = DEV_N – CAS_N, is the relative increase in the response to a deviant tone, compared to the control. A positive iPE reflects predictive activity, as opposed to SSA (Ruhnau et al., 2012), and quantifies the proportion of prediction error accounting for nMM (Taaseh et al., 2011). Therefore, the relation **iMM = iRS + iPE** provides a functional, quantitative decomposition of nMM (Figure 32D). The distribution of these indices across stations reveals that both iMM and iPE increase along the auditory pathway, from *fo*-IC to *ho*-AC (Figure 34G-L).

Summary statistics for these normalized responses and indices are shown in Figure 35A and 4b, respectively. The iPE shows a distinct increase in two ways: (1) from first- to higher-order stations, and (2) from IC to MGB to AC (Figure 35B). To validate these observations statistically, I fitted a linear model for the iPE using *nucleus* (IC, MGB, AC) and *hierarchy* (*fo*, *ho*) as categorical factors. The resulting model was:

$$\mathbf{iPE} = 0.012 + 0.020^{*}\boldsymbol{ho} - 0.136^{*}\mathbf{MGB} + 0.092^{*}\mathbf{AC} + 0.185^{*}\boldsymbol{ho}^{*}\mathbf{MGB} + 0.158^{*}\boldsymbol{ho}^{*}\mathbf{AC},$$

with a significant effect of *hierarchy* ($F=37.16$, $p=1.40\cdot10^{-9}$) and *nucleus* ($F=46.35$, $p=3.15\cdot10^{-20}$), and a significant *hierarchy*nucleus* interaction ($F=3.48$, $p=0.031$). Therefore, both trends are

significant and robust from midbrain to cortex. In particular, the significant *hierarchy* effect means that the small average iPE seen in *ho*-IC (iPE = 0.012 + 0.020 = **0.032**) is nevertheless statistically significant (Figure 35B), consistent with a significant difference in absolute spike counts (DEV–CAS in Table 3; Figure 34J). Overall, this analysis demonstrates a gradual emergence of a prediction error component in responses of single neurons as information progresses through the auditory pathway, both in bottom-up and in first- to higher-order directions, with a mutual potentiation of these two effects.

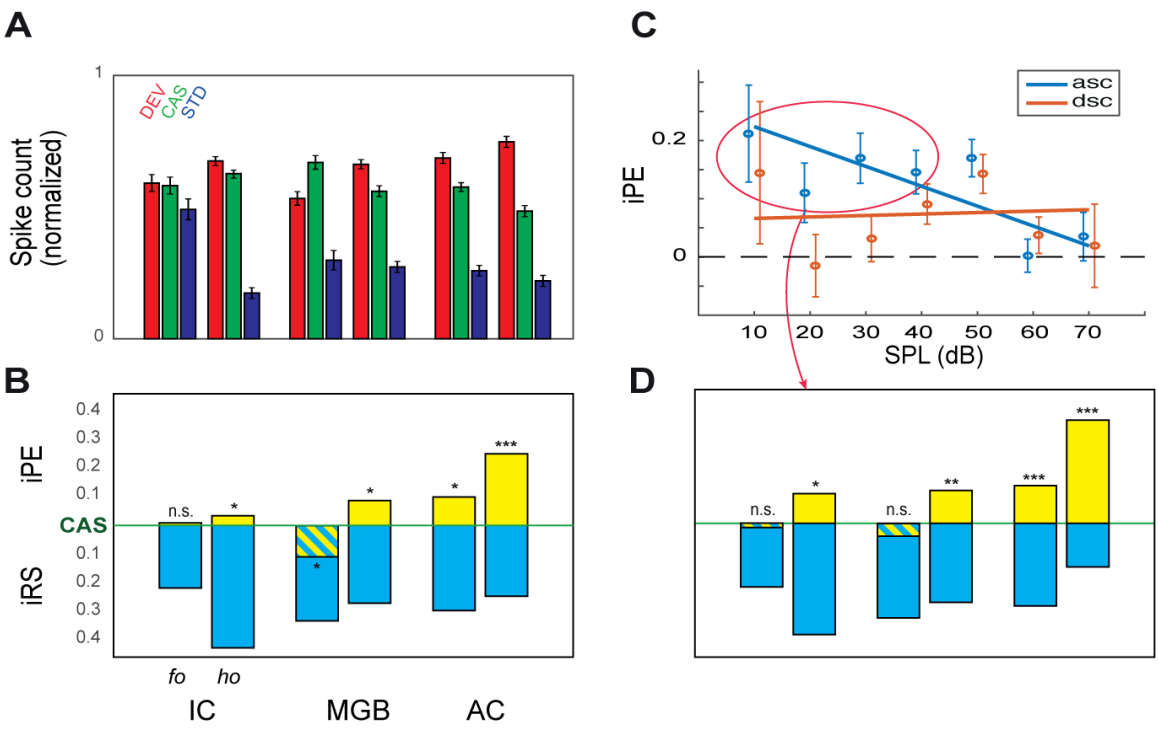

Figure 35: Emergence of iPE along the auditory hierarchy. A. Average normalized responses (mean ± SEM) to the three conditions (DEVN, STDN, CASN) within each station. **B.** These same normalized responses are representd with respect to the CAS control condition, so that the indices are represented by their differences (iPE is upwards-positive, iRS is downwards-positive). Asterisks denote statistical significance of iPE against zero median (Table 3) **C.** Linear model fitted for the iPE, using SPL and Direction (ascending/descending) as predictors. Error bars denote mean and SEM for each SPL and Direction. **D.** The same as in (B), but using only recordings for ascending deviant tones at intensities ≤ 40 dB SPL.

According to previous modeling work, change-sensitivity in single neurons is expected to be maximal for stimulus ranges where the firing rate of the neuron is below saturation (Abbott et al., 1997). Consistent with this hypothesis, a common observation in the pool of recorded neurons was that using low stimulation intensities it was easier to produce deviance-specific responses, particularly for ascending deviants (e.g. Figure 33D). To test these observations at the population level, I fitted a different model for the iPE, using *SPL* (in Bels = dB SPL/10) and *direction* (ascending, ASC, or descending, DSC) of deviant tones (see Figure 32C) as

predictors. The model showed a significant effect of *SPL* (F=4.59, p=0.03) and a *SPL*direction* interaction (F=6.66, p=0.01):

iPE = 0.064 + 0.194***ASC** + 0.003***SPL** – 0.037***ASC*****SPL**,

which indicates that the iPE is expected to be much higher for ascending deviants at intensities below 40 dB SPL (Figure 35C). Indeed, I observed a distinct increase in the iPE within all stations, under these stimulation conditions (Figure 35D), particularly in *ho*-AC, where prediction error accounted for around two thirds of the iMM. This effect could facilitate perception under challenging sensory conditions, by increasing the gain of prediction error responses at early processing stages (Auksztulewicz and Friston, 2016b). These findings run parallel to previous observations in single neurons of the primary visual cortex, where cortical feedback improves figure-background discrimination of low-salience stimuli (Hupé et al., 1998).

Prediction error in single neurons correlates with a large-scale mismatch response in the auditory cortex

I also recorded local field potentials (LFP), simultaneously to single neuron spikes, from the same electrode, to explore the direct correlation between prediction error in spike responses and large-scale mismatch responses (such as the MMN). I averaged LFP responses for each condition and station, as well as the difference between DEV and CAS conditions, which I called the "prediction error potential" (Shiramatsu et al., 2013; Harms et al., 2014): PEP = $LFP_{DEV} - LFP_{CAS}$ (Figure 36). A significant early PEP was already detectable within *ho*-IC and *ho*-MGB (Figure 36D,E). In the auditory cortex, the PEP was strong and significant in both *fo*-AC and *ho*-AC, showing three major deflections (Figure 36C,F): a fast negative deflection (N1; 35–50 ms after change onset), a slower positive deflection (P2; 70–120 ms), and a third, late, negative deflection (N2; beyond 150 ms). Importantly, epidural MMN peaks between 60 and 120 ms in rats (Harms et al., 2015), the same range of the P2 recorded here for the PEP, and can be positive when recorded from inside the brain (Fishman and Steinschneider, 2012). Then, the iPE was re-computed for 12 different time windows (20 ms width, from –50 to 190 ms respect to stimulus onset), for each neuron/tone combination separately, and averaged within each station (Figure 36). The iPE showed a clear modulation over time in both *fo*-AC and *ho*-AC stations (Friedman test, not corrected for 6 independent tests). Each individual iPE value was also tested against zero, and this analysis revealed a significant iPE within *fo*-AC between 60–100 ms after change onset, and in *ho*-AC between 40–200 ms, and seemingly beyond (Figure 36C,F).

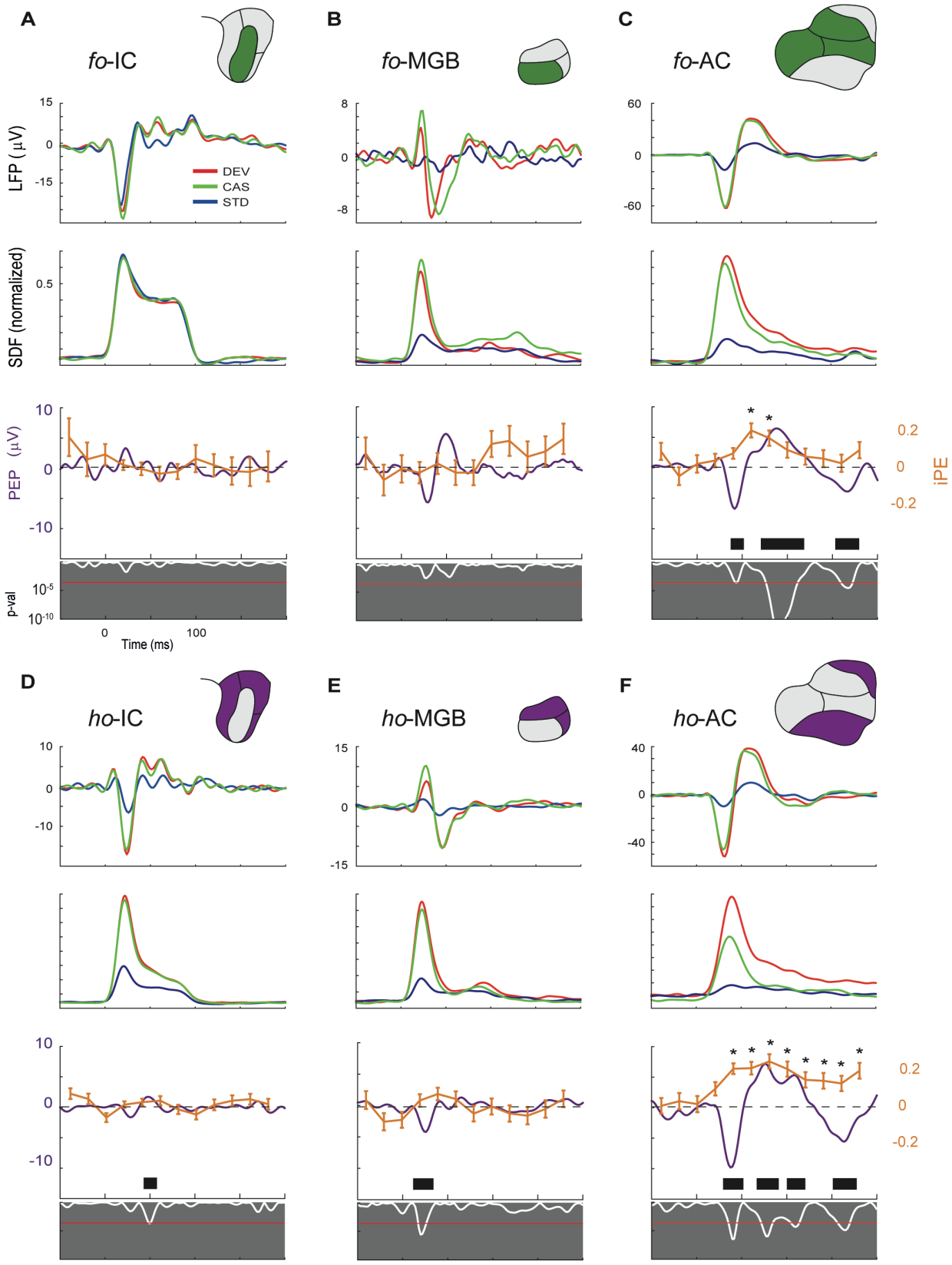

Figure 36: Correlation of iPE and the local-field prediction error signal (PEP). Population grand-averages for different response measures, computed for each processing station separately: (1) Average local field potentials (LFP) across tested tones and recording sites for the different conditions. (2) Average firing rate profiles, as spike-

density functions (SDF, normalized to better match the iPE traces shown below). (3) Average "local-field prediction error signal" (PEP = LFPDEV − LFPCAS; white trace: instantaneous p-value for the PEP, paired t-test against equal means; red horizontal line: critical threshold with Bonferroni correction for 200 comparisons, FWER<0.05; thick black bars: time intervals for which average PEP is significant). (4) Along with the PEP trace, the time course of the average iPE is plotted in orange (mean ± SEM, asterisks indicate a significant iPE for the corresponding time window; Wilcoxon signed rank test with Bonferroni correction for 12 comparisons, FWER<0.05). Highest iPE values are concurrent in time and location (auditory cortex; panels C-F) with the strongest PEP.

Table 3: Summary of principal dataset for Study 2. For each auditory station: Number of recorded neurons and tested neuron/tone combinations (points). Median values for baseline-corrected spike counts (spk) to the different conditions. Median differences between the former measures and associated p-values against zero (Friedman test with post-hoc multiple comparison, Fisher's Least Significant Difference method, uncorrected for 6 independent tests). Median indices of neuronal mismatch (iMM), repetition suppression (iRS) and prediction error (iPE), computed from each of the two control sequences (CAS or MAS), and their corresponding p-values (note that p-values are the same for absolute differences and normalized indices, since these indices are median differences between normalized responses, and the non-parametric comparison is independent of scaling).

	fo-IC	*ho*-IC	*fo*-MGB	*ho*-MGB	*fo*-AC	*ho*-AC
# Neurons	22	56	24	35	35	36
# Points	114	523	77	225	250	306
DEV (spk)	2.55	0.99	0.64	0.68	0.95	0.98
STD (spk)	1.93	0.22	0.20	0.14	0.24	0.21
CAS (spk)	2.37	0.97	0.71	0.55	0.77	0.59
MAS (spk)	2.51	0.95	0.90	0.65	0.85	0.52
DEV-STD (spk)	0.62	0.77	0.44	0.54	0.71	0.77
p-val	0.000	0.000	0.000	0.000	0.000	0.000
CAS-STD (spk)	0.44	0.76	0.51	0.40	0.53	0.38
p-val	0.000	0.000	0.000	0.000	0.000	0.000
DEV-CAS (spk)	**0.18**	**0.019**	**-0.07**	**0.13**	**0.18**	**0.39**
p-val	0.779	0.020	0.019	0.023	0.019	0.000
MAS-STD (spk)	0.57	0.73	0.70	0.50	0.60	0.31
p-val	0.003	0.000	0.000	0.000	0.000	0.000
DEV-MAS (spk)	0.04	0.04	-0.26	0.03	0.11	0.46
p-val	0.190	0.155	0.003	0.671	0.049	0.000
iMM_{CAS}	0.127	0.493	0.324	0.496	0.505	0.609
p-val	0.000	0.000	0.000	0.000	0.000	0.000
iRS_{CAS}	0.013	0.461	0.447	0.446	0.398	0.334
p-val	0.000	0.000	0.000	0.000	0.000	0.000
iPE_{CAS}	**-0.002**	**0.032**	**-0.122**	**0.050**	**0.107**	**0.275**
p-val	0.779	0.020	0.019	0.023	0.019	0.000
iMM_{MAS}	0.147	0.485	0.303	0.505	0.508	0.611
p-val	0.000	0.000	0.000	0.000	0.000	0.000
iRS_{MAS}	0.091	0.463	0.445	0.494	0.439	0.343
p-val	0.003	0.000	0.000	0.000	0.000	0.000
iPE_{MAS}	0.055	0.023	-0.143	0.010	0.069	0.267
p-val	0.190	0.155	0.003	0.671	0.049	0.000

DISCUSSION

In Study 1, I compared the level of SSA in primary and higher-order auditory cortex to validate SSA as a candidate neural correlate of the MMN. To study the topographic organization of SSA I mapped the whole rat auditory cortex with MUA recordings from middle layers III/IV, using an oddball paradigm. I demonstrate that SSA occurs beyond A1, and its properties differ between primary and non-primary fields. Major findings in Study 1 are: (1) Highest SSA is sharply segregated to non-primary fields, creating a distinct topographic gradient of SSA within the auditory cortex. (2) High SSA is present in non-primary fields up to 200 ms after stimulus onset, and it remains stronger than in primary fields during the first 100 ms of the neuronal responses. (3) In all cortical fields, SSA is correlated in time and strength with the difference wave seen in both the fast (Nd) and slower (Pd) deflections of the LFP. As additional novel findings, I show that: (4) SSA produces a delay in the responses to standard tones, as compared to deviants, and this delay is longer in non-primary fields. (5) SSA is significantly higher for high frequencies of stimulation, and this dependence is more pronounced in primary fields. (6) SSA occurs faster and reaches a much lower plateau in the non-primary fields.

My data sharply contrast with previous studies showing that SSA level in A1 neurons is independent of their CF and in which less than 4% neurons showed a latency effect (Ulanovsky et al., 2004). But the presence of strong SSA in spiking responses at 50-100 ms and beyond represents the major difference with previous SSA studies. Only very recently, two studies in mouse auditory cortex (Chen et al., 2015; Natan et al., 2015) and one in rat somatosensory cortex (Musall et al., 2015) found SSA in either subthreshold V_m fluctuations of layer II/III pyramidal neurons (Chen et al., 2015) or spiking responses of inhibitory interneurons (Chen et al., 2015; Natan et al., 2015) and layer IV pyramidal neurons (Musall et al., 2015) occurring >50-100 ms after stimulus onset. Importantly, we recorded mainly form layer IIIb/IV neurons, receiving direct thalamocortical inputs, which are more likely to show long-latency spiking responses (Metherate and Cruikshank, 1999). Finally, previous studies reported SSA for LFP in A1, but they failed to show any correlation between MMN-like components of the LFP and SSA. Some did not find significant spiking activity for latencies beyond 50 ms (von der Behrens et al., 2009; Fishman and Steinschneider, 2012), or observed SSA only for the fast Nd (Farley et al., 2010); others did not measure MUA (Szymanski et al., 2009) or their analysis was restricted to the fast Nd only (Taaseh et al., 2011). Such a correlation has only been described in the somatosensory cortex (Musall et al., 2015).

Additionally, in Study 2, I could confirm that single neuron responses to deviant tones in the oddball paradigm reflect genuine deviance detection, as opposed to just adaptation to repetition, thus showing that these responses meet the critical condition to be considered as genuine mismatch responses. Moreover, the highest iPE values, reflecting prediction error in single neuron responses, also correlate in time and location (*ho*-AC) with a large-scale mismatch wave (the PEP), putatilvely corresponding to the MMN in the rat (Shiramatsu et al., 2013; Harms et al., 2015).

Thus, in these two studies, I provide unequivocal evidence to support the notion that single neuron responses to oddball stimulation along the auditory pathway constitute the neuronal correlate of large-scale indices of deviance detection recorded epidurally. In particular, I demonstrate that the responses of single neurons in higher-order auditory cortex directly underlie the generation of the MMN.

Completing the picture of SSA in the auditory pathway

One key aspect of my data in Study 1 is the high coincidence in the relative position of the fields across animals and in comparison with previous mapping studies (Polley et al., 2007; Pandya et al., 2008; Higgins et al., 2010; Profant et al., 2013). My analysis revealed a systematic meta-organization of SSA in the auditory cortex of the rat (Polley et al., 2007; Higgins et al., 2010), such that the CSI gradient shows a steep increase at the boundaries between primary and non-primary fields (Figure 26B). In particular, the sharp CSI enhancement between A1 and PAF (Figure 26D) bears striking resemblance with the same border found previously for bandwidth and latency (Pandya et al., 2008). These results conform with previous studies that showed SSA in A1 (Ulanovsky et al., 2003; von der Behrens et al., 2009; Farley et al., 2010; Taaseh et al., 2011; Fishman and Steinschneider, 2012; Hershenhoren et al., 2014; Chen et al., 2015; Natan et al., 2015; Nir et al., 2015) and extend their findings, as I present new SSA properties hitherto unknown. Importantly, the distribution of SSA indices in my A1 sample is largely equivalent to those shown in previous studies of SSA in the rat or mouse A1 that used similar paradigm parameters (Taaseh et al., 2011; Natan et al., 2015; Nir et al., 2015) making further comparisons more reliable. To the best of my knowledge, there were no previous studies of SSA outside A1, although higher SSA levels were expected to be found in non-primary fields, since neurons in non-primary cortical areas are known to show fast adaptation (Irvine and Huebner, 1979; Schreiner and Cynader, 1984). In particular, many studies independently reported that PAF neurons in the rat adapt strongly even to slow repetition rates (Doron et al., 2002; Polley et al., 2007; Pandya et al., 2008), and novel sounds produced greater cellular activity than familiar sounds in auditory association cortex in area Te3 (Wan et al., 2001), where the SRAF is located (Kimura et al., 2007). There is also strong evidence of enhanced adaptation in in non-primary areas of the auditory cortex from large-scale brain responses (ERP, MEG, fMRI) in both animals (King et al., 1995; Pincze et al., 2001; Jung et al., 2013; Shiramatsu et al., 2013) and humans (Kropotov et al., 2000; Jääskeläinen et al., 2004; Opitz et al., 2005; Maess et al., 2007). My findings also parallel the topography of subcortical SSA (Figure 31). Previous studies consistently found stronger SSA in the non-primary (or non-lemniscal) subdivisions of the IC (Malmierca et al., 2009; Duque et al., 2012; Ayala and Malmierca, 2013) and MGB (Kraus et al., 1994; Antunes et al., 2010). Importantly, an identical dependence of SSA on frequency of stimulation as well as a delay in onset latency of responses to standards have already been shown in the IC (Duque et al., 2012).

Before proceeding any further, I should draw attention to three major caveats of Study 1. First, anesthesia reduces neuronal responsiveness to auditory stimuli, as well as spontaneous firing, and may change some receptive field properties (Zurita et al., 1994; Gaese and Ostwald, 2001; Noda and Takahashi, 2015), and thus, an increased sensitivity to anesthetics in higher-order fields may lead to an overestimation of the SSA seen in those areas. However, I observed

high spontaneous rates, as well as strong, sustained responses to deviants in non-primary fields (Figure 27A; baseline-corrected spike counts within 0-200 ms, mean ± SEM: A1, **3.2** ± 0.1; AAF, **2.8** ± 0.1; VAF, **4.7** ± 0.2; SRAF, **3.9** ± 0.2; PAF, **2.6** ± 0.2). I used urethane as anesthetic because it preserves balanced neural activity better than other agents (Hara and Harris, 2002), it retains the higher-order processing capabilities of the auditory cortex (Capsius and Leppelsack, 1996) and shows no significant effects on SSA levels, at least in the IC (Duque and Malmierca, 2015). Most importantly, MMN-like responses have been successfully recorded from anesthetized (Ruusuvirta et al., 1998; Tikhonravov et al., 2010; Astikainen et al., 2011; Shiramatsu et al., 2013) and awake (Nakamura et al., 2011; Jung et al., 2013; Harms et al., 2014) animals alike (for review, see (Todd et al., 2013)). Second, the MMN is a negative-going component, in contrast to the positive late potential (Pd) examined here. Depending on the location of recording and anesthetic state, epidural MMN recordings in rats can be positive in polarity (Nakamura et al., 2011; Harms et al., 2014), an effect commonly observed in urethane-anesthetized preparations (Ruusuvirta et al., 1998; Astikainen et al., 2011). Moreover, an inversion of the LFP has been extensively described using laminar probes in A1 (Szymanski et al., 2009; Fishman and Steinschneider, 2012), such that positivities in layers IIIb/IV may appear as negativities in superficial layers. Third, there are some discrepancies between the SSA seen in MUA and in LFP data. Namely, whereas the MUA shows prominent activity between 100–200 ms (i.e., beyond the rat-MMN range; Figure 27B) the LFP is relatively flat within this time window (Figure 30A). Similar late-spiking activity has been observed in parvalbumin-positive inhibitory interneurons (Chen et al., 2015) and interpreted as delayed reverberating network activity specifically triggered by deviant stimuli, but we cannot rule out that MUA includes activity from thalamocortical afferents in layers IIIb/IV, which would not produce a prominent LFP component. Alternatively, the late enhancement of SSA (100–200 ms) seen in the primary fields (Figure 27B,C) might result from processing in the non-primary fields, subsequently transmitted downwards through the massive feedback corticocortical connections (Figure 31) (Kimura et al., 2004, 2007; Carrasco and Lomber, 2010; Musall et al., 2015). A more relevant discrepancy is that the difference-wave amplitude for the later Pd component of the LFP is comparable between primary and non-primary auditory cortex, and even significantly smaller in PAF than in A1 or AAF (Figure 30B), not supporting the notion of enhanced SSA in non-primary fields. However, previous ERP studies (Jung et al., 2013; Shiramatsu et al., 2013) failed to find differences in the MMN amplitude between primary and non-primary fields. One simple reason for this could be that ERPs and LFPs are large-scale potentials, reflecting overall synaptic activity within a wide volume of tissue (Buzsáki et al., 2012), most probably spanning the boundaries between fields. Therefore, local measures at the cellular level such as MUA are much better indicators of specific differences between fields. Furthermore, it is consistent to find higher SSA at the MUA than at the LFP level (i.e., output vs. input, respectively) within any particular area, as also shown at the single-neuron level (Hershenhoren et al., 2014). Also, the amplitude of the difference wave is an absolute measure, whereas SSA is commonly expressed as a contrast such as the CSI. When computed this way, SSA for the Pd amplitude is already higher in non-primary than in primary fields, yet this difference is much sharper for the MUA, reflecting the operations carried out by non-primary fields to their already-adapted inputs.

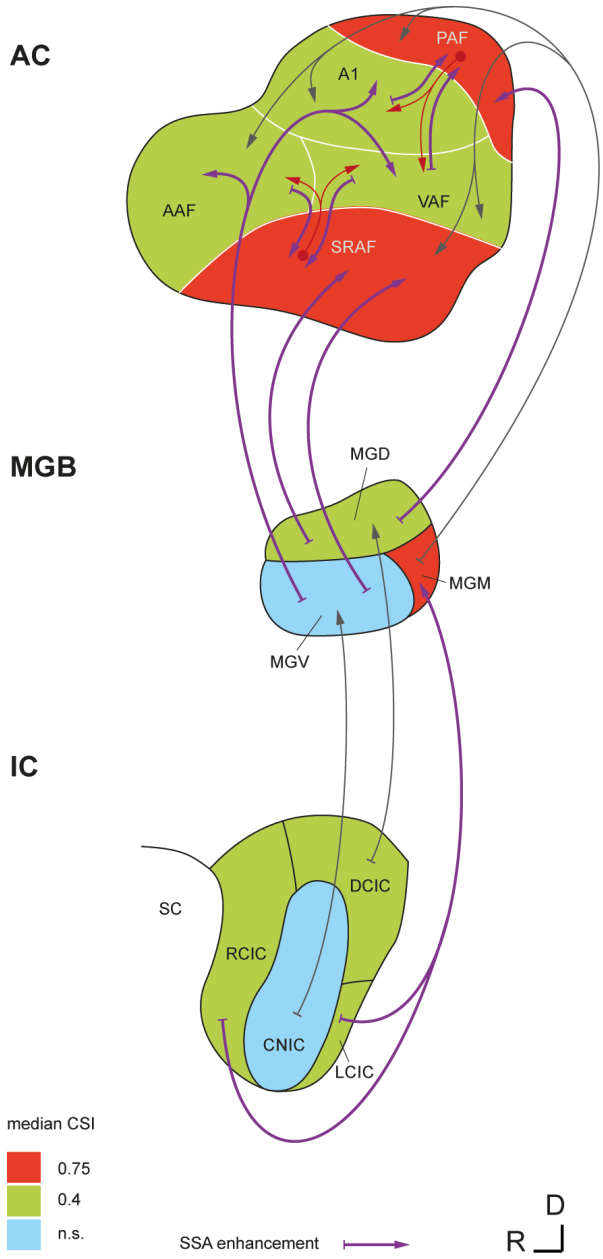

Figure 31. Emergence of SSA in the non-lemniscal auditory pathway. Simplified wiring diagram showing SSA levels and ascending connections of the auditory brain where SSA occurs. SSA is virtually absent from lemniscal parts of the IC (CNIC, central nucleus of the IC) and MGB (MGV, ventral division of the MGB), but it is high in their non-lemniscal subdivisions (RCIC, DCIC and LCIC, rostral, dorsal and lateral cortices of the IC, respectively; MGD and MGM, dorsal and medial divisions of the MGB, respectively), showing levels comparable to those seen in primary cortical fields. Extreme levels of SSA are found only in non-primary fields of the auditory cortex and in the MGM. Thus, SSA undergoes a significant enhancement at both lemniscal and non-lemniscal thalamocortical projections. A potential influence of non-primary fields on high late-SSA seen in primary fields is represented by the red arrows. Median CSI values in the IC and MGB are from Antunes et al. (2010) and Duque et al. (2012), using similar paradigm parameters.

SSA as a neuronal correlate of MMN

The mechanisms and location of the neural generators of SSA and their relation to MMN are still a subject of debate (Grimm and Escera, 2012; Escera and Malmierca, 2014; Malmierca et al., 2014; Nelken, 2014). In the lemniscal pathway (Figure 31), SSA undergoes a first enhancement at the thalamocortical synapses from the ventral division of the MGB to A1 (Ulanovsky et al., 2003; Antunes et al., 2010). In Study 1 I show a further enhancement of SSA in non-primary cortical fields, which integrate the thalamocortical projection from non-lemniscal MGB (Smith et al., 2012) and the corticocortical projection from primary fields (Carrasco et al., 2015) and redirect their output to prefrontal and limbic brain regions involved in spatial attention and emotional memory (Kimura et al., 2004, 2007). Thus, Study 1 confirms that SSA is a prevalent property of the non-lemniscal auditory pathway, even at the cortical level (Figure 31). This organization may underlie its functional significance, as a higher-order stage of sensory processing beyond the faithful representation of the auditory stimuli that predominates in the lemniscal pathway (Atiani et al., 2014). Cumulating evidence indicates the existence of a hierarchy of processing stages for regularity encoding in the auditory brain, with later response components showing sensitivity for changes in more complex aspects of the acoustic scene (Costa-Faidella et al., 2011a; Grimm and Escera, 2012; Malmierca et al., 2014). Repetition positivity (RP) has been proposed as the electrophysiological correlate of the memory trace formation required for subsequent change detection and, in turn, rapid SSA in auditory cortex is likely to contribute to its generation (Haenschel et al., 2005; Garrido et al., 2009a). Here we show very strong SSA in non-primary auditory cortex, supposed to contain the main generators of the MMN in humans (Alho, 1995; Alho et al., 1998; Kropotov et al., 2000; Opitz et al., 2005; Maess et al., 2007), cats (Pincze et al., 2001) and rats (Shiramatsu et al., 2013), that resembles MMN in several ways. First, SSA results in stronger responses to deviants than to standards in the oddball paradigm, to the extent that responses to standards can get totally suppressed in some recordings from non-primary fields. Critically, I show strong SSA in these areas between 50-100 ms, correlated with a consistent difference wave at the slow Pd component of the LFP (Figure 30A). The latency of this Pd deflection (60-80 ms) is considerably shorter than the human MMN (150-200 ms), but matches perfectly the range of MMN-like potentials in the rat (Ruusuvirta et al., 1998; Tikhonravov et al., 2010; Astikainen et al., 2011; Nakamura et al., 2011; Jung et al., 2013; Shiramatsu et al., 2013; Harms et al., 2014), which tend to occur on average 50-100 ms after stimulus onset, probably due to the smaller size of the rat brain (Harms et al., 2015). Interestingly, this SSA resembles RP in the first standard presentations (Figure 29B) and matches stimulus statistics at multiple time scales (Ulanovsky et al., 2004; Costa-Faidella et al., 2011b). I also show stronger SSA for high- than for low-frequency tones, paralleling a commonly observed effect of frequency in both animal (Astikainen et al., 2011; Nakamura et al., 2011; Harms et al., 2014) and human (Pratt et al., 2009; Peter et al., 2010) MMN recordings.

At this juncture, it is important to note that the slower Pd component of the difference wave peaked with the same latency throughout the entire auditory cortex (Figure 30B), and so did its epidural counterpart in the rat (Shiramatsu et al., 2013). By contrast, the fast Nd deflection of the LFP occurs earlier in primary than in non-primary fields (Figure 30B), suggesting a lemniscal origin and bottom-up propagation. Therefore, a higher degree of

reciprocal interaction between fields is likely involved in the generation of the Pd, consistent with the idea that intracortical processing contributes to SSA at longer latencies (Javitt et al., 1994; Ulanovsky et al., 2003; Szymanski et al., 2009; Musall et al., 2015; Natan et al., 2015). Thus, MMN-like potentials may be readily recorded from both primary and non-primary auditory cortex, but non-primary fields seem to contribute critically to their generation at the microcircuit level (Molholm et al., 2005; Opitz et al., 2005).

In conclusion, in Study 1, I demonstrate that strong SSA occurs in non-primary auditory cortex at the latency range of the MMN in the rat. This finding overcomes the two major discrepancies hitherto alleged against the suggestion that SSA in the auditory cortex may underlie the generation of the MMN (Nelken and Ulanovsky, 2007; Fishman, 2014), namely, its anatomical location and its temporal development. I provide empirical evidence of the missing link between SSA in single neurons and scalp-recorded potentials, thus bridging the gap between animal physiology studies and the human MMN. Given the wide use of the MMN as a tool in clinical and cognitive neuroscience (Näätänen, 1995; Näätänen et al., 2007, 2012; Todd et al., 2013), such a connection is potentially of high relevance for future research in these fields.

SSA as a neuronal correlate of predictive coding

Study 2 provides evidence, hitherto very scarce, that the hierarchical predictive activity of perceptual systems is detectable at the cellular level, even subcortically. Specifically, oddball responses of individual neurons, from midbrain to cortex, reflect predictive processing and underlie large-scale electrophysiological indicators of deviance detection. After quantitatively decomposing neuronal mismatch responses (nMM; Figure 32D) into repetition suppression (iRS) and prediction error (iPE), the data show a systematic increase in the proportion of prediction error accounting for nMM as the sensory signal propagates up the auditory hierarchy (Figure 35B,D). The highest iPE values are reached within the higher-order auditory cortex, where they correlate with a simultaneously recorded, large-scale prediction error potential (PEP; Figure 36F), and extend into late evoked potentials, suggesting an influence from higher-association or prefrontal cortices (Maess et al., 2007). These results are consistent with the predictive coding account of mismatch responses, while at the same time highlight the role of subcortical structures in perception (Güntürkün and Bugnyar, 2016), providing a novel extension of the mostly corticocentric predictive coding literature (Friston, 2009; Parvizi, 2009; Bastos et al., 2012).

Previous attempts to show predictive activity in auditory neurons were inconclusive (Farley et al., 2010; Taaseh et al., 2011; Fishman and Steinschneider, 2012), and were limited to multi-unit activity recordings in primary auditory cortex (but see (Meyer and Olson, 2011; Zmarz and Keller, 2016) for compelling evidence in single visual neurons). However, a recent study in mouse A1 (Chen et al., 2015) and another in rat barrel cortex (Musall et al., 2015) showed deviance detection in late responses of single units, using the MAS control sequence. Although the CAS sequence is arguably a better control for repetition effects than the MAS sequence (Ruhnau et al., 2012), only one animal study has previously applied it, using epidural recordings, and yielding also inconclusive results (Harms et al., 2014). My results, using single-unit

recordings, were comparable or even more robust for the CAS than for the MAS control (Table 3), in agreement with human studies (Ruhnau et al., 2012). The finding that the contribution of prediction error to nMM supersedes that of repetition suppression within the higher-order auditory cortex (Figure 35B,D), is consistent with studies of brain sources of MMN in animals (Kraus et al., 1994; Shiramatsu et al., 2013) and humans (Opitz et al., 2005; Maess et al., 2007) using similar controls for repetition effects. This hierarchical transformation of nMM, dominated by repetition suppression at lower hierarchical levels of the auditory system, with a gradual emergence of prediction error at higher levels (Figure 35,B,D), confirms that lower levels are mostly sensitive to global stimulus probability, while higher-order levels are more sensitive to local relationships between sounds (transitional probabilities), exactly as observed in human MMN studies (Winkler and Schröger, 2015; Koelsch et al., 2016). Thus, my data are consistent with passive SSA (Figure 32E) underlying oddball responses in first-order midbrain and thalamus (Taaseh et al., 2011) (Figure 35B). By contrast, they support a generative mechanism of Bayesian inference being at play in auditory cortex and higher-order subcortical stations of perceptual processing (Stefanics et al., 2014). The contrast between first- and higher-order nMM is particularly clear within the auditory thalamus (compare Figure 32E and Figure 35B). Thus, higher-order midbrain and thalamus behave like the auditory cortex with regard to prediction error, which is the novel extension of the predictive coding scholarship. Finally, asymmetries in the direction of frequency-change detection (ascending vs. descending) have also been found in both animal (Harms et al., 2014) and human (Peter et al., 2010) MMN studies.

Concluding remarks

At the functional level, adaptation and deviance detection confabulate to segregate incoming sensory events into two separate streams of information processing: (a) A lemniscal stream of primary processing that represents even the less informative details of the scene, and (b) a non-lemniscal stream of higher-order processing that only represents changing aspects of the auditory scene, which pop out from the background. Thus, as anticipated by Barlow, the segregation of sensory events based on their informational content is indeed one of the neurophysiological substrates of auditory scene analysis and stream segregation.

These results set an important milestone in the evolution of the research carried out in our laboratory (Auditory Neuroscience Unit, INCYL), marking the end of a first, physiologically-oriented stage—which might be called "the SSA stage"—and the entry into a new, more cognitive-oriented stage—the "mismatch detection stage". On the one hand, with Study 1, I have completed the picture of SSA in the auditory system, by setting the last stone on it, namely, the description of SSA in non-lemniscal fields of the auditory cortex. On the other hand, with Study 2, I have confirmed that responses to deviant tones are indeed special, beyond the fact that they pop-out over the background of attenuated standards. They show indices of prediction error, which is a qualitative difference with respect to the classical SSA notion. The discovery that single neuron responses to simple oddball stimulation represent actual prediction error opens up a whole new family of research lines that could be followed by subsequent research projects. Among them, we can indicate the most important ones:

- ✓ Demonstrate mismatch detection for more complex types of rules, such as arbitrary relationships between successive stimuli.
- ✓ Demonstrate mismatch detection for complex sounds beyond pure tones, such as for spectrotemporally modulated or natural sounds.
- ✓ Perform manipulations such as reversible deactivation of frontal cortex or higher-order areas, optogenetic deactivation of specific cell populations, pharmacologic manipulations at the single cell level (microiontophoresis), etc. to dissociate the cellular mechanisms of repetition suppression and prediction error effects.
- ✓ Investigate specific alterations of the "adaptation" (repetition suppression) or "deviance detection" (prediction error) components of neuronal responses within clinical targets such as animal models of aging, autism, schizophrenia or attention disorders.

CONCLUSIONS

I present strong evidence linking animal SSA to the human MMN, a result thus far missing in animal research. Furthermore, my results demonstrate that prediction error is an intrinsic component of responses of single auditory neurons, emerging even from subcortical levels, and strengthen the case for the predictive coding theory of perceptual processing. In addition, I show that neuronal predictive activity underlies the generation of large-scale mismatch responses in animal models, and parallels important properties of human MMN. These are promising results for translational research into the cellular mechanisms that are disrupted in schizophrenia and other brain disorders characterized by reductions in large-scale mismatch responses, such as MMN. The conclusions of this thesis and their relevance for scientific advancement are the following:

1. Neurons in higher-order cortical regions show extreme SSA levels, almost twice as high as in primary cortical regions.
2. SSA as a prevalent property of the non-lemniscal auditory pathway, from midbrain to cortex.
3. The anatomical location and temporal development of SSA in auditory cortex matches well those of simultaneously recorded MMN in the rat.
4. Responses of single neurons to deviant tones in the oddball paradigm reflect a significant degree of deviance detection in addition to SSA.
5. Single neuron activity in response to oddball stimulation underlies the generation of MMN and earlier indices of deviance detection.
6. Responses of single neurons under oddball stimulation reflect the predictive activity of the brain, and in particular, responses to deviant tones represent prediction error at the single cell level.
7. The representation of prediction error along the auditory pathway follows a hierarchical pattern which is highly consistent with the postulates of the Hierarchical Predictive Coding Framework.
8. These results provide empirical support for the predictive coding account of MMN, which is increasing but still scarce.

REFERENCES

Abbott LF, Varela JA, Sen K, Nelson SB (1997) Synaptic depression and cortical gain control. Science 275:220–224.

Abolafia JM, Vergara R, Arnold MM, Reig R, Sanchez-Vives MV (2011) Cortical auditory adaptation in the awake rat and the role of potassium currents. Cereb Cortex 21:977–990.

Adrian ED, Zotterman Y (1926) The impulses produced by sensory nerve-endings: Part II. The response of a Single End-Organ. J Physiol (Lond) 61:151–171.

Aghamolaei M, Zarnowiec K, Grimm S, Escera C (2016) Functional dissociation between regularity encoding and deviance detection along the auditory hierarchy. Eur J Neurosci 43:529–535.

Akatsuka K, Wasaka T, Nakata H, Kida T, Hoshiyama M, Tamura Y, Kakigi R (2007) Objective examination for two-point stimulation using a somatosensory oddball paradigm: an MEG study. Clin Neurophysiol 118:403–411.

Alain C, Achim A, Woods DL (1999) Separate memory-related processing for auditory frequency and patterns. Psychophysiology 36:737–744.

Alain C, Cortese F, Picton TW (1998) Event-related brain activity associated with auditory pattern processing. Neuroreport 9:3537–3541.

Alain C, Woods DL, Ogawa KH (1994) Brain indices of automatic pattern processing. Neuroreport 6:140–144.

Alho K (1995) Cerebral generators of mismatch negativity (MMN) and its magnetic counterpart (MMNm) elicited by sound changes. Ear Hear 16:38–51.

Alho K, Winkler I, Escera C, Huotilainen M, Virtanen J, Jääskeläinen IP, Pekkonen E, Ilmoniemi RJ (1998) Processing of novel sounds and frequency changes in the human auditory cortex: magnetoencephalographic recordings. Psychophysiology 35:211–224.

Althen H, Grimm S, Escera C (2011) Fast detection of unexpected sound intensity decrements as revealed by human evoked potentials. PLoS ONE 6:e28522.

Althen H, Grimm S, Escera C (2013) Simple and complex acoustic regularities are encoded at different levels of the auditory hierarchy. Eur J Neurosci 38:3448–3455.

Anderson LA, Malmierca MS (2013) The effect of auditory cortex deactivation on stimulus-specific adaptation in the inferior colliculus of the rat. Eur J Neurosci 37:52–62.

Antunes FM, Malmierca MS (2011) Effect of auditory cortex deactivation on stimulus-specific adaptation in the medial geniculate body. J Neurosci 31:17306–17316.

Antunes FM, Nelken I, Covey E, Malmierca MS (2010) Stimulus-specific

adaptation in the auditory thalamus of the anesthetized rat. PLoS ONE 5:e14071.

Astikainen P, Cong F, Ristaniemi T, Hietanen JK (2013) Event-related potentials to unattended changes in facial expressions: detection of regularity violations or encoding of emotions? Front Hum Neurosci 7:557.

Astikainen P, Lillstrang E, Ruusuvirta T (2008) Visual mismatch negativity for changes in orientation--a sensory memory-dependent response. Eur J Neurosci 28:2319–2324.

Astikainen P, Stefanics G, Nokia M, Lipponen A, Cong F, Penttonen M, Ruusuvirta T (2011) Memory-based mismatch response to frequency changes in rats. PLoS ONE 6:e24208.

Atiani S, David SV, Elgueda D, Locastro M, Radtke-Schuller S, Shamma SA, Fritz JB (2014) Emergent selectivity for task-relevant stimuli in higher-order auditory cortex. Neuron 82:486–499.

Auksztulewicz R, Friston K (2016a) Repetition suppression and its contextual determinants in predictive coding. Cortex 80:125–140.

Auksztulewicz R, Friston K (2016b) Repetition suppression and its contextual determinants in predictive coding. Cortex.

Ayala YA, Malmierca MS (2013) Stimulus-specific adaptation and deviance detection in the inferior colliculus. Front Neural Circuits 6:89.

Ayala YA, Malmierca MS (2015) Cholinergic Modulation of Stimulus-Specific Adaptation in the Inferior Colliculus. J Neurosci 35:12261–12272.

Ayala YA, Pérez-González D, Duque D, Nelken I, Malmierca MS (2013) Frequency discrimination and stimulus deviance in the inferior colliculus and cochlear nucleus. Front Neural Circuits 6:119.

Ayala YA, Pérez-González D, Duque D, Palmer, AR, Malmierca, MS (2016) Extracellular recording of neuronal activity combined with microiontophoretic application of neuroactive substances in awake mice. JOVE.

Baldeweg T (2006) Repetition effects to sounds: evidence for predictive coding in the auditory system. Trends Cogn Sci 10:93–94.

Barlow H (1961) Possible principles underlying the transformation of sensory messages. In: Sensory Communication, pp 217–234. Cambridge, Massachusetts: MIT Press.

Bartlett EL, Smith PH (1999) Anatomic, intrinsic, and synaptic properties of dorsal and ventral division neurons in rat medial geniculate body. J Neurophysiol 81:1999–2016.

Bartlett EL, Stark JM, Guillery RW, Smith PH (2000) Comparison of the fine structure of cortical and collicular terminals in the rat medial geniculate body. Neuroscience 100:811–828.

Bastos AM, Usrey WM, Adams RA, Mangun GR, Fries P, Friston KJ (2012) Canonical microcircuits for predictive coding. Neuron 76:695–711.

Bäuerle P, von der Behrens W, Kössl M, Gaese BH (2011) Stimulus-specific adaptation in the gerbil primary auditory thalamus is the result of a fast frequency-specific habituation and is regulated by the corticofugal system. J Neurosci 31:9708–9722.

Bendixen A, SanMiguel I, Schröger E (2012) Early electrophysiological indicators for predictive processing in audition: a review. Int J Psychophysiol 83:120–131.

Bendor D (2015) The role of inhibition in a computational model of an auditory cortical neuron during the encoding of temporal information. PLoS Comput Biol 11:e1004197.

Benucci A, Saleem AB, Carandini M (2013) Adaptation maintains population homeostasis in primary visual cortex. Nat Neurosci 16:724–729.

Bordi F, LeDoux JE (1994) Response properties of single units in areas of rat auditory thalamus that project to the amygdala. I. Acoustic discharge patterns and frequency receptive fields. Exp Brain Res 98:261–274.

Bregman AS (1990) Auditory Scene Analysis. MIT Press Available at: https://mitpress.mit.edu/books/auditory-scene-analysis [Accessed April 11, 2016].

Bullock DC, Palmer AR, Rees A (1988) Compact and easy-to-use tungsten-in-glass microelectrode manufacturing workstation. Med Biol Eng Comput 26:669–672.

Buzsáki G, Anastassiou CA, Koch C (2012) The origin of extracellular fields and currents--EEG, ECoG, LFP and spikes. Nat Rev Neurosci 13:407–420.

Cacciaglia R, Escera C, Slabu L, Grimm S, Sanjuán A, Ventura-Campos N, Ávila C (2015) Involvement of the human midbrain and thalamus in auditory deviance detection. Neuropsychologia.

Capsius B, Leppelsack HJ (1996) Influence of urethane anesthesia on neural processing in the auditory cortex analogue of a songbird. Hear Res 96:59–70.

Carandini M, Ferster D (1997) A tonic hyperpolarization underlying contrast adaptation in cat visual cortex. Science 276:949–952.

Carrasco A, Kok MA, Lomber SG (2015) Effects of core auditory cortex deactivation on neuronal response to simple and complex acoustic signals in the contralateral anterior auditory field. Cereb Cortex 25:84–96.

Carrasco A, Lomber SG (2010) Reciprocal modulatory influences between tonotopic and nontonotopic cortical fields in the cat. J Neurosci 30:1476–1487.

Carrasco A, Lomber SG (2011) Neuronal activation times to simple, complex, and natural sounds in cat primary and nonprimary auditory cortex. Journal of Neurophysiology 106:1166–1178.

Chen I-W, Helmchen F, Lütcke H (2015) Specific Early and Late Oddball-

Evoked Responses in Excitatory and Inhibitory Neurons of Mouse Auditory Cortex. J Neurosci 35:12560–12573.

Chung S, Li X, Nelson SB (2002) Short-term depression at thalamocortical synapses contributes to rapid adaptation of cortical sensory responses in vivo. Neuron 34:437–446.

Clifford CWG, Webster MA, Stanley GB, Stocker AA, Kohn A, Sharpee TO, Schwartz O (2007) Visual adaptation: neural, psychological and computational aspects. Vision Res 47:3125–3131.

Clifford CW, Wenderoth P, Spehar B (2000) A functional angle on some after-effects in cortical vision. Proc Biol Sci 267:1705–1710.

Condon CD, Weinberger NM (1991) Habituation produces frequency-specific plasticity of receptive fields in the auditory cortex. Behav Neurosci 105:416–430.

Cooke JE, Zhang H, Kelly JB (2007) Detection of sinusoidal amplitude modulated sounds: deficits after bilateral lesions of auditory cortex in the rat. Hear Res 231:90–99.

Cornella M, Leung S, Grimm S, Escera C (2012) Detection of Simple and Pattern Regularity Violations Occurs at Different Levels of the Auditory Hierarchy. PLoS ONE 7:e43604.

Cornella M, Leung S, Grimm S, Escera C (2013) Regularity encoding and deviance detection of frequency modulated sweeps: human middle- and long-latency auditory evoked potentials. Psychophysiology 50:1275–1281.

Costa-Faidella J, Baldeweg T, Grimm S, Escera C (2011a) Interactions between "what" and "when" in the auditory system: temporal predictability enhances repetition suppression. J Neurosci 31:18590–18597.

Costa-Faidella J, Grimm S, Slabu L, Díaz-Santaella F, Escera C (2011b) Multiple time scales of adaptation in the auditory system as revealed by human evoked potentials. Psychophysiology 48:774–783.

Csépe V, Karmos G, Molnár M (1987) Evoked potential correlates of stimulus deviance during wakefulness and sleep in cat--animal model of mismatch negativity. Electroencephalogr Clin Neurophysiol 66:571–578.

Czigler I, Balázs L, Winkler I (2002) Memory-based detection of task-irrelevant visual changes. Psychophysiology 39:869–873.

Dean I, Harper NS, McAlpine D (2005) Neural population coding of sound level adapts to stimulus statistics. Nat Neurosci 8:1684–1689.

DeFelipe J et al. (2013) New insights into the classification and nomenclature of cortical GABAergic interneurons. Nat Rev Neurosci 14:202–216.

Dehaene S, Meyniel F, Wacongne C, Wang L, Pallier C (2015) The Neural Representation of Sequences: From Transition Probabilities to Algebraic Patterns and Linguistic Trees. Neuron 88:2–19.

Denève S, Machens CK (2016) Efficient codes and balanced networks. Nat Neurosci 19:375–382.

Dhruv NT, Carandini M (2014) Cascaded effects of spatial adaptation in the early visual system. Neuron 81:529–535.

Díaz-Quesada M, Maravall M (2008) Intrinsic mechanisms for adaptive gain rescaling in barrel cortex. J Neurosci 28:696–710.

Donishi T, Kimura A, Okamoto K, Tamai Y (2006) "Ventral" area in the rat auditory cortex: a major auditory field connected with the dorsal division of the medial geniculate body. Neuroscience 141:1553–1567.

Doron NN, Ledoux JE, Semple MN (2002) Redefining the tonotopic core of rat auditory cortex: physiological evidence for a posterior field. J Comp Neurol 453:345–360.

Dragoi V, Sharma J, Miller EK, Sur M (2002) Dynamics of neuronal sensitivity in visual cortex and local feature discrimination. Nat Neurosci 5:883–891.

Dragoi V, Sharma J, Sur M (2000) Adaptation-induced plasticity of orientation tuning in adult visual cortex. Neuron 28:287–298.

Drew PJ, Abbott LF (2006) Models and properties of power-law adaptation in neural systems. J Neurophysiol 96:826–833.

Duque D, Ayala YA, Malmierca MS (2015) Deviance detection in auditory subcortical structures: what can we learn from neurochemistry and neural connectivity? Cell Tissue Res.

Duque D, Malmierca MS (2015) Stimulus-specific adaptation in the inferior colliculus of the mouse: anesthesia and spontaneous activity effects. Brain Struct Funct 220:3385–3398.

Duque D, Malmierca MS, Caspary DM (2014) Modulation of stimulus-specific adaptation by GABA(A) receptor activation or blockade in the medial geniculate body of the anaesthetized rat. J Physiol 592:729–743.

Duque D, Pérez-González D, Ayala YA, Palmer AR, Malmierca MS (2012) Topographic distribution, frequency, and intensity dependence of stimulus-specific adaptation in the inferior colliculus of the rat. J Neurosci 32:17762–17774.

Duque D, Wang X, Nieto-Diego J, Krumbholz K, Malmierca MS (2016) Neurons in the inferior colliculus of the rat show stimulus-specific adaptation for frequency, but not for intensity. Sci Rep 6:24114.

Dutta A, Wagner H, Gutfreund Y (2016) Responses to Pop-Out Stimuli in the Barn Owl's Optic Tectum Can Emerge through Stimulus-Specific Adaptation. J Neurosci 36:4876–4887.

Edeline J-M (2012) Beyond traditional approaches to understanding the functional role of neuromodulators in sensory cortices. Front Behav Neurosci 6:45.

Eggermont JJ (2014) Animal models of auditory temporal processing. Int J Psychophysiol.

Eggermont JJ (2015) Animal models of auditory temporal processing. Int J Psychophysiol 95:202–215.

Escera C, Alho K, Winkler I, Näätänen R (1998) Neural mechanisms of involuntary attention to acoustic novelty and change. J Cogn Neurosci 10:590–604.

Escera C, Leung S, Grimm S (2014) Deviance detection based on regularity encoding along the auditory hierarchy: electrophysiological evidence in humans. Brain Topogr 27:527–538.

Escera C, Malmierca MS (2014) The auditory novelty system: an attempt to integrate human and animal research. Psychophysiology 51:111–123.

Escera C, Yago E, Corral M-J, Corbera S, Nuñez MI (2003) Attention capture by auditory significant stimuli: semantic analysis follows attention switching. Eur J Neurosci 18:2408–2412.

Fairhall AL, Lewen GD, Bialek W, de Ruyter Van Steveninck RR (2001) Efficiency and ambiguity in an adaptive neural code. Nature 412:787–792.

Farley BJ, Quirk MC, Doherty JJ, Christian EP (2010) Stimulus-specific adaptation in auditory cortex is an NMDA-independent process distinct from the sensory novelty encoded by the mismatch negativity. J Neurosci 30:16475–16484.

Felleman DJ, Van Essen DC (1991) Distributed hierarchical processing in the primate cerebral cortex. Cereb Cortex 1:1–47.

Fishman YI (2014) The mechanisms and meaning of the mismatch negativity. Brain Topogr 27:500–526.

Fishman YI, Steinschneider M (2012) Searching for the mismatch negativity in primary auditory cortex of the awake monkey: deviance detection or stimulus specific adaptation? J Neurosci 32:15747–15758.

Friston K (2005) A theory of cortical responses. Philos Trans R Soc Lond B Biol Sci 360:815–836.

Friston K (2009) The free-energy principle: a rough guide to the brain? Trends Cogn Sci 13:293–301.

Froemke RC (2015) Plasticity of cortical excitatory-inhibitory balance. Annu Rev Neurosci 38:195–219.

Froemke RC, Merzenich MM, Schreiner CE (2007) A synaptic memory trace for cortical receptive field plasticity. Nature 450:425–429.

Gaese BH, Ostwald J (2001) Anesthesia changes frequency tuning of neurons in the rat primary auditory cortex. J Neurophysiol 86:1062–1066.

Games KD, Winer JA (1988) Layer V in rat auditory cortex: projections to the

inferior colliculus and contralateral cortex. Hear Res 34:1–25.

Garrido MI, Friston KJ, Kiebel SJ, Stephan KE, Baldeweg T, Kilner JM (2008) The functional anatomy of the MMN: a DCM study of the roving paradigm. Neuroimage 42:936–944.

Garrido MI, Kilner JM, Kiebel SJ, Stephan KE, Baldeweg T, Friston KJ (2009a) Repetition suppression and plasticity in the human brain. Neuroimage 48:269–279.

Garrido MI, Kilner JM, Stephan KE, Friston KJ (2009b) The mismatch negativity: a review of underlying mechanisms. Clin Neurophysiol 120:453–463.

Garrido MI, Sahani M, Dolan RJ (2013) Outlier responses reflect sensitivity to statistical structure in the human brain. PLoS Comput Biol 9:e1002999.

Giard MH, Perrin F, Pernier J, Bouchet P (1990) Brain generators implicated in the processing of auditory stimulus deviance: a topographic event-related potential study. Psychophysiology 27:627–640.

Gimenez TL, Lorenc M, Jaramillo S (2015) Adaptive categorization of sound frequency does not require the auditory cortex in rats. J Neurophysiol 114:1137–1145.

Gomes H, Bernstein R, Ritter W, Vaughan HG, Miller J (1997) Storage of feature conjunctions in transient auditory memory. Psychophysiology 34:712–716.

Grill-Spector K, Henson R, Martin A (2006) Repetition and the brain: neural models of stimulus-specific effects. Trends Cogn Sci (Regul Ed) 10:14–23.

Grimm S, Escera C (2012) Auditory deviance detection revisited: evidence for a hierarchical novelty system. Int J Psychophysiol 85:88–92.

Grimm S, Escera C, Nelken I (2015) Early indices of deviance detection in humans and animal models. Biol Psychol.

Grimm S, Escera C, Slabu L, Costa-Faidella J (2011) Electrophysiological evidence for the hierarchical organization of auditory change detection in the human brain. Psychophysiology 48:377–384.

Guillery RW, Sherman SM (2002) Thalamic relay functions and their role in corticocortical communication: generalizations from the visual system. Neuron 33:163–175.

Güntürkün O, Bugnyar T (2016) Cognition without Cortex. Trends Cogn Sci 20:291–303.

Haenschel C, Vernon DJ, Dwivedi P, Gruzelier JH, Baldeweg T (2005) Event-related brain potential correlates of human auditory sensory memory-trace formation. J Neurosci 25:10494–10501.

Hanna J, Mejias S, Schelstraete M-A, Pulvermüller F, Shtyrov Y, Van der Lely HKJ (2014) Early activation of Broca's area in grammar processing as revealed by the syntactic mismatch negativity and distributed source analysis. Cogn Neurosci 5:66–76.

Hara K, Harris RA (2002) The anesthetic mechanism of urethane: the effects on neurotransmitter-gated ion channels. Anesth Analg 94:313–318.

Harms L, Fulham WR, Todd J, Budd TW, Hunter M, Meehan C, Penttonen M, Schall U, Zavitsanou K, Hodgson DM, Michie PT (2014) Mismatch negativity (MMN) in freely-moving rats with several experimental controls. PLoS One 9:e110892.

Harms L, Michie PT, Näätänen R (2015) Criteria for determining whether mismatch responses exist in animal models: Focus on rodents. Biol Psychol.

Harms L, Michie PT, Näätänen R (2016) Criteria for determining whether mismatch responses exist in animal models: Focus on rodents. Biol Psychol 116:28–35.

Hershenhoren I, Taaseh N, Antunes FM, Nelken I (2014) Intracellular correlates of stimulus-specific adaptation. J Neurosci 34:3303–3319.

Higgins NC, Storace DA, Escabí MA, Read HL (2010) Specialization of binaural responses in ventral auditory cortices. J Neurosci 30:14522–14532.

Horváth J, Czigler I, Jacobsen T, Maess B, Schröger E, Winkler I (2008) MMN or no MMN: no magnitude of deviance effect on the MMN amplitude. Psychophysiology 45:60–69.

Hu B (2003) Functional organization of lemniscal and nonlemniscal auditory thalamus. Exp Brain Res 153:543–549.

Hupé JM, James AC, Payne BR, Lomber SG, Girard P, Bullier J (1998) Cortical feedback improves discrimination between figure and background by V1, V2 and V3 neurons. Nature 394:784–787.

Imaizumi K, Lee CC (2014) Frequency transformation in the auditory lemniscal thalamocortical system. Front Neural Circuits 8:75.

Irvine DR, Huebner H (1979) Acoustic response characteristics of neurons in nonspecific areas of cat cerebral cortex. J Neurophysiol 42:107–122.

Isaacson JS, Scanziani M (2011) How inhibition shapes cortical activity. Neuron 72:231–243.

Jääskeläinen IP, Ahveninen J, Bonmassar G, Dale AM, Ilmoniemi RJ, Levänen S, Lin F-H, May P, Melcher J, Stufflebeam S, Tiitinen H, Belliveau JW (2004) Human posterior auditory cortex gates novel sounds to consciousness. Proc Natl Acad Sci U S A 101:6809–6814.

Jacobsen T, Schröger E (2001) Is there pre-attentive memory-based comparison of pitch? Psychophysiology 38:723–727.

Javitt DC, Schroeder CE, Steinschneider M, Arezzo JC, Vaughan HG Jr (1992) Demonstration of mismatch negativity in the monkey. Electroencephalogr Clin Neurophysiol 83:87–90.

Javitt DC, Steinschneider M, Schroeder CE, Vaughan HG, Arezzo JC (1994)

Detection of stimulus deviance within primate primary auditory cortex: intracortical mechanisms of mismatch negativity (MMN) generation. Brain Res 667:192–200.

Jin DZ, Dragoi V, Sur M, Seung HS (2005) Tilt aftereffect and adaptation-induced changes in orientation tuning in visual cortex. J Neurophysiol 94:4038–4050.

Jung F, Stephan KE, Backes H, Moran R, Gramer M, Kumagai T, Graf R, Endepols H, Tittgemeyer M (2013) Mismatch responses in the awake rat: evidence from epidural recordings of auditory cortical fields. PLoS One 8:e63203.

Kekoni J, Hämäläinen H, Saarinen M, Gröhn J, Reinikainen K, Lehtokoski A, Näätänen R (1997) Rate effect and mismatch responses in the somatosensory system: ERP-recordings in humans. Biol Psychol 46:125–142.

Kelly JB, Kavanagh GL (1986) Effects of auditory cortical lesions on pure-tone sound localization by the albino rat. Behav Neurosci 100:569–575.

Khouri L, Nelken I (2015) Detecting the unexpected. Curr Opin Neurobiol 35:142–147.

Kim KJ, Rieke F (2001) Temporal contrast adaptation in the input and output signals of salamander retinal ganglion cells. J Neurosci 21:287–299.

Kimura A, Donishi T, Okamoto K, Imbe H, Tamai Y (2007) Efferent connections of the ventral auditory area in the rat cortex: implications for auditory processing related to emotion. Eur J Neurosci 25:2819–2834.

Kimura A, Donishi T, Okamoto K, Tamai Y (2004) Efferent connections of "posterodorsal" auditory area in the rat cortex: implications for auditory spatial processing. Neuroscience 128:399–419.

Kimura A, Donishi T, Okamoto K, Tamai Y (2005) Topography of projections from the primary and non-primary auditory cortical areas to the medial geniculate body and thalamic reticular nucleus in the rat. Neuroscience 135:1325–1342.

Kimura A, Donishi T, Sakoda T, Hazama M, Tamai Y (2003) Auditory thalamic nuclei projections to the temporal cortex in the rat. Neuroscience 117:1003–1016.

Kimura M, Katayama J 'ichi, Ohira H, Schröger E (2009) Visual mismatch negativity: new evidence from the equiprobable paradigm. Psychophysiology 46:402–409.

King AJ, Nelken I (2009) Unraveling the principles of auditory cortical processing: can we learn from the visual system? Nat Neurosci 12:698–701.

King C, McGee T, Rubel EW, Nicol T, Kraus N (1995) Acoustic features and acoustic changes are represented by different central pathways. Hear Res 85:45–52.

Klein C, von der Behrens W, Gaese BH (2014) Stimulus-specific adaptation in field potentials and neuronal responses to frequency-modulated tones in the primary auditory cortex. Brain Topogr 27:599–610.

Koelsch S, Busch T, Jentschke S, Rohrmeier M (2016) Under the hood of

statistical learning: A statistical MMN reflects the magnitude of transitional probabilities in auditory sequences. Sci Rep 6:19741.

Kohn A (2007) Visual adaptation: physiology, mechanisms, and functional benefits. J Neurophysiol 97:3155–3164.

Kohn A, Movshon JA (2003) Neuronal adaptation to visual motion in area MT of the macaque. Neuron 39:681–691.

Kohn A, Movshon JA (2004) Adaptation changes the direction tuning of macaque MT neurons. Nat Neurosci 7:764–772.

Kraus N, McGee T, Littman T, Nicol T, King C (1994) Nonprimary auditory thalamic representation of acoustic change. J Neurophysiol 72:1270–1277.

Kropotov JD, Alho K, Näätänen R, Ponomarev VA, Kropotova OV, Anichkov AD, Nechaev VB (2000) Human auditory-cortex mechanisms of preattentive sound discrimination. Neurosci Lett 280:87–90.

La Camera G, Rauch A, Thurbon D, Lüscher H-R, Senn W, Fusi S (2006) Multiple time scales of temporal response in pyramidal and fast spiking cortical neurons. J Neurophysiol 96:3448–3464.

Lee CC (2015) Exploring functions for the non-lemniscal auditory thalamus. Front Neural Circuits 9:69.

Lee CC, Sherman SM (2011) On the classification of pathways in the auditory midbrain, thalamus, and cortex. Hear Res 276:79–87.

Leung S, Cornella M, Grimm S, Escera C (2012) Is fast auditory change detection feature specific? An electrophysiological study in humans. Psychophysiology 49:933–942.

Leung S, Recasens M, Grimm S, Escera C (2013) Electrophysiological index of acoustic temporal regularity violation in the middle latency range. Clin Neurophysiol 124:2397–2405.

Lieder F, Stephan KE, Daunizeau J, Garrido MI, Friston KJ (2013) A neurocomputational model of the mismatch negativity. PLoS Comput Biol 9:e1003288.

Li J et al. (2017) Primary Auditory Cortex is Required for Anticipatory Motor Response. Cereb Cortex:1–18.

Llano DA, Sherman SM (2008) Evidence for nonreciprocal organization of the mouse auditory thalamocortical-corticothalamic projection systems. J Comp Neurol 507:1209–1227.

Lohvansuu K, Hämäläinen JA, Tanskanen A, Bartling J, Bruder J, Honbolygó F, Schulte-Körne G, Démonet J-F, Csépe V, Leppänen PHT (2013) Separating mismatch negativity (MMN) response from auditory obligatory brain responses in school-aged children. Psychophysiology 50:640–652.

Lomber SG, Malhotra S (2008) Double dissociation of “what” and “where”

processing in auditory cortex. Nat Neurosci 11:609–616.

Lomber SG, McMillan AJ (2011) Functional Specialization in Primary and Non-primary Auditory Cortex. In: The Auditory Cortex (Winer JA, Schreiner CE, eds), pp 189–208. New York, NY: Springer.

Maess B, Jacobsen T, Schröger E, Friederici AD (2007) Localizing pre-attentive auditory memory-based comparison: magnetic mismatch negativity to pitch change. Neuroimage 37:561–571.

Malmierca MS (2003) The structure and physiology of the rat auditory system: an overview. Int Rev Neurobiol 56:147–211.

Malmierca MS (2015) Chapter 29 - Auditory System. In: The Rat Nervous System (Fourth Edition) (Paxinos G, ed), pp 865–946. San Diego: Academic Press.

Malmierca MS, Anderson LA, Antunes FM (2015) The cortical modulation of stimulus-specific adaptation in the auditory midbrain and thalamus: a potential neuronal correlate for predictive coding. Front Syst Neurosci 9:19.

Malmierca MS, Cristaudo S, Pérez-González D, Covey E (2009) Stimulus-specific adaptation in the inferior colliculus of the anesthetized rat. J Neurosci 29:5483–5493.

Malmierca MS, Izquierdo MA, Cristaudo S, Hernández O, Pérez-González D, Covey E, Oliver DL (2008) A discontinuous tonotopic organization in the inferior colliculus of the rat. The Journal of Neuroscience 28:4767–4776.

Malmierca MS, Rees A, Le Beau FE, Bjaalie JG (1995) Laminar organization of frequency-defined local axons within and between the inferior colliculi of the guinea pig. J Comp Neurol 357:124–144.

Malmierca MS, Sanchez-Vives MV, Escera C, Bendixen A (2014) Neuronal adaptation, novelty detection and regularity encoding in audition. Front Syst Neurosci 8:111.

Maravall M (2013) Adaptation and sensory coding. In: Principles of Neural Coding.

Maravall M, Alenda A, Bale MR, Petersen RS (2013) Transformation of adaptation and gain rescaling along the whisker sensory pathway. PLoS ONE 8:e82418.

Maravall M, Petersen RS, Fairhall AL, Arabzadeh E, Diamond ME (2007) Shifts in coding properties and maintenance of information transmission during adaptation in barrel cortex. PLoS Biol 5:e19.

May PJC, Tiitinen H (2010) Mismatch negativity (MMN), the deviance-elicited auditory deflection, explained. Psychophysiology 47:66–122.

Merrill EG, Ainsworth A (1972) Glass-coated platinum-plated tungsten microelectrodes. Med Biol Eng 10:662–672.

Metherate R, Cruikshank SJ (1999) Thalamocortical inputs trigger a propagating

envelope of gamma-band activity in auditory cortex in vitro. Exp Brain Res 126:160–174.

Meyer T, Olson CR (2011) Statistical learning of visual transitions in monkey inferotemporal cortex. Proc Natl Acad Sci USA 108:19401–19406.

Molholm S, Martinez A, Ritter W, Javitt DC, Foxe JJ (2005) The neural circuitry of pre-attentive auditory change-detection: an fMRI study of pitch and duration mismatch negativity generators. Cereb Cortex 15:545–551.

Moran RJ, Campo P, Symmonds M, Stephan KE, Dolan RJ, Friston KJ (2013) Free energy, precision and learning: the role of cholinergic neuromodulation. J Neurosci 33:8227–8236.

Mountcastle VB (1997) The columnar organization of the neocortex. Brain 120 (Pt 4):701–722.

Movshon JA, Lennie P (1979) Pattern-selective adaptation in visual cortical neurones. Nature 278:850–852.

Müller JR, Metha AB, Krauskopf J, Lennie P (1999) Rapid adaptation in visual cortex to the structure of images. Science 285:1405–1408.

Mumford D (1992) On the computational architecture of the neocortex. II. The role of cortico-cortical loops. Biol Cybern 66:241–251.

Musall S, Haiss F, Weber B, von der Behrens W (2015) Deviant Processing in the Primary Somatosensory Cortex. Cereb Cortex.

Musall S, von der Behrens W, Mayrhofer JM, Weber B, Helmchen F, Haiss F (2014) Tactile frequency discrimination is enhanced by circumventing neocortical adaptation. Nat Neurosci 17:1567–1573.

Näätänen R (1992) Attention and Brain Function. Routledge.

Näätänen R (1995) The mismatch negativity: a powerful tool for cognitive neuroscience. Ear Hear 16:6–18.

Näätänen R, Jacobsen T, Winkler I (2005) Memory-based or afferent processes in mismatch negativity (MMN): a review of the evidence. Psychophysiology 42:25–32.

Näätänen R, Kujala T, Escera C, Baldeweg T, Kreegipuu K, Carlson S, Ponton C (2012) The mismatch negativity (MMN)--a unique window to disturbed central auditory processing in ageing and different clinical conditions. Clin Neurophysiol 123:424–458.

Näätänen R, Lehtokoski A, Lennes M, Cheour M, Huotilainen M, Iivonen A, Vainio M, Alku P, Ilmoniemi RJ, Luuk A, Allik J, Sinkkonen J, Alho K (1997) Language-specific phoneme representations revealed by electric and magnetic brain responses. Nature 385:432–434.

Näätänen R, Paavilainen P, Rinne T, Alho K (2007) The mismatch negativity (MMN) in basic research of central auditory processing: a review. Clin Neurophysiol

118:2544–2590.

Näätänen R, Picton T (1987) The N1 wave of the human electric and magnetic response to sound: a review and an analysis of the component structure. Psychophysiology 24:375–425.

Näätänen R, Tervaniemi M, Sussman E, Paavilainen P, Winkler I (2001) "Primitive intelligence" in the auditory cortex. Trends Neurosci 24:283–288.

Nakamura T, Michie PT, Fulham WR, Todd J, Budd TW, Schall U, Hunter M, Hodgson DM (2011) Epidural Auditory Event-Related Potentials in the Rat to Frequency and duration Deviants: Evidence of Mismatch Negativity? Front Psychol 2:367.

Natan RG, Briguglio JJ, Mwilambwe-Tshilobo L, Jones S, Aizenberg M, Goldberg EM, Geffen MN (2015) Complementary control of sensory adaptation by two types of cortical interneurons. Elife 4:e09868.

Nelken I (2004) Processing of complex stimuli and natural scenes in the auditory cortex. Current Opinion in Neurobiology 14:474–480.

Nelken I (2014) Stimulus-specific adaptation and deviance detection in the auditory system: experiments and models. Biol Cybern 108:655–663.

Nelken I, Ulanovsky N (2007) Mismatch negativity and stimulus-specific adaptation in animal models. J Psychophysiol 21:214–223.

Nieto-Diego J, Malmierca MS (2016) Topographic Distribution of Stimulus-Specific Adaptation across Auditory Cortical Fields in the Anesthetized Rat. PLoS Biol 14:e1002397.

Nir Y, Vyazovskiy VV, Cirelli C, Banks MI, Tononi G (2015) Auditory responses and stimulus-specific adaptation in rat auditory cortex are preserved across NREM and REM sleep. Cereb Cortex 25:1362–1378.

Noda T, Takahashi H (2015) Anesthetic effects of isoflurane on the tonotopic map and neuronal population activity in the rat auditory cortex. Eur J Neurosci 42:2298–2311.

Opitz B, Schröger E, von Cramon DY (2005) Sensory and cognitive mechanisms for preattentive change detection in auditory cortex. Eur J Neurosci 21:531–535.

Oswald A-MM, Schiff ML, Reyes AD (2006) Synaptic mechanisms underlying auditory processing. Curr Opin Neurobiol 16:371–376.

Pandya PK, Rathbun DL, Moucha R, Engineer ND, Kilgard MP (2008) Spectral and temporal processing in rat posterior auditory cortex. Cereb Cortex 18:301–314.

Parvizi J (2009) Corticocentric myopia: old bias in new cognitive sciences. Trends Cogn Sci 13:354–359.

Pause BM, Krauel K (2000) Chemosensory event-related potentials (CSERP) as a key to the psychology of odors. Int J Psychophysiol 36:105–122.

Pérez-González D, Hernández O, Covey E, Malmierca MS (2012) GABA(A)-Mediated Inhibition Modulates Stimulus-Specific Adaptation in the Inferior Colliculus. PLoS ONE 7:e34297.

Pérez-González D, Malmierca MS (2014) Adaptation in the auditory system: an overview. Front Integr Neurosci 8:19.

Pérez-González D, Malmierca MS, Covey E (2005) Novelty detector neurons in the mammalian auditory midbrain. Eur J Neurosci 22:2879–2885.

Peter V, McArthur G, Thompson WF (2010) Effect of deviance direction and calculation method on duration and frequency mismatch negativity (MMN). Neurosci Lett 482:71–75.

Phillips DP, Irvine DR (1981) Responses of single neurons in physiologically defined primary auditory cortex (AI) of the cat: frequency tuning and responses to intensity. J Neurophysiol 45:48–58.

Phillips HN, Blenkmann A, Hughes LE, Kochen S, Bekinschtein TA, Cam-Can, Rowe JB (2016) Convergent evidence for hierarchical prediction networks from human electrocorticography and magnetoencephalography. Cortex 82:192–205.

Picton TW (2010) Human Auditory Evoked Potentials. Plural Pub.

Pincze Z, Lakatos P, Rajkai C, Ulbert I, Karmos G (2001) Separation of mismatch negativity and the N1 wave in the auditory cortex of the cat: a topographic study. Clin Neurophysiol 112:778–784.

Pincze Z, Lakatos P, Rajkai C, Ulbert I, Karmos G (2002) Effect of deviant probability and interstimulus/interdeviant interval on the auditory N1 and mismatch negativity in the cat auditory cortex. Brain Res Cogn Brain Res 13:249–253.

Polley DB, Read HL, Storace DA, Merzenich MM (2007) Multiparametric auditory receptive field organization across five cortical fields in the albino rat. J Neurophysiol 97:3621–3638.

Popper AN, Fay RR (1992) The Mammalian Auditory Pathway: Neurophysiology. Springer.

Pratt H, Starr A, Michalewski HJ, Dimitrijevic A, Bleich N, Mittelman N (2009) Auditory-evoked potentials to frequency increase and decrease of high- and low-frequency tones. Clin Neurophysiol 120:360–373.

Profant O, Burianová J, Syka J (2013) The response properties of neurons in different fields of the auditory cortex in the rat. Hear Res 296:51–59.

Puccini GD, Sanchez-Vives MV, Compte A (2007) Integrated mechanisms of anticipation and rate-of-change computations in cortical circuits. PLoS Comput Biol 3:e82.

Pulvermüller F, Shtyrov Y (2003) Automatic processing of grammar in the human brain as revealed by the mismatch negativity. Neuroimage 20:159–172.

Pulvermüller F, Shtyrov Y, Hasting AS, Carlyon RP (2008) Syntax as a reflex: neurophysiological evidence for early automaticity of grammatical processing. Brain Lang 104:244–253.

Puschmann S, Sandmann P, Ahrens J, Thorne J, Weerda R, Klump G, Debener S, Thiel CM (2013) Electrophysiological correlates of auditory change detection and change deafness in complex auditory scenes. Neuroimage 75:155–164.

Qin L, Sato Y (2004) Suppression of auditory cortical activities in awake cats by pure tone stimuli. Neurosci Lett 365:190–194.

Rao RP, Ballard DH (1999) Predictive coding in the visual cortex: a functional interpretation of some extra-classical receptive-field effects. Nat Neurosci 2:79–87.

Rauschecker JP, Romanski LM (2011) Auditory Cortical Organization: Evidence for Functional Streams. In: The Auditory Cortex (Winer JA, Schreiner CE, eds), pp 99–116. Springer US. Available at: http://link.springer.com/chapter/10.1007/978-1-4419-0074-6_4 [Accessed April 4, 2017].

Recanzone GH, Schreiner CE, Sutter ML, Beitel RE, Merzenich MM (1999) Functional organization of spectral receptive fields in the primary auditory cortex of the owl monkey. J Comp Neurol 415:460–481.

Recasens M, Grimm S, Capilla A, Nowak R, Escera C (2014) Two sequential processes of change detection in hierarchically ordered areas of the human auditory cortex. Cereb Cortex 24:143–153.

Reches A, Gutfreund Y (2008) Stimulus-specific adaptations in the gaze control system of the barn owl. J Neurosci 28:1523–1533.

Rieke F (1999) Spikes: Exploring the Neural Code. MIT Press.

Ritter W, Deacon D, Gomes H, Javitt DC, Vaughan HG (1995) The mismatch negativity of event-related potentials as a probe of transient auditory memory: a review. Ear Hear 16:52–67.

Robinson BL, Harper NS, McAlpine D (2016) Meta-adaptation in the auditory midbrain under cortical influence. Nat Commun 7:13442.

Robinson BL, McAlpine D (2009) Gain control mechanisms in the auditory pathway. Curr Opin Neurobiol 19:402–407.

Ruhnau P, Herrmann B, Schröger E (2012) Finding the right control: the mismatch negativity under investigation. Clin Neurophysiol 123:507–512.

Rutkowski RG, Miasnikov AA, Weinberger NM (2003) Characterisation of multiple physiological fields within the anatomical core of rat auditory cortex. Hear Res 181:116–130.

Ruusuvirta T, Penttonen M, Korhonen T (1998) Auditory cortical event-related potentials to pitch deviances in rats. Neurosci Lett 248:45–48.

Saldaña E, Feliciano M, Mugnaini E (1996) Distribution of descending projections

from primary auditory neocortex to inferior colliculus mimics the topography of intracollicular projections. J Comp Neurol 371:15–40.

Saldaña E, Merchán MA (1992) Intrinsic and commissural connections of the rat inferior colliculus. J Comp Neurol 319:417–437.

Sanchez-Vives MV, Nowak LG, McCormick DA (2000) Cellular mechanisms of long-lasting adaptation in visual cortical neurons in vitro. J Neurosci 20:4286–4299.

Schinkel-Bielefeld N, David SV, Shamma SA, Butts DA (2012) Inferring the role of inhibition in auditory processing of complex natural stimuli. J Neurophysiol 107:3296–3307.

Schreiner CE, Cynader MS (1984) Basic functional organization of second auditory cortical field (AII) of the cat. J Neurophysiol 51:1284–1305.

Schröger E, Bendixen A, Denham SL, Mill RW, Bőhm TM, Winkler I (2014) Predictive regularity representations in violation detection and auditory stream segregation: from conceptual to computational models. Brain Topogr 27:565–577.

Schwartz O, Pillow JW, Rust NC, Simoncelli EP (2006) Spike-triggered neural characterization. J Vis 6:484–507.

Schwindt PC, Spain WJ, Foehring RC, Stafstrom CE, Chubb MC, Crill WE (1988) Multiple potassium conductances and their functions in neurons from cat sensorimotor cortex in vitro. J Neurophysiol 59:424–449.

Seriès P, Stocker AA, Simoncelli EP (2009) Is the homunculus "aware" of sensory adaptation? Neural Comput 21:3271–3304.

Shannon CE, Weaver W (1998) The Mathematical Theory of Communication. University of Illinois Press.

Sherman SM (2007) The thalamus is more than just a relay. Curr Opin Neurobiol 17:417–422.

Sherman SM, Guillery RW (1996) Functional organization of thalamocortical relays. J Neurophysiol 76:1367–1395.

Sherman SM, Guillery RW (2011) Distinct functions for direct and transthalamic corticocortical connections. J Neurophysiol 106:1068–1077.

Shiga T, Althen H, Cornella M, Zarnowiec K, Yabe H, Escera C (2015) Deviance-Related Responses along the Auditory Hierarchy: Combined FFR, MLR and MMN Evidence. PLoS ONE 10:e0136794.

Shinozaki N, Yabe H, Sutoh T, Hiruma T, Kaneko S (1998) Somatosensory automatic responses to deviant stimuli. Brain Res Cogn Brain Res 7:165–171.

Shipp S (2007) Structure and function of the cerebral cortex. Current Biology 17:R443–R449.

Shiramatsu TI, Kanzaki R, Takahashi H (2013) Cortical mapping of mismatch

negativity with deviance detection property in rat. PLoS One 8:e82663.

Sillito AM, Cudeiro J, Jones HE (2006) Always returning: feedback and sensory processing in visual cortex and thalamus. Trends Neurosci 29:307–316.

Simoncelli EP, Paninski L, Pillow J, Schwartz O (2004) Characterization of neural responses with stochastic stimuli. In: The Cognitive Neurosciences III, 3rd ed. MIT Press.

Slabu L, Escera C, Grimm S, Costa-Faidella J (2010) Early change detection in humans as revealed by auditory brainstem and middle-latency evoked potentials. Eur J Neurosci 32:859–865.

Slabu L, Grimm S, Escera C (2012) Novelty detection in the human auditory brainstem. J Neurosci 32:1447–1452.

Smith PH, Uhlrich DJ, Manning KA, Banks MI (2012) Thalamocortical projections to rat auditory cortex from the ventral and dorsal divisions of the medial geniculate nucleus. J Comp Neurol 520:34–51.

Solomon SG, Kohn A (2014) Moving sensory adaptation beyond suppressive effects in single neurons. Curr Biol 24:R1012–R1022.

Stefanics G, Kremláček J, Czigler I (2014) Visual mismatch negativity: a predictive coding view. Front Hum Neurosci 8:666.

Stefanics G, Kremláček J, Czigler I (2016) Mismatch negativity and neural adaptation: Two sides of the same coin. Response: Commentary: Visual mismatch negativity: a predictive coding view. Front Hum Neurosci 10:13.

Storace DA, Higgins NC, Chikar JA, Oliver DL, Read HL (2012) Gene expression identifies distinct ascending glutamatergic pathways to frequency-organized auditory cortex in the rat brain. J Neurosci 32:15759–15768.

Storace DA, Higgins NC, Read HL (2010) Thalamic label patterns suggest primary and ventral auditory fields are distinct core regions. The Journal of Comparative Neurology 518:1630–1646.

Summerfield C, de Lange FP (2014) Expectation in perceptual decision making: neural and computational mechanisms. Nat Rev Neurosci 15:745–756.

Summerfield C, Trittschuh EH, Monti JM, Mesulam MM, Egner T (2008) Neural repetition suppression reflects fulfilled perceptual expectations. Nat Neurosci 11:1004–1006.

Sutter ML, Shamma SA (2011) The Relationship of Auditory Cortical Activity to Perception and Behavior. In: The Auditory Cortex (Winer JA, Schreiner CE, eds), pp 189–208. New York, NY: Springer.

Swanson LR (2016) The Predictive Processing Paradigm Has Roots in Kant. Front Syst Neurosci 10:79.

Szymanski FD, Garcia-Lazaro JA, Schnupp JWH (2009) Current source density

profiles of stimulus-specific adaptation in rat auditory cortex. J Neurophysiol 102:1483–1490.

Taaseh N, Yaron A, Nelken I (2011) Stimulus-specific adaptation and deviance detection in the rat auditory cortex. PLoS One 6:e23369.

Takahashi H, Nakao M, Kaga K (2005) Interfield differences in intensity and frequency representation of evoked potentials in rat auditory cortex. Hear Res 210:9–23.

Tervaniemi M, Maury S, Näätänen R (1994) Neural representations of abstract stimulus features in the human brain as reflected by the mismatch negativity. Neuroreport 5:844–846.

Tikhonravov D, Neuvonen T, Pertovaara A, Savioja K, Ruusuvirta T, Näätänen R, Carlson S (2010) Dose-related effects of memantine on a mismatch negativity-like response in anesthetized rats. Neuroscience 167:1175–1182.

Todd J, Harms L, Schall U, Michie PT (2013) Mismatch negativity: translating the potential. Front Psychiatry 4:171.

Ulanovsky N, Las L, Farkas D, Nelken I (2004) Multiple time scales of adaptation in auditory cortex neurons. J Neurosci 24:10440–10453.

Ulanovsky N, Las L, Nelken I (2003) Processing of low-probability sounds by cortical neurons. Nat Neurosci 6:391–398.

Umbricht D, Vyssotki D, Latanov A, Nitsch R, Lipp H-P (2005) Deviance-related electrophysiological activity in mice: is there mismatch negativity in mice? Clin Neurophysiol 116:353–363.

von der Behrens W, Bäuerle P, Kössl M, Gaese BH (2009) Correlating stimulus-specific adaptation of cortical neurons and local field potentials in the awake rat. J Neurosci 29:13837–13849.

Wacongne C, Changeux J-P, Dehaene S (2012) A neuronal model of predictive coding accounting for the mismatch negativity. J Neurosci 32:3665–3678.

Wacongne C, Labyt E, van Wassenhove V, Bekinschtein T, Naccache L, Dehaene S (2011) Evidence for a hierarchy of predictions and prediction errors in human cortex. Proc Natl Acad Sci USA 108:20754–20759.

Wang X, Lu T, Bendor D, Bartlett E (2008) Neural coding of temporal information in auditory thalamus and cortex. Neuroscience 157:484–494.

Wan H, Warburton EC, Kuśmierek P, Aggleton JP, Kowalska DM, Brown MW (2001) Fos imaging reveals differential neuronal activation of areas of rat temporal cortex by novel and familiar sounds. Eur J Neurosci 14:118–124.

Wark B, Lundstrom BN, Fairhall A (2007) Sensory adaptation. Curr Opin Neurobiol 17:423–429.

Wehr M, Zador AM (2003) Balanced inhibition underlies tuning and sharpens spike timing in auditory cortex. Nature 426:442–446.

Wehr M, Zador AM (2005) Synaptic mechanisms of forward suppression in rat auditory cortex. Neuron 47:437–445.

Weinberger NM (2004) Specific long-term memory traces in primary auditory cortex. Nat Rev Neurosci 5:279–290.

Whitmire CJ, Stanley GB (2016) Rapid Sensory Adaptation Redux: A Circuit Perspective. Neuron 92:298–315.

Winer JA (2006) Decoding the auditory corticofugal systems. Hear Res 212:1–8.

Winer JA, Saint Marie RL, Larue DT, Oliver DL (1996) GABAergic feedforward projections from the inferior colliculus to the medial geniculate body. Proc Natl Acad Sci USA 93:8005–8010.

Winer JA, Schreiner CE (2011) The Auditory Cortex. Springer.

Winkler I (2007) Interpreting the Mismatch Negativity. Journal of Psychophysiology 21:147–163.

Winkler I, Czigler I (2012) Evidence from auditory and visual event-related potential (ERP) studies of deviance detection (MMN and vMMN) linking predictive coding theories and perceptual object representations. Int J Psychophysiol 83:132–143.

Winkler I, Karmos G, Näätänen R (1996) Adaptive modeling of the unattended acoustic environment reflected in the mismatch negativity event-related potential. Brain Res 742:239–252.

Winkler I, Schröger E (2015) Auditory perceptual objects as generative models: Setting the stage for communication by sound. Brain Lang 148:1–22.

Yabe H, Tervaniemi M, Reinikainen K, Näätänen R (1997) Temporal window of integration revealed by MMN to sound omission. Neuroreport 8:1971–1974.

Yaron A, Hershenhoren I, Nelken I (2012) Sensitivity to complex statistical regularities in rat auditory cortex. Neuron 76:603–615.

Yarrow S, Razak KA, Seitz AR, Seriès P (2014) Detecting and quantifying topography in neural maps. PLoS One 9:e87178.

Yu X-J, Xu X-X, He S, He J (2009) Change detection by thalamic reticular neurons. Nat Neurosci 12:1165–1170.

Zhang LI, Tan AYY, Schreiner CE, Merzenich MM (2003) Topography and synaptic shaping of direction selectivity in primary auditory cortex. Nature 424:201–205.

Zmarz P, Keller GB (2016) Mismatch Receptive Fields in Mouse Visual Cortex. Neuron 92:766–772.

Zurita P, Villa AE, de Ribaupierre Y, de Ribaupierre F, Rouiller EM (1994) Changes of single unit activity in the cat's auditory thalamus and cortex associated to different anesthetic conditions. Neurosci Res 19:303–316.

APPENDIX I: SUMMARY IN SPANISH

INTRODUCCIÓN

Las neuronas de la corteza auditiva (AC) muestran una propiedad denominada adaptación a estímulos específicos (*stimulus-specific adaptation*, SSA), que ayuda al sistema auditivo a responder de inmediato a cambios inesperados en el ambiente auditivo. Estas respuestas neuronales adaptadas están estrechamente ligadas al denominado "potencial de disparidad" (MMN, del inglés "mismatch negativity"), un componente de los potenciales evocados auditivos registrados en humanos bajo determinados paradigmas de estimulación. El objetivo fundamental de este trabajo es localizar y estudiar detalladamente las neuronas que se consideran responsables de la generación de estos componentes de disparidad en la corteza auditiva y otros núcleos subcorticales de la vía auditiva en animales. Es importante señalar que la rata es buen modelo experimentar para estudiar el MMN y otros fenómenos relacionados, ya que se ha demostrado que en este animal (así como en otros roedores) se pueden registrar unos potenciales evocados auditivos análogos a los observados en humanos, y que comparten con ellos algunas de sus propiedades más características. No obstante, existen también algunas diferencias en los detalles de la morfología de estos potenciales entre animales y humanos. En particular, dado el menor tamaño del cerebro en la rata, los picos de estos potenciales ocurren mucho antes en el tiempo con respecto al estímulo (50-100 ms) que en humanos (150-300 ms).

La detección automática de estímulos inesperados es una función importante de los sistemas sensoriales (Ranganath and Rainer, 2003; Whitmire and Stanley, 2016). El cerebro responde automáticamente a estos eventos discrepantes con el contexto actual, y esta actividad de respuesta a la discrepancia se puede detectar fácilmente usando métodos de registro no invasivos, como el electroencefalograma. El MMN es una de estas respuestas a la disparidad (Näätänen et al., 2007), generada en la corteza cerebral auditiva primaria y secundaria (Opitz et al., 2005; Maess et al., 2007) cuando un estímulo raro interrumpe una secuencia de tonos regular. Durante los últimos 40 años, el MMN se ha utilizado como una importante herramienta en investigación básica y en diagnóstico clínico (Näätänen et al., 2012), ya que está alterada en pacientes con esquizofrenia y otros desórdenes cerebrales (Michie et al., 2016).

Pero más allá de sus aplicaciones prácticas, estas respuestas a la discrepancia proporcionan la única evidencia disponible hasta ahora de la denominada "teoría general de la codificación predictiva" (predictive coding framework), que trata de explicar en términos computacionales el funcionamiento en general de los sistemas sensoriales y sentar las bases teóricas de la percepción (Friston, 2005, 2009; Bastos et al., 2012). Según esta teoría, los sistemas sensoriales están continuamente tratando de anticiparse a las entradas sensoriales, y envían predicciones hacia estaciones de procesamiento inferiores para cancelar las respuestas neuronales evocadas por los estímulos que se consiguen predecir correctamente. Así, las respuestas a la discrepancia se interpretarían dentro de esta teoría como la suma de miles de respuestas neuronales que señalarían un error de predicción (Bendixen et al., 2012; Schröger et al., 2014; Stefanics et al., 2014; Phillips et al., 2016).

Sin embargo, a nivel celular, se ha sugerido que las respuestas a la discrepancia podrían explicarse por un mecanismo neuronal más simple (May and Tiitinen, 2010; Fishman, 2014)—que no involucra la generación de "predicciones" ni de "errores de predicción"—a saber, adaptación a estímulos específicos, es decir, SSA (Ulanovsky et al., 2003; Malmierca et al., 2009; Escera and Malmierca, 2014), basada en la depresión sináptica dependiente de actividad (Grill-Spector et al., 2006; Mill et al., 2011). Las neuronas que muestran esta propiedad se encuentran en regiones específicas del cerebro auditivo, especialmente en regiones de orden superior dentro de la jerarquía auditiva (Escera and Malmierca, 2014; Nieto-Diego and Malmierca, 2016), y tienen la capacidad de atenuar sus respuestas a estímulos repetitivos, pero responden fuertemente a otros estímulos diferentes. Sin embargo, no está claro si esta actividad neuronal refleja simplemente SSA, o además también cierto grado de actividad predictiva.

Afortunadamente, existe una manera de distinguir entre estas dos explicaciones, usando un diseño experimental que incluye, además de secuencias tipo oddball (Figura 32C), otras secuencias de control que permiten separar la atenuación a la repetición de los errores de predicción (Figura 32D,E) (Ruhnau et al., 2012; Harms et al., 2015). Nosotros hemos usado estas secuencias tonales, que normalmente se aplican solo en estudios de percepción auditiva en humanos (Escera and Malmierca, 2014; Schröger et al., 2014), para revelar que las respuestas neuronales en el cerebro auditivo de la rata efectivamente reflejan esta actividad predictiva a nivel celular. Se trata por tanto de un descubrimiento muy importante para comprender la fisiología de la percepción auditiva, y de la percepción en general, porque unifica tres descripciones coexistentes de la percepción de la discrepancia, a distintos niveles de análisis: neurofisiológico, cognitivo y teórico.

HIPÓTESIS Y OBJETIVOS

Dados los antecedentes arriba presentados, este trabajo de investigación se vertebra en torno a una serie de hipótesis, principalmente:

1. El fenómeno de la SSA, definida como una respuesta diferencial a estímulos "standard" y "deviant" dentro del paradigma *oddball*, tiene lugar en las áreas de orden superior de la corteza auditiva, además de en las áreas primarias.
2. Esta SSA en áreas corticales de orden superior ocurre dentro de un rango de latencias más cercano al MMN en la rata, dado que las respuestas neuronales en áreas no primarias tienden a presentar latencias de respuesta más largas (Schreiner and Cynader, 1984; Polley et al., 2007).
3. Las respuestas de unidades neuronales aisladas a los tonos discrepantes (deviant) en el paradigma *oddball* son un correlato neuronal de la detección de la disparidad (deviance detection), además de SSA.
4. Las respuestas aumentadas a los estímulos discrepantes a lo largo de la vía auditiva son la representación neuronal de una señal de error de predicción, que irá creciendo a medida que se asciende en la jerarquía de procesamiento del sistema auditivo, tal y como postula la teoría de la codificación predictiva (Predictive Coding Framework).

Por tanto, el principal objetivo de esta investigación es validar la SSA como un correlato neuronal del MMN, que subyace a la detección de la discrepancia al nivel celular. Más específicamente, para contratar las hipótesis anteriores, se fijan los siguientes objetivos:

1. Crear un mapa fisiológico de SSA que recubra toda la corteza auditiva de la rata, incluyendo áreas primarias y no primarias (o de orden superior), para detectar cualquier principio de organización de la SSA en gradientes o metagradientes (Polley et al., 2007).
2. Investigar el nivel de SSA a lo largo de distintos rangos temporales en las respuestas neuronales, especialmente dentro de las áreas no primarias. Analizar cualquier variación significativa del nivel de SSA a lo largo del transcurso de la respuesta, desde el inicio o respuesta temprana (onset) hasta la extinción de la respuesta (offset).
3. Utilizar los controles de adaptación "many-standards" y "en cascada" para investigar si las respuestas neuronales al paradigma oddball reflejan detección de la disparidad, además de SSA.
4. Realizar estos registros en varias estaciones a lo largo de la jerarquía de procesamiento del sistema auditivo, al menos aquellas donde la SSA ha sido investigada anteriormente: colículo inferior, tálamo auditivo y corteza auditiva, para estudiar cualquier progresión sistemática del error de predicción a lo largo de la vía.

Los Objetivos 1 y 2 serán abordados en el Estudio 1, mediante la creación de mapas topográficos de SSA. Para ello se utilizará un paradigma *oddball* y registros multiunidad en la capa IV de las distintas áreas corticales auditivas. Los Objetivos 3 y 4, más ambiciosos, se intentarán responder en el Estudio 2, y requerirán el uso de las secuencias de control, además del paradigma *oddball*, y registros cuidadosos de unidades bien aisladas en todas las estaciones de la vía.

MATERIALES Y MÉTODOS

Se han realizado experimentos utilizando ratas hembra de la variedad Long-Evans, anestesiadas con uretano, un anestésico que produce un nivel de analgesia y anestesia profundos, pero no altera significativamente las propiedades de respuesta neurofisiológica básicas de las neuronas de la vía auditiva. También se aplican otros fármacos como corticoides (cortexona) para evitar la inflamación y el edema cerebral durante la cirugía, bloquentes de la secreción bronquial (atropina) y anestésicos locales (lidocaína). Después de anestesiar al animal se le realiza una prueba de umbrales de audición (ABR) para descartar algún déficit auditivo.

Durante la cirugía se expone el hueso temporal izquierdo y se practica una craneotomía de unos 3x4 mm para dejar expuesta la mayor parte la corteza auditiva. Además se practica una punción de la cisterna magna para liberar la presión del líquido cefalorraquídeo e impedir la evaginación del cerebro durante los registros. Finalmente se cubre con gel de agarosa templado toda la superficie cerebral y ósea expuesta, para evitar la desecación y la protrusión de la superficie cerebral y reducir los movimientos de pulsión del tejido nervioso que repercuten negativamente sobre la estabilidad de los registros.

Para localizar los registros dentro de una de las cinco subdivisiones de la corteza auditiva de la rata se utilizó como referencia el mapa de Polley et al. 2007. Las coordenadas de cada penetración del electrodo se anotan cuidadosamente a partir de una macrofotografía del área de registro sobre la que se superpone una cuadrícula micrométrica. Además, en algunos lugares de registro seleccionados se realiza una lesión electrolítica para su posterior localización precisa durante el procesamiento histológico del tejido.

Para buscar la respuesta neuronal al sonido se utilizaron ráfagas de ruido blanco de 40 ms a intensidad moderada (20-60 dB SPL). En cada lugar de registro se obtuvo lo que se denomina "área de respuesta en frecuencia" (*frequency response área*, FRA) de la neurona, aplicando una secuencia pseudoaleatoria de tonos puros a diferente frecuencia e intensidad. Para calcular el índice de SSA (*common SSA index*, CSI) se utiliza un paradigma *oddball* seleccionando dos estímulos de distinta frecuencia en torno a la frecuencia preferida de la neurona (BF). Para este primer experimento se utiliza un contraste de frecuencias lo más amplio posible ($\Delta f>0.2$).

RESULTADOS

En el Estudio 1, he comparado los niveles de SSA en las cortezas auditivas primaria y de orden superior, para validar la SSA como un correlato neuronal del MMN. Para estudiar la organización topográfica de la SSA realicé un mapeado completo de la corteza auditiva de la rata con registros multiunidad en las capas III/IV, usando un paradigma *oddball*. En este estudio he podido demostrar que la SSA ocurre más allá de A1, y que sus propiedades difieren entre las cortezas primarias y de orden superior. Los principales hallazgos del Estudio 1 son: (1) Los niveles más altos de SSA están altamente segregados hacia las áreas corticales de orden superior (no primarias), creando un gradiente de SSA característico y bien definido dentro de la corteza auditiva (Figura 25 y Figura 26). (2) Los niveles de SSA en las cortezas no primarias se mantienen muy altos durante toda la respuesta neuronal, hasta 200 ms después del estímulo, y se mantienen significativamente más altos que en las áreas primarias durante los primeros 100 ms de la respuesta (Figura 27). (3) En todas las áreas corticales la SSA se correlaciona en el tiempo y en intensidad con la señal diferencia registrada en los componentes rápido (Nd) y lento (Pd) de los potenciales de campo local (LFP; Figura 30). (4) La SSA produce un retraso en las respuestas a estímulos repetitivos (standard), y este retraso es mayor en las áreas no primarias. (5) La SSA es significativamente más alta para frecuencias de estimulación agudas, y esta dependencia es más pronunciada en las áreas primarias (Figura 28). (6) La SSA ocurre más rápidamente, y alcanza un estado estacionario mucho más bajo, en las áreas corticales de orden superior (Figura 29).

Por tanto, en el Estudio 1 he demostrado que la SSA ocurre no solo en las áreas primarias de la Corteza Auditiva (A1, VAF y SRAF), como ya se sabía, sino que también puede observarse en áreas secundarias (SRAF y PAF). Es más, la SSA es mucho más intensa en estas áreas secundarias. La SSA observada en las respuestas neuronales individuales está correlacionada en el espacio y en el tiempo con los potenciales de campo local (LFP), que son el correlato electrofisiológico del MMN cuando se registra desde el interior del tejido. La SSA es una propiedad fundamental de las estaciones de orden superior del sistema auditivo, y uno de los mecanismos celulares íntimamente relacionados con la generación del MMN.

En el Estudio 2, he registrado las respuestas de neuronas en distintas estaciones de procesamiento de la vía auditiva (Figura 31 y 32), ordenadas jerárquicamente desde las más inferiores (como el núcleo central de colículo inferior) hasta las más superiores (como la corteza auditiva secundaria, ver Figura 32B). En un primer análisis, comoparé las respuestas de toda nuestra muestra entre tres diferentes condiciones de presentación de los tonos: standard o repetitivo (STD), deviant o discrepante, (DEV), y control en cascada o estímulo neutro (CAS) (Figura 32C), observando que las respuestas DEV son en general significativamente mayores que al CAS, sobre todo en estaciones de procesamiento superior (Figura 34D-F). Después, he normalizado todas las respuestas neuronales entre 0 y 1 (Figura 34G-L), para descomponer la diferencia entre las respuestas a los estímulos repetitivos (STD) y discrepantes (DEV) en dos factores distintos (ver Figura 32D): atenuación a la repetición (iRS) y error de predicción (iPE). Y lo más importante es que pude observar una emergencia progresiva del componente iPE, es decir, del error de predicción, a medida que se asciende hacia estaciones de procesamiento superior (Figura 35). Este resultado ha sido validado estadísticamente, ajustando un modelo lineal robusto a los datos de iPE en las distintas estaciones, y he encontrado dos factores que influyen significativamente en aumentar este error de predicción: el nivel anatómico (colículo inferior, tálamo y corteza) y el nivel jerárquico (primer orden y orden superior). Esto encaja perfectamente con la teoría de la codificación predictiva, que postula que la generación de predicciones y errores de predicción es un proceso universal que ocurre a todos los niveles de procesamiento sensorial; pero además nuestros datos extienden esta teoría a estaciones subcorticales, lo cual es un descubrimiento muy novedoso y una demostración de que el procesamiento subcortical es fundamental para la percepción.

Finalmente, he podido demostrar que esta actividad en neuronas individuales está acompañada de un potencial cerebral registrado a mayor escala, comparable con el MMN en humanos, y que se sabe que refleja la actividad predictiva del cerebro (Figura 36). Por tanto, la actividad neuronal que hemos identificado, se puede considerar la responsable de estos potenciales de disparidad que están alterados en la esquizofrenia o el autismo, y esto abre una puerta de valor incalculable para estudios traslacionales en modelos animales (Todd et al., 2013; Harms et al., 2015; Michie et al., 2016).

DISCUSIÓN

Los datos del Estudio 1 contrastan con estudios previos de SSA, que indicaban que los niveles de SSA en A1 eran independientes de su frecuencia característica (CF), y en los que menos de un 4% de las neuronas mostraron un efecto en la latencia de respuesta (Ulanovsky et al., 2004). Pero la presencia de SSA alta en las respuestas neuronales entre 50 y 100 ms e incluso más tarde, representa la principal diferencia con respecto a estudios previos de SSA. Solo muy recientemente, dos estudios en la corteza auditiva del ratón (Chen et al., 2015; Natan et al., 2015) y uno en la corteza somatosensorial de la rata (Musall et al., 2015) encontraron SSA en respuestas subumbrales en neuronas piramidales de la capa II/III, o en respuestas neuronales extracelulares en interneuronas inhibitorias (Chen et al., 2015; Natan et al., 2015) y en neuronas piramidales de la capa IV(Musall et al., 2015), que ocurrían más allá de los 50-100 ms después del estímulo.

Además, en el Estudio 2, he podido confirmar que las respuestas de unidades neuronales aisladas a estímulos discrepantes (deviant) son el resultado de un proceso genuino de detección de la disparidad (deviance detection), y no solamente de la adaptación a la repetición. Así, he podido demostrar que estas respuestas cumplen el requisito fundamental para ser consideradas como respuestas a la disparidad genuinas. Es más, los altos índices de error de predicción (iPE), que reflejan señales de error en las respuestas de neuronas individuales, también se correlacionan en el tiempo y en la localización anatómica (ho-AC) con un potencial de error de predicción (PEP) registrado a gran escala, que se corresponde con el MMN en la rata (Shiramatsu et al., 2013; Harms et al., 2015).

Algunos estudios previos intentaron demostrar detección de la disparidad en unidades neuronales de la corteza auditiva primaria, pero estos estudios no pudieron alcanzar ningún resultado concluyente (Farley et al., 2010; Taaseh et al., 2011; Fishman and Steinschneider, 2012), quizá porque se limitaron a registrar actividad multiunidad en la corteza auditiva primaria. No obstante, un estudio reciente en la corteza auditiva primaria del ratón (Chen et al., 2015) y otro en la corteza somatosensorial de la rata (Musall et al., 2015) encontraron signos de detección de la discrepancia en respuestas neuronales tardías, utilizando en control "many-standards". A pesar de que el control "en cascada" está considerado un mejor control de adaptación que el "many-standards" (Ruhnau et al., 2012), solo un estudio en animales lo ha utilizado, en registros epidurales, y sin alcanzar tampoco resultados concluyentes (Harms et al., 2014).

Así pues, en estos dos estudios, proporciono pruebas concluyentes que apoyan la teoría de que las respuestas de unidades neuronales aisladas a estimulación con el paradigma oddball, a distintos niveles de la vía auditiva, constituyen el correlato neuronal de los indicadores electrofisiológicos de detección de la discrepancia (deviance detection) registrados epiduralmente mediante EEG. En particular, he demostrado que las respuestas de unidades neuronales en las cortezas auditivas de orden superior subyacen directamente a la generación del MMN.

CONCLUSIONES

En conjunto, los resultados de los dos estudios incluidos en esta tesis permiten extraer las siguientes conclusiones:

1. Las neuronas de regiones corticales auditivas de orden superior muestran niveles muy altos de SSA, significativamente mayores que en las áreas primarias de la corteza auditiva.
2. La SSA es una propiedad predominante de la vía auditiva no lemniscal, desde el mesencéfalo hasta la corteza auditiva.
3. La localización anatómica y el curso temporal de la SSA en la corteza auditiva se corresponden con los del MMN registrado simultáneamente en la rata.
4. Las respuestas de unidades neuronales aisladas a tonos discrepantes en un paradigma *oddball* son resultado de un proceso de detección de la discrepancia, además de SSA.

5. La actividad de unidades neuronales aisladas en respuesta al paradigma *oddball* es la base de la generación del MMN y otros indicadores tempranos de detección de la discrepancia.
6. Las respuestas neuronales a la estimulación con el paradigma *oddball* demuestran la actividad predictiva del cerebro auditivo, in en particular, las respuestas a tonos discrepantes representan error de predicción a nivel celular.
7. La representación del error de predicción a lo largo de la vía auditiva sigue un patrón jerárquico consistente con los postulados de la Teoría de la Codificación Predictiva Jerárquica.
8. Estos resultados proporcionan pruebas empíricas de la generación del MMN basada en codificación predictiva, para lo cual hay aún escasez de evidencia experimental.

APPENDIX II: ORIGINAL PUBLICATIONS

PLOS | BIOLOGY

RESEARCH ARTICLE

Topographic Distribution of Stimulus-Specific Adaptation across Auditory Cortical Fields in the Anesthetized Rat

Javier Nieto-Diego[1,2], **Manuel S. Malmierca**[1,2,3]*

1 Auditory Neuroscience Laboratory, Institute of Neuroscience of Castilla y León (INCYL), Salamanca, Spain, **2** Salamanca Institute for Biomedical Research (IBSAL), Salamanca, Spain, **3** Department of Cell Biology and Pathology, Faculty of Medicine, University of Salamanca, Salamanca, Spain

* msm@usal.es

Citation: Nieto-Diego J, Malmierca MS (2016) Topographic Distribution of Stimulus-Specific Adaptation across Auditory Cortical Fields in the Anesthetized Rat. PLoS Biol 14(3): e1002397. doi:10.1371/journal.pbio.1002397

Academic Editor: Robert Zatorre, McGill University, CANADA

Received: August 25, 2015

Accepted: February 1, 2016

Published: March 7, 2016

Data Availability Statement: All relevant data are within the paper and its Supporting Information files.

Funding: This work was funded by Spanish MINECO (Grant BFU2013-43608-P to MSM), Spanish JCYL (Grant JCYL-SA343-U14 to MSM) and the European Social Fund/Spanish JCYL (Ph.D. Fellowship to JND under the Operational Programme ESF Castilla y León 2007–2013). The funders had no role in study design, data collection and analysis, decision to publish, or preparation of the manuscript.

Competing Interests: The authors have declared that no competing interests exist.

Abstract

Stimulus-specific adaptation (SSA) in single neurons of the auditory cortex was suggested to be a potential neural correlate of the mismatch negativity (MMN), a widely studied component of the auditory event-related potentials (ERP) that is elicited by changes in the auditory environment. However, several aspects on this SSA/MMN relation remain unresolved. SSA occurs in the primary auditory cortex (A1), but detailed studies on SSA beyond A1 are lacking. To study the topographic organization of SSA, we mapped the whole rat auditory cortex with multiunit activity recordings, using an oddball paradigm. We demonstrate that SSA occurs outside A1 and differs between primary and nonprimary cortical fields. In particular, SSA is much stronger and develops faster in the nonprimary than in the primary fields, paralleling the organization of subcortical SSA. Importantly, strong SSA is present in the nonprimary auditory cortex within the latency range of the MMN in the rat and correlates with an MMN-like difference wave in the simultaneously recorded local field potentials (LFP). We present new and strong evidence linking SSA at the cellular level to the MMN, a central tool in cognitive and clinical neuroscience.

Author Summary

Sensory systems automatically detect salient events in a monotonous ambient background. In humans, this change detection process is indexed by the mismatch negativity (MMN), a mid-late component of the auditory-evoked potentials that has become a central tool in cognitive and clinical neuroscience over the last 40 years. However, the neuronal correlate of MMN remains controversial. Stimulus-specific adaptation (SSA) is a special type of adaptation recorded at the neuronal level in the auditory pathway. Attenuating the response only to repetitive, background stimuli is a very efficient mechanism to enhance the saliency of any upcoming deviant or novel stimulus. Thus, SSA was originally proposed as a neural correlate of the MMN, but previous studies in the auditory cortex reported SSA only at very early latencies (circa 20–30 ms) and only within the primary auditory cortex (A1), whereas MMN analogs in the rat occur later, between 50 and 100 ms

Abbreviations: AAF, anterior auditory field; A1, primary auditory cortex; CF, characteristic frequency; CNIC, central nucleus of the inferior colliculus; CSI, common stimulus-specific adaptation index; DCIC, dorsal cortex of the inferior colliculus; DW, difference wave; ERP, event-related potential; FRA, frequency response area; IC, inferior colliculus; LCIC, lateral cortex of the inferior colliculus; LFP, local field potential; MEG, magnetoencephalography; MGB, medial geniculate body; MGD, dorsal division of the MGB; MGM, medial division of the MGB; MGV, ventral division of the MGB; MMN, mismatch negativity; MUA, multiunit activity; Nd, negative deflection of the LFP; PAF, posterior auditory field; Pd, positive deflection of the LFP; RCIC, rostral cortex of the inferior colliculus; RP, repetition positivity; SI, stimulus-specific adaptation index; SRAF, suprarhinal auditory field; SSA, stimulus-specific adaptation; VAF, ventral auditory field.

after change onset, and are generated mainly within nonprimary fields. Here, we report very strong SSA in nonprimary fields within the latency range of the MMN in the rat, providing empirical evidence of the missing link between single neuron response studies in animal models and the human MMN.

Introduction

A critical function of the brain is to identify uncommon and potentially important stimuli while ignoring irrelevant ambient backgrounds [1–3]. In humans, this ability is reflected by an electrophysiological brain response called mismatch negativity (MMN), a mid-late (150–200 ms) deflection of the auditory event-related potentials (ERP) that is elicited by uncommon, but not by repetitive, sounds [4–7] and serves to automatically redirect attention toward potentially relevant stimuli [8]. Importantly, the MMN signal is altered in patients with schizophrenia and other psychiatric disorders and can be used as an index of cognitive decline in normal and pathological neurodegenerative processes [9,10]. The MMN has been extensively studied using the "oddball" paradigm, in which infrequently occurring sounds, i.e., "deviant" tones, are randomly interspersed among frequent monotonous sounds, i.e., "standard" tones. MMN studies have advanced our knowledge on many aspects of change and novelty detection, but scalp recordings limit our ability to pinpoint its regions of generation.

Recent studies over the past decade have taken advantage of the oddball paradigm to study adaptation in single auditory neurons. Stimulus-specific adaptation (SSA) may be a counterpart phenomenon to MMN that is studied in single neurons using this paradigm [11]. As in MMN, neurons showing SSA adapt to frequently occurring stimuli (standards) yet respond strongly to rare stimuli (deviants). Within the auditory system, SSA was originally reported in the primary auditory cortex (A1) [12] as a higher level of adaptation to a specific stimulus, different from firing rate adaptation resulting from changes in the intrinsic properties of the neuron. SSA shares many properties with the MMN, and it is important because it may be a neural correlate of the MMN, or at least one of its early generators [11,13]. The basic properties of SSA have been studied in great detail not only in A1 but also in the subcortical inferior colliculus (IC) [14–16] and medial geniculate body (MGB) [17,18]. One important difference between SSA in the auditory cortex and subcortical stations is their anatomical location. SSA is strong and widespread only in the nonlemniscal regions of the IC and MGB [16], while SSA has been described as strong and widespread in lemniscal A1 [12,19]. However, detailed studies on SSA within the different cortical fields beyond A1 are lacking. Since SSA is stronger in the nonlemniscal regions of the IC and MGB, it is reasonable to hypothesize that SSA in the nonprimary regions of the auditory cortex would also be stronger than in A1. Indeed, previous studies on the general response properties of the auditory cortex reported that nonprimary neurons in the cat [20,21] and rat [22–24] auditory cortex adapt more strongly than in A1. Even studies in human subjects have shown differential adaptation between primary and nonprimary cortical areas [25–27]. Moreover, two recent studies that mapped auditory ERPs in the rat showed robust MMN-like responses in nonprimary auditory cortical fields [28,29].

The main goal of the present study was to generate a complete and fine-grained map of SSA across all known cortical fields in the rat. Despite interspecies differences, the rat auditory cortex shares many common anatomical and physiological features with other species [23,30,31], including primary and nonprimary regions. Primary regions of the auditory cortex are characterized by a thick, dense, granular layer and receive major layer IIIb/IV thalamocortical projection from the first-order (or lemniscal) auditory thalamus. The nonprimary auditory cortex is

formed by surrounding regions that subsequently process input from primary regions and receive major layer IIIb/IV projection from the higher-order (or nonlemniscal) auditory thalamus [31]. Detailed electrophysiological mapping studies [23,24,32] have identified at least five tonotopically organized fields in the rat auditory cortex. The A1, the anterior auditory field (AAF), and the ventral auditory field (VAF) are all considered primary fields [23,33]. Additionally, two distinct nonprimary regions have been identified: the posterior auditory field (PAF), located in the dorsocaudal border of A1; and the suprarhinal auditory field (SRAF), in the ventral margin of the auditory cortex [23,31,34,35]. Unfortunately, there are no specific stains or molecular markers that cause one cortical region in the rat to stand out unambiguously from another, but they show a robust organization of multiple response properties that follow a particular spatial organization [23,36]. Our results demonstrate that, although SSA is indeed present in A1 and the other two primary fields, it is markedly stronger in the nonprimary fields PAF and SRAF, consistent with the SSA observed in nonlemniscal parts of the IC and MGB. Another important finding in our data is that SSA observed in auditory cortex is robust up to 200 ms after stimulus onset, well within the latency range of the MMN-like potentials in the rat [37]. These data suggest the existence of a hierarchically organized system for SSA processing [13] and reinforce the notion that nonprimary SSA is a more direct neural correlate of the MMN than the SSA observed in A1.

Results

To study the topographic distribution of SSA across the auditory cortex, we recorded a total of 816 multiunit activity (MUA) clusters from layers IIIb/IV within all cortical fields from the left auditory cortex in 12 animals (total number of recordings by field: A1, 167; AAF, 121; VAF, 164; SRAF, 169; PAF, 119). Local field potentials (LFPs) were simultaneously recorded from the same electrode in four of the animals. In each animal, we made a microelectrode mapping (15–25 tracks/mm^2) covering at least three fields (Fig 1A shows an example with 132 recording sites from all fields). Most recordings (89%) were made between 300 and 600 μm in depth, corresponding to cortical layers IIIb/IV [31]. Five auditory cortical fields were identified according to tone frequency response topographies. The limits and relative position of the auditory fields were determined for each animal at the end of the experiment, using the characteristic frequency (CF) gradient as the main reference landmark (Fig 1B). We consistently observed distinct tonotopic gradients within the different fields [23,32,36], with a high-frequency reversal between VAF and AAF (rostrally), a low-frequency reversal between A1 and PAF (dorsocaudally), and a high-frequency reversal between VAF and SRAF (ventrally). We identified the boundary between A1 and VAF as a 90°-shift in the CF gradient in the ventral low-frequency border of A1, and the boundary between A1 and AAF as an absence of tone-evoked responses in the ventral, high-frequency border of A1 (Fig 1B). We used these boundaries to assign each recording to a given field.

At every recording site, the frequency response area (FRA) was computed, and we presented an oddball paradigm (two sequences of 250 trials, 10% deviants, 300 ms onset-to-onset interval, 0.5 octaves frequency separation) using a pair of pure tones from the FRA, at 20–30 dB above CF threshold, which elicited clear responses of similar magnitude. Fig 2 shows representative MUA recordings from each auditory cortex field. Fig 2A shows their FRAs and the pair of stimuli f_1 and f_2 selected for the oddball paradigm, and Fig 2B shows comparative responses to each frequency when presented as either standard (blue) or deviant (red) in the oddball paradigm.

SSA Is Stronger in Nonprimary Fields

The main aim of this study was to quantify and compare SSA levels between the five cortical fields. Thus, we computed the stimulus-specific adaptation index (SI) for each stimulus, SI(f_1)

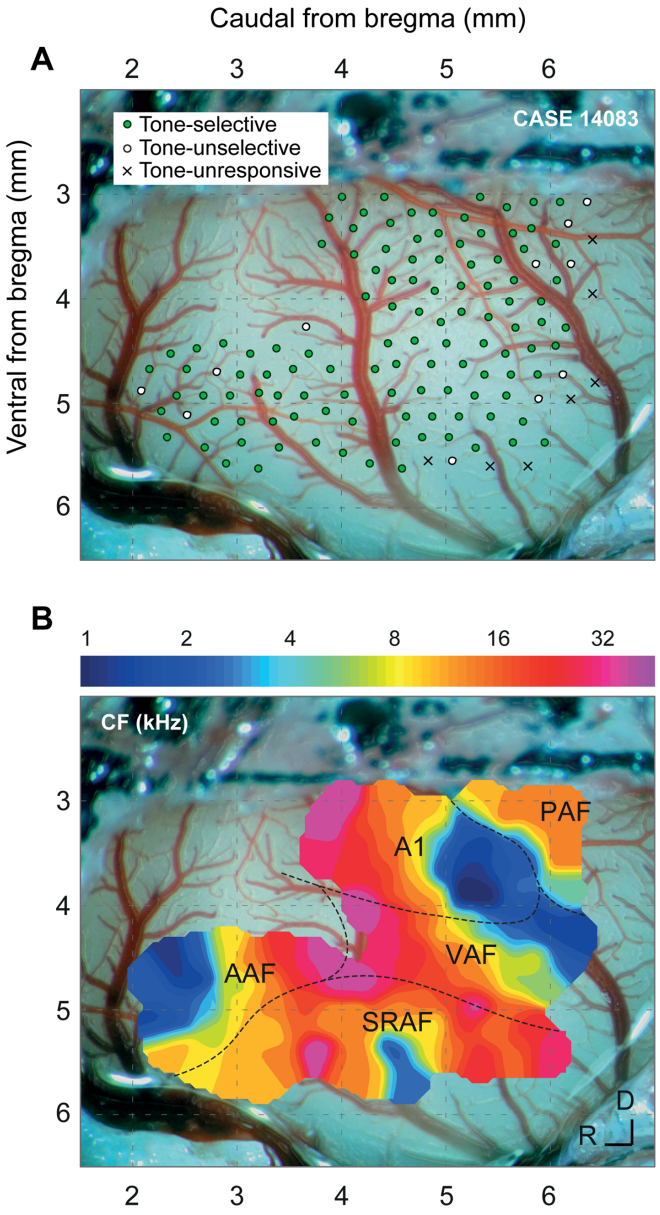

Fig 1. Experimental setup. A. Sample case with 132 MUA recording sites from layers IIIb/IV throughout the cortical fields in one representative animal. At every site, the CF was determined (if possible), and we presented an oddball paradigm (c.f., Fig 2). Sites are classified according to pure-tone selectivity (Selective: tone-responsive with a clear CF; Unselective: tone-responsive, but with a lack of a clear CF; Unresponsive: no significant responses to pure tones). **B.** Outline of the different cortical fields in this particular case, as derived from the tonotopic gradients. Each field shows a characteristic CF gradient [23], with A1 being the most easily identifiable.

doi:10.1371/journal.pbio.1002397.g001

and SI(f_2), and the common SSA index (CSI) for every recording site, using baseline-corrected spike counts during stimulus presentation (5 to 80 ms from stimulus onset; see Materials and Methods). Fig 3A shows a series of scatterplots illustrating the joint distribution of SI(f_1) and SI (f_2), for the whole population and for each field separately, and Fig 3B illustrates corresponding histograms of CSI distributions (total number of recording sites included in this analysis, as detailed in Materials and Methods, are also indicated). In all cases, points are symmetrically

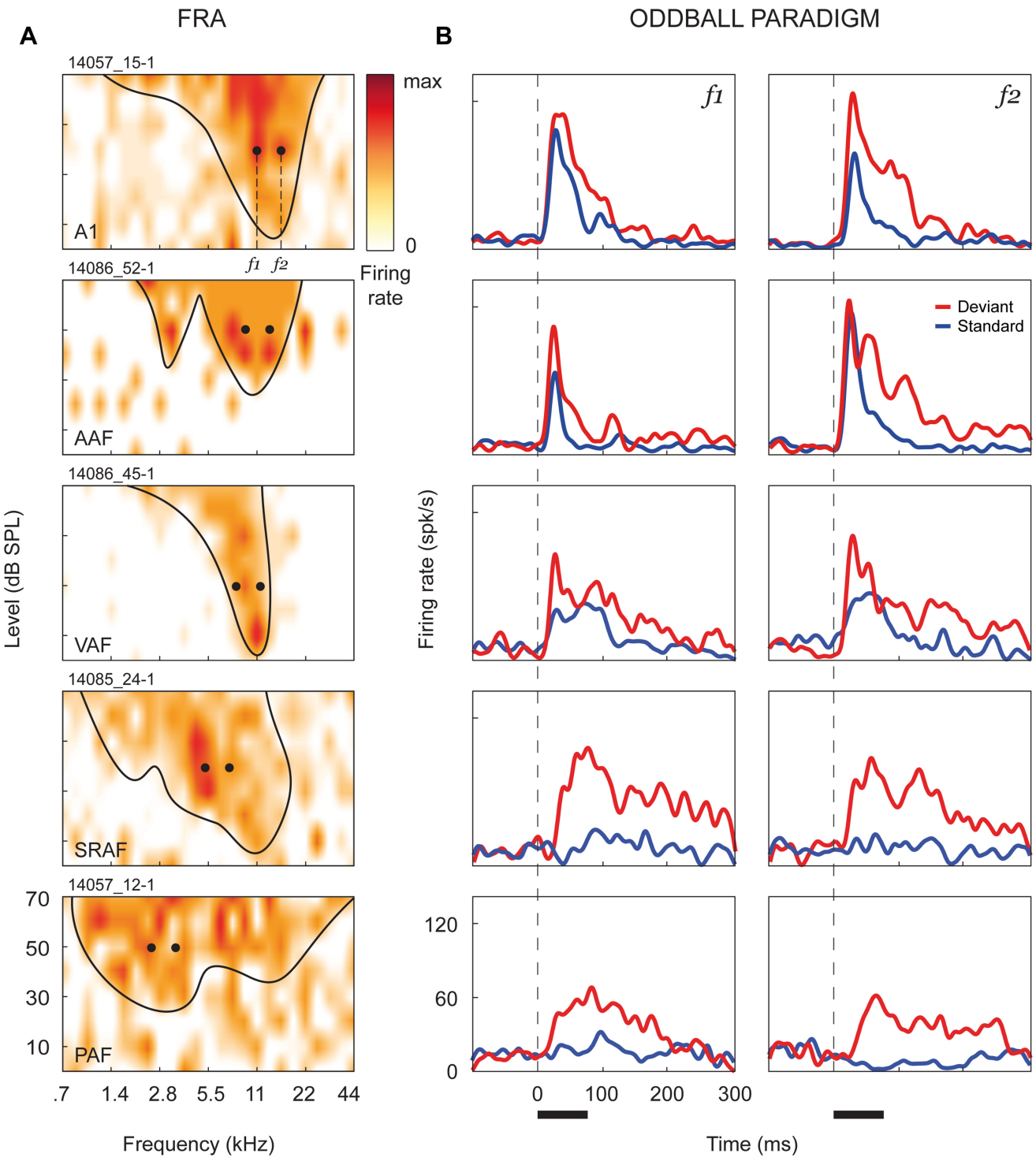

Fig 2. Stimulation paradigm. A. Representative FRAs from each auditory cortex field. Firing rate (red shading, normalized to max response) is represented as a function of frequency and intensity of the tones presented, and the frequency-tuning curve has been outlined (minimum sound intensity that elicits a firing rate over 20%–40% of the maximum firing for each frequency, excluding isolated "islands" of spontaneous activity). We selected a pair of frequencies, separated by 0.5 octaves, that elicited responses of similar magnitude at 20–30 dB above threshold. These frequencies were then presented within an oddball paradigm (250 tones, 10% deviants, 300 ms onset-to-onset interval, 75 ms tone duration). **B.** Corresponding responses to the oddball paradigm. Each plot compares spike-density functions (see Materials and Methods) in response to the same frequency, computed from the 25 deviant trials (red) and the 25 standard trials just preceding a deviant (blue). Responses to standard tones were significantly reduced in all fields as compared to deviants, but this adaptation is much stronger in the nonprimary fields (SRAF and PAF). Black horizontal bar: stimulus duration.

doi:10.1371/journal.pbio.1002397.g002

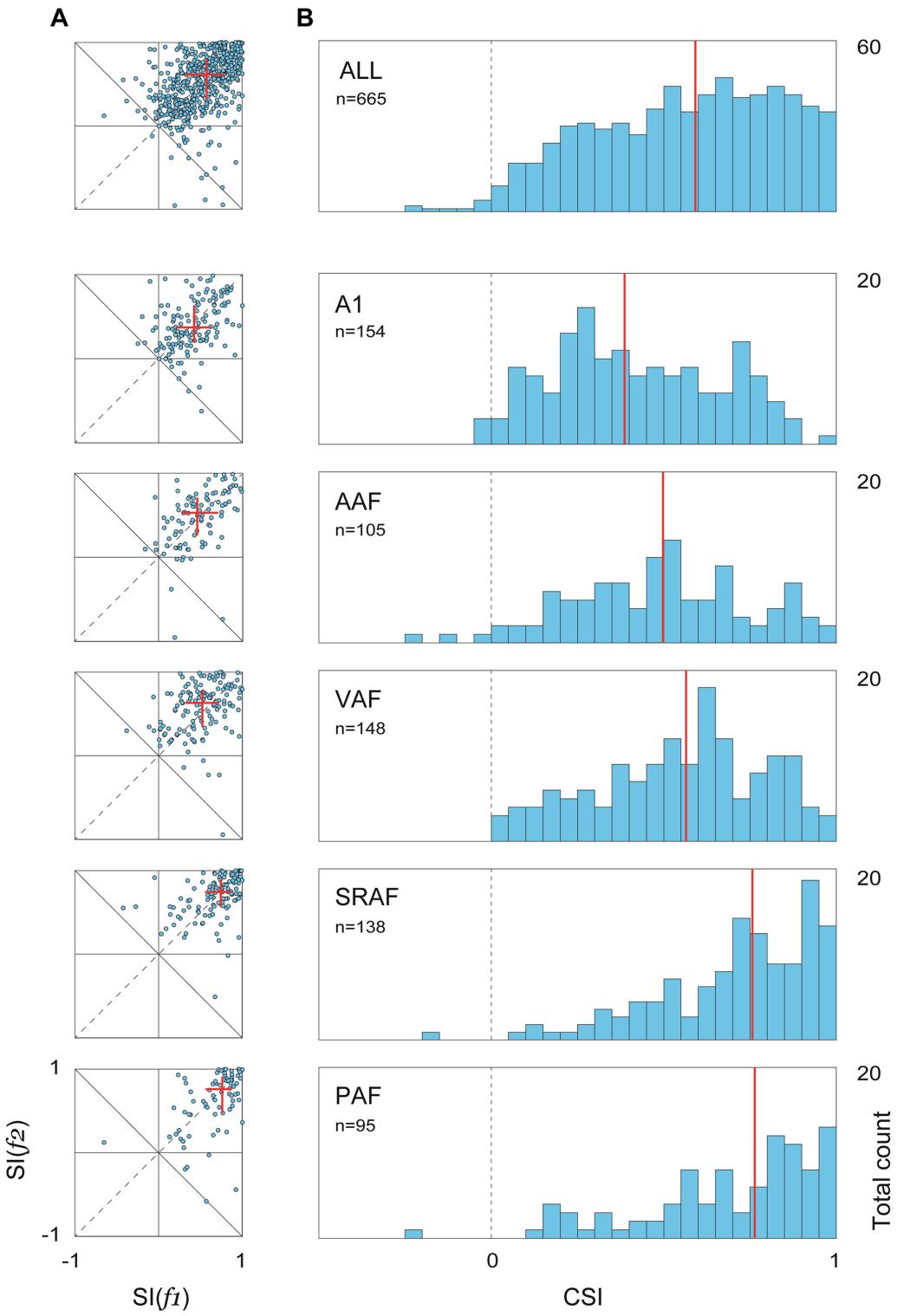

Fig 3. Distribution of SSA indexes within each field. A. Distribution of frequency-specific SSA indexes for the whole population and for each field separately. Red lines represent median and inter-quartile range for SI(f_1) and SI(f_2), showing a progressive increase in SSA from primary to nonprimary fields. **B.** Corresponding distributions of the CSI. In the primary fields, distributions are symmetrical and centered in medium-CSI values, but in the nonprimary fields, CSI distributions are sharply skewed to extreme levels of SSA. Red lines show distribution medians, which were statistically different between every primary and nonprimary field (see text). Underlying data for this figure can be found in S2 Data.

doi:10.1371/journal.pbio.1002397.g003

clustered around the main diagonal, with no significant differences between the median SI(f_1) and SI(f_2) for any field (paired Wilcoxon signed rank test, $p > 0.1$ in all fields), indicating that adaptation was equal on average for f_1 and f_2. The drift of the population medians toward the upper-right corner (Fig 3A) reveals a gradual shift of the cloud of points, from A1 to PAF fields, toward higher levels of SSA. The global population shows a CSI distribution that is slightly skewed to the right (Fig 3B, top panel). The origin of this skewness emerges once we split these distributions into the five cortical fields: the CSI distributions for the primary fields, especially A1 and AAF, are more symmetrical, centered on medium CSI values, and span the full range of possible values (Fig 3B). The same distributions for the nonprimary fields, SRAF and PAF, on the other hand, are clearly asymmetric, sharply skewed to the right toward the extreme positive CSI values, with a virtual absence of low CSI values. Moreover, the center of the distribution progressively moves to the right (i.e., toward higher CSI values) from A1 to PAF, (CSI, [Q_1, median, Q_3]: A1, [0.22, 0.38, 0.61]; AAF, [0.32, 0.50, 0.68]; VAF, [0.39, 0.56, 0.72]; SRAF, [0.57, 0.76, 0.90]; PAF, [0.56, 0.76, 0.89]), with the median CSI in every primary field being significantly smaller than in every nonprimary field (Kruskall-Wallis test, $\chi^2(4) = 121.43$, $p < 5\times10^{-24}$).

Correcting for baseline activity was required to measure the actual evoked response, given the high spontaneous rates seen in many recordings, particularly from the nonprimary fields (spontaneous firing rate, mean ± SEM: A1, 8.2 ± 0.7 spk/s; AAF, 7.3 ± 0.6 spk/s; VAF, 10.7 ± 0.7 spk/s; SRAF, 9.2 ± 0.6 spk/s; PAF, 13.0 ± 1.0 spk/s). This correction may have a major impact when using a contrast index such as the CSI [38], so that higher CSI values in nonprimary fields could result in part from this procedure. Therefore, we repeated the CSI calculation using the absolute spike counts for the same time window. As expected, all CSI values were overall reduced, but the same trend was observed between fields, since median CSI in all fields were lower than in SRAF; only CSI levels in PAF were differentially affected, so that they were no longer higher than in primary fields (CSI without baseline correction, [Q_1, median, Q_3]: A1, [0.14, 0.24, 0.40]; AAF, [0.18, 0.30, 0.45]; VAF, [0.21, 0.32, 0.42]; SRAF, [0.26, 0.39, 0.52]; PAF, [0.17, 0.25, 0.42]). However, given the higher spontaneous rate relative to evoked activity seen in PAF, uncorrected CSI does not faithfully represent the strong SSA (i.e., contrast) clearly observed in responses from this field (Fig 2B). Therefore, we kept using these corrected measures for the rest of the analyses.

Consistent with previous studies [23], nonprimary fields showed longer response onset latencies than primary fields for both deviant (mean ± SEM: A1, 11.6 ± 1.2 ms; AAF, 11.1 ± 1.1 ms; VAF, 17.3 ± 1.5 ms; SRAF, 27.0 ± 2.0 ms; PAF, 23.9 ± 2.2 ms; Kruskal-Wallis test, $\chi^2(4) = 152.78$, $p < 10^{-31}$) and standard tones (A1, 16.7 ± 1.7 ms; AAF, 22.5 ± 3.3 ms; VAF, 29.8 ± 3.5 ms; SRAF, 45.8 ± 4.7 ms; PAF, 50.0 ± 8.0 ms; $\chi^2(4) = 77.59$, $p < 10^{-15}$). From these figures, it is apparent that onset latency was significantly delayed for standards as compared to deviants in all five fields (onset latency difference, standard–deviant, mean ± SEM: A1, 7.6 ± 1.5 ms; AAF, 13.6 ± 3.1 ms; VAF, 18.0 ± 3.1 ms; SRAF, 23.2 ± 3.8 ms; PAF, 31.8 ± 7.2 ms; all significantly greater than zero, Wilcoxon signed rank test, $p < 0.01$ in all cases). Thus, in addition to an overall reduction in spike counts, SSA also produced a delay in onset latency to the standard tones. Furthermore, this delay was significantly longer in nonprimary fields than in primary fields A1 and AAF (Kruskal-Wallis test, $\chi^2(4) = 34.13$, $p < 10^{-6}$).

SSA Is Topographically Organized in the Auditory Cortex

The sharp differences in SSA levels observed between primary and nonprimary fields derive from a distinct topographic organization of adaptation throughout the whole auditory cortex (Fig 4). The absolute position of the map with respect to bregma differed between animals by

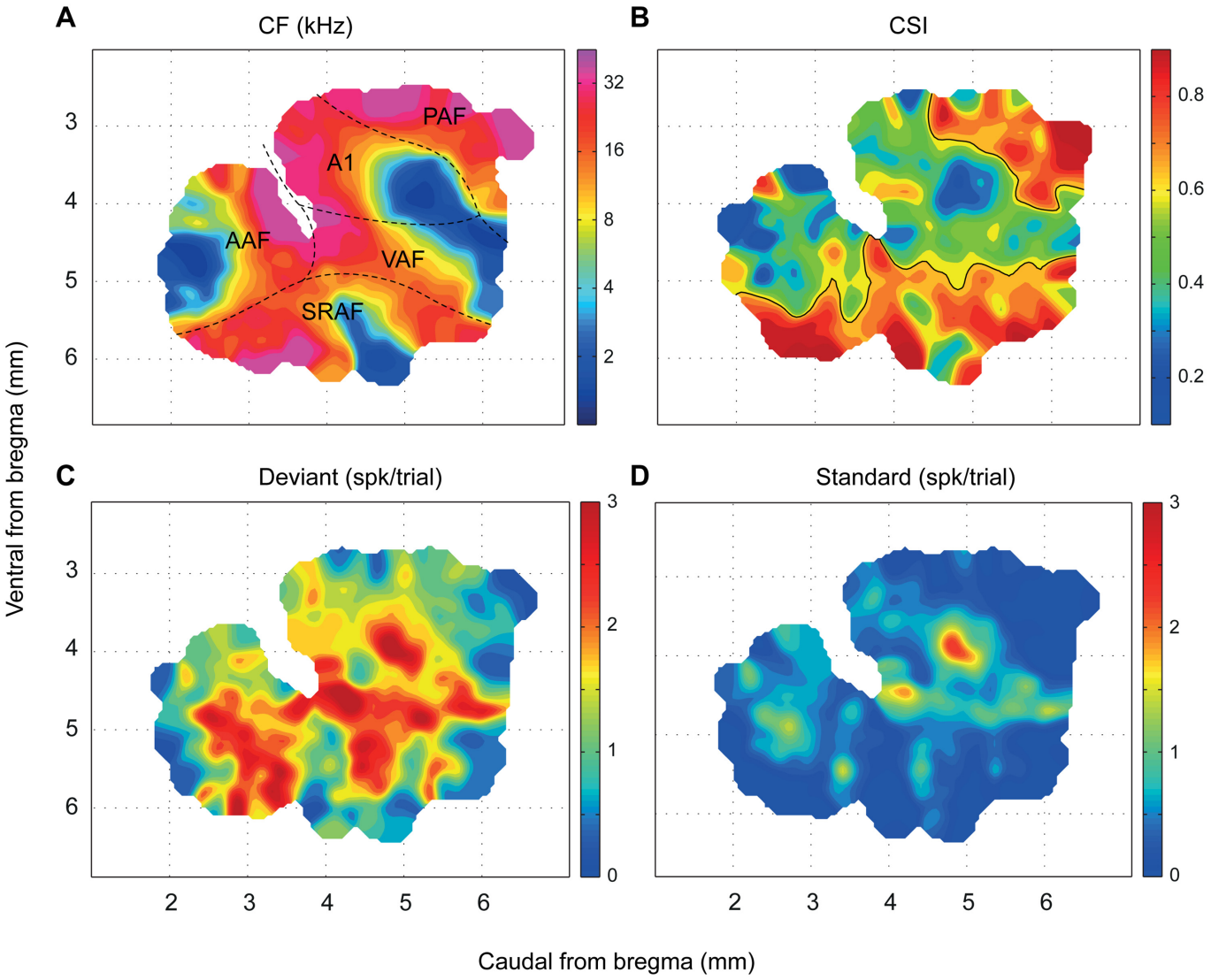

Fig 4. Topographic distribution of SSA throughout the auditory cortex. A. Synthetic map of the auditory cortex showing the location of the five cortical fields. The CF was used as the main reference to put into register the individual maps from the 12 animals. The high topographical correlation of the CF (see text) confirmed the robustness of the alignment. **B.** Topographic distribution of SSA in the auditory cortex. The CSI follows a statistically significant topography within the auditory cortex (see text), with the highest values being confined to the nonprimary fields. **C,D.** Topographic distribution of the responses to deviant and standard tones, respectively, from which the CSI was computed. Responses to standard tones were almost zero in the nonprimary fields. Data underlying these maps can be found in S3 Data.

doi:10.1371/journal.pbio.1002397.g004

up to 0.6 mm, but the relative position and orientation of the five cortical fields were highly conserved from one animal to the next. Thus, we constructed a synthetic map of CSI from all available data. Using the CF gradient as the main reference landmark, an appropriate shift was applied to each map to maximize the degree of CF coincidence between them (Fig 4A; cf. Fig 1 in [23] and Fig 1 in [36]). We quantified the quality of the alignment as the local coincidence of CF values. The resulting correlation of CF between neighboring sites was next to maximal (Topological product, $P_T = 0.9686$, permutation test, $p < 0.001$) [39]. Fig 4B shows the CSI map, while Fig 4C and 4D show the corresponding maps of the response to deviant and standard stimuli (within the stimulus-fitted window), from which the CSI was computed. The CSI follows a statistically significant topographic distribution (Topological product, $P_T = 0.2342$,

permutation test, $p < 0.001$), meaning that neighboring sites are likely to have more similar CSI values than more distant ones. To better determine the nature of this topography, we traced a boundary following the median iso-CSI contour (Fig 4B; median population CSI = 0.60) whenever this line enclosed a region of area greater than 0.5 mm^2. This procedure revealed an emergent organization of SSA, showing a large region of low-to-medium CSI values that covers the central and rostral portions of the auditory cortex and two separate and distinct high-CSI regions confined to the posterodorsal and ventral margins of the map, respectively (Fig 4B). Remarkably, the CSI-based boundary that defines the posterodorsal high-CSI region matches almost perfectly the boundary between A1 and PAF previously traced from the CF gradient reversal (Fig 4A). Similarly, the iso-CSI contour that separates the ventral high-CSI region matches very well the caudal SRAF/VAF and rostral SRAF/AAF boundaries.

Finally, these high-SSA regions revealed in Fig 4B can be seen also as regions of extremely low spike count to the standard stimuli in Fig 4D. Indeed, the "CSI" and "Standard" maps are almost complementary, such that regions of extreme CSI values correspond to those with virtually no response to standard stimuli, while regions of low-medium CSI match those with significant response to standards. This observation reveals a strong CSI dependence on the standard response being low, rather than on the deviant response being high. In fact, CSI was negatively correlated with both deviant (DEV) and standard (STD) response strength, yet much more strongly to the standard (Spearman correlation coefficient, $\rho[CSI,DEV] = -0.19$, $p < 10^{-6}$; $\rho[CSI,STD] = -0.81$, $p < 10^{-152}$). This also indicates that CSI values tend to be higher for neurons with an overall lower firing rate, as confirmed by a subsequent analysis (*v.i.*).

SSA Occurs at the Late Component of the Response

SSA was suggested as a potential neural correlate for the MMN, but previous studies neglected an analysis of the responses to deviant and standard tones at different temporal courses during stimulus presentation and beyond. Since we observed responses of long durations to deviant tones in many recordings (deviant response offset, mean ± SEM: A1, 162.6 ± 5.7 ms; AAF, 149.8 ± 6.9 ms; VAF, 194.2 ± 4.6 ms; SRAF, 196.4 ± 4.4 ms; PAF, 167.9 ± 7.4 ms), we wanted to further investigate the variation of the CSI across different components of the neural response. Hence, we computed baseline-corrected spike counts for different time intervals after stimulus onset (Fig 5A): onset (5–30 ms), sustained (30–80 ms), offset (80–105 ms), and late (105–200 ms). Corresponding CSI distributions and their topography for these different time windows are shown in Fig 5B and 5C, respectively.

First, we compared median CSI between fields for every time window separately. For the onset, sustained, and offset components, we found the same trend already observed for the stimulus-fitted response window: the median CSI in every primary field was significantly lower than in every nonprimary field, and lowest of all in A1 (Fig 5B; Kruskall-Wallis test, onset: $\chi^2(4) = 73.95$, $p < 10^{-14}$, sustained: $\chi^2(4) = 109.81$, $p < 10^{-22}$; offset: $\chi^2(4) = 60.95$, $p < 10^{-11}$). The CSI for the late component of the response, however, behaved differently. At this time window, there were no significant differences in SSA between fields (Fig 5B; Kruskall-Wallis test, $\chi^2(4) = 7.78$, $p > 0.1$).

Then, we compared CSI levels within each field for the four time windows to analyze the trend of SSA throughout the different response components. Within nonprimary fields, we found no significant differences between median CSIs measured at the four different time windows (Fig 5B; Friedman test, SRAF: $\chi^2(3) = 5.03$, $p > 0.1$; PAF: $\chi^2(3) = 4.72$, $p > 0.1$). By contrast, a highly significant window effect was found for the three primary fields (Friedman test, A1: $\chi^2(3) = 109.58$, $p < 10^{-22}$; AAF: $\chi^2(3) = 18.18$, $p < 0.001$; VAF: $\chi^2(3) = 55.3$, $p < 10^{-11}$). Post-hoc comparisons revealed that this effect was due to a specific increase of CSI at the late

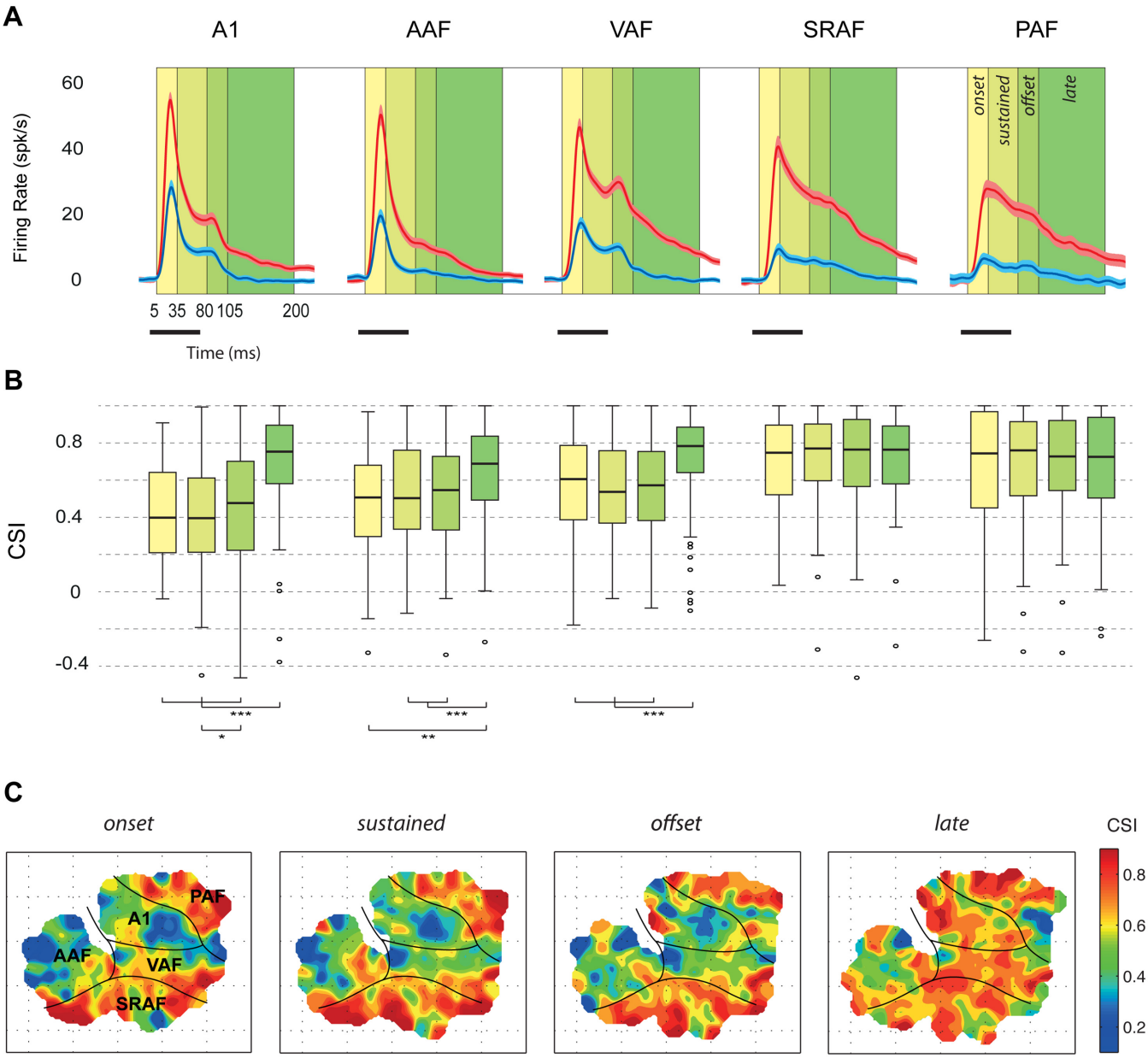

Fig 5. Variation of the CSI throughout the neural response. A. Grand-average responses (baseline-corrected firing rate, mean ± SEM) to standard (blue) and deviant (red) tones within each field. Many recordings showed significant responses beyond 100 ms from stimulus onset. **B.** Distribution of CSI values (thick bar: median, box: interquartile range, whiskers: full range excluding outliers) computed at different time windows with respect to stimulus presentation. In the nonprimary fields, SSA was high through the entire response. In primary fields, median CSI was lower than in nonprimary fields from onset to offset components but not for the late component, which showed CSI levels as high as in the nonprimary fields. **C.** Topographic distribution of SSA for the four different time windows. Note that only the late-component CSI is high throughout the entire auditory cortex. Underlying data for this figure can be found in S4 Data.

doi:10.1371/journal.pbio.1002397.g005

component (Fig 5B), with no significant differences between median CSI measured at the onset, sustained, or offset components of the response, except for a slightly significant increase from the sustained to the offset component in A1, consistent with the overall trend. Therefore, SSA in the nonprimary fields is maintained high throughout the entire response (Fig 5B and 5C). By contrast, SSA in the primary fields is moderate during stimulus presentation, followed

by a specific enhancement in late components (Fig 5B and 5C), in which SSA reaches the same levels found in nonprimary fields.

SSA Depends on Neuronal Firing Rate and Frequency of Stimulation

Upon visual inspection, regions with lowest SSA in the CSI landscape seemed to coincide with low-CF regions of the auditory cortex, particularly within A1 (Fig 4A and 4B). Since a strong dependence of SSA on frequency and intensity of pure-tone stimulation has been shown in the IC [15], we wanted to test whether a similar dependence was present in the auditory cortex. Fig 6A shows a spotlight-average map of the SI across all frequency/intensity combinations tested in the whole set of recordings. High SSA is sharply skewed toward the high frequencies and low intensities of stimulation. When we analyzed primary and nonprimary fields separately (Fig 6B and 6C), we observed that this dependence of the SI on frequency and intensity was more evident within primary (Fig 6B) than nonprimary fields (Fig 6C). Additionally, average firing rate had a topographical distribution in the dataset and was different between cortical areas (Fig 4C and 4D). Since firing rate may also have a strong impact on the amount of adaptation [17], the topography of SSA could result in part from a topography of firing rates. Finally, the observed effect of stimulus intensity on the SI (Fig 6) might be an indirect consequence of the effect of firing rate, with higher intensities of stimulation producing higher firing rates and, therefore, lower SSA.

To address these observations quantitatively, we fit a multivariate linear regression model for the SI, following a stepwise strategy ("fitlm" function in Matlab, with robust fitting options; sample data used to fit this model can be found in S5 Data). First, we used average spike count (*SPK*, as the sum of average response to deviant and standard stimuli) and frequency of stimulation (*OCT*, in octaves with respect to 1 kHz) as predictors. The resulting model was:

$$\mathrm{SI} = 0.51 - 0.046 \cdot SPK + 0.057 \cdot OCT \ (\mathrm{F}_{2,1215} = 166, p < 5 \times 10^{-64}).$$

This model accounted for 21.3% of the variability of the SI, but, more importantly, it provided a specific quantification of each effect: on average, SI decreases 0.046 points per spike of the response, while it increases 0.057 points per octave of the stimulus. Then, we added intensity of stimulation (*SPL*, in dB SPL) to the model, obtaining:

$$\mathrm{SI} = 0.72 - 0.051 \cdot SPK + 0.050 \cdot OCT - 0.003 \cdot SPL \ (\mathrm{F}_{3,1214} = 122, p < 5 \times 10^{-69}).$$

Thus, SI is also negatively correlated to intensity of stimulation. This model, however, explained 23% of the variability of the SI, only 1.7% more than the previous one. Therefore, most of the dependence of the SI on *SPL* is already explained by its dependence on *SPK*, confirming the fact that higher intensities produce lower SSA because of a higher firing rate. Therefore, we removed *SPL* from the model and replaced it with *FIELD* as a categorical factor. Now, the explanatory power of the model increased to 30.6%, mainly due to overall higher SI in the nonprimary fields:

$$\mathrm{SI} = 0.41 + 0.12 \cdot VAF + 0.24 \cdot SRAF + 0.20 \cdot PAF - 0.04 \cdot SPK + 0.05 \cdot OCT \ (\mathrm{F}_{6,1211} = 90.6, p < 10^{-94}).$$

According to this model, mean SI is 0.41 in A1 and AAF (not significantly different from each other), 0.53 (0.41 + 0.12) in VAF ($p < 5{\times}10^{-9}$), 0.65 in SRAF ($p < 5{\times}10^{-28}$), and 0.61 in PAF ($p < 5{\times}10^{-16}$), and this difference cannot be explained by differences in firing rate within fields, since the *FIELD* factor explains an extra 9.3% of the SI variability. Note also that these

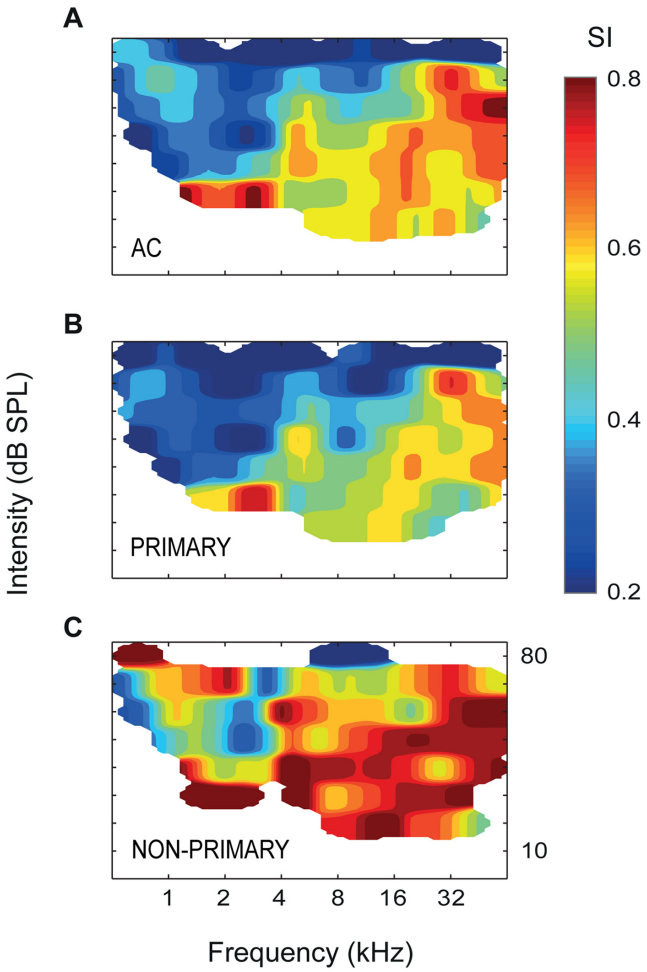

Fig 6. Dependence of SSA on the frequency and intensity of stimulation. A. Averaged SI for different values of frequency and intensity used in the oddball paradigm, for the whole set of recordings throughout the auditory cortex. SSA is significantly higher for high frequencies and low intensities of stimulation. **B.** The same effect of frequency and intensity on SSA is apparent when using all data from primary fields alone, with a virtual absence of SSA for low frequencies and high intensities of stimulation. **C.** In the nonprimary fields, this frequency and intensity dependence is weaker than in the primary fields. Underlying data for this figure can be found in S5 Data.

doi:10.1371/journal.pbio.1002397.g006

are mean values and, therefore, lower than the median values shown in Fig 3, given the rightward skewness of the distributions.

As a final step, we tested this model for interactions between *FIELD* and the other three predictors separately, and we found significant interactions only between *FIELD* and *OCT*:

$$\mathrm{SI} = 0.19 - 0.24 \cdot \mathit{VAF} + 0.36 \cdot \mathit{SRAF} + 0.36 \cdot \mathit{PAF} + 0.078 \cdot \mathit{OCT} - 0.042 \cdot \mathit{VAF} \cdot \mathit{OCT} - 0.031 \cdot \mathit{SRAF} \cdot \mathit{OCT} - 0.034 \cdot \mathit{PAF} \cdot \mathit{OCT} \; (\mathrm{F}_{9,1208} = 43.8, p < 5 \times 10^{-68}),$$

indicating that the effect of frequency was weaker in VAF ($p < 0.005$), SRAF ($p < 0.05$), and PAF ($p < 0.05$) than in A1 and AAF. Therefore, the dependence of SSA on firing rate (and, indirectly, on intensity of stimulation) is comparable among the five fields, but the observed dependence of SSA on frequency of stimulation is mainly due to the fact that A1 and AAF show lower SSA for low frequencies of stimulation, as illustrated in Figs 4A, 4B and 6B.

Incidentally, A1 and AAF are the cortical fields that show the most clear tonotopic gradient, each the mirror reversal of the other (Fig 4A) [23].

Since frequency and intensity of oddball stimulation were selected according to the frequency tuning and threshold of each recording site, and since there is a tendency for tuning bandwidth in auditory cortex to decrease as a function of CF [40,41], differences in SSA between fields could simply reflect differences in tuning bandwidth or CF threshold in the auditory cortex. To check this possibility, we analyzed the correlation between CSI and frequency tuning characteristics in our sample. Distributions of tuning bandwidth and threshold in our sample were consistent with previous mapping work in the rat [23]. Particularly, PAF and AAF featured the broadest tuning bandwidth and highest response thresholds (bandwidth 30 dB above threshold, in octaves, mean ± SEM: A1, 1.89 ± 0.06; AAF, 2.30 ± 0.1; VAF, 1.75 ± 0.06; SRAF, 1.98 ± 0.08; PAF, 2.95 ± 0.16; CF threshold in dB SPL, mean ± SEM: A1, 23.7 ± 0.9; AAF, 29.3 ± 1.3; VAF, 14.8 ± 0.9; SRAF, 22.5 ± 1.1; PAF, 28.3 ± 1.3). Both bandwidth and threshold in AAF and PAF were different from the other fields, but not from each other (Kruskal-Wallis test, bandwidth: $\chi^2(4) = 55.60$, $p < 5\times10^{-11}$; threshold: $\chi^2(4) = 96.03$, $p < 10^{-20}$). By contrast, CSI was 50% higher in PAF than in AAF, as already shown (Fig 3B). Similarly, CF threshold in VAF was significantly lower than in A1 or AAF, but the median CSI was not different between these primary fields (Fig 3B). Indeed, correlation between CSI and either tuning bandwidth or threshold was extremely weak in our sample (Spearman correlation coefficient: $\rho[CSI,BW30] = 0.083$, $p = 0.04$; $\rho[CSI,THR] = -0.09$, $p = 0.02$). These considerations demonstrate that the distinct topography of SSA that we have found is genuine and not an artifactual effect of differences in other response properties between cortical fields.

Different Time Course of Adaptation in Primary and Nonprimary Fields

In order to study the dynamics of adaptation to the repetitive stimuli over time, we averaged responses to standard and deviant stimuli across recordings for every trial number within the sequence and plotted them in relation to the time elapsed since the beginning of the sequence, separately for each field (Fig 7A). Then, we fitted these responses to different simple models. None of the models tested could explain any amount of the variance of the deviant responses, indicating that deviant responses did not show dependence on trial number within any field. In sharp contrast, a power law model of three parameters, $y(t) = a \cdot t^b + c$, yielded very good quality fits for the responses to standards in all fields, explaining about 80% of their variability (adjusted r^2: A1, 0.80; AAF, 0.74; VAF, 0.84; SRAF, 0.83; PAF, 0.69) and indicating that SSA in all fields matches stimulus statistics at many timescales [42].

The most obvious difference between fields was that nonprimary fields reached a much lower plateau at their final steady-state responses (gray dashed line in Fig 7B; *c* parameter (spk/trial): A1, 0.84; AAF, 0.50; VAF, 0.60; SRAF, 0.22; PAF, 0.17; all significantly different from each other as derived from the 95% confidence intervals reported by the "fit" function in Matlab). Also, according to this model, adaptation was fastest in PAF, slowest in VAF, and not significantly different between the other three fields (*b* parameter: A1, –0.78; AAF, –0.93; VAF, –0.68; SRAF, –0.73; PAF, –1.32). This result indicates a distinct high sensitivity of PAF to repetitive stimuli, needing only a few presentations to reach its fully adapted state. This phenomenon can be readily appreciated when analyzing the responses to the first 10 standard trials of the sequence (Fig 7B). Responses to standards in the nonprimary fields adapt below half their initial strength with three (PAF) or four (SRAF) presentations of a stimulus (black arrows in Fig 7B), whereas in the primary fields it takes up to six (A1) presentations to produce this same relative reduction. Therefore, adaptation occurs faster and is stronger in nonprimary than in primary fields.

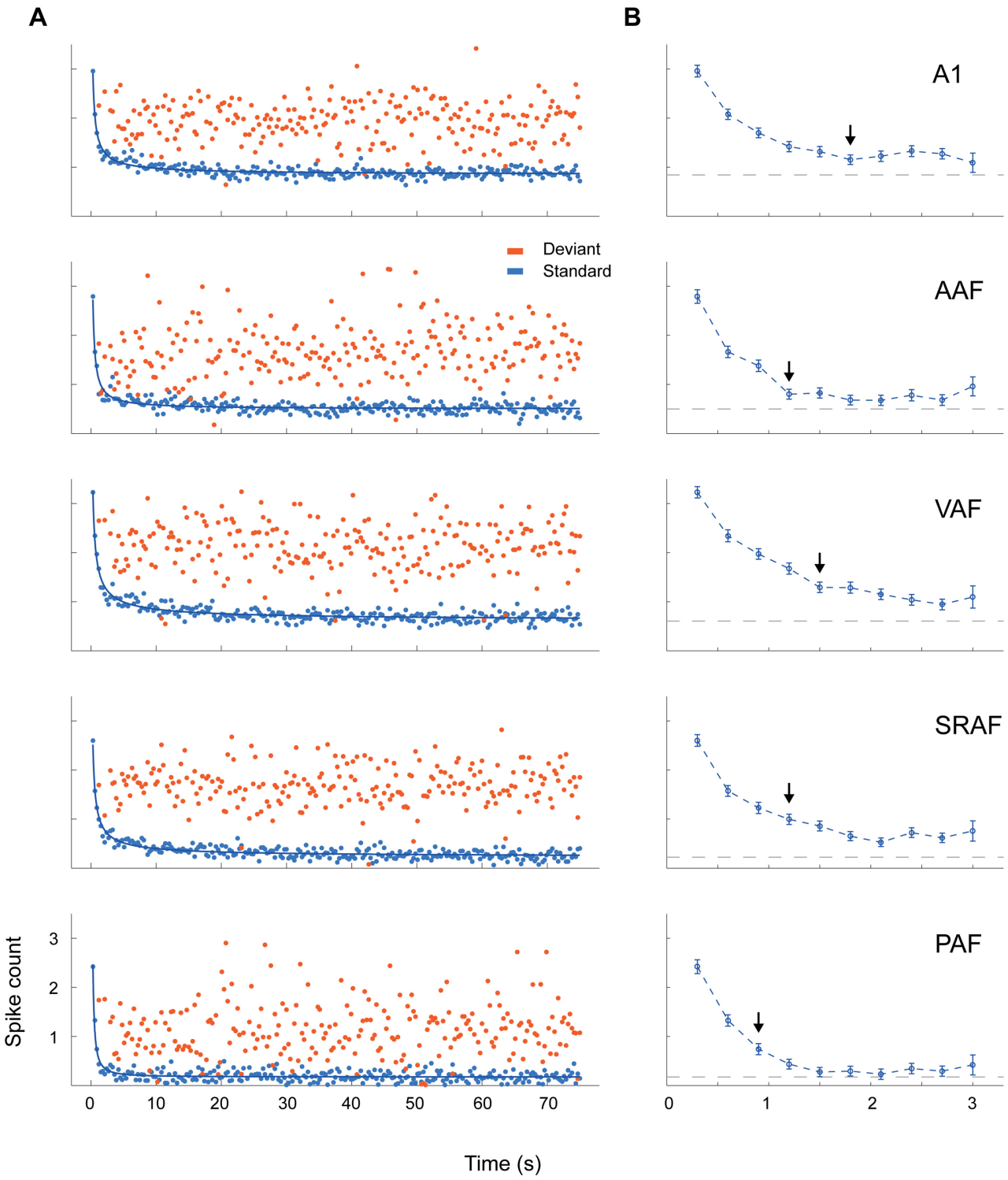

Fig 7. Time course of adaptation within each field. A. Average responses within each auditory cortex field in relation to the order of tone presentation, plotted for standard (blue) and deviant (red) tones separately. The course of standard responses over time followed a power law (thick blue lines), indicating that SSA matches stimulus statistics at many timescales. **B.** Detail of the average (mean ± SEM) standard responses for the first 10 presentations within the sequence. The arrows indicate the trial number in which the response has fallen significantly below half of the response to the first tone presentation. Gray dashed lines indicate the steady-state plateau reached by standard responses at the end of the sequence (constant parameter of the power-law fit). Adaptation occurred faster in PAF than in any other field (see text), and reached a much lower plateau in nonprimary than in primary fields. Underlying data for this figure can be found in S6 Data.

doi:10.1371/journal.pbio.1002397.g007

SSA in the Auditory Cortex Correlates with the Difference Wave of the Local Field Potentials

Whereas SSA in spike responses is a local measure at the neuron level, the MMN is a large-scale brain potential. One reasonable way to bridge this gap is to probe the correlation between adaptation of neural responses and LFP, which represent average synaptic activity in local cortical circuits [43]. Thus, we recorded LFP simultaneously with MUA in four out of the 12 animals, with a total yield of 268 recording sites (A1, 49; AAF, 48; VAF, 55; SRAF, 54; PAF, 42; Unlocalized, 20). We averaged the recorded LFP waveforms evoked by standard and deviant tones for each field separately and computed the difference wave (DW) at every time point after stimulus onset (Fig 8A). In all five cortical fields, these potentials showed the typical morphology in response to pure tones [44,45], with a fast negative deflection (Nd) followed by a slower positive deflection (Pd). These two components were present in responses to both standard and deviant tones, but their amplitudes were, in all cases, smaller for the standards, giving rise to a DW of similar shape but varying amplitudes (Fig 8A). For each recording, the peak amplitude and peak latency of the DW was measured for the Nd and Pd components, within a time window in which the DW reached statistical significance at the whole population level (16–37.6 ms for Nd and 41.5–86.7 ms for Pd, respectively, paired *t* test, Bonferroni correction for 268 comparisons, $p < 0.05$).

Peak amplitude of the DW at the Nd component showed a clear trend to be larger in primary than in nonprimary fields, being significantly smaller in PAF than in the three primary fields and smaller in SRAF than in AAF (Fig 8B; one-way ANOVA, $F_{4,243} = 8.24$, $p < 5\times10^{-6}$). This trend was still present, albeit much less clear, for the Pd component of the DW, being significantly smaller in PAF than in A1 and AAF but not different between the other fields (Fig 8B; one-way ANOVA, $F_{4,243} = 3.74$, $p < 0.01$). Thus, the fast Nd component of the DW showed a topographical distribution within the auditory cortex, whereas the slower Pd component of the DW showed a more homogenous distribution across cortical fields. A similar pattern was apparent for the peak latencies of each of these components (Fig 8B). The Nd component of the DW peaked earlier in the primary than in the nonprimary fields, significantly so between A1 or AAF and SRAF or PAF (mean ± SEM: A1: 24.6 ± 0.9 ms; AAF: 24.8 ± 0.8 ms; VAF: 28.3 ± 0.6 ms; SRAF: 31.1 ± 0.8 ms; PAF: 32.0 ± 1.7 ms; one-way ANOVA, $F_{4,243} = 11.78$, $p < 5\times10^{-8}$). Peak latencies for the Pd component, on the other hand, were not statistically different between fields (mean ± SEM: A1: 61.7 ± 2.0 ms; AAF: 57.4 ± 2.2 ms;, VAF: 59.5 ± 2.0 ms;, SRAF: 59.8 ± 1.7 ms; PAF: 61.4 ± 2.1 ms; one-way ANOVA, $F_{4,243} = 0.70$, $p = 0.59$). The steady progression of the Nd peak latency is consistent with a bottom-up propagation of the signal from primary to nonprimary fields, whereas the homogeneity of the Pd peak latency suggests a stronger contribution of intracortical processing and reciprocal interaction between fields.

To facilitate a more direct comparison between SSA for the MUA and for the LFP components, we also computed CSI values for the Nd and Pd peaks of the LFP (S8 Data). Overall, SSA at both components of the LFP was appreciably lower than for the MUA (paired signed rank test for the whole set of recordings with LFP; CSI-Nd versus CSI-onset, z-score = 6.98, $p < 5\times10^{-12}$; CSI-Pd versus CSI-sustained, z-score = 10.12, $p < 5\times10^{-24}$), but it followed the same trend to be lower in the primary than in nonprimary fields (Median CSI-Nd: A1, 0.32; AAF, 0.31; VAF, 0.45; SRAF, 0.50; PAF, 0.47; Kruskall-Wallis test, $\chi^2(4) = 21.12$, $p < 5\times10^{-4}$. Median CSI-Pd: A1, 0.25; AAF, 0.24; VAF, 0.33; SRAF, 0.37; PAF, 0.40; Kruskall-Wallis test, $\chi^2(4) = 13.09$, $p < 0.05$). Furthermore, CSI-Nd and CSI-Pd were strongly correlated with their corresponding CSI values at comparable time windows (Spearman correlation coefficient: ρ [CSI-Nd, CSI-onset] = 0.66, $p < 10^{-40}$; ρ[CSI-Pd, CSI-sustained] = 0.43, $p < 5\times10^{-12}$; ρ [CSI-Pd, CSI-offset] = 0.21, $p < 0.005$).

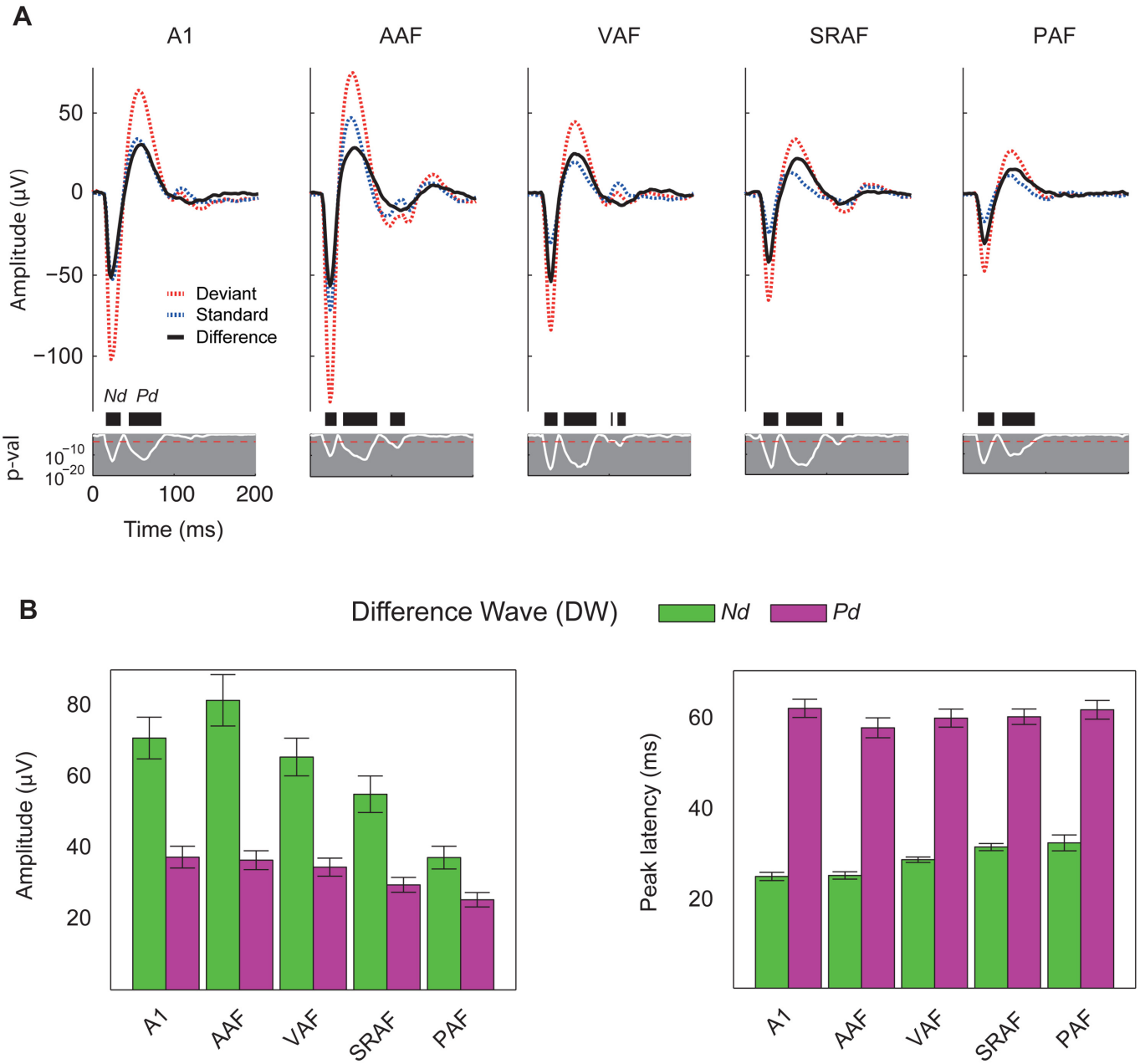

Fig 8. Adaptation in the LFP. A. Grand-average LFP traces in response to deviant (red) and standard (blue) tones, and the resulting difference wave (black), averaged for each cortical field separately. Two components of the difference wave (DW) were analyzed: the fast negative deflection (Nd) and the slower positive deflection (Pd). Note also a small but significant deflection of the LFP at longer latencies (>100 ms) in anteroventral fields (AAF, VAF, and SRAF). White line: *p*-value of the DW. Black thick bars: time intervals showing a significant DW. Red dotted horizontal line: Bonferroni-corrected critical *p*-value (bilateral *t* test). **B.** Peak amplitude and latency (mean ± SEM) of the Nd and Pd components of the DW within each cortical field. Note that the mean of the amplitudes/latencies of the individual DW components are not equal to the peak amplitude/latency of the same component in the grand-averaged DW. Underlying data for the charts in panel B can be found in S7 Data.

doi:10.1371/journal.pbio.1002397.g008

Discussion

In this account, we compared the level of SSA in primary and higher-order auditory cortex to validate SSA as a candidate neural correlate of the MMN. To study the topographic organization of SSA, we mapped the whole rat auditory cortex with MUA recordings from middle

layers IIIb/IV using an oddball paradigm. We demonstrate that SSA occurs beyond A1, and its properties differ between primary and nonprimary fields. Our major findings are: (1) Highest SSA is sharply segregated to nonprimary fields, creating a distinct topographic gradient of SSA within the auditory cortex. (2) High SSA is present in nonprimary fields up to 200 ms after stimulus onset, and it remains stronger than in primary fields during the first 100 ms of the neuronal responses. (3) In all cortical fields, SSA is correlated in time and strength with the difference wave seen in both the fast (Nd) and slower (Pd) deflections of the LFP. As additional novel findings, we show that (4) SSA produces a delay in the responses to standard tones, as compared to deviants, and this delay is longer in nonprimary fields. (5) SSA is significantly higher for high frequencies of stimulation, and this dependence is more pronounced in primary fields. (6) SSA occurs faster and reaches a much lower plateau in the nonprimary fields.

One key aspect of our data is the high coincidence in the relative position of the fields across animals and in comparison with previous mapping studies [23,24,32,36]. Our analysis revealed a systematic meta-organization of SSA in the auditory cortex of the rat [23,36], such that the CSI gradient shows a steep increase at the boundaries between primary and nonprimary fields (Fig 4B). In particular, the sharp CSI enhancement between A1 and PAF (Fig 4D) bears striking resemblance with the same border found previously for bandwidth and latency [24]. Our results conform with previous studies that showed SSA in A1 [12,19,44–50] and extend their findings, as we present new SSA properties hitherto unknown. Importantly, the distribution of SSA indices in our A1 sample is largely equivalent to those shown in previous studies of SSA in the rat or mouse A1 that used similar paradigm parameters [19,47,50], making further comparisons more reliable. To the best of our knowledge, there were no previous studies of SSA outside A1, although higher SSA levels were expected to be found in nonprimary fields, since neurons in nonprimary cortical areas are known to show fast adaptation [20,21]. In particular, many studies independently reported that PAF neurons in the rat adapt strongly even to slow repetition rates [22–24], and novel sounds produced greater cellular activity than familiar sounds in auditory association cortex in area Te3 [51], where the SRAF is located [35]. There is also strong evidence of enhanced adaptation in nonprimary areas of the auditory cortex from large-scale brain responses (ERP, magnetoencephalography [MEG], fMRI) in both animals [28,29,52,53] and humans [25–27,54]. Our findings also parallel the topography of subcortical SSA (Fig 9). Previous studies consistently found stronger SSA in the nonprimary (or nonlemniscal) subdivisions of the IC [14–16] and MGB [17,55]. Importantly, an identical dependence of SSA on frequency of stimulation as well as a delay in onset latency of responses to standards have already been shown in the IC [15].

Our data sharply contrast with previous studies showing that the SSA level in A1 neurons is independent of their CF and in which less than 4% of neurons showed a latency effect [56]. However, the presence of strong SSA in spiking responses at 50–100 ms and beyond represents the major difference with previous SSA studies. Only very recently, two studies in mouse auditory cortex [49,50] and one in rat somatosensory cortex [57] found SSA in either subthreshold V_m fluctuations of layer II/III pyramidal neurons [49] or spiking responses of inhibitory interneurons [49,50] and layer IV pyramidal neurons [57] occurring more than 50–100 ms after stimulus onset. Importantly, we recorded mainly form layer IIIb/IV neurons, receiving direct thalamocortical inputs, which are more likely to show long-latency spiking responses [58]. Finally, previous studies reported SSA for LFP in A1, but they failed to show any correlation between MMN-like components of the LFP and SSA. Some did not find significant spiking activity for latencies beyond 50 ms [44,45] or observed SSA only for the fast Nd [46]; others did not measure MUA [59], or their analysis was restricted to the fast Nd only [19]. Such a correlation has only been described in the somatosensory cortex [57].

The mechanisms and location of the neural generators of SSA and their relation to MMN are still subjects of debate [11,13,60,61]. In the lemniscal pathway (Fig 9), SSA undergoes a first

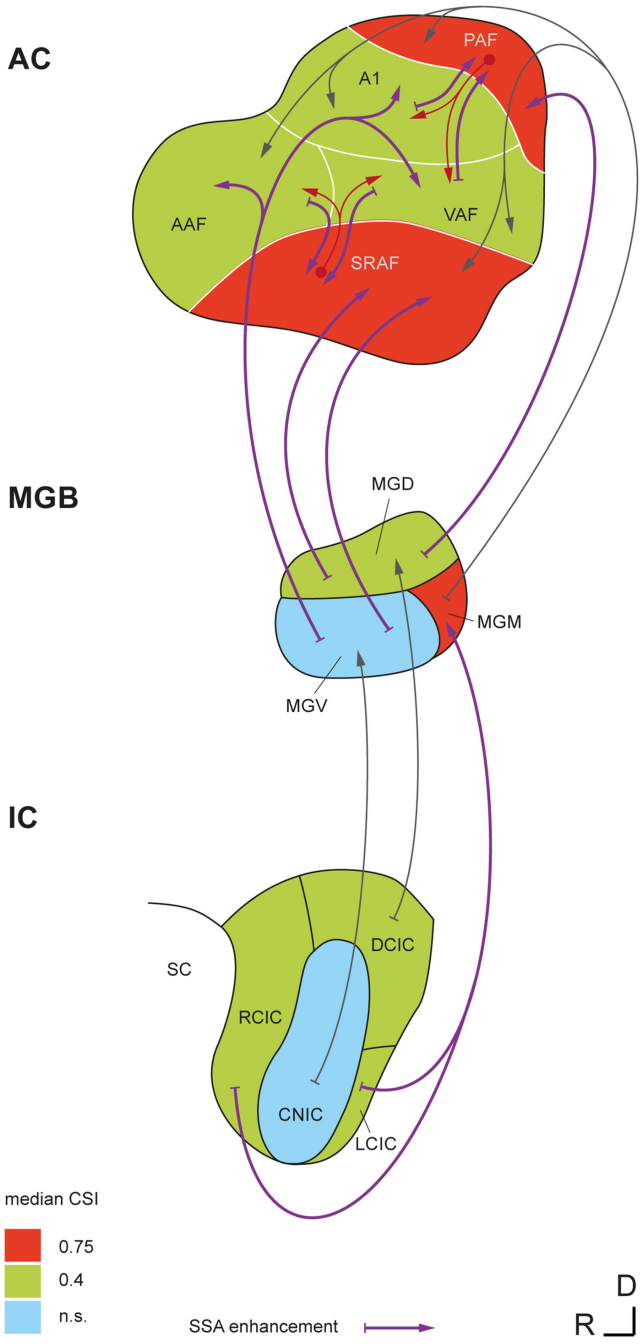

Fig 9. Emergence of SSA in the nonlemniscal auditory pathway. Simplified wiring diagram showing SSA levels and ascending connections of the auditory brain in which SSA occurs. SSA is virtually absent from lemniscal parts of the IC (central nucleus of the IC [CNIC]) and MGB (ventral division of the MGB [MGV]), but it is high in their nonlemniscal subdivisions (rostral, dorsal, and lateral cortices of the IC [RCIC, DCIC, and LCIC, respectively]; dorsal and medial divisions of the MGB [MGD and MGM, respectively]), showing levels comparable to those seen in primary cortical fields. Extreme levels of SSA are found only in nonprimary fields of the auditory cortex and in the MGM. Thus, SSA undergoes a significant enhancement at both lemniscal and nonlemniscal thalamocortical projections. A potential influence of nonprimary fields on high late-SSA seen in primary fields is represented by the red arrows. Median CSI values in the IC and MGB are from [17] and [15], using similar paradigm parameters.

doi:10.1371/journal.pbio.1002397.g009

enhancement at the thalamocortical synapses from the ventral division of the MGB to A1 [12,17]. Here, we show a further enhancement of SSA in nonprimary cortical fields, which integrate the thalamocortical projection from nonlemniscal MGB [31] and the corticocortical projection from primary fields [62] and redirect their output to prefrontal and limbic brain regions involved in spatial attention and emotional memory [34,35]. Thus, our study confirms that SSA is a prevalent property of the nonlemniscal auditory pathway, even at the cortical level (Fig 9). This organization may underlie its functional significance as a higher-order stage of sensory processing beyond the faithful representation of the auditory stimuli that predominates in the lemniscal pathway [63]. Cumulating evidence indicates the existence of a hierarchy of processing stages for regularity encoding in the auditory brain, with later response components showing sensitivity for changes in more complex aspects of the acoustic scene [13,60,64]. Repetition positivity (RP) has been proposed as the electrophysiological correlate of the memory trace formation required for subsequent change detection and, in turn, rapid SSA in auditory cortex is likely to contribute to its generation [65,66]. Here, we show very strong SSA in nonprimary auditory cortex, supposed to contain the main generators of the MMN in humans [25,27,54,67,68], cats [53], and rats [29], that resembles MMN in several ways. First, SSA results in stronger responses to deviants than to standards in the oddball paradigm, to the extent that responses to standards can get totally suppressed in some recordings from nonprimary fields. Critically, we show strong SSA in these areas between 50 and 100 ms, correlated with a consistent difference wave at the slow Pd component of the LFP (Fig 8A). The latency of this Pd deflection (60–80 ms) is considerably shorter than the human MMN (150–200 ms) but matches perfectly the range of MMN-like potentials in the rat [28,29,69–73], which tend to occur, on average, 50–100 ms after stimulus onset, probably due to the smaller size of the rat brain [37]. Interestingly, this SSA resembles RP in the first standard presentations (Fig 7B) and matches stimulus statistics at multiple time scales [56,74]. We also show stronger SSA for high- than for low-frequency tones, paralleling a commonly observed effect of frequency in both animal [71–73] and human [75,76] MMN recordings. Therefore, we present strong evidence linking animal SSA to the human MMN, a result thus far missing in animal research. Importantly, we show that an MMN-like difference signal can readily result from SSA to standard tones that leaves responses to deviants unaffected (Fig 7A). Additionally, our LFP recordings show that the same components were present in responses to both standard and deviant tones (Fig 8A), consistent with the view that the MMN is a differentially adapted obligatory component of the ERPs. If so, our results would suggest a purely SSA explanation for the MMN [6,7,26].

Before we conclude, we should draw attention to three major caveats of our study. First, anesthesia reduces neuronal responsiveness to auditory stimuli as well as spontaneous firing, and may change some receptive field properties [77–79]; thus, an increased sensitivity to anesthetics in higher-order fields may lead to an overestimation of the SSA seen in those areas. However, we observed high spontaneous rates as well as strong, sustained responses to deviants in nonprimary fields (Fig 5A; baseline-corrected spike counts within 0 and 200 ms, mean ± SEM: A1, 3.2 ± 0.1; AAF, 2.8 ± 0.1; VAF, 4.7 ± 0.2; SRAF, 3.9 ± 0.2; PAF, 2.6 ± 0.2). We used urethane as anesthetic because it preserves balanced neural activity better than other agents [80], retains the higher-order processing capabilities of the auditory cortex [81], and shows no significant effects on SSA levels, at least in the IC [82]. Most importantly, MMN-like responses have been successfully recorded from anesthetized [29,69–71] and awake [28,72,73] animals alike (for review, see [10]). Second, the MMN is a negative-going component, in contrast to the positive late potential (Pd) examined here. Depending on the location of recording and anesthetic state, epidural MMN recordings in rats can be positive in polarity [72,73], an effect commonly observed in urethane-anesthetized preparations [69,71]. Moreover, an inversion of the LFP has been extensively described using laminar probes in A1 [45,59], such that

positivities in layers IIIb/IV may appear as negativities in superficial layers. Third, there are some discrepancies between the SSA seen in MUA and in LFP data. Namely, whereas the MUA shows prominent activity between 100 and 200 ms (i.e., beyond the rat-MMN range), the LFP is relatively flat within this time window. Similar late-spiking activity has been observed in parvalbumin-positive inhibitory interneurons [49] and interpreted as delayed reverberating network activity specifically triggered by deviant stimuli, but we cannot rule out that MUA includes activity from thalamocortical afferents in layers IIIb/IV, which would not produce a prominent LFP component. Alternatively, the late enhancement of SSA (100–200 ms) seen in the primary fields (Fig 5B and 5C) might result from processing in the nonprimary fields, subsequently transmitted downwards through the massive feedback corticocortical connections (Fig 9) [34,35,57,83]. A more relevant discrepancy is that the difference-wave amplitude for the later Pd component of the LFP is comparable between primary and nonprimary auditory cortex and even significantly smaller in PAF than in A1 or AAF (Fig 8B), not supporting the notion of enhanced SSA in nonprimary fields. However, previous ERP studies [28,29] failed to find differences in the MMN amplitude between primary and nonprimary fields. One simple reason for this could be that ERPs and LFPs are large-scale potentials, reflecting overall synaptic activity within a wide volume of tissue [43], most probably spanning the boundaries between fields. Therefore, local measures at the cellular level, such as MUA, are much better indicators of specific differences between fields. Furthermore, it is consistent to find higher SSA at the MUA than at the LFP level (i.e., output versus input, respectively) within any particular area, as also shown at the single-neuron level [48]. Additionally, the amplitude of the difference wave is an absolute measure, whereas SSA is commonly expressed as a contrast, such as the CSI. When computed this way, SSA for the Pd amplitude is already higher in nonprimary than in primary fields, yet this difference is much sharper for the MUA, reflecting the operations carried out by nonprimary fields to their already-adapted inputs.

At this juncture, it is important to note that the slower Pd component of the difference wave peaked with the same latency throughout the entire auditory cortex (Fig 8B), and so did its epidural counterpart in the rat [29]. By contrast, the fast Nd deflection of the LFP occurs earlier in primary than in nonprimary fields (Fig 8B), suggesting a lemniscal origin and bottom-up propagation. Therefore, the higher degree of reciprocal interaction between fields is likely involved in the generation of the Pd, consistent with the idea that intracortical processing contributes to SSA at longer latencies [12,50,57,59,84]. Thus, MMN-like potentials may be readily recorded from both primary and nonprimary auditory cortex, but nonprimary fields seem to contribute critically to their generation at the microcircuit level [27,85].

In conclusion, we demonstrate that strong SSA occurs in nonprimary auditory cortex at the latency range of the MMN in the rat. This finding overcomes the two main discrepancies hitherto alleged against the suggestion that SSA in the auditory cortex may underlie the generation of the MMN [7,86], namely, its anatomical location and its temporal development. We provide empirical evidence of the missing link between SSA in single neurons and scalp-recorded potentials, thus bridging the gap between animal physiology studies and the human MMN. Given the wide use of the MMN as a tool in clinical and cognitive neuroscience [9,10,87,88], such a connection is potentially of high relevance for future research in these fields.

Materials and Methods

Surgical Procedures

The experimental protocols were approved by, and used methods conforming to the standards of, the University of Salamanca Animal Care Committee and the European Union (Directive 2010/63/EU) for the use of animals in neuroscience research. Experiments were performed on

12 adult female Long-Evans rats with body weights within 200 and 250 g. Surgical anesthesia was induced and maintained with urethane (1.5 g/kg, i.p.), with supplementary doses (0.5 g/kg, i.p.) given as needed. Dexamethasone (0.25 mg/kg) and atropine sulfate (0.1 mg/kg) were administered at the beginning of the surgery and every 10 h thereafter to reduce brain edema and the viscosity of bronchial secretions, respectively. Prior to surgery and recording sessions, we recorded auditory brainstem responses (ABR) with subcutaneous electrodes to ensure the animal had normal hearing. ABRs were collected using Tucker-Davis Technologies (TDT) software (BioSig) and hardware (RX6 Multifunction Processor) following standard procedures (0.1 ms clicks presented at a 21/s rate, delivered in 10 dB ascending steps from 10 to 90 dB SPL). The animal was then placed in a stereotaxic frame in which the ear bars were replaced by hollow specula that accommodated a sound delivery system.

After the animal reached a surgical plane of anesthesia, the trachea was cannulated for artificial ventilation and a cisternal drain was introduced to prevent brain hernia. Corneal and hindpaw withdrawal reflexes were monitored to ensure that a moderately deep anesthetic plane was maintained as uniformly as possible throughout the recording procedure. Isotonic glucosaline solution was administered periodically (5–10 ml every 6–8 h, s.c.) throughout the experiment to prevent dehydration. Body temperature was monitored with a rectal probe and maintained between 37 and 38°C with a homoeothermic blanket system (Cibertec). The skin and temporal muscles over the left side of the skull were reflected, and a 6 × 5 mm craniotomy was made in the left temporal bone to expose the entire auditory cortex. The dura was removed and the exposed cortex and surrounding area were covered with a thin, transparent layer of agar to prevent desiccation and to stabilize the recordings.

At the end of the surgery, a magnified picture (25×) of the exposed cortex was taken with a digital SLR camera (D5100, Nikon) coupled to the surgical microscope (Zeiss) through a lens adapter (TTI Medical). The picture included a pair of reference points previously marked on the dorsal ridge of the temporal bone, indicating the absolute scale and position of the image with respect to the bregma. This picture was displayed on a computer screen, and a micrometric grid was overlapped to guide and mark the placement of the electrode for every recording made. Recording sites (150–250 μm spacing; Fig 1A) were evenly distributed across the cortical region of interest while avoiding blood vessels. The vascular pattern was used as a local reference to mark the position of every recording site in the picture, but otherwise differed largely between animals. To confirm the actual depth and cortical layer of the recorded neurons, at the end of the experiment we made electrolytic lesions at one to four of the recording sites at the same depth that recordings were made.

Electrophysiological Recording Procedures

Experiments were performed inside a sound-insulated and electrically shielded chamber. Sounds were generated using an RX6 Multifunction Processor (TDT) and delivered monaurally (to the right ear) in a closed system through a Beyer DT-770 earphone (0.1–45 kHz) fitted with a custom-made cone and coupled to a small tube (12-gauge hypodermic) sealed in the ear. The sound system response was flattened with a finite impulse response (FIR) filter, and the output of the system was calibrated in situ using a ¼-in condenser microphone (model 4136, Brüel & Kjær), a conditioning amplifier (Nexus, Brüel & Kjær), and a dynamic signal analyzer (Photon +, Brüel & Kjær). The output of the system had a flat spectrum at 76 dB SPL (±3 dB) between 500 Hz and 45 kHz, and the second and third harmonic components in the signal were $\leq$ 40 dB below the level of the fundamental at the highest output level (90 dB SPL) [14].

MUA was recorded with self-manufactured glass-coated tungsten electrodes (1–5 MΩ impedance at 1 kHz) [89,90]. A single electrode was positioned orthogonal to the pial surface

(forming a 30° angle with the horizontal plane) and advanced 350–550 μm into the thalamorecipient layers IIIb–IV using a piezoelectric micromanipulator (Sensapex) until we observed a strong spiking activity synchronized with the train of searching stimuli. The signal was amplified (1000×) and band-pass filtered (1 Hz to 3 kHz) with a differential amplifier (DAM-80, WPI). This analog signal was digitized at a 12K sampling rate and further amplified and band-pass filtered for action potentials (between 500 Hz and 3 kHz). Spike waveforms and relative times in respect to the start of the recording were displayed and stored in a PC running Windows XP (Microsoft). A bilateral threshold for automatic action potential detection was set at about two to three standard deviations of the background noise. In a subset of the experiments, the digital signal was further filtered for LFP (between 3 and 50 Hz), decimated to a 508 Hz sampling rate and stored in continuous form for posterior analysis. Stimulus generation and neuronal response visualization were controlled online with custom software created with the OpenEx suite (TDT) and Matlab (Mathworks).

Sounds used for stimulation were white noise bursts or pure tones with 5 ms rise-fall ramps. Sounds used for searching for neuronal activity were trains of noise bursts or pure tones (1–8 stimulus per second). We used short stimulus duration for searching (30 ms) to prevent strong adaptation. In addition, type (noise, pure tone) and parameters (frequency, intensity, presentation rate) of the search stimuli were varied manually when necessary to facilitate release from adaptation and, thus, prevent overlooking responses with high SSA. Once a suitable recording site was reached, the FRA was determined using 75 ms pure tones at varying frequencies and intensities (Fig 2A; 0.5–44 kHz logarithmically spaced at 0.25 octave steps, 0–70 dB SPL at 10 dB steps, 375 ms onset-to-onset interval, one to three randomized repetitions of each stimulus). The FRA was displayed on a computer screen using custom software, and the frequency-tuning curve was automatically outlined as the minimum sound intensity that elicited a firing rate over 20%–40% of the maximum firing for each frequency. Thus, the minimum response threshold and CF were computed for each site (excluding isolated "islands" of spontaneous activity), and two frequencies (f_1, f_2) were selected to use in the oddball paradigm [12] at 20–30 dB above threshold. The two stimuli were selected so as to evoke strong responses of similar magnitude at that recording site. In some cases, one or more extra pairs of stimuli were selected to ensure at least one recording met this requirement. Two oddball sequences with fixed parameters (250 trials each, 75 ms stimulus duration, 0.5 octaves frequency separation, 10% deviant probability, 300 ms onset-to-onset interval, minimum of three standard tones before a deviant) were presented for every pair of stimuli thus selected. In one of the sequences, the low frequency (f_1) was the "standard" and the high frequency (f_2) was the "deviant," and in the other sequence their roles were swapped. The order of presentation of these two sequences was randomized across sites.

Data Analysis

Peristimulus time histograms (PSTH) were generated for every stimulus and condition tested. Only the last standard tones preceding each deviant were used for the analyses, except for the time course analysis, where all standard trials were analyzed. Every PSTH was analyzed to test for significant auditory responses and to extract several different metrics of response strength and latency. For these analyses, the original PSTH was smoothed with a 6 ms gaussian kernel ("ksdensity" function in Matlab) in 1 ms steps to estimate the spike-density function (SDF) over time, and the baseline spontaneous firing rate (SFR) was determined as the average firing rate during the 75 ms preceding stimulus onset. For any given time window, the excitatory response was measured as the area below the SDF and above the baseline SFR. This measure will be referred to as "baseline-corrected spike count" (BCSC). To test for statistical significance of the

BCSC we used a Monte Carlo approach. First, 1000 simulated PSTHs were generated using a Poisson model with a constant firing rate equal to the SFR. Then, a "null distribution" of BCSC was generated from this collection of PSTHs, following these same steps. Finally, the *p*-value of the original BCSC was empirically computed as $p = (g + 1) / (N + 1)$, where g is the count of "null" measures greater than or equal to BCSC and $N = 1000$ is the size of the "null" sample. Note that using this approach, the minimum *p*-value that can be obtained is $1/1001 \approx 0.001$.

When a significant evoked activity was detected, onset and offset latencies of the whole excitatory response were computed as follows. First, a "noise" threshold was computed, as the firing rate below which the pure-spontaneous simulated SDFs remained 97.5% of the time. Every SDF, including the simulated ones, was scanned for stretches of "signal" above this threshold, and the amount of "signal" for each stretch was measured as the area below the SDF and above the SFR during that particular interval. Using the distribution of all the signal stretches thus found within the 1,000 pure-spontaneous SDFs, a Monte Carlo test was used to compute empirical *p*-values for every stretch of signal found in the target SDF under study. For each significant signal stretch ($p < 0.05$), the start/end times (T_{on}, T_{off}) were determined as the time points when the SDF trace cuts the noise threshold, and onset/offset latencies of the whole excitatory response (*ONSET*, *OFFSET*) were defined as the T_{on}/T_{off} of the first/last significant excitatory component of the response, respectively. Peak firing rate amplitude was defined as the maximum firing rate reached by the SDF within the analysis window, minus the SFR baseline, and peak latency as the time point respect stimulus onset that this peak takes place. Finally, the duration of the whole significant response interval was defined as *OFFSET*–*ONSET*, and the duration of the strong peak of the response, or "half-peak response duration," was measured as the total length of time that the SDF remains above 50% of the peak amplitude.

In order to quantify and compare SSA levels between the five fields, we computed the frequency-specific SSA index for each stimulus, SI(f_1) and SI(f_2), and the common SSA index (CSI) for every recording site in the usual way [12]:

$$SI(f_i) = \frac{DEV(f_i) - STD(f_i)}{DEV(f_i) + STD(f_i)}\ ; \quad i = 1, 2$$

$$CSI = \frac{\sum DEV(f_i) - \sum STD(f_i)}{\sum DEV(f_i) + \sum STD(f_i)}\ ; \quad i = 1, 2$$

Where DEV(f_i), STD(f_i) are baseline-corrected spike counts in response to frequency f_i when it was a deviant and standard, respectively. The CSI was calculated only for recordings with significant auditory responses to at least one frequency in the oddball paradigm (either as deviant or as standard). In cases in which more than one stimulus pair was tested at the same recording site, we selected only one to compute SSA for that site, according to the following criteria: (1) Recordings with significant responses to both frequencies (either as deviant or as standard) were always preferred to recordings with significant response to only one of them. (2) We selected the recording with most similar responses to f_1 and f_2 (as deviants); the similarity between responses was measured as their ratio, f_1/f_2 or f_2/f_1, whichever was less than 1. (3) If there were two or more recordings with similar deviant-to-deviant ratios (difference of ratios < 0.1), we selected the one with the lowest sound level (SPL) used for stimulation.

For the analysis of the LFP signal, we aligned the recorded wave to the onset of the stimulus for every trial and computed the mean LFP for every recording site and stimulus condition (deviant, standard) as well as the difference wave (DW = deviant−standard). Then, grand-averages were computed for deviant, standard, and DW across the whole auditory cortex and for every field separately. The *p*-value of the grand-averaged DW was determined for every time

point with a two-tailed *t* test, Bonferroni-corrected for 204 comparisons (overall significance level of 0.05), and the time intervals in which a significant DW was observed were computed. For each individual (mean) LFP wave, the peak amplitude and latency were computed within two time windows: [10–40 ms] and [50–90 ms], corresponding to the first Nd and second Pd seen in the grand-averages within all fields. When comparing response features between fields, such as onset latency or CSI, we used nonparametric Kruskall-Wallis or Friedman tests, given the non-normal nature of these measures. Each of these tests was followed by a post-hoc multiple comparison test, using the Dunn-Sidak method at a 5% significance level, to detect specific differences between fields. For the sake of readability, *p*-values for all tests are reported using an upper bound equal to the minimum power of ten or half a power of ten that is greater than the actual *p*-value (e.g., $p < 5{\cdot}10^{-6}$).

For the time course analysis, we first computed the average standard and deviant response at each absolute position within the sequence for all neurons tested within each cortical field separately. A single-trial spike count for any given PSTH was computed as the number of spikes between the previously determined *ONSET* and *OFFSET* times, minus the baseline SFR. Then, we fitted these time series to different models (linear, exponential, double exponential, polynomial inverse, and power law with two or three coefficients) using the "fit" function in Matlab, which also computes the coefficient of determination (adjusted-r^2) of the whole fit and confidence intervals for the fitted parameters.

To quantify the topographical organization of a feature map and test for statistical significance thereof, we used the "MapTools" library in Matlab, applying the topographic product statistic [39]. This metric was used instead of other alternatives (Pearson and Spearman linear correlation, Zrehen measure, etc.) due to the highly non-normal nature of the data under study (i.e., CSI) and assuming a local, linear nature of the topography of the CSI. To generate averaged maps for CF, CSI, and other response features, we followed a spotlight-average approach: starting with the set of sample points in which actual recordings were made and the associated values of the feature, we computed the averaged feature value for any other point in the map from its nearest neighbors. Specifically, we placed a bivariate Gaussian kernel of 100-μm radius,

$$\ker(x,y) = \frac{1}{2\pi r} \cdot \exp\left\{\frac{\sqrt{x^2+y^2}}{2r^2}\right\},$$

centered on every sample point and multiplied it by its associated feature value. Then we summed all these functions over the entire map and divided the result by the sum of all kernels at every point, to compute a weighted average throughout the whole surface. Thus, the feature value *V* at every point of the map was calculated as:

$$V(x,y) = \frac{\Sigma_{i=0}^{n} v_i \cdot ker(x-x_i, y-y_i)}{\Sigma_{i=0}^{n} ker(x-x_i, y-y_i)},$$

where *x*, *y* are the coordinates of a generic point in the map, and x_i, y_i ($i = 1, \ldots, n$) are the sample points used to generate the map. To impose a limit on the influence span for every point, this weighted average was computed only for points where the sum of all kernels (denominator in the last formula) was greater than 0.05. Further, to avoid single-point averages, we computed *V(x,y)* only when at least two neighboring sample points had been used for averaging.

To combine data from different animals, we followed an iterative process to improve the quality of the alignment in successive stages. We first generated the CF map for the case with the greatest number of recordings (shown in Fig 1). Then, we applied a manual shift to each of the remaining maps in turn so as to put them into register with the former. We used the CF gradient, the "unresponsive spot" at the wedge between A1, AAF, and VAF, and the low-

frequency centers in A1, AAF, and SRAF as main references to determine, for each animal, the absolute position of the map with respect to the bregma [23]. Finally, we computed the topographic product statistic for the whole set of aligned recordings. This alignment was refined and the test statistic was recalculated until no improvement was detected in the correlation. We repeated this process for every animal until the alignment was completed.

Supporting Information

S1 Data. Full dataset used in reported results and figures. Organized into four spreadsheets: "Recording site," list of all MUA recordings made, including those that didn't show good responses to pure tones or otherwise could not be tested with the oddball paradigm; "Oddball (MUA)," list of all MUA recordings that could be tested with the oddball paradigm (one selected recording per multiunit), contains main stimulation parameters, response measures, and SSA indexes; "Time Course," contains trial-by-trial spike counts used to fit the time course of SSA and generate Fig 7; "Oddball (LFP)," list of all recording sites with LFP recordings made, contains main responses and adaptation measures reported for the Nd and Pd deflections of the LFP.
(XLSX)

S2 Data. Selected dataset (full SSA index sample) underlying Fig 3.
(XLSX)

S3 Data. Selected dataset used to generate the maps in Fig 4. Contains separate spreadsheets for Fig 4A (map of CF, all recordings with a well-defined CF) and Fig 4B–4D (maps of adaptation, all recordings tested with the oddball paradigm).
(XLSX)

S4 Data. Selected dataset (CSI measures at different time windows) underlying boxplots and maps in Fig 5B and 5C.
(XLSX)

S5 Data. Selected dataset (tone frequency, intensity, firing rate, and SI for each tone [*f1* and *f2*, separately]) used to fit the linear model for the SI described in Results and to generate SI maps in Fig 6.
(XLSX)

S6 Data. Average trial-by-trial spike counts used to fit the time course of SSA within each field and generate Fig 7.
(XLSX)

S7 Data. Selected dataset (amplitude and latency of the Nd and Pd difference) underlying barplots in Fig 8B.
(XLSX)

S8 Data. Selected dataset (SSA for the Nd and Pd components) reported in Results but not shown in any figure.
(XLSX)

Acknowledgments

We thank Drs. Dexter Irvine, Patricia Michie, Alan Palmer, Heather Read, and Adrian Rees for their comments on previous versions of the manuscript and for their constructive criticisms.

We are especially grateful to Dr. Heather Read for helpful suggestions for recording from the auditory cortex and determining the boundaries of the cortical fields.

Author Contributions

Conceived and designed the experiments: JND MSM. Performed the experiments: JND. Analyzed the data: JND. Contributed reagents/materials/analysis tools: JND. Wrote the paper: JND MSM.

References

1. Ranganath C, Rainer G. Neural mechanisms for detecting and remembering novel events. Nat Rev Neurosci. 2003; 4:193–202. doi: 10.1038/nrn1052 PMID: 12612632
2. Kaya EM, Elhilali M. Investigating bottom-up auditory attention. Front Hum Neurosci. 2014; 8:327. doi: 10.3389/fnhum.2014.00327 PMID: 24904367
3. Malmierca MS, Anderson LA, Antunes FM. The cortical modulation of stimulus-specific adaptation in the auditory midbrain and thalamus: a potential neuronal correlate for predictive coding. Front Syst Neurosci. 2015; 9:19. doi: 10.3389/fnsys.2015.00019 PMID: 25805974
4. Näätänen R, Gaillard AW, Mäntysalo S. Early selective-attention effect on evoked potential reinterpreted. Acta Psychol (Amst). 1978; 42:313–29. doi: 10.1016/0001-6918(78)90006-9
5. Winkler I, Karmos G, Näätänen R. Adaptive modeling of the unattended acoustic environment reflected in the mismatch negativity event-related potential. Brain Res. 1996; 742:239–52. doi: 10.1016/S0006-8993(96)01008-6 PMID: 9117400
6. May PJC, Tiitinen H. Mismatch negativity (MMN), the deviance-elicited auditory deflection, explained. Psychophysiology. 2010; 47:66–122. doi: 10.1111/j.1469-8986.2009.00856.x PMID: 19686538
7. Fishman YI. The mechanisms and meaning of the mismatch negativity. Brain Topogr. 2014; 27:500–26. doi: 10.1007/s10548-013-0337-3 PMID: 24276221
8. Escera C, Alho K, Winkler I, Näätänen R. Neural mechanisms of involuntary attention to acoustic novelty and change. J Cogn Neurosci. 1998; 10:590–604. PMID: 9802992
9. Näätänen R, Kujala T, Escera C, Baldeweg T, Kreegipuu K, Carlson S, et al. The mismatch negativity (MMN)—a unique window to disturbed central auditory processing in ageing and different clinical conditions. Clin Neurophysiol. 2012; 123:424–58. doi: 10.1016/j.clinph.2011.09.020 PMID: 22169062
10. Todd J, Harms L, Schall U, Michie PT. Mismatch negativity: translating the potential. Front Psychiatry. 2013; 4:171. doi: 10.3389/fpsyt.2013.00171 PMID: 24391602
11. Nelken I. Stimulus-specific adaptation and deviance detection in the auditory system: experiments and models. Biol Cybern. 2014; 108:655–63. doi: 10.1007/s00422-014-0585-7 PMID: 24477619
12. Ulanovsky N, Las L, Nelken I. Processing of low-probability sounds by cortical neurons. Nat Neurosci. 2003; 6:391–8. doi: 10.1038/nn1032 PMID: 12652303
13. Grimm S, Escera C. Auditory deviance detection revisited: evidence for a hierarchical novelty system. Int J Psychophysiol. 2012; 85:88–92. doi: 10.1016/j.ijpsycho.2011.05.012 PMID: 21669238
14. Malmierca MS, Cristaudo S, Pérez-González D, Covey E. Stimulus-specific adaptation in the inferior colliculus of the anesthetized rat. J Neurosci. 2009; 29:5483–93. doi: 10.1523/JNEUROSCI.4153-08.2009 PMID: 19403816
15. Duque D, Pérez-González D, Ayala YA, Palmer AR, Malmierca MS. Topographic distribution, frequency, and intensity dependence of stimulus-specific adaptation in the inferior colliculus of the rat. J Neurosci. 2012; 32:17762–74. doi: 10.1523/JNEUROSCI.3190-12.2012 PMID: 23223296
16. Ayala YA, Malmierca MS. Stimulus-specific adaptation and deviance detection in the inferior colliculus. Front Neural Circuits. 2013; 6:89. doi: 10.3389/fncir.2012.00089 PMID: 23335883
17. Antunes FM, Nelken I, Covey E, Malmierca MS. Stimulus-specific adaptation in the auditory thalamus of the anesthetized rat. PLoS ONE. 2010; 5:e14071. doi: 10.1371/journal.pone.0014071 PMID: 21124913
18. Antunes FM, Malmierca MS. Effect of auditory cortex deactivation on stimulus-specific adaptation in the medial geniculate body. J Neurosci. 2011; 31:17306–16. doi: 10.1523/JNEUROSCI.1915-11.2011 PMID: 22114297
19. Taaseh N, Yaron A, Nelken I. Stimulus-specific adaptation and deviance detection in the rat auditory cortex. PLoS ONE. 2011; 6:e23369. doi: 10.1371/journal.pone.0023369 PMID: 21853120

20. Irvine DR, Huebner H. Acoustic response characteristics of neurons in nonspecific areas of cat cerebral cortex. J Neurophysiol. 1979; 42:107–22. PMID: 430107

21. Schreiner CE, Cynader MS. Basic functional organization of second auditory cortical field (AII) of the cat. J Neurophysiol. 1984; 51:1284–305. PMID: 6737031

22. Doron NN, Ledoux JE, Semple MN. Redefining the tonotopic core of rat auditory cortex: physiological evidence for a posterior field. J Comp Neurol. 2002; 453:345–60. doi: 10.1002/cne.10412 PMID: 12389207

23. Polley DB, Read HL, Storace DA, Merzenich MM. Multiparametric auditory receptive field organization across five cortical fields in the albino rat. J Neurophysiol. 2007; 97:3621–38. doi: 10.1152/jn.01298.2006 PMID: 17376842

24. Pandya PK, Rathbun DL, Moucha R, Engineer ND, Kilgard MP. Spectral and temporal processing in rat posterior auditory cortex. Cereb Cortex. 2008; 18:301–14. doi: 10.1093/cercor/bhm055 PMID: 17615251

25. Kropotov JD, Alho K, Näätänen R, Ponomarev VA, Kropotova OV, Anichkov AD, et al. Human auditory-cortex mechanisms of preattentive sound discrimination. Neurosci Lett. 2000; 280:87–90. doi: 10.1016/S0304-3940(00)00765-5 PMID: 10686384

26. Jääskeläinen IP, Ahveninen J, Bonmassar G, Dale AM, Ilmoniemi RJ, Levänen S, et al. Human posterior auditory cortex gates novel sounds to consciousness. Proc Natl Acad Sci U S A. 2004; 101:6809–14. doi: 10.1073/pnas.0303760101 PMID: 15096618

27. Opitz B, Schröger E, von Cramon DY. Sensory and cognitive mechanisms for preattentive change detection in auditory cortex. Eur J Neurosci. 2005; 21:531–5. doi: 10.1111/j.1460-9568.2005.03839.x PMID: 15673452

28. Jung F, Stephan KE, Backes H, Moran R, Gramer M, Kumagai T, et al. Mismatch responses in the awake rat: evidence from epidural recordings of auditory cortical fields. PLoS ONE. 2013; 8:e63203. doi: 10.1371/journal.pone.0063203 PMID: 23646197

29. Shiramatsu TI, Kanzaki R, Takahashi H. Cortical mapping of mismatch negativity with deviance detection property in rat. PLoS ONE. 2013; 8:e82663. doi: 10.1371/journal.pone.0082663 PMID: 24349330

30. Takahashi H, Nakao M, Kaga K. Interfield differences in intensity and frequency representation of evoked potentials in rat auditory cortex. Hear Res. 2005; 210:9–23. doi: 10.1016/j.heares.2005.05.014 PMID: 16213681

31. Smith PH, Uhlrich DJ, Manning KA, Banks MI. Thalamocortical projections to rat auditory cortex from the ventral and dorsal divisions of the medial geniculate nucleus. J Comp Neurol. 2012; 520:34–51. doi: 10.1002/cne.22682 PMID: 21618239

32. Profant O, Burianová J, Syka J. The response properties of neurons in different fields of the auditory cortex in the rat. Hear. Res. 2013; 296:51–9. doi: 10.1016/j.heares.2012.11.021 PMID: 23220149

33. Storace DA, Higgins NC, Chikar JA, Oliver DL, Read HL. Gene expression identifies distinct ascending glutamatergic pathways to frequency-organized auditory cortex in the rat brain. J Neurosci. 2012; 32:15759–68. doi: 10.1523/JNEUROSCI.1310-12.2012 PMID: 23136415

34. Kimura A, Donishi T, Okamoto K, Tamai Y. Efferent connections of "posterodorsal" auditory area in the rat cortex: implications for auditory spatial processing. Neuroscience. 2004; 128:399–419. doi: 10.1016/j.neuroscience.2004.07.010 PMID: 15350651

35. Kimura A, Donishi T, Okamoto K, Imbe H, Tamai Y. Efferent connections of the ventral auditory area in the rat cortex: implications for auditory processing related to emotion. Eur J Neurosci. 2007; 25:2819–34. doi: 10.1111/j.1460-9568.2007.05519.x PMID: 17459110

36. Higgins NC, Storace DA, Escabí MA, Read HL. Specialization of binaural responses in ventral auditory cortices. J Neurosci. 2010; 30:14522–32. doi: 10.1523/JNEUROSCI.2561-10.2010 PMID: 20980610

37. Harms L, Michie PT, Näätänen R. Criteria for determining whether mismatch responses exist in animal models: Focus on rodents. Biol Psychol. 2015; doi: 10.1016/j.biopsycho.2015.07.006

38. Klein C, von der Behrens W, Gaese BH. Stimulus-specific adaptation in field potentials and neuronal responses to frequency-modulated tones in the primary auditory cortex. Brain Topogr. 2014; 27:599–610. doi: 10.1007/s10548-014-0376-4 PMID: 24863565

39. Yarrow S, Razak KA, Seitz AR, Seriès P. Detecting and quantifying topography in neural maps. PLoS ONE. 2014; 9:e87178. doi: 10.1371/journal.pone.0087178 PMID: 24505279

40. Phillips DP, Irvine DR. Responses of single neurons in physiologically defined primary auditory cortex (A1) of the cat: frequency tuning and responses to intensity. J Neurophysiol. 1981; 45:48–58. PMID: 7205344

41. Recanzone GH, Schreiner CE, Sutter ML, Beitel RE, Merzenich MM. Functional organization of spectral receptive fields in the primary auditory cortex of the owl monkey. J Comp Neurol. 1999; 415:460–81. doi: 10.1002/(SICI)1096-9861(19991227)415:4<460::AID-CNE4>3.0.CO;2-F PMID: 10570456

42. Drew PJ, Abbott LF. Models and properties of power-law adaptation in neural systems. J Neurophysiol. 2006; 96:826–33. doi: 10.1152/jn.00134.2006 PMID: 16641386

43. Buzsáki G, Anastassiou CA, Koch C. The origin of extracellular fields and currents—EEG, ECoG, LFP and spikes. Nat Rev Neurosci. 2012; 13:407–20. doi: 10.1038/nrn3241 PMID: 22595786

44. von der Behrens W, Bäuerle P, Kössl M, Gaese BH. Correlating stimulus-specific adaptation of cortical neurons and local field potentials in the awake rat. J Neurosci. 2009; 29:13837–49. doi: 10.1523/JNEUROSCI.3475-09.2009 PMID: 19889995

45. Fishman YI, Steinschneider M. Searching for the mismatch negativity in primary auditory cortex of the awake monkey: deviance detection or stimulus specific adaptation? J Neurosci. 2012; 32:15747–58. doi: 10.1523/JNEUROSCI.2835-12.2012 PMID: 23136414

46. Farley BJ, Quirk MC, Doherty JJ, Christian EP. Stimulus-specific adaptation in auditory cortex is an NMDA-independent process distinct from the sensory novelty encoded by the mismatch negativity. J Neurosci. 2010; 30:16475–84. doi: 10.1523/JNEUROSCI.2793-10.2010 PMID: 21147987

47. Nir Y, Vyazovskiy VV, Cirelli C, Banks MI, Tononi G. Auditory responses and stimulus-specific adaptation in rat auditory cortex are preserved across NREM and REM sleep. Cereb Cortex. 2015; 25:1362–78. doi: 10.1093/cercor/bht328 PMID: 24323498

48. Hershenhoren I, Taaseh N, Antunes FM, Nelken I. Intracellular correlates of stimulus-specific adaptation. J Neurosci. 2014; 34:3303–19. doi: 10.1523/JNEUROSCI.2166-13.2014 PMID: 24573289

49. Chen I-W, Helmchen F, Lütcke H. Specific Early and Late Oddball-Evoked Responses in Excitatory and Inhibitory Neurons of Mouse Auditory Cortex. J Neurosci. 2015; 35:12560–73. doi: 10.1523/JNEUROSCI.2240-15.2015 PMID: 26354921

50. Natan RG, Briguglio JJ, Mwilambwe-Tshilobo L, Jones S, Aizenberg M, Goldberg EM, et al. Complementary control of sensory adaptation by two types of cortical interneurons. Elife. 2015; 4:e09868. doi: 10.7554/eLife.09868 PMID: 26460542

51. Wan H, Warburton EC, Kuśmierek P, Aggleton JP, Kowalska DM, Brown MW. Fos imaging reveals differential neuronal activation of areas of rat temporal cortex by novel and familiar sounds. Eur J Neurosci. 2001; 14:118–24. doi: 10.1046/j.0953-816x.2001.01625.x PMID: 11488955

52. King C, McGee T, Rubel EW, Nicol T, Kraus N. Acoustic features and acoustic changes are represented by different central pathways. Hear Res. 1995; 85:45–52. PMID: 7559178

53. Pincze Z, Lakatos P, Rajkai C, Ulbert I, Karmos G. Separation of mismatch negativity and the N1 wave in the auditory cortex of the cat: a topographic study. Clin Neurophysiol. 2001; 112:778–84. doi: 10.1016/S1388-2457(01)00509-0 PMID: 11336892

54. Maess B, Jacobsen T, Schröger E, Friederici AD. Localizing pre-attentive auditory memory-based comparison: magnetic mismatch negativity to pitch change. Neuroimage. 2007; 37:561–71. doi: 10.1016/j.neuroimage.2007.05.040 PMID: 17596966

55. Kraus N, McGee T, Littman T, Nicol T, King C. Nonprimary auditory thalamic representation of acoustic change. J Neurophysiol. 1994; 72:1270–7. PMID: 7807210

56. Ulanovsky N, Las L, Farkas D, Nelken I. Multiple time scales of adaptation in auditory cortex neurons. J Neurosci. 2004; 24:10440–53. doi: 10.1523/JNEUROSCI.1905-04.2004 PMID: 15548659

57. Musall S, Haiss F, Weber B, von der Behrens W. Deviant Processing in the Primary Somatosensory Cortex. Cereb Cortex. 2015; doi: 10.1093/cercor/bhv283

58. Metherate R, Cruikshank SJ. Thalamocortical inputs trigger a propagating envelope of gamma-band activity in auditory cortex in vitro. Exp Brain Res. 1999; 126:160–74. PMID: 10369139

59. Szymanski FD, Garcia-Lazaro JA, Schnupp JWH. Current source density profiles of stimulus-specific adaptation in rat auditory cortex. J Neurophysiol. 2009; 102:1483–90. doi: 10.1152/jn.00240.2009 PMID: 19571199

60. Malmierca MS, Sanchez-Vives MV, Escera C, Bendixen A. Neuronal adaptation, novelty detection and regularity encoding in audition. Front Syst Neurosci. 2014; 8:111. doi: 10.3389/fnsys.2014.00111 PMID: 25009474

61. Escera C, Malmierca MS. The auditory novelty system: an attempt to integrate human and animal research. Psychophysiology. 2014; 51:111–23. doi: 10.1111/psyp.12156 PMID: 24423134

62. Carrasco A, Kok MA, Lomber SG. Effects of core auditory cortex deactivation on neuronal response to simple and complex acoustic signals in the contralateral anterior auditory field. Cereb Cortex. 2015; 25:84–96. doi: 10.1093/cercor/bht205 PMID: 23960202

63. Atiani S, David SV, Elgueda D, Locastro M, Radtke-Schuller S, Shamma SA, et al. Emergent selectivity for task-relevant stimuli in higher-order auditory cortex. Neuron. 2014; 82:486–99. doi: 10.1016/j.neuron.2014.02.029 PMID: 24742467

64. Costa-Faidella J, Baldeweg T, Grimm S, Escera C. Interactions between "what" and "when" in the auditory system: temporal predictability enhances repetition suppression. J Neurosci. 2011; 31:18590–7. doi: 10.1523/JNEUROSCI.2599-11.2011 PMID: 22171057

65. Haenschel C, Vernon DJ, Dwivedi P, Gruzelier JH, Baldeweg T. Event-related brain potential correlates of human auditory sensory memory-trace formation. J Neurosci. 2005; 25:10494–501. doi: 10.1523/JNEUROSCI.1227-05.2005 PMID: 16280587

66. Garrido MI, Kilner JM, Kiebel SJ, Stephan KE, Baldeweg T, Friston KJ. Repetition suppression and plasticity in the human brain. Neuroimage. 2009; 48:269–79. doi: 10.1016/j.neuroimage.2009.06.034 PMID: 19540921

67. Alho K. Cerebral generators of mismatch negativity (MMN) and its magnetic counterpart (MMNm) elicited by sound changes. Ear Hear. 1995; 16:38–51. PMID: 7774768

68. Alho K, Winkler I, Escera C, Huotilainen M, Virtanen J, Jääskeläinen IP, et al. Processing of novel sounds and frequency changes in the human auditory cortex: magnetoencephalographic recordings. Psychophysiology. 1998; 35:211–24. PMID: 9529947

69. Ruusuvirta T, Penttonen M, Korhonen T. Auditory cortical event-related potentials to pitch deviances in rats. Neurosci Lett. 1998; 248:45–8. doi: 10.1016/S0304-3940(98)00330-9 PMID: 9665660

70. Tikhonravov D, Neuvonen T, Pertovaara A, Savioja K, Ruusuvirta T, Näätänen R, et al. Dose-related effects of memantine on a mismatch negativity-like response in anesthetized rats. Neuroscience. 2010; 167:1175–82. doi: 10.1016/j.neuroscience.2010.03.014 PMID: 20298759

71. Astikainen P, Stefanics G, Nokia M, Lipponen A, Cong F, Penttonen M, et al. Memory-based mismatch response to frequency changes in rats. PLoS ONE. 2011; 6:e24208. doi: 10.1371/journal.pone.0024208 PMID: 21915297

72. Nakamura T, Michie PT, Fulham WR, Todd J, Budd TW, Schall U, et al. Epidural Auditory Event-Related Potentials in the Rat to Frequency and duration Deviants: Evidence of Mismatch Negativity? Front Psychol. 2011; 2:367. doi: 10.3389/fpsyg.2011.00367 PMID: 22180747

73. Harms L, Fulham WR, Todd J, Budd TW, Hunter M, Meehan C, et al. Mismatch negativity (MMN) in freely-moving rats with several experimental controls. PLoS ONE. 2014; 9:e110892. doi: 10.1371/journal.pone.0110892 PMID: 25333698

74. Costa-Faidella J, Grimm S, Slabu L, Díaz-Santaella F, Escera C. Multiple time scales of adaptation in the auditory system as revealed by human evoked potentials. Psychophysiology. 2011; 48:774–83. doi: 10.1111/j.1469-8986.2010.01144.x PMID: 20946129

75. Pratt H, Starr A, Michalewski HJ, Dimitrijevic A, Bleich N, Mittelman N. Auditory-evoked potentials to frequency increase and decrease of high- and low-frequency tones. Clin Neurophysiol. 2009; 120:360–73. doi: 10.1016/j.clinph.2008.10.158 PMID: 19070543

76. Peter V, McArthur G, Thompson WF. Effect of deviance direction and calculation method on duration and frequency mismatch negativity (MMN). Neurosci Lett. 2010; 482:71–5. doi: 10.1016/j.neulet.2010.07.010 PMID: 20630487

77. Zurita P, Villa AE, de Ribaupierre Y, de Ribaupierre F, Rouiller EM. Changes of single unit activity in the cat's auditory thalamus and cortex associated to different anesthetic conditions. Neurosci Res. 1994; 19:303–16. PMID: 8058206

78. Gaese BH, Ostwald J. Anesthesia changes frequency tuning of neurons in the rat primary auditory cortex. J Neurophysiol. 2001; 86:1062–6. PMID: 11495976

79. Noda T, Takahashi H. Anesthetic effects of isoflurane on the tonotopic map and neuronal population activity in the rat auditory cortex. Eur J Neurosci. 2015; 42:2298–311. doi: 10.1111/ejn.13007 PMID: 26118739

80. Hara K, Harris RA. The anesthetic mechanism of urethane: the effects on neurotransmitter-gated ion channels. Anesth Analg. 2002; 94:313–8. PMID: 11812690

81. Capsius B, Leppelsack HJ. Influence of urethane anesthesia on neural processing in the auditory cortex analogue of a songbird. Hear Res. 1996; 96:59–70. PMID: 8817307

82. Duque D, Malmierca MS. Stimulus-specific adaptation in the inferior colliculus of the mouse: anesthesia and spontaneous activity effects. Brain Struct Funct. 2015; 220:3385–98. doi: 10.1007/s00429-014-0862-1 PMID: 25115620

83. Carrasco A, Lomber SG. Reciprocal modulatory influences between tonotopic and nontonotopic cortical fields in the cat. J Neurosci. 2010; 30:1476–87. doi: 10.1523/JNEUROSCI.5708-09.2009 PMID: 20107075

84. Javitt DC, Steinschneider M, Schroeder CE, Vaughan HG, Arezzo JC. Detection of stimulus deviance within primate primary auditory cortex: intracortical mechanisms of mismatch negativity (MMN) generation. Brain Res. 1994; 667:192–200. PMID: 7697356

85. Molholm S, Martinez A, Ritter W, Javitt DC, Foxe JJ. The neural circuitry of pre-attentive auditory change-detection: an fMRI study of pitch and duration mismatch negativity generators. Cereb Cortex. 2005; 15:545–51. doi: 10.1093/cercor/bhh155 PMID: 15342438

86. Nelken I, Ulanovsky N. Mismatch negativity and stimulus-specific adaptation in animal models. J Psychophysiol. 2007; 21:214–23. doi: 10.1027/0269-8803.21.34.214

87. Näätänen R. The mismatch negativity: a powerful tool for cognitive neuroscience. Ear Hear. 1995; 16:6–18. PMID: 7774770

88. Näätänen R, Paavilainen P, Rinne T, Alho K. The mismatch negativity (MMN) in basic research of central auditory processing: a review. Clin Neurophysiol. 2007; 118:2544–90. doi: 10.1016/j.clinph.2007.04.026 PMID: 17931964

89. Merrill EG, Ainsworth A. Glass-coated platinum-plated tungsten microelectrodes. Med Biol Eng. 1972; 10:662–72. PMID: 5076431

90. Bullock DC, Palmer AR, Rees A. Compact and easy-to-use tungsten-in-glass microelectrode manufacturing workstation. Med Biol Eng Comput. 1988; 26:669–72. PMID: 3256764

Title

Hierarchical Prediction Error in Neuronal Responses along the Auditory Neuraxis

Authors

Javier Nieto-Diego[1,3], Guillermo V Carbajal[1,3], Gloria G Parras[1,3], Carles Escera[4,5] & Manuel S Malmierca[1,2,3]*

Affiliations

[1] Auditory Neuroscience Laboratory, Institute of Neuroscience of Castilla y León (INCYL), Salamanca, Spain.

[2] Department of Cell Biology and Pathology, Faculty of Medicine, University of Salamanca, Salamanca, Spain.

[3] The Salamanca Institute for Biomedical Research (IBSAL), Salamanca, Spain.

[4] Brainlab-Cognitive Neuroscience Research Group, Department of Clinical Psychology and Psychobiology, University of Barcelona, Barcelona, Catalonia-Spain.

[5] Institute of Neurosciences, University of Barcelona, Barcelona, Catalonia-Spain.

Contact Information

* msm@usal.es

Abstract

Current theories of brain function depict perception as a reciprocal interchange of predictions and prediction error signals between hierarchically organized processing stations. A growing family of large-scale brain responses to perceptual mismatches supports this postulate. However, the predictive activity of the brain and its hierarchical organization remains to be demonstrated at the neuronal level. We recorded single-neuron activity during oddball stimulation, and used novel control sequences to separate prediction error from adaptation effects. Our results reveal a hierarchical organization of prediction error along the central auditory system, present already at subcortical levels and gradually increasing towards the higher-order auditory cortex. We demonstrate that the predictive activity of sensory systems is detectable at the neuronal level and highlight the role of subcortical structures in perception.

Main Text

Unexpected events are likely to convey relevant information, and their prompt detection is fundamental for survival [1,2]. Brain responses to the perceptual mismatch between expected and actual sensory inputs have been extensively recorded in all sensory systems including auditory [3], visual [4], somatosensory [5] and olfactory [6] modalities, and are thought to underlie the brain's ability to resolve auditory objects [7], proving themselves a key to understanding perceptual processing [4,8,9]. Auditory mismatch responses are typically obtained with non-invasive brain recordings using *oddball* sequences [9], in which a repetitive (standard) tone is randomly replaced by a different (deviant) tone with a low probability. Over the past 40 years, a particular mismatch response recorded from the human scalp with electroencephalography, the so-called mismatch negativity (MMN) [10], has become a valuable

tool in cognitive and clinical neuroscience [11], especially as a reliable biomarker of schizophrenia and other brain disorders [12].

At the theoretical level, large-scale mismatch responses provide empirical support to the hierarchical predictive coding framework—a neurobiologically informed and unifying account of general brain function [13–15]—, seamlessly fitting it as the sum of thousands of neuronal prediction error signals [4,16–18]. According to this theory, the classical notion that brain activity evoked by a sensory event is a neuronal representation of the occurrence of that particular event, is only half of the story. This may be true for the first/lower processing stations of sensory systems. However, at the same time, higher stations are constantly trying to anticipate the future, and send descending signals to actively suppress this evoked, ascending neuronal activity. Therefore, as the sensory signal propagates up the hierarchy of sensory systems, neuronal responses progressively switch from representing the stimulus itself to represent sensory prediction error to that stimulus. This is why neuronal responses to standard tones show repetition suppression, or response attenuation with stimulus repetition [19,20], that propagates back from higher to lower stations [21], whereas deviant tones produce a large prediction error signal, which is relayed bottom-up, facilitating the task of automatic deviance detection [22,23].

However, at the cellular level, mismatch responses could also arise from a simpler neurophysiological mechanism [24,25], namely, stimulus-specific adaptation (SSA) [26], or response decrement with stimulus repetition [2] that leaves neuronal responses to different stimuli—e.g. the deviant—almost unaffected. SSA is a widespread property of auditory neurons, increasing from midbrain [27] through the thalamus [28] to primary [29,30] and higher-order [30] auditory cortex, and assumed to be due to synaptic depression [3,29,31]. Therefore, single neuron responses along the auditory pathway show a differential response to standard and deviant tones under oddball stimulation, just as MMN but at the cellular level [3,26]. Yet,

whereas it is now clear that large-scale mismatch responses indeed reflect the predictive activity of the auditory and other sensory systems [4,17], even at early processing stages [18] including subcortical midbrain and thalamus [3], and also in animal models [32–34], this predictive activity remains to be demonstrated at the neuronal level.

In this study, we recorded individual responses of subcortical and cortical neurons along the rat auditory pathway, using recently developed control sequences to separate repetition suppression from prediction error under oddball stimulation [29,35–37]. Our data show that differential responses to deviant and standard tones in oddball sequences indeed reflect active predictive activity, instead of a mere SSA in single neurons, and that this predictive activity emerges hierarchically from subcortical structures. These results unify three coexisting views of perceptual deviance detection at different levels of description: neuronal physiology, cognitive neuroscience and the theoretical predictive coding framework.

Results

Evidence of prediction error in single auditory neurons

The predictive coding framework assumes that the same operations (generation of predictions and prediction errors) would take place at every hierarchical level of sensory systems [13], and this could in principle include subcortical processing stations [19]. Unfortunately, there is a severe dearth of evidence for this, since research on predictive brain activity has until recently focused on cortical responses of varying source and latency [17,18], and the role of subcortical structures in cognition, albeit increasingly acknowledged [38,39], remains largely unexplored. In order to collect a representative sample from different processing stations along the auditory pathway, we recorded a total of 207 neurons (Table 1) from the auditory midbrain (IC), thalamus (MGB) and cortex (AC) of anesthetized rats, while stimulating the animal with sequences of pure tones (Fig. 1). Recorded neurons were further

grouped into "first-order" (*fo*) or "higher-order" (*ho*), depending on their particular location within each nuclei [3,30], thus leading to 6 different processing stations (*fo*-IC, *ho*-IC, *fo*-MGB, *ho*-MGB, *fo*-AC, *ho*-AC; Fig. 1B; see Methods). This distinction was made because higher-order (or non-primary) auditory regions represent a higher hierarchical level of processing [40] and are known to be more sensitive to acoustic change and contextual influences than first-order (or primary) ones [3,30,41].

For each recorded neuron, we presented a set of oddball sequences, using tones selected from the neuron's frequency-response area (FRA), and a "neuronal mismatch response" (nMM) was computed as the difference between responses to deviant (DEV) and standard (STD) conditions for each tone (Fig. 1D). To determine whether this difference (usually DEV > STD) reflected predictive activity, instead of (or in addition to) just SSA, we also presented two cascaded (CAS) sequences (ascending and descending) and one many-standards (MAS) sequence as controls [36,37] (Fig. 1C), containing all tones used in oddball sequences (see Methods). The main rationale behind this design is that, in the CAS/MAS control conditions, each tone has the same (low, 10%) probability of occurrence as a DEV tone in the oddball sequence, so it is not repetitive (as the STD), and therefore is free of repetition effects (e.g. repetition suppression), but it does not stand out from the statistical context (as the DEV), and therefore it is not perceived as a deviant [36,37]. Thus, responses to CAS/MAS control conditions are used as the reference yardstick with respect to which repetition suppression and prediction error effects can be discriminated (Fig. 1D). If the neuronal mismatch response (nMM = DEV – STD) is caused entirely by SSA to the STD tone, responses to DEV and CAS/MAS control conditions should remain comparable through all hierarchical levels, or if anything, the response to DEV tones should undergo a slightly stronger suppression than to the controls, due to cross-frequency adaptation [29] (Fig. 1E). By contrast, under the predictive coding framework, deviance detection is based on Bayesian

117 inference [15], such that stronger prediction errors will be produced as more sensory evidence
118 accumulates to increase the confidence and precision of current predictions [4,19,22]. Therefore,
119 stronger prediction errors should be elicited by DEV than by CAS/MAS tones, due to the
120 lack of sequential stimulus repetitions in the controls [4,36], and this effect should increase up
121 the hierarchy (Fig. 1E), since higher-order processing stations are able to code for more
122 complex regularities [3,18,23,42].

123 Individual responses of representative neurons are shown in Fig. 2. Responses of first-
124 order neurons are mostly dependent on tone frequency, with little sensitivity to the different
125 conditions, particularly at subcortical levels (Fig. 2A,B). However, in *fo*-AC (Fig. 2C), and
126 most clearly in higher-order neurons (Fig. 2E-F), strong response suppression to STD
127 condition is apparent, but also, a higher firing rate in response to DEV tones, as compared to
128 both MAS and CAS control conditions, was consistent across tested frequencies. This is, as
129 just explained, the signature of prediction error at the single neuron level [29,32].

130 In the following, we will present only the results using the cascaded sequence as
131 control, since it was designed as an improvement to the many-standards sequence that
132 controls for additional factors beyond presentation rate of the deviant tone [36,37] (see Materials
133 and Methods, *Experimental Design*). However, the results using either CAS/MAS condition
134 as a control were commensurable (Table 1), with no remarkable differences between them
135 (Wilcoxon signed-rank test, $z = -0.125$, $p = 0.9$).

136 *The contribution of prediction error to nMM increases along the auditory hierarchy*

137 Single neuron responses to the three conditions (DEV, STD, CAS) for all tones tested
138 in all neurons are represented in Fig. 3A-F, separately for each processing station. Each pair
139 of conditions, within each station, was tested for a difference in medians (Table 1). As
140 expected, responses to DEV condition were stronger than to STD condition within all stations

(Fig. 3A-F; Table 1). This is a well described neuronal behavior across the auditory pathway [3], which has been referred to as SSA in previous studies [26], even though it was postulated to be the neuronal mechanism underlying deviance detection [29]. Indeed, this nMM results mostly from suppression of the response to the repetitive STD condition (repetition suppression), since responses to STD were significantly weaker than to CAS condition within all stations (Table 1). Critically, responses to DEV tones were significantly higher than to CAS already within the *ho*-IC (Fig. 3D; Table 1), and this difference increased progressively in the *ho*-MGB, and *ho*-AC (Fig. 3E,F), where it was most apparent. Therefore, neuronal responses showed clear signs of prediction error at the population level, within all higher-order stations, but also within *fo*-AC (Fig. 3C; Table 1), consistent with the observed effects in individual cases (Fig. 2C-F).

To quantify the relative contribution of repetition suppression and prediction error to nMM in neuronal responses, and to facilitate comparisons between different neurons/stations, we normalized the neural responses to the three conditions (DEV, STD, CAS) for each neuron/tone combination. We applied Euclidean vector normalization (Fig. 3G), such that all normalized responses (DEV_N, STD_N, CAS_N) ranged between 0 and 1. Then, we computed three indices as the difference between normalized responses to pairs of conditions, ranging between −1 and +1 (Fig. 3G). The "index of neuronal mismatch", **iMM** = $DEV_N - STD_N$, is the relative difference in responses to STD and DEV tones in the oddball paradigm. The iMM is quantitatively equivalent to the typical "SSA index" [26], used in previous studies (Fig. S1). The "index of neuronal repetition suppression", **iRS** = $CAS_N - STD_N$, is the relative reduction of the response to a standard tone, as compared to the control. Thus, the iRS quantifies repetition effects [20]. Finally, and most importantly for this study, the "index of neuronal prediction error", **iPE** = $DEV_N - CAS_N$, is the relative increase in the response to a deviant tone, compared to the control. A positive iPE reflects predictive activity, as opposed

166 to SSA [36], and quantifies the proportion of prediction error accounting for nMM [29].
167 Therefore, the relation **iMM = iRS + iPE** provides a functional, quantitative decomposition
168 of nMM (Fig. 1D). The distribution of these indices across stations reveals that both iMM
169 and iPE increase along the auditory pathway, from *fo*-IC to *ho*-AC (Fig. 3G-L).

170 Summary statistics for these normalized responses and indices are shown in Fig. 4A
171 and 4B, respectively. The iPE shows a distinct increase in two ways: (1) from first- to higher-
172 order stations, and (2) from IC to MGB to AC (Fig. 4B). To validate these observations
173 statistically, we fitted a linear model for the iPE using *nucleus* (IC, MGB, AC) and *hierarchy*
174 (*fo*, *ho*) as categorical factors. The resulting model was:

175 **iPE** = 0.012 + 0.020****ho*** – 0.136***MGB** + 0.092***AC** + 0.185****ho******MGB** +
176 0.158****ho******AC**,

177 with a significant effect of *hierarchy* ($F=37.16$, $p=1.40\cdot10^{-9}$) and *nucleus* ($F=46.35$,
178 $p=3.15\cdot10^{-20}$), and a significant *hierarchy*nucleus* interaction ($F=3.48$, $p=0.031$). Therefore,
179 both trends are significant and robust from midbrain to cortex. In particular, the significant
180 *hierarchy* effect means that the small average iPE seen in *ho*-IC (iPE = 0.012 + 0.020 =
181 **0.032**) is nevertheless statistically significant (Fig. 4B), consistent with a significant
182 difference in absolute spike counts (DEV−CAS in Table 1; Fig. 3J). Overall, this analysis
183 demonstrates a gradual emergence of a prediction error component in responses of single
184 neurons as information progresses through the auditory pathway, both in bottom-up and in
185 first- to higher-order directions, with a mutual potentiation of these two effects.

186 According to previous modeling work, change-sensitivity in single neurons is
187 expected to be maximal for stimulus ranges where the firing rate of the neuron is below
188 saturation [43]. Consistent with this hypothesis, a common observation in the pool of recorded
189 neurons was that using low stimulation intensities it was easier to produce deviance-specific

responses, particularly for ascending deviants (e.g. Fig. 2D). To test these observations at the population level, we fitted a different model for the iPE, using *SPL* (in Bels = dB SPL/10) and *direction* (ascending, ASC, or descending, DSC) of deviant tones (see Fig. 1C) as predictors. The model showed a significant effect of *SPL* (F=4.59, p=0.03) and a *SPL*direction* interaction (F=6.66, p=0.01):

$$\mathbf{iPE} = 0.064 + 0.194*\mathbf{ASC} + 0.003*\mathbf{SPL} - 0.037*\mathbf{ASC}*\mathbf{SPL},$$

which indicates that the iPE is expected to be much higher for ascending deviants at intensities below 40 dB SPL (Fig. 4C). Indeed, we observed a distinct increase in the iPE within all stations, under these stimulation conditions (Fig. 4D), particularly in *ho*-AC, where prediction error accounted for around two thirds of the iMM. This effect could facilitate perception under challenging sensory conditions, by increasing the gain of prediction error responses at early processing stages [19]. These findings run parallel to previous observations in single neurons of the primary visual cortex, where cortical feedback improves figure-background discrimination of low-salience stimuli [44].

Prediction error in single neurons correlates with a large-scale mismatch response in the auditory cortex

We also recorded local field potentials (LFP), simultaneously to single neuron spikes, from the same electrode, to explore the direct correlation between prediction error in spike responses and large-scale mismatch responses (such as the MMN). We averaged LFP responses for each condition and station, as well as the difference between DEV and CAS conditions, which we called the "prediction error potential" [33,37]: $PEP = LFP_{DEV} - LFP_{CAS}$ (Fig. 5). A significant early PEP was already detectable within *ho*-IC and *ho*-MGB (Fig. 5D,E). In the auditory cortex, the PEP was strong and significant in both *fo*-AC and *ho*-AC, showing three major deflections (Fig. 5C,F): a fast negative deflection (N1; 35−50 ms after

change onset), a slower positive deflection (P2; 70−120 ms), and a third, late, negative deflection (N2; beyond 150 ms). Importantly, epidural MMN peaks between 60 and 120 ms in rats [32], the same range of the P2 recorded here for the PEP, and can be positive when recorded from inside the brain [45]. Then, the iPE was re-computed for 12 different time windows (20 ms width, from –50 to 190 ms respect to stimulus onset), for each neuron/tone combination separately, and averaged within each station (Fig. 5). The iPE showed a clear modulation over time in both *fo*-AC and *ho*-AC stations (Friedman test, not corrected for 6 independent tests). Each individual iPE value was also tested against zero, and this analysis revealed a significant iPE within *fo*-AC between 60−100 ms after change onset, and in *ho*-AC between 40−200 ms, and seemingly beyond (Fig. 5C,F). In summary, the highest iPE values, reflecting prediction error in single neuron responses, correlate in time and location (*ho*-AC) with a large-scale mismatch wave (the PEP), putatilvely corresponding to the MMN in the rat [32,33].

Discussion

This study provides evidence, hitherto unavailable, that the hierarchical predictive activity of perceptual systems is detectable at the cellular level, even subcortically. Specifically, oddball responses of individual neurons, from midbrain to cortex, reflect predictive processing and underlie large-scale electrophysiological indicators of deviance detection. After quantitatively decomposing neuronal mismatch responses (nMM; Fig. 1D) into repetition suppression (iRS) and prediction error (iPE), the data show a systematic increase in the proportion of prediction error accounting for nMM as the sensory signal propagates up the auditory hierarchy (Fig. 4B,D). The highest iPE values are reached within the higher-order auditory cortex, where they correlate with a simultaneously recorded, large-scale prediction error potential (Fig. 5F), and extend into late evoked potentials, suggesting

238 an influence from higher-association or prefrontal cortices [46]. These results are in total
239 agreement with the predictive coding account of mismatch responses, while at the same time
240 highlight the role of subcortical structures in perception [39], providing a novel extension of the
241 mostly corticocentric predictive coding literature [14,15,38].

242 Previous attempts to show predictive activity in auditory neurons were inconclusive
243 [29,45,47], and were limited to multi-unit activity recordings in primary auditory cortex (but see
244 [48,49] for compelling evidence in single visual neurons). However, a recent study in mouse A1
245 [50] and another in rat barrel cortex [51] showed deviance detection in late responses of single
246 units, using the MAS control sequence. Although the CAS sequence is arguably a better
247 control for repetition effects than the MAS sequence [36], only one animal study has previously
248 applied it, using epidural recordings, and yielding also inconclusive results [37]. Our results,
249 using single-unit recordings, were comparable or even more robust for the CAS than for the
250 MAS control (Table 1), in agreement with human studies [36]. Our finding that the contribution
251 of prediction error to nMM supersedes that of repetition suppression within the higher-order
252 auditory cortex (Fig. 4B,D), is consistent with studies of brain sources of MMN in animals
253 [33,41] and humans [42,46] using similar controls for repetition effects. This hierarchical
254 transformation of nMM, dominated by repetition suppression at lower hierarchical levels of
255 the auditory system, with a gradual emergence of prediction error at higher levels (Fig.
256 4B,D), confirms that lower levels are mostly sensitive to global stimulus probability, while
257 higher-order levels are more sensitive to local relationships between sounds (transitional
258 probabilities), exactly as observed in human MMN studies [52,53]. Thus, our data are consistent
259 with passive SSA (Fig. 1e) underlying oddball responses in first-order midbrain and thalamus
260 [29] (Fig. 4B). By contrast, they support a generative mechanism of Bayesian inference being at
261 play in auditory cortex and higher-order subcortical stations of perceptual processing [4]. The
262 contrast between first- and higher-order nMM is particularly clear within the auditory

thalamus (compare Fig. 1E and 4B). Thus, higher-order midbrain and thalamus behave like the auditory cortex with regard to prediction error, which is the novel extension of the predictive coding scholarship. Finally, asymmetries in the direction of frequency-change detection (ascending vs. descending) have also been found in both animal [37] and human [54] MMN studies.

In conclusion, our results demonstrate that prediction error is an intrinsic component of responses of single auditory neurons, emerging even from subcortical levels, and strengthen the case for the predictive coding theory of perceptual processing. In addition, we show that neuronal predictive activity underlies the generation of large-scale mismatch responses in animal models, and parallels important properties of human MMN. These are promising results for translational research into the cellular mechanisms that are disrupted in schizophrenia and other brain disorders characterized by reductions in large-scale mismatch responses, such as MMN.

Methods

Experimental Design

The goal of the present experiments was to test responses of single neurons of the central auditory system of the rat for signs of predictive activity under oddball stimulation. We recorded extracellular single neuron activity in response to sinusoidal tones in different auditory centers of the rat brain (Fig. 1a,b). Rats were deeply anesthetized prior to surgery preparation and during the whole recording session. One single neuron was recorded at a time, using one tungsten electrode inserted into the brain, and local field potential (LFP) activity was simultaneously recorded from the same electrode. Surgical, electrophysiological and histological procedures are detailed below.

An important part of our experimental design was to record a substantial sample of neurons from the major anatomical regions representing the hierarchical organization of the central auditory system, both at cortical and subcortical levels. The inferior colliculus (IC) of the midbrain is the main convergence hub of the subcortical auditory system [3,55]. The medial geniculate body (MGB) is the auditory section of the thalamus, and relies all ascending inputs to the auditory cortex (AC), considered the highest hierarchical level of the auditory system. All these auditory processing stations contain first- and higher-order divisions [56]. First-order divisions receive their main ascending input from the brainstem (central nucleus of the IC), or from first-order division of the preceding nucleus (ventral division of the MGB and cortical fields A1, VAF and AAF), and comprise the so-called "lemniscal" auditory pathway, where the auditory information is initially processed. Higher-order divisions are integration centers for more elaborate processing of abstract properties of the stimulation, and receive their main inputs from heterogeneous sources. The cortical regions of the IC are considered higher-order, as well as the dorsal and medial divisions of the MGB. Finally, the cortical fields SRAF and PAF receive their main ascending input from the higher-order MGB, and thus represent the highest level of the auditory hierarchy in the rat [30,57].

All stimuli presented were sinusoidal pure tones of 75 ms duration, including 5 ms raise/fall ramps. For each recorded neuron, the frequency-response area (FRA) was first computed, as the map of response magnitude for each frequency/intensity combination (Fig. 2). To obtain this FRA, a randomized sequence of tones was presented at a 4 Hz rate, randomly varying frequency and intensity of the presented tones (3-5 repetitions of all tones). Then, we selected 10 evenly-spaced tones (0.5 octave separation) at a fixed sound intensity (usually 20-30 dB above minimal response threshold), so that at least two of them fell within the FRA or close to its limits (see Fig. 1c and Fig. 2). These 10 frequencies were used to create the control sequences shown in Fig. 1c. Additionally, adjacent pairs of them were used to

311 present different oddball sequences. All sequences were 400 tones in length, at the same,
312 constant presentation rate of 3 Hz (for AC) or 4 Hz (for IC and MGB). A faster presentation
313 rate was used for subcortical recordings, to compensate for the relative slowing down of pre-
314 ferred repetition rates from brainstem to cortex [58].

315 To test the specific contribution of deviance to the neuronal responses, we used oddball
316 sequences [9,26] (Fig. 1c). An oddball sequence consisted of a repetitive tone (the standard),
317 occasionally replaced by a different tone (the deviant), with a p=0.1 probability, in a pseu-
318 dorandom fashion. The first 10 tones of the sequence were always the standard tone, and a
319 minimum of 3 standard tones always preceded each deviant. Oddball sequences were either
320 ascending or descending, depending on whether the deviant was of a higher or lower fre-
321 quency than the standard, respectively (Fig. 1c). To control for the overall presentation rate of
322 the target tone, as it reduces neuronal responses at high rates, we used two different control
323 sequences, namely, the many-standards and cascaded sequences [29,36] (Fig. 1c). The many-
324 standards control sequence was a random presentation of the 10 selected tones, such that each
325 of them appeared the same number of times in an unpredictable order, with the only con-
326 straint that a single tone was never repeated in a row. Two cascaded control sequences, as-
327 cending and descending, were built as a repetitive series of groups of the 10 tones, arranged
328 by ascending/descending frequency, respectively (Fig. 1c). Since all sequences were 400
329 stimuli long, at the same presentation rate, a tone appeared with the same overall presentation
330 rate in the DEV, MAS and CAS conditions, a total of 40 times along the 400-stimuli se-
331 quence. The cascaded sequence was recently designed as an improvement to the many-
332 standards, that controls for additional key factors beyond presentation rate of the deviant tone
333 [36,37]. First, the tone immediately preceding a deviant is the same in the oddball (a standard)
334 and cascaded sequences. This improves the estimation of the overall adaptation state of the
335 system by the time the deviant tone is played, and controls for the potential sensitivity of the

neuron to a rise or fall in frequency between two successive tones. Second, the cascaded sequence mimics the regular structure of the oddball sequence, with the important difference that now the target tone *conforms* to the rule, instead of being a deviant.

Thus, using this design, every tone presented as a deviant was also presented as a standard (in a different oddball sequence) and in the context of the many-standards and cascaded control sequences. These four conditions, and by extension also response measures to them, will be denoted DEV, STD, MAS and CAS, respectively. Note that there were two variants of the DEV condition (ascending/descending), which were compared with the corresponding ascending/descending CAS condition. The STD condition was averaged, for each frequency, across ascending/descending versions of the oddball sequence (as indicated in Fig. 1c). The order of presentation of these sequences was randomized across neurons, with a silent pause of ~30 seconds between sequences. If the neuron could be held for long enough, the same protocol was repeated at different sound intensities.

Surgical procedures

Experiments were performed on 36 adult, female Long-Evans rats with body weights between 200–250 g. The experimental protocols were approved by, and used methods conforming to the standards of, the University of Salamanca Animal Care Committee and the European Union (Directive 2010/63/EU) for the use of animals in neuroscience research. Each individual animal was used to record from only one auditory station, either IC, MGB or AC. The initial surgical procedures were identical in each case, and the electrophysiological procedures differed only in the location of the craniotomy, and placement/orientation of the recording electrode, for each different station.

Surgical anesthesia was induced and maintained with urethane (1.5 g/kg, i.p.), with supplementary doses (0.5 g/kg, i.p.) given as needed. Dexamethasone (0.25 mg/kg) and atropine

sulfate (0.1 mg/kg) were administered at the beginning of the surgery and every 10 h thereafter to reduce brain edema and the viscosity of bronchial secretions, respectively. After the animal reached a surgical plane of anesthesia, the trachea was cannulated for artificial ventilation and a cisternal drain was introduced to prevent brain hernia. The animal was then placed in a stereotaxic frame in which the ear bars were replaced by hollow specula that accommodated a sound delivery system. Corneal and hind-paw withdrawal reflexes were monitored to ensure that a moderately deep anesthetic plane was maintained as uniformly as possible throughout the recording procedure. Isotonic glucosaline solution was administered periodically (5–10 ml every 6–8 hours, s.c.) throughout the experiment to prevent dehydration. Body temperature was monitored with a rectal probe and maintained between 37–38°C with a homoeothermic blanket system (Cibertec).

For IC and MGB recordings, a craniotomy was performed in the left parietal bone to expose the cerebral cortex overlying the left IC/MGB. The dura was removed, and the electrode was advanced with an angle of 20º for the IC, and in a vertical direction for the MGB. For AC recordings, the skin and temporal muscles over the left side of the skull were reflected and a 6×5 mm craniotomy was made in the left temporal bone to expose the entire auditory cortex (see Figure 1 in ref. [30]). The dura was removed and the exposed cortex and surrounding area were covered with a transparent layer of agar to prevent desiccation and to stabilize the recordings. The electrode was positioned orthogonal to the pial surface, forming a 30º angle with the horizontal plane, to penetrate through all the cortical layers of one same cortical column.

Electrophysiological recording procedures

Experiments were performed inside a sound-insulated and electrically-shielded chamber. All sounds were generated using an RX6 Multifunction Processor (TDT) and delivered mon-

aurally (to the right ear) in a closed system through a Beyer DT-770 earphone (0.1–45 kHz) fitted with a custom-made cone and coupled to a small tube (12 gauge hypodermic) sealed in the ear. The sound system response was flattened with a finite impulse response (FIR) filter, and the output of the system was calibrated in situ using a ¼-inch condenser microphone (model 4136, Brüel & Kjær), a conditioning amplifier (Nexus, Brüel & Kjær) and a dynamic signal analyzer (Photon+, Brüel & Kjær). The output of the system had a flat spectrum at 76 dB SPL (±3 dB) between 500 Hz and 45 kHz, and the second and third harmonic components in the signal were ≤ 40 dB below the level of the fundamental at the highest output level (90 dB SPL). Prior to surgery and recording sessions, we recorded auditory brainstem responses (ABR) with subcutaneous electrodes to ensure the animal had normal hearing. ABRs were collected using TDT software (BioSig) and hardware (RX6 Multifunction Processor) following standard procedures (0.1 ms clicks presented at a 21/s rate, delivered in 10 dB ascending steps from 10 to 90 dB SPL).

Action potentials and local field potentials (LFP) were recorded with hand-manufactured, glass-coated tungsten electrodes [59] (1–4 MΩ impedance at 1 kHz). One individual electrode was used to record one single neuron at a time. The electrode was advanced using a piezoelectric micromanipulator (Sensapex) until we observed a strong spiking activity synchronized with the train of searching stimuli. The signal was amplified (1000×) and band-pass filtered (1 Hz to 3 kHz) with an alternate current differential amplifier (DAM-80, WPI). This analog signal was digitized at a 12K sampling rate and further band-pass filtered (with a second TDT-RX6 module) separately for action potentials (between 500 Hz and 3 kHz) and LFP (between 3 and 50 Hz). Stimulus generation and neuronal response processing and visualization were controlled online with custom software created with the OpenEx suite (TDT) and Matlab (Mathworks). A unilateral threshold for automatic action potential detection was manually set at about 2–3 standard deviations of the background noise. Spike waveforms

were displayed on the screen, and overlapped on each other in a pile-plot to facilitate isolation of single units. Only when all snippet waveforms were identical and clearly separable form other smaller units and the background noise, the recorded action potentials were considered to belong to a single unit.

Sounds used for stimulation were white noise bursts or pure tones with 5 ms rise-fall ramps. Sounds used for searching for neuronal activity were trains of noise bursts or pure tones (1–8 stimulus per second). We used short stimulus duration for searching (30 ms) to prevent strong adaptation. In addition, type (white noise, narrowband noise, pure tone) and parameters (frequency, intensity, presentation rate) of the search stimuli were varied manually when necessary to facilitate release from adaptation, and thus prevent overlooking responses with high SSA. Once a single neuron was isolated and confirmed to be stable, the whole stimulation protocol was applied, as described in the first section "Experimental Design".

Histological procedures and anatomical localization of recording sites

AC experiments. At the end of the surgery, a magnified picture (25×) of the exposed cortex was taken [30] with a digital SLR camera (D5100, Nikon) coupled to the surgical microscope (Zeiss) through a lens adapter (TTI Medical). The picture included a pair of reference points previously marked on the dorsal ridge of the temporal bone, indicating the absolute scale and position of the image with respect to bregma. This picture was displayed on a computer screen and a micrometric grid was overlapped to guide and mark the placement of the electrode for every recording made. Recording sites (250–500 μm spacing) were evenly distributed across the cortical region of interest while avoiding blood vessels. The vascular pattern was used as a local reference to mark the position of every recording site in the picture, but otherwise differed largely between animals. To confirm the actual depth and cortical lay-

er of the recorded neurons, at the end of the experiment we made electrolytic lesions at one to four of the recording sites, at the same depth that recordings were made. Five auditory cortical fields were identified according to tone frequency response topographies [30]. The limits and relative position of the auditory fields were determined for each animal at the end of the experiment, using the characteristic frequency (CF; the tone frequency that elicits a significant neuronal response at the lowest intensity) gradient as the main reference landmark [30,57]. We consistently observed distinct tonotopic gradients within the different fields, with a high-frequency reversal between VAF and AAF (rostrally), a low-frequency reversal between A1 and PAF (dorsocaudally) and a high-frequency reversal between VAF and SRAF (ventrally). We identified the boundary between A1 and VAF as a 90° shift in the CF gradient in the ventral low-frequency border of A1, and the boundary between A1 and AAF as an absence of tone-evoked responses in the ventral, high-frequency border of A1 [30]. We used these boundaries to assign each recording to a given field. The CF of each recording track was computed as the average CF of all neurons recorded in that track, including a fast multi-unit activity FRA recording made between 400-550 μm depth, corresponding to layers IIIb-IV of the auditory cortex.

IC and MGB experiments. Each recording track was marked with electrolytic lesions for subsequent histological localization of the neurons recorded. At the end of the experiment, the animal was given a lethal dose of sodium pentobarbital and perfused transcardially with phosphate buffered saline (0.5% $NaNO_3$ in PBS) followed by fixative (a mixture of 1% paraformaldehyde and 1% glutaraldehyde in rat Ringer's solution). After fixation and dissection, the brain tissue was cryoprotected in 30% sucrose and sectioned on a freezing microtome in the transverse or sagittal planes into 40 mm-thick sections. Sections were Nissl stained with 0.1% cresyl violet to facilitate identification of cytoarchitectural boundaries. Recording sites were marked on standard sections from a rat brain atlas (Paxinos and Watson, 6th Edition)

458 and neurons were assigned to one of the main divisions of the IC (central nucleus, dorsal,
459 lateral or rostral cortex) or the MGB (ventral, dorsal and medial division), respectively. The
460 stained sections with the lesions were used to localize each track mediolaterally, dorsoven-
461 trally and rostrocaudally in the Paxinos atlas. To determine the main IC or MGB subdivi-
462 sions, cytoarchitectonic criteria, i.e., cell shape and size, Nissl staining patterns and cell pack-
463 ing density, were used. This information was complemented and confirmed by the stereotaxic
464 coordinates used during the experiment to localize the IC/MGB. After assigning a section to
465 each track/lesion, the electrophysiological coordinates from each experiment and recording
466 unit, i.e., beginning and end of the IC/MGB, as well as the depth of the neuron, were used as
467 complementary references to localize each neuron within a track.

468 *Statistical Analysis*

469 All data analyses were performed with the Matlab^{TM} software, using the built-in func-
470 tions, the Statistics and Machine Learning toolbox, or custom scripts and functions developed
471 in our laboratory. Peri-stimulus time histograms (PSTH) were generated for each stimu-
472 lus/condition tested. Only the last STD tones preceding each DEV tone were used for the
473 analyses. A PSTH was a histogram of action potential density over time (in action potentials
474 per second, or Hz) from −75 to 250 ms around stimulus onset, using the 40 trials available for
475 each tone and condition. Every PSTH was smoothed with a 6 ms gaussian kernel ("ksdensi-
476 ty" function in Matlab) in 1 ms steps to estimate the spike-density function (SDF) over time,
477 and the baseline spontaneous firing rate (SFR) was determined as the average firing rate (in
478 Hz) during the 75 ms preceding stimulus onset. For any given time window, the excitatory
479 response was measured as the area below the SDF and above the baseline SFR (positive area
480 patches only, to avoid negative response values). This measure will be referred to as "base-
481 line-corrected spike count".

We used two types of sequences to control for repetition effects (*v.s. Experimental Design*), namely the many-standards and cascaded sequences (Fig. 1d). However, only one of them is required to decompose neuronal mismatch into repetition suppression and prediction error (Fig. 1d). In the following, we describe the analysis performed using the CAS condition as control, since the analysis using the MAS sequence is completely analogous. Baseline-corrected spike count responses of a neuron to the same tone in the three conditions (DEV, STD, CAS) were normalized using the formulas:

$DEV_N = DEV/N;$

$STD_N = STD/N;$

$CAS_N = CAS/N;$

Where

$$N = \sqrt{DEV^2 + STD^2 + CAS^2}$$

is the Euclidean norm of the vector (DEV, STD, CAS) defined by the three responses. This normalization procedure always results in a value ranging 0 to 1, and has a straightforward geometrical interpretation (Fig. 3b,h): Normalized values are the coordinates of a 3D unit vector (DEV_N, STD_N, CAS_N) with the same direction of the original vector (DEV, STD, CAS), and thus the same proportions between the three response measures. From these normalized responses, indices of neuronal mismatch (iMM), repetition suppression (iRS), and prediction error (iPE) were computed as:

iMM = $DEV_N - STD_N$,

iRS = $CAS_N - STD_N$,

iPE = $DEV_N - CAS_N$,

These indices, consequently, always range between -1 and 1, and provide the following quantitative decomposition of neuronal mismatch (Fig. 1d) into repetition suppression and prediction error:

iMM = iRS + iPE

As shown if Fig. S1, the iMM is largely equivalent to the typical SI, or "SSA index", commonly used in most previous studies of SSA in single units [26,29]:

SI = (DEV-STD)/(DEV+STD)

For the analysis of the LFP signal, we aligned the recorded wave to the onset of the stimulus for every trial, and computed the mean LFP for every recording site and stimulus condition (DEV, STD, CAS), as well as the "prediction error potential" (PEP = $LFP_{DEV} - LFP_{CAS}$). Then, grand-averages were computed for all conditions, for each auditory station separately. The p-value of the grand-averaged PEP was determined for every time point with a two-tailed t-test (Bonferroni-corrected for 200 comparisons, with family-wise error rate FWER<0.05), and we computed the time intervals where PEP was significantly different from zero (Fig. 5).

All statistical tests used were distribution-free tests (or "nonparametric", namely the Wilcoxon signed-rank test and Friedman test), given the non-normal nature of our dataset (baseline-corrected spike counts, normalized responses, indices of neuronal mismatch, repetition suppression and prediction error). Only the difference wave for the LFPs (PEP in Fig. 5) was tested using a t-test, since each LFP trace is itself an average of 40 waves, and thus approximately normal (according to the Central Limit Theorem). Linear models used to test significant average iPE within each auditory station (Fig. 4b,d) and significant effects of *nucleus*, *hierarchy*, *SPL*, *direction*, and interactions between them, were fitted using the 'fitlm' function in Matlab, with robust options.

References

1. Ranganath, C. & Rainer, G. Neural mechanisms for detecting and remembering novel events. *Nat Rev Neurosci* **4,** 193–202 (2003).

2. Whitmire, C. J. & Stanley, G. B. Rapid Sensory Adaptation Redux: A Circuit Perspective. *Neuron* **92,** 298–315 (2016).

3. Escera, C. & Malmierca, M. S. The auditory novelty system: an attempt to integrate human and animal research. *Psychophysiology* **51,** 111–123 (2014).

4. Stefanics, G., Kremláček, J. & Czigler, I. Visual mismatch negativity: a predictive coding view. *Front Hum Neurosci* **8,** 666 (2014).

5. Ostwald, D. *et al.* Evidence for neural encoding of Bayesian surprise in human somatosensation. *Neuroimage* **62,** 177–188 (2012).

6. Pause, B. M. & Krauel, K. Chemosensory event-related potentials (CSERP) as a key to the psychology of odors. *Int J Psychophysiol* **36,** 105–122 (2000).

7. Winkler, I., Denham, S. L. & Nelken, I. Modeling the auditory scene: predictive regularity representations and perceptual objects. *Trends Cogn Sci* **13,** 532–540 (2009).

8. Näätänen, R., Astikainen, P., Ruusuvirta, T. & Huotilainen, M. Automatic auditory intelligence: an expression of the sensory-cognitive core of cognitive processes. *Brain Res Rev* **64,** 123–136 (2010).

9. Dehaene, S., Meyniel, F., Wacongne, C., Wang, L. & Pallier, C. The Neural Representation of Sequences: From Transition Probabilities to Algebraic Patterns and Linguistic Trees. *Neuron* **88,** 2–19 (2015).

10. Näätänen, R., Paavilainen, P., Rinne, T. & Alho, K. The mismatch negativity (MMN) in basic research of central auditory processing: a review. *Clin Neurophysiol* **118,** 2544–2590 (2007).

11. Näätänen, R. *et al.* The mismatch negativity (MMN)--a unique window to disturbed central auditory processing in ageing and different clinical conditions. *Clin Neurophysiol* **123,** 424–458 (2012).

12. Michie, P. T., Malmierca, M. S., Harms, L. & Todd, J. The neurobiology of MMN and implications for schizophrenia. *Biol Psychol* **116,** 90–97 (2016).

13. Friston, K. A theory of cortical responses. *Philos Trans R Soc Lond B Biol Sci* **360,** 815–836 (2005).

14. Bastos, A. M. *et al.* Canonical microcircuits for predictive coding. *Neuron* **76,** 695–711 (2012).

15. Friston, K. The free-energy principle: a rough guide to the brain? *Trends Cogn Sci* **13,** 293–301 (2009).

16. Schröger, E. *et al.* Predictive regularity representations in violation detection and auditory stream segregation: from conceptual to computational models. *Brain Topogr* **27,** 565–577 (2014).

17. Phillips, H. N. *et al.* Convergent evidence for hierarchical prediction networks from human electrocorticography and magnetoencephalography. *Cortex* **82,** 192–205 (2016).

18. Bendixen, A., SanMiguel, I. & Schröger, E. Early electrophysiological indicators for predictive processing in audition: a review. *Int J Psychophysiol* **83,** 120–131 (2012).

19. Auksztulewicz, R. & Friston, K. Repetition suppression and its contextual determinants in predictive coding. *Cortex* **80,** 125–140 (2016).

20. Baldeweg, T. Repetition effects to sounds: evidence for predictive coding in the auditory system. *Trends Cogn Sci* **10,** 93–94 (2006).

21. Garrido, M. I. *et al.* Repetition suppression and plasticity in the human brain. *Neuroimage* **48,** 269–279 (2009).

22. Garrido, M. I., Kilner, J. M., Stephan, K. E. & Friston, K. J. The mismatch negativity: a review of underlying mechanisms. *Clin Neurophysiol* **120,** 453–463 (2009).

23. Wacongne, C., Changeux, J.-P. & Dehaene, S. A neuronal model of predictive coding accounting for the mismatch negativity. *J Neurosci* **32,** 3665–3678 (2012).

24. May, P. J. C. & Tiitinen, H. Mismatch negativity (MMN), the deviance-elicited auditory deflection, explained. *Psychophysiology* **47,** 66–122 (2010).

25. Fishman, Y. I. The mechanisms and meaning of the mismatch negativity. *Brain Topogr* **27,** 500–526 (2014).

26. Ulanovsky, N., Las, L. & Nelken, I. Processing of low-probability sounds by cortical neurons. *Nat Neurosci* **6,** 391–398 (2003).

27. Malmierca, M. S., Cristaudo, S., Pérez-González, D. & Covey, E. Stimulus-specific adaptation in the inferior colliculus of the anesthetized rat. *J Neurosci* **29,** 5483–5493 (2009).

28. Antunes, F. M. & Malmierca, M. S. An overview of stimulus-specific adaptation in the auditory thalamus. *Brain Topogr* **27,** 480–499 (2014).

29. Taaseh, N., Yaron, A. & Nelken, I. Stimulus-specific adaptation and deviance detection in the rat auditory cortex. *PLoS One* **6,** e23369 (2011).

30. Nieto-Diego, J. & Malmierca, M. S. Topographic Distribution of Stimulus-Specific Adaptation across Auditory Cortical Fields in the Anesthetized Rat. *PLoS Biol.* **14,** e1002397 (2016).

31. Grill-Spector, K., Henson, R. & Martin, A. Repetition and the brain: neural models of stimulus-specific effects. *Trends Cogn. Sci. (Regul. Ed.)* **10,** 14–23 (2006).

32. Harms, L., Michie, P. T. & Näätänen, R. Criteria for determining whether mismatch responses exist in animal models: Focus on rodents. *Biol Psychol* **116,** 28–35 (2016).

33. Shiramatsu, T. I., Kanzaki, R. & Takahashi, H. Cortical mapping of mismatch negativity with deviance detection property in rat. *PLoS One* **8,** e82663 (2013).

34. Todd, J., Harms, L., Schall, U. & Michie, P. T. Mismatch negativity: translating the potential. *Front Psychiatry* **4,** 171 (2013).

35. Jacobsen, T. & Schröger, E. Is there pre-attentive memory-based comparison of pitch? *Psychophysiology* **38,** 723–727 (2001).

36. Ruhnau, P., Herrmann, B. & Schröger, E. Finding the right control: the mismatch negativity under investigation. *Clin Neurophysiol* **123,** 507–512 (2012).

37. Harms, L. *et al.* Mismatch negativity (MMN) in freely-moving rats with several experimental controls. *PLoS One* **9,** e110892 (2014).

38. Parvizi, J. Corticocentric myopia: old bias in new cognitive sciences. *Trends Cogn Sci* **13,** 354–359 (2009).

39. Güntürkün, O. & Bugnyar, T. Cognition without Cortex. *Trends Cogn Sci* **20,** 291–303 (2016).

40. Atiani, S. *et al.* Emergent selectivity for task-relevant stimuli in higher-order auditory cortex. *Neuron* **82,** 486–499 (2014).

41. Kraus, N., McGee, T., Littman, T., Nicol, T. & King, C. Nonprimary auditory thalamic representation of acoustic change. *J Neurophysiol* **72,** 1270–1277 (1994).

42. Opitz, B., Schröger, E. & von Cramon, D. Y. Sensory and cognitive mechanisms for preattentive change detection in auditory cortex. *Eur J Neurosci* **21,** 531–535 (2005).

43. Abbott, L. F., Varela, J. A., Sen, K. & Nelson, S. B. Synaptic depression and cortical gain control. *Science* **275,** 220–224 (1997).

44. Hupé, J. M. *et al.* Cortical feedback improves discrimination between figure and background by V1, V2 and V3 neurons. *Nature* **394,** 784–787 (1998).

45. Fishman, Y. I. & Steinschneider, M. Searching for the mismatch negativity in primary auditory cortex of the awake monkey: deviance detection or stimulus specific adaptation? *J Neurosci* **32,** 15747–15758 (2012).

46. Maess, B., Jacobsen, T., Schröger, E. & Friederici, A. D. Localizing pre-attentive auditory memory-based comparison: magnetic mismatch negativity to pitch change. *Neuroimage* **37,** 561–571 (2007).

47. Farley, B. J., Quirk, M. C., Doherty, J. J. & Christian, E. P. Stimulus-specific adaptation in auditory cortex is an NMDA-independent process distinct from the sensory novelty encoded by the mismatch negativity. *J Neurosci* **30,** 16475–16484 (2010).

48. Meyer, T. & Olson, C. R. Statistical learning of visual transitions in monkey inferotemporal cortex. *Proc. Natl. Acad. Sci. U.S.A.* **108,** 19401–19406 (2011).

49. Zmarz, P. & Keller, G. B. Mismatch Receptive Fields in Mouse Visual Cortex. *Neuron* **92,** 766–772 (2016).

50. Chen, I.-W., Helmchen, F. & Lütcke, H. Specific Early and Late Oddball-Evoked Responses in Excitatory and Inhibitory Neurons of Mouse Auditory Cortex. *J Neurosci* **35,** 12560–12573 (2015).

51. Musall, S., Haiss, F., Weber, B. & von der Behrens, W. Deviant Processing in the Primary Somatosensory Cortex. *Cereb Cortex* (2015). doi:10.1093/cercor/bhv283

52. Koelsch, S., Busch, T., Jentschke, S. & Rohrmeier, M. Under the hood of statistical learning: A statistical MMN reflects the magnitude of transitional probabilities in auditory sequences. *Sci Rep* **6,** 19741 (2016).

53. Winkler, I. & Schröger, E. Auditory perceptual objects as generative models: Setting the stage for communication by sound. *Brain Lang* **148,** 1–22 (2015).

54. Peter, V., McArthur, G. & Thompson, W. F. Effect of deviance direction and calculation method on duration and frequency mismatch negativity (MMN). *Neurosci Lett* **482,** 71–75 (2010).

55. Malmierca, M. S. The structure and physiology of the rat auditory system: an overview. *Int. Rev. Neurobiol.* **56,** 147–211 (2003).

56. Lee, C. C. & Sherman, S. M. On the classification of pathways in the auditory midbrain, thalamus, and cortex. *Hear. Res.* **276,** 79–87 (2011).

57. Polley, D. B., Read, H. L., Storace, D. A. & Merzenich, M. M. Multiparametric auditory receptive field organization across five cortical fields in the albino rat. *J Neurophysiol* **97,** 3621–3638 (2007).

58. Eggermont, J. J. Animal models of auditory temporal processing. *Int J Psychophysiol* **95,** 202–215 (2015).

59. Bullock, D. C., Palmer, A. R. & Rees, A. Compact and easy-to-use tungsten-in-glass microelectrode manufacturing workstation. *Med Biol Eng Comput* **26,** 669–672 (1988).

Acknowledgements

We thank Drs. Bernhard Englitz, Alan Palmer, Patrick May, Daniel Polley, José Luis Peña, Juanita Todd, Ryszard Auksztulewicz, Christoph Schreiner, Iria SanMiguel and Adrian Rees for their comments on a previous version of the manuscript and for their constructive criticisms.

Financial support was kindly provided by the Spanish MINECO (BFU2013-43608-P & SAF2016-75803-P) and JCYL (SA343U14) to MSM and a Explora-Ciencia grant (PSI2013-49348-EXPLORA) to MSM and CE. CE was also supported by the Generalitat de Catalunya (SGR2014-177) and by the Icrea Acadèmia Distinguished Professor Award. JND held a fellowship from the European Social Fund/Spanish JCYL (Operational Programme ESF Castilla y León 2007–2013). GGP held a fellowship from the Spanish MINECO (BES-2014-069113).

Author contributions

The experiments were performed at the Neurobiology of Hearing Laboratory, Institute of Neuroscience of Castilla y León- INCYL, University of Salamanca, Salamanca, Spain. The contribution of each author to the following aspects of the study is as stated: (1) collection of data: JND, GVC and GGP; (2) conception and design of experiments: JND and MSM; (3) analysis, interpretation of data and conceptual advice: JND, GVC; GGP; CE and MSM; (5) writing of the manuscript: JND and MSM. All authors approved the final version of the manuscript.

Figures

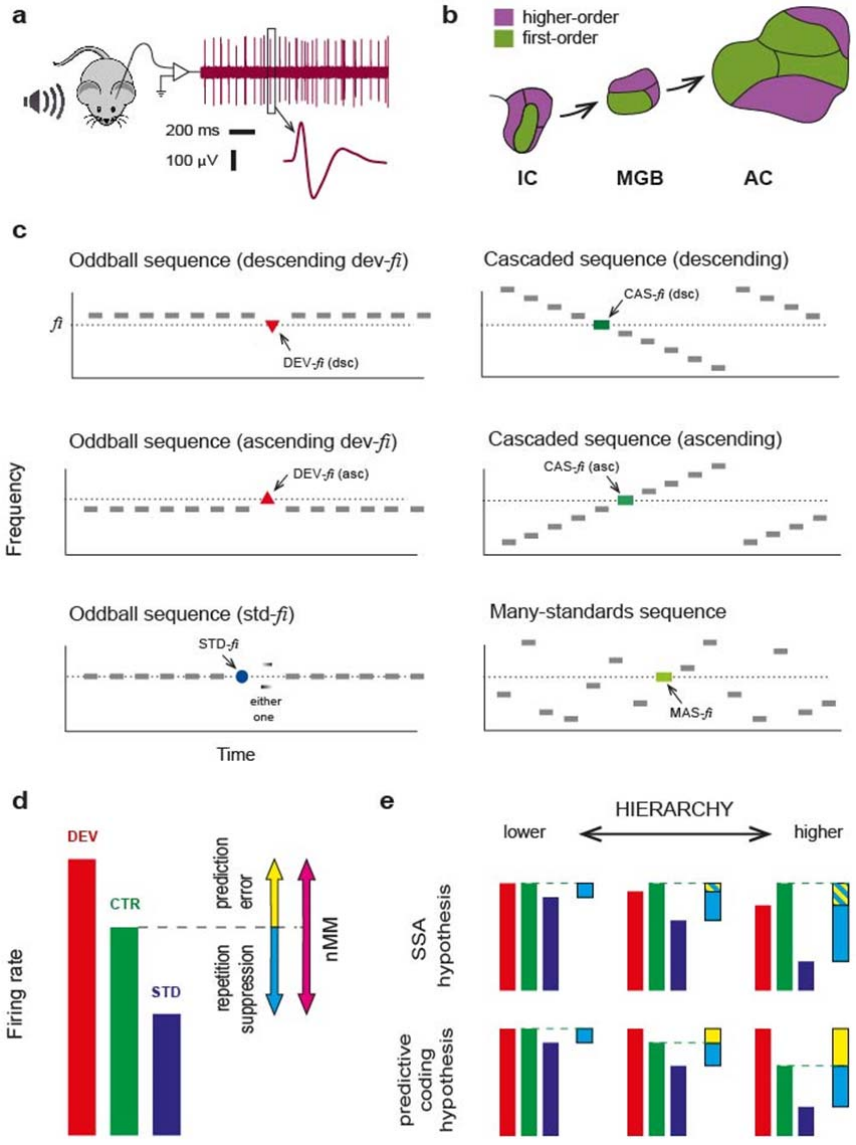

Figure 1: Experimental design. **a**. Sketch of experimental setup. Isolated neurons were recorded from different auditory nuclei of anesthetized rats, while stimulating with pure tones. **b.** Schematic representation of the major nuclei in the rat auditory pathway form midbrain to cortex [3,30], divided into first- and higher-order regions. **c.** Stimulation sequences. For each recorded neuron, 10 tones of evenly-spaced frequencies were selected to construct these stimulation sequences. Using this design, each tone f_i (i=1...10) lying inside the

690 neuron's receptive field could be presented in two experimental conditions (DEV and STD,
691 in separate oddball sequences), and two control conditions (CAS/MAS) for adaptation
692 effects. Note that ascending/descending DEV tones will be compared to the corresponding
693 version of the CAS condition (see Methods). **d.** Decomposition of neuronal mismatch
694 responses (nMM=DEV−STD) to the oddball sequence using either one of the control
695 conditions. **e.** Predicted scenarios under two competing mechanisms explaining nMM. If SSA
696 is the main mechanism underlying nMM, responses to STD tones will be more suppressed
697 the more synapses information traverses along the auditory hierarchy, and responses to
698 control (CAS/MAS) tones would be equal to, or stronger than, to DEV tones, since the
699 average intertonal distance is larger in the controls than in oddball sequences [29]. By contrast,
700 if nMM reflects Bayesian inference, responses to DEV tones would be progressively larger
701 than to the controls as the information propagates up the auditory hierarchy [4].

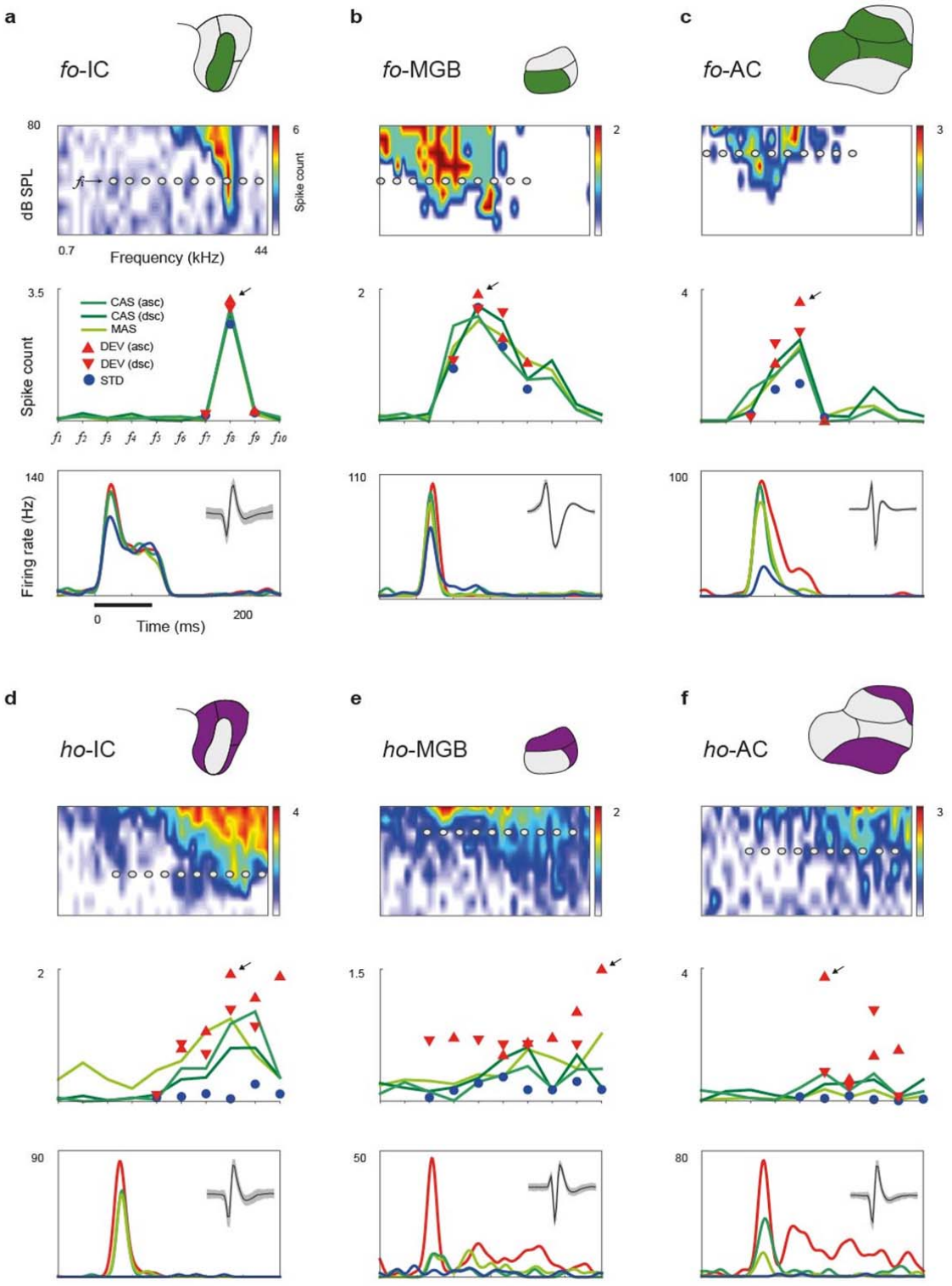

Figure 2: Prediction error in sample neuronal responses. a-f. Each panel shows responses of representative neurons within each station of the auditory pathway: (1) The FRA

(representation of neuronal sensitivity to different frequency/intensity combinations) and the 10 tones selected to create the control sequences for that particular neuron (see Methods). (2) Measured responses of the neuron to each tone (baseline-corrected spike counts, averaged within 0−180 ms after tone onset), for all conditions tested. (3) Sample PSTH for each condition, for the tone with the highest response (either ascending or descending; indicated with an arrow). Stimulus duration is represented by the thick, horizontal line, and the isolated spike (mean ± SEM) is shown in the small inset. Note that both repetition suppression (STD < CTR) and prediction error (DEV > CTR) can be observed in responses to some tones, and this is particularly consistent for higher-order neurons (panels D-F).

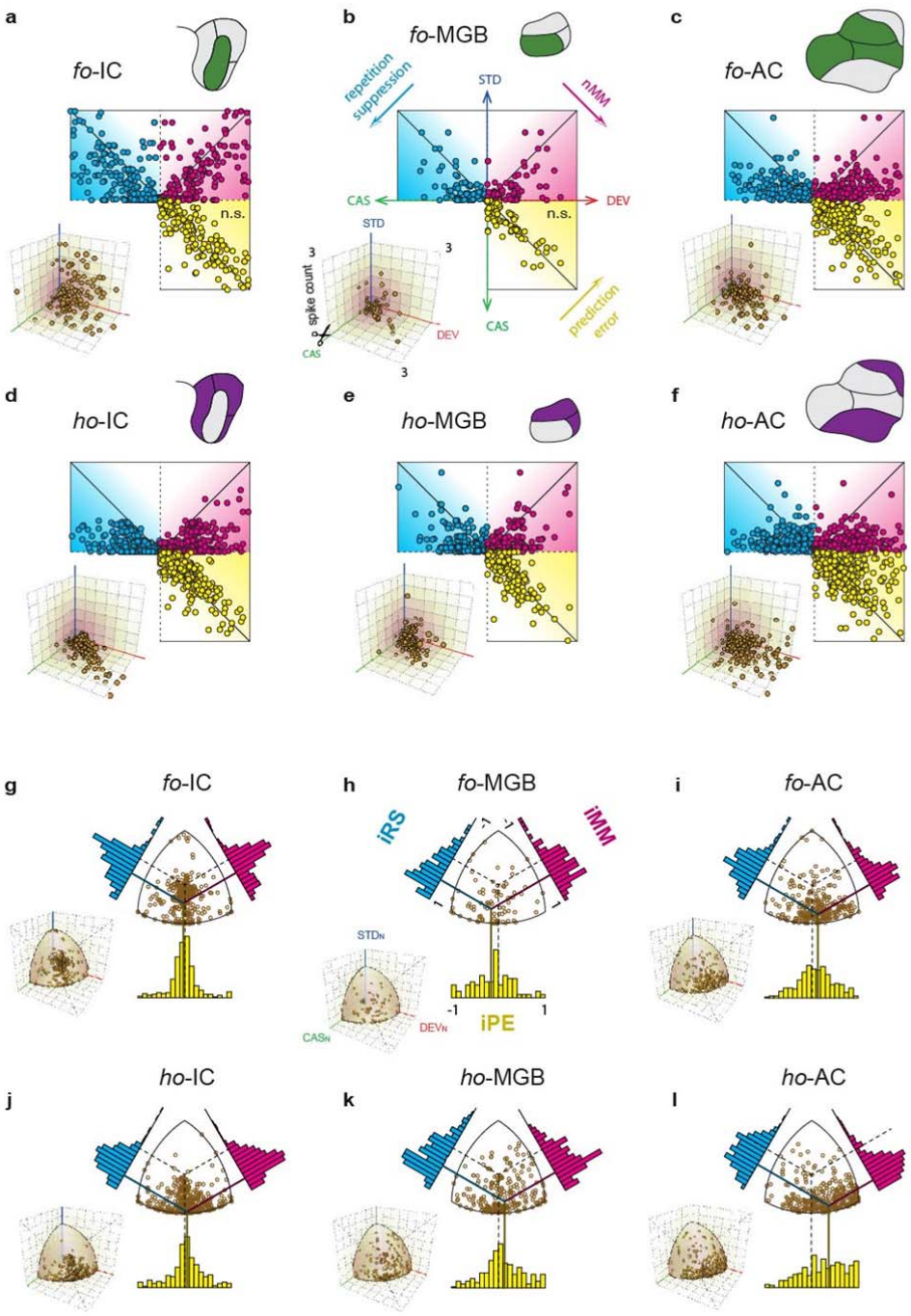

714

715 **Figure 3. Prediction error at the population level**. **a-f**. Responses to the three conditions

716 (DEV, STD, CAS; for all tones tested in all neurons) were represented on a 3D scatter,

717 separately for each station. These points were then orthogonally projected onto the three

718 "walls", to compare two responses at a time, and then the "box" was unfolded (after "cutting"

along the CAS axes) to create the main, flat diagrams. Thus, each 2D point represents the response (baseline-corrected spike count) of a single neuron to one given tone for a pair of conditions. The clouds of magenta and blue points concentrate below the diagonal in all stations, indicating neuronal mismatch and repetition suppression, respectively, at the population level. The cloud of yellow points remains unbiased in lower stations (a,b), but is displaced above the diagonal in higher stations, especially in AC (c,f). This indicates an important contribution of prediction error to neuronal responses in these stations. **g-l**. Distribution of normalized responses and indices of neuronal mismatch (iMM), repetition suppression (iRS) and prediction error (iPE). Each point in the 3D scatters from panels a-f represents a vector in response space (DEV, STD, CAS). The normalization is just the radial projection of this point onto the unit sphere centered on the origin (small insets), so the resulting vector (DEV_N, STD_N, CAS_N,) is a scaled version of the former. The flat diagram is a zenith view of the 3D sphere. Each diagonal (dotted black lines) represents the line where the corresponding index is zero, and the index will increase or decrease as a projected point moves away from this line. Histograms represent index distributions, with their means indicated by colored lines. Note the overall shift of the mean iPE towards positive values, from IC through MGB to AC, and from first- to higher-order divisions.

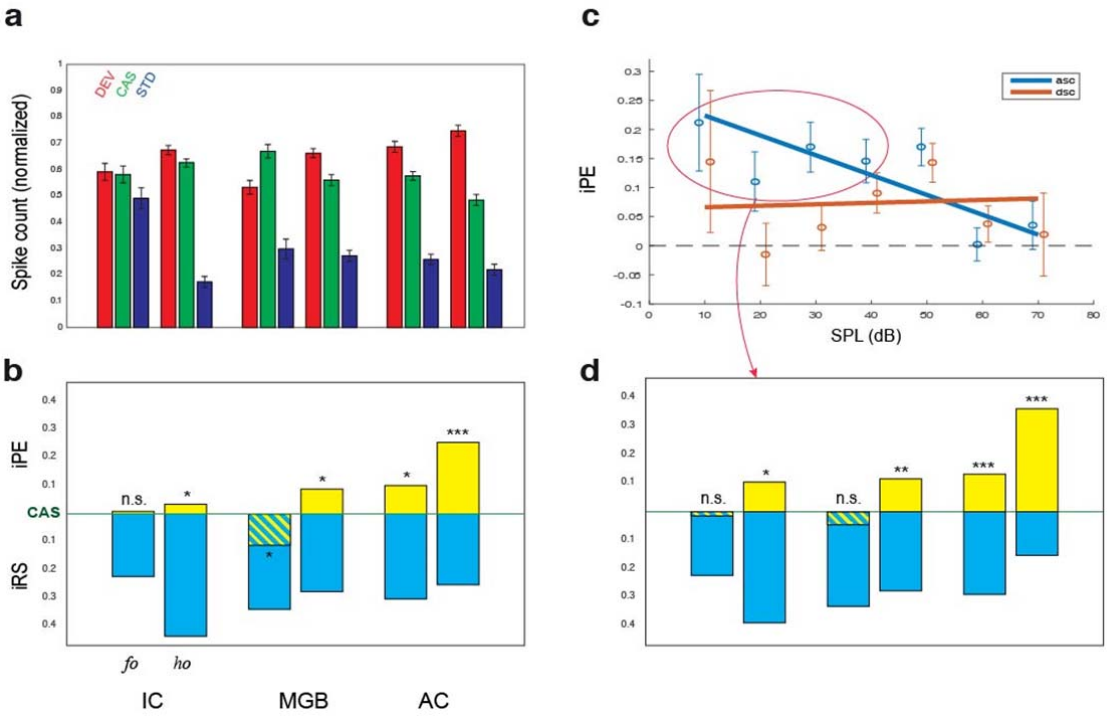

736

737 **Figure 4: Emergence of iPE along the auditory hierarchy. a**. Average normalized
738 responses (mean ± SEM) to the three conditions (DEV_N, STD_N, CAS_N) within each station.
739 **b**. These same normalized responses are represented with respect to the CAS control
740 condition, so that the indices are represented by their differences (iPE is upwards-positive,
741 iRS is downwards-positive). Asterisks denote statistical significance of iPE against zero
742 median (Table 1) **c**. Linear model fitted for the iPE, using SPL and Direction
743 (ascending/descending) as predictors. Error bars denote mean and SEM for each SPL and
744 Direction. **d**. The same as in (b), but using only recordings for ascending deviant tones at
745 intensities ≤ 40 dB SPL.

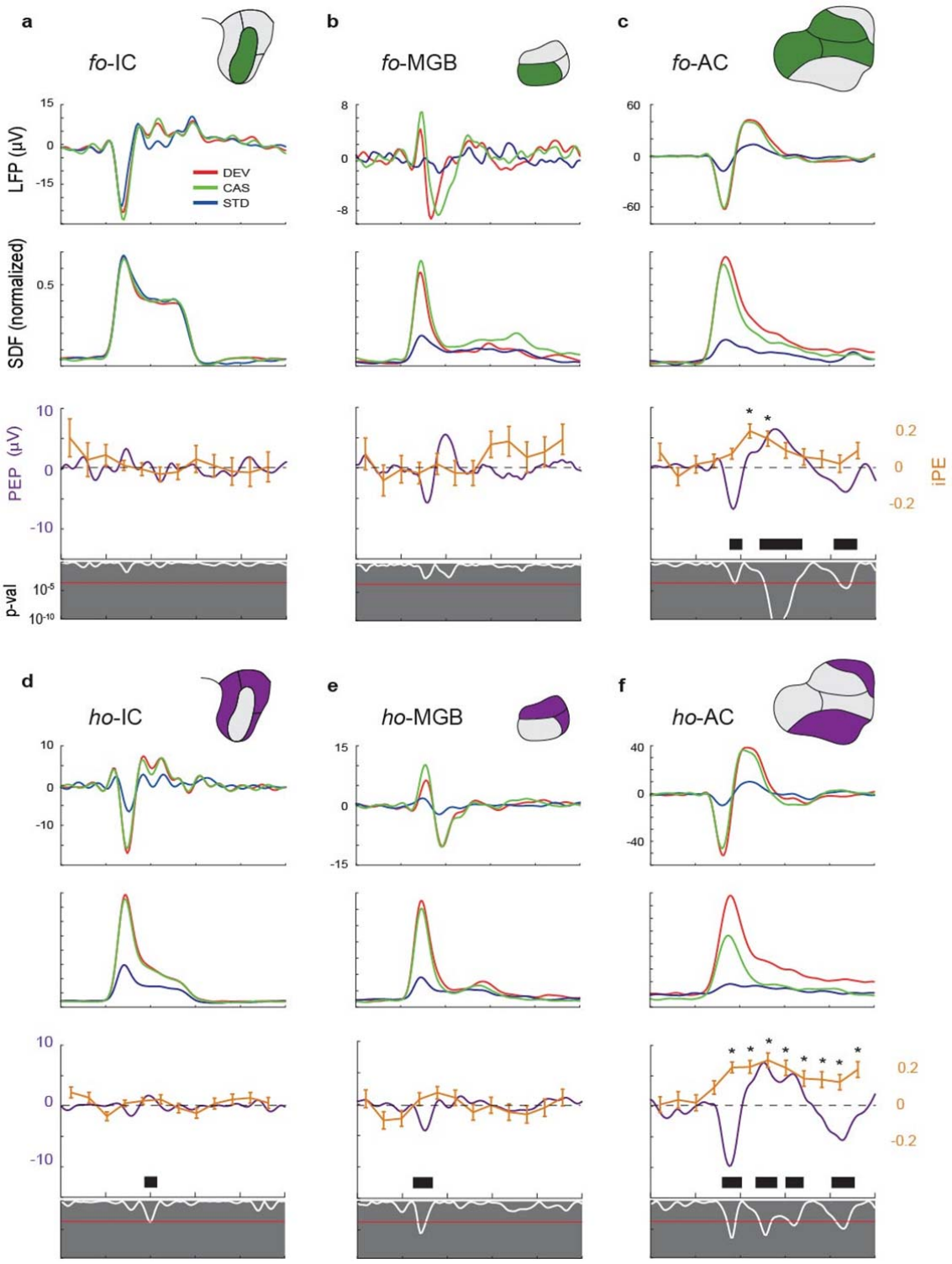

746

747 **Figure 5: Correlation of iPE and the local-field prediction error signal (PEP).** Population

748 grand-averages for different response measures, computed for each processing station

separately: (1) Average local field potentials (LFP) across tested tones and recording sites for the different conditions. (2) Average firing rate profiles, as spike-density functions (SDF, normalized to better match the iPE traces shown below). (3) Average "local-field prediction error signal" (PEP = $LFP_{DEV} - LFP_{CAS}$; white trace: instantaneous p-value for the PEP, paired t-test against equal means; red horizontal line: critical threshold with Bonferroni correction for 200 comparisons, FWER<0.05; thick black bars: time intervals for which average PEP is significant). (4) Along with the PEP trace, the time course of the average iPE is plotted in orange (mean ± SEM, asterisks indicate a significant iPE for the corresponding time window; Wilcoxon signed rank test with Bonferroni correction for 12 comparisons, FWER<0.05). Highest iPE values are concurrent in time and location (auditory cortex; panels C-F) with the strongest PEP.

Tables

Table 1: Summary of principal dataset. For each auditory station: Number of recorded neurons and tested neuron/tone combinations (points). Median values for baseline-corrected spike counts (spk) to the different conditions. Median differences between the former measures, and associated p-values against zero (Friedman test with post-hoc multiple comparison, Fisher's Least Significant Difference method, uncorrected for 6 independent tests). Median indices of neuronal mismatch (iMM), repetition suppression (iRS) and prediction error (iPE), computed from each of the two control sequences (CAS or MAS), and their corresponding p-values (note that p-values are the same for absolute differences and normalized indices, since these indices are median differences between normalized responses, and the non-parametric test is independent of scaling). Values related to predictive neuronal activity are highlighted in bold case, since they represent the most significant result of this research.

773

	fo-IC	*ho*-IC	*fo*-MGB	*ho*-MGB	*fo*-AC	*ho*-AC
# Neurons	22	56	24	35	35	36
# Points	114	523	77	225	250	306
DEV (spk)	2.55	0.99	0.64	0.68	0.95	0.98
STD (spk)	1.93	0.22	0.20	0.14	0.24	0.21
CAS (spk)	2.37	0.97	0.71	0.55	0.77	0.59
MAS (spk)	2.51	0.95	0.90	0.65	0.85	0.52
DEV−STD (spk)	0.62	0.77	0.44	0.54	0.71	0.77
p-val	0.000	0.000	0.000	0.000	0.000	0.000
CAS−STD (spk)	0.44	0.76	0.51	0.40	0.53	0.38
p-val	0.000	0.000	0.000	0.000	0.000	0.000
DEV−CAS (spk)	0.18	**0.019**	−0.07	**0.13**	**0.18**	**0.39**
p-val	0.779	0.020	0.019	0.023	0.019	0.000
MAS−STD (spk)	0.57	0.73	0.70	0.50	0.60	0.31
p-val	0.003	0.000	0.000	0.000	0.000	0.000
DEV−MAS (spk)	0.04	0.04	−0.26	0.03	**0.11**	**0.46**
p-val	0.190	0.155	0.003	0.671	0.049	0.000
iMM_{CAS}	0.127	0.493	0.324	0.496	0.505	0.609
p-val	0.000	0.000	0.000	0.000	0.000	0.000
iRS_{CAS}	0.013	0.461	0.447	0.446	0.398	0.334
p-val	0.000	0.000	0.000	0.000	0.000	0.000
iPE_{CAS}	−0.002	**0.032**	−0.122	**0.050**	**0.107**	**0.275**
p-val	0.779	0.020	0.019	0.023	0.019	0.000
iMM_{MAS}	0.147	0.485	0.303	0.505	0.508	0.611
p-val	0.000	0.000	0.000	0.000	0.000	0.000
iRS_{MAS}	0.091	0.463	0.445	0.494	0.439	0.343
p-val	0.003	0.000	0.000	0.000	0.000	0.000
iPE_{MAS}	0.055	0.023	−0.143	0.010	**0.069**	**0.267**
p-val	0.190	0.155	0.003	0.671	0.049	0.000

774

775

Supplementary Materials

Figure S1: Quantitative comparison between iMM and the "classical" SI. The SI trace is plotted as a function of the DEV/STD ratio, since it does not take into account the control condition. Different iMM traces are plotted (dashed lines), as a function of the relative magnitude of the response to control condition with respect to DEV response (CTR/DEV), from low (CTR=0.2*DEV) to high (CTR=1.2*DEV) hypothetical responses to the control. The two indices (the SI and the iMM for different CTR response magnitudes) take values very close to each other under most conditions, except for very extreme and rare cases in which the response to the control condition is much larger than DEV of much smaller than STD.